Multiple roles of integrin-α3 in the development and maintenance of the neuromuscular junction

Alexander Jacob Ross

Institute of Child Health,

University College London

2015

A thesis submitted to University College London in fulfilment of the requirements for the degree of Doctor of Philosophy

I, Alexander Jacob Ross, confirm that the work presented in this thesis is my own. Where information has been derived from other sources, I confirm that this has been indicated in the thesis.

Abstract

The neuromuscular junction (NMJ) is the synaptic contact between motoneurons and muscle, where neurotransmission results in the contraction of the muscle fibres. The basal lamina instructs NMJ development at virtually every stage. Largely, the functions of the basal lamina are mediated through interactions with cell surface adhesion receptors; however, less is known about the identities and roles of these at the NMJ. Integrin-α3 is an extracellular matrix receptor that has previously been identified at the NMJ active zones, the sites of neurotransmitter release in the presynaptic terminus. As integrin-α3 binds to laminin-α4 and other active zone components, my hypothesis is that it may be important for relaying signals provided by the basal lamina during NMJ development. In this study, the integrin-α3 knockout mouse was used to explore the functions of this protein at the NMJ. Mutants displayed defects in active zone assembly and developmental motoneuron patterning. NMJs frequently resembled those found in aged animals, and in some cases, nerve terminals were detached from the synaptic cleft. Finally, electrophysiological analysis revealed defects in neurotransmission at mutant NMJs, including reduced efficiency of synaptic vesicle release, and impaired sensitivity of nerve terminals to external Ca^{2+}. Previous studies have implicated integrin-α3 in muscle development; however, I find no expression of integrin-α3 in the muscle, and no defects in myogenesis in integrin-α3 mutants. These results indicate multiple roles for integrin-α3 at the NMJ, for active zone assembly, adhesion of nerve terminal, morphological integrity and neurotransmission. To my knowledge, this study identifies for the first time a cell surface receptor for the anchorage of pre- and postsynaptic elements at the NMJ. These results suggest that alterations in integrin-α3 expression or function may underlie some of the changes associated with ageing at the NMJ, and that mutations in its encoding gene may cause myasthenic syndromes.

Table of Contents

List of figures and tables

Acknowledgments

I would like to thank my primary supervisor Francesco Conti for his excellent guidance, both experimental and theoretical, and for the very many fruitful (and animated) discussions about "what might be going on". Also for the help in navigating the fields of neuromuscular junction development and synaptic physiology, both of which were new to us, and outside the expertise of the department. To my secondary supervisor Jennifer Morgan for all the help and encouragement throughout the experimental and writing phases of the project. I would also like to thank Lizzy Stevens for her constant love and support during my PhD. Also for putting up with me during the write-up, and for your hard work with the corrections - I'm sorry to have inflicted that on you! Also to my Mum and Dad for the huge amount of support and help you have given me over the years. I would not be writing this thesis if it wasn't for you. Thanks go to my friends for their understanding and patience while I was in the final stages.

Another set of thanks go to all the collaborators who have done an excellent and often arduous job with all the research. To Mark Turmaine for giving up huge amounts of time, both his own and of the availability of the electron microscope, while I booked never-ending sessions to look for NMJs. Also for his keen and experienced eye which helped no end. To Richard Webster for diligently pursuing and dissecting the electrophysiological defects in the mice, days and days of work which was a lot more complicated than expected. Also for his patience in helping us to understand the principles of electrophysiology. To Kairbaan Hodivala-Dilke for continuing to house the mice for several years, and for the very useful suggestions. To Tanguy Lechertier, Louise Reynolds, Bruce Williams and Julie Holdsworth for all the help with the mice, and for dealing with multiple administrative nightmares associated with the transfer of mice to Oxford. Also to Bertrand Vernay, for all his invaluable help with imaging, particularly the 3D deconvolution.

Abbreviations

AChR: acetylcholine receptor

AChE: acetylcholinesterase

ADP: adenosine diphosphate

ATP: adenosine triphosphate

BCAM: basal cell adhesion molecule

BMD: Becker muscular dystrophy

BSA: bovine serum albumin

ChAT: choline acetyltransferase

CMS: congenital myasthenic syndrome

CNS: central nervous system

DGC: dystrophin-associated glycoprotein complex

DMD: Duchenne muscular dystrophy

dNTP: deoxynucleotide triphosphate

ECM: extracellular matrix

EDTA: ethylenediaminetetraacetic acid

EM: electron microscopy

EOM: extraocular muscle

EPP: endplate potential

EPSC: excitatory postsynaptic current

FAK: focal adhesion kinase

ILK: integrin-linked kinase

IMP: intramembranous particle

IQR: interquartile range

LEMS: Lambert-Eaton myasthenic syndrome

LTP: long-term potentiation

MAPK: mitogen-activated protein kinase

MEPP: miniature endplate potential

MEPSC: miniature excitatory postsynaptic current

MRF: myogenic regulatory factor

MTJ: myotendinous junction

MuSK: muscle-specific kinase

MyHC: myosin heavy chain

NCAM: neural cell adhesion molecule

NMJ: neuromuscular junction

nNOS: neuronal nitric oxide synthase

NSF: N-ethylmaleimide-sensitive factor

Pax: paired box (transcription factor)

PBS: phosphate buffered saline

PCR: polymerase chain reaction

PFA: paraformaldehyde

PSF: point spread function

PSI: plexin-semaphorin-integrin (domain)

RIM-BP: RIM-binding protein

RRP: readily releasable pool

SD: standard deviation

SEM: standard error of the mean

SM: Sec1/Munc18-like

SNARE: soluble NSF attachment protein receptor

SR: sarcoplasmic reticulum

STED: stimulated emission depletion (microscopy)

STF: short-term facilitation

SV2: synaptic vesicle protein 2

TBE: Tris/borate/EDTA (buffer)

TA: *Tibialis anterior* (muscle)

t-SNARE: target membrane SNARE protein

UGC: utrophin associated glycoprotein complex

VGCC: voltage-gated calcium channel

VGSC: voltage-gated sodium channel

v-SNARE: vesicle SNARE protein

1. Introduction

1.1. Skeletal muscle

Skeletal muscles are the organs that generate voluntary movement. At each end, they bind to bones via tendons, and their contraction exerts force on the skeleton, driving motion. There are over 650 skeletal muscles in the human body, and by mass they account for the largest set of organs. They are at the centre of a diverse range of motor functions, including walking, breathing, speech, eye movement, and maintenance of posture. The large number of muscles means that these actions can be carried out with great control and precision (MacIntosh et al., 2006). Movement is coordinated initially in the motor cortex of the brain. Information is transmitted by upper motoneurons to the ventral horn of the spinal column. Here, the cell bodies of the α-motoneurons reside, and these relay signals to the muscles via their axons. The spinal column is divided down its length by vertebrae, and at each level, there is a different population of motoneurons, responsible for innervating its own set of muscles. Sensory nerves also converge at different levels of the spinal cord. Their cell bodies are located just outside the spinal column, in bundles called dorsal root ganglia, and these neurons receive sensory information from their target tissue, and transmit it to the spinal cord. Short interneurons in the spinal cord connect sensory neurons and motoneurons, allowing reflex movements to occur in response to sensation. This pathway allows the bypassing of the brain to occur, so that reflex action can be executed rapidly (Le Douarin and Smith, 1988).

Skeletal muscle consists of many myofibres, the contractile cells that span the entire length of the muscle. Multiple myofibres are first bundled into groups called fascicles, and several of these are in turn bundled together to form the muscle. Each level of structural hierarchy is associated with its own layer of surrounding connective tissue: the epimysium over the outer surface of the entire muscle; the perimysium around each fascicle; and finally the endomysium ensheathing individual myofibres (**Fig 1.1A**). Skeletal muscle is one of three types of muscle in the body, the others being cardiac and smooth muscle. Skeletal muscle is controlled by the

voluntary or somatic nervous system, while the latter two are controlled by the involuntary or autonomic nervous system (Batters et al., 2014).

At the cellular level, the myofibres are multinucleated cells with a single syncytium, formed by many cell fusion events between myogenic precursor cells called myoblasts. Larger muscles may contain myofibres with tens of thousands of myonuclei, each one contributed by a single myoblast (Morgan and Partridge, 2003). Each myofibre is filled with rod-like structures known as myofibrils, which stretch from end to end; these consist primarily of actin and myosin filaments that provide contractile properties. The myofibril is divided along its length into segments called sarcomeres, the basic contractile unit of the muscle. These are ~2 μm long, and are bounded at each end by protein-rich bands called Z-lines. Actin (the 'thin' filaments) spans from the Z-lines towards the centre of the sarcomere, which is demarcated by a band called the M-line. Spanning from the M-line are filaments of myosin (the 'thick' filaments) and these intercalate with the thin actin filaments (**Fig 1.1B, C**). Upon stimulation, the two types of filaments slide over each other, resulting in shortening of the sarcomeres, and muscle contraction. The structural unit of the myofibre is also common to the cardiac muscle, with most of the components and mechanisms of contraction being the same. Owing to the to banded appearance of the sarcomeres, skeletal and cardiac muscles are often referred to as striated muscle (Lopes and Elliott, 2014; MacIntosh et al., 2006).

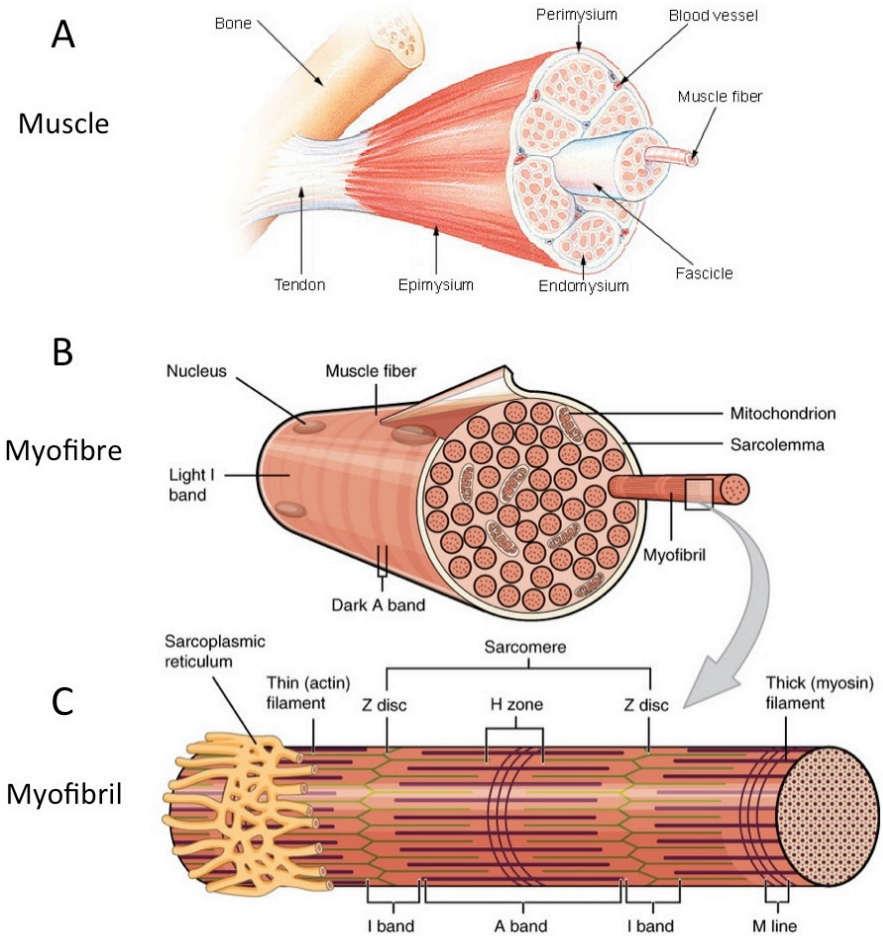

Fig 1.1. Structure of skeletal muscle. (A) Depiction of a skeletal muscle, with linkage to bones via the tendons. The epimysium is the connective tissue that surrounds the whole muscle; the perimysium that which surrounds the fascicles (groups of myofibres); and the endomysium that which surrounds individual myofibres. (B) The structure of one myofibre, with nuclei at the periphery of the cytoplasm, and dense packing of myofibrils. (C) The structure of one myofibril. The individual units of contraction are the sarcomeres, which are bordered at each end by the Z-disks. Actin (thin filaments) extend from the Z-disks, and intercalate with myosin (thick filaments). The central region of the sarcomere is known as the M-line. (A) Image publicly available from National Institute of Health (http://training.seer.cancer.gov/anatomy/muscular/structure.html). (B, C) "1022 Muscle Fibers (small)", from OpenStax College (http://cnx.org/content/col11496/1.6/), under Creative Commons license CC BY 3.0.

The molecular mechanisms that govern contraction are well understood. Upon stimulation by a motoneuron, the plasma membrane of the muscle fibre (the sarcolemma) becomes depolarized, and an action potential spreads into the T-tubules, which are deep invaginations into the cell. Electrical stimulation here results in the opening of L-type voltage-gated calcium channels (VGCCs). The mechanical interactions involved in channel activation result in the opening of calcium channels on the adjacent sarcoplasmic reticulum (SR), an organelle that surrounds the myofibrils. Thus, Ca^{2+} floods out from its store in the SR and into the cytoplasm, and binds to troponin C, which is found on the thin filaments. This in turn results in conformational changes in tropomyosin, another protein associated with the thin filaments, and allows the myosin head to bind to the thin filaments through the unmasking of a binding site. At this stage, adenosine diphosphate (ADP) and inorganic phosphate are associated with myosin, and the release of these results in a conformational change referred to as the power stroke, whereby the myosin head shifts and pulls on the thin filament for sarcomere contraction. Adenosine triphosphate (ATP) now binds to myosin, causing it to detach from the thin filament, and hydrolysis of ATP to ADP and inorganic phosphate provides the energy for myosin to adopt its initial conformation (**Fig 1.2**). This cycle can be repeated multiple times, until stimulation stops, and Ca^{2+} is pumped back into the SR (Bárány, 1967).

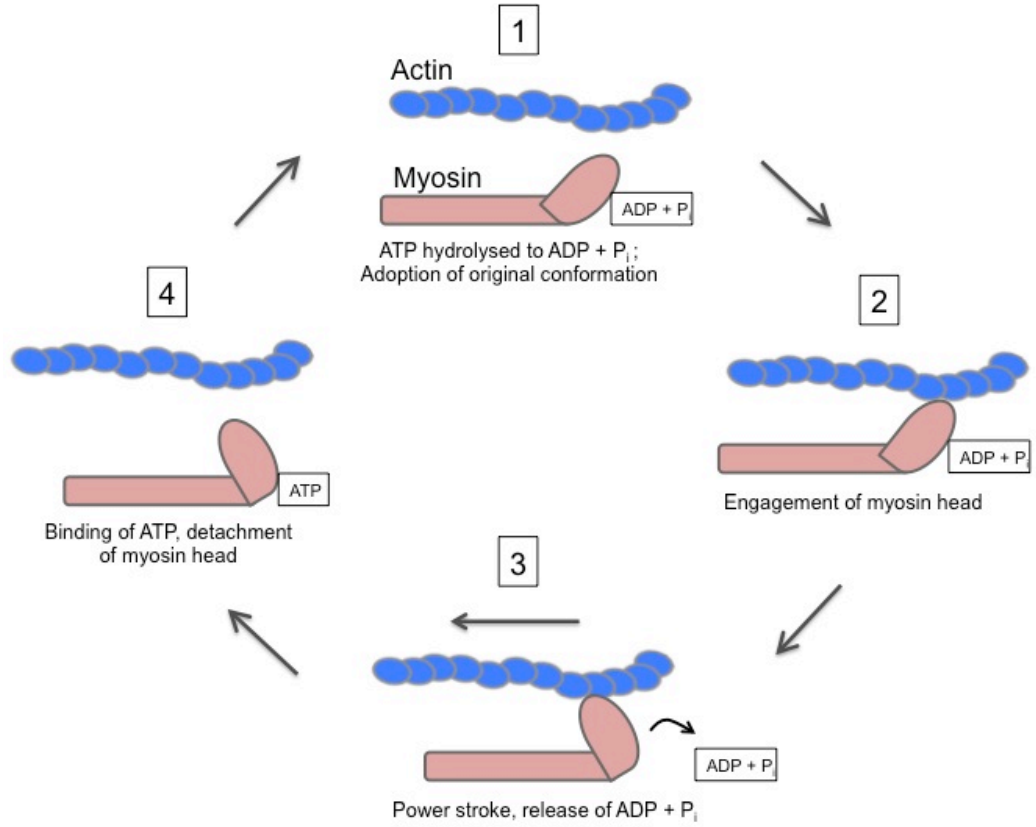

Fig 1.2. Muscle contraction. The interaction of myosin and actin results in muscle contraction, whereby the sarcomeres shorten as the Z-disks draw inwards towards the M-line. Myosin heads are unbound to actin filaments at rest (step 1). On entry of Ca^{2+}, myosin heads are able to engage actin (step 2). Following this, adenosine diphosphate (ADP) and inorganic phosphate (P_i) held in the myosin head are released, and the head tilts, thus pulling on the actin filament (step 3). Adenosine triphosphate (ATP) is now able to bind to the myosin head, and actin is released (step 4). The hydrolysis of ATP provides the energy for myosin to adopt its original conformation (step 1). The action of multiple myosin and actin molecules results in shortening of the sarcomere.

Myofibres are divided into several categories (fibre types), depending on their contractile properties. Generally, these are classed as Type I or slow twitch fibres, and type II or fast twitch fibres. Type I fibres are responsible for sustained contraction with low levels of fatigue, utilising slow myosin ATPase activity. A high myoglobin and mitochondrial content confers an aerobic metabolic profile on these fibres. In contrast, type II fibres are responsible for shorter bursts of strong contraction, relying on fast myosin ATPase activity, and anaerobic metabolism for rapid generation of ATP. As such, they have a lower myoglobin content, as they do not require significant oxygen storage. Type II fibres are further divided into two major categories, IIa and IIb. Type IIa fibres are often considered to be a hybrid of type I and II fibres. They are better at generating quick bursts of force than type I fibres, relying on a mixture of aerobic and anaerobic respiration, but fatigue more quickly. Type IIb fibres have the fastest twitch response, depending on anaerobic metabolism, but fatigue more quickly than the other types (Scott et al., 2001).

The functional capacities of different muscles are defined partially by the composition of fast and slow fibres. As such, muscles involved in posture, particularly those of the neck, tend to have a higher type I fibre content, generating prolonged contraction, but at a relatively low force. The low fatigability of these fibres is also a key factor in endurance, and athletes who compete in activities such as marathons tend to possess more type I fibres (through a probable mixture of genetics and training). In contrast, muscles of the arm tend to contain a higher proportion of the fast type IIb fibres, and athletes who compete in activities such as sprinting tend to possess more of these fibres, due to their association with short bursts of high activity (Daugaard and Richter, 2001).

Contraction at the level of the whole muscle is organised and directed by motor units. Each myofibre is innervated by a single axonal branch of a motoneuron, and neurotransmission occurs across the neuromuscular junction (NMJ), the synapse between the motoneuron and the postsynaptic muscle. One motoneuron can innervate many myofibres (hundreds in larger

muscles), by multiple branching of the efferent axon. A motor unit therefore consists of all the myofibres that are innervated by a particular motoneuron. Myofibres of each motor unit are of the same fibre type. Strong contraction for a larger muscle load is achieved by the recruitment of more motor units: this begins with the smallest in size and ends with the largest. In addition, slow motor units are recruited before fast ones (Mendell, 2005; Milner-Brown et al., 1973). The motor unit system confers several advantages on the process of muscle contraction. Firstly, motor units are recruited as and when needed, adjusting for the quantity of the load, ensuring that fatigue is minimal. Secondly, overall contraction can be fine-tuned across the whole range of outputs of the muscle (Llewellyn et al., 2010).

1.2. Structural arrangement of myofibres

The myofibres are ensheathed by a layer of extracellular matrix (ECM) known as the basement membrane, a mesh-like network of largely filamentous proteins. The basement membrane is found in nearly all cellular systems of animals, and has crucial roles in structural support and a diverse range of cell signalling events, including survival, differentiation, proliferation and regeneration (Hynes, 2009). At the sarcolemma, the costameres are arranged at regular intervals; these are small areas where cell surface adhesion complexes are concentrated. The costameres are linked to the Z-lines of the outer myofibrils through molecular complexes, and remain in precise register with them. On the extracellular leaf, the costameres bind to components of the basement membrane, via adhesion receptors (Ervasti, 2003). The continuum of molecular interactions between the basal lamina, the costameres and the Z-lines of the myofibrils is an essential part of the structural and mechanical stability of muscle, a characteristic that is particularly important in this tissue, in which large forces are generated (Batchelor and Winder, 2006; Godfrey et al., 2011; Lapidos et al., 2004). At the end of the fibre is the myotendinous junction (MTJ), which as the name suggests, is the interface between the muscle fibre and the tendon. Here, deep interlocking invaginations between muscle and tendon allow strong adhesion, via cell surface receptors and basal lamina constituents (Nagano et al., 1998). Together, the myofibrils, costameres, sarcolemma, basal lamina and MTJ are

crucial for the lateral transmission of force during contraction. Below, the different molecular constituents of these muscle elements will be discussed in more detail.

1.2.1. The basement membrane and basal lamina

The basement membrane that surrounds the myofibre is divided into two main layers. The outermost layer is known as the reticular lamina, which consists mostly of a dense mesh of fibrillar collagens. The innermost layer of the basement membrane is referred to as the basal lamina, which contains various proteins including laminins, non-fibrillar collagens, perlecan and nidogens; this part is in direct contact with the myofibre. The basal lamina contains various proteins arranged in a network (**Fig 1.3**). EM observations allowed the basal lamina to be further distinguished into two layers: the lamina densa, the outer electron-dense layer, which is assumed to constitute the main structural mesh; and the lamina lucida, the electron-lucent inner leaf, which is assumed to include the protein elements that interact with the cell membrane. The overall structure of the basement membrane as a whole can therefore be considered as three layers. From outermost to innermost, these are the reticular lamina, the lamina densa and the lamina lucida, the latter two comprising the basal lamina (Merker, 1994). The components of the basal lamina tend to be heavily glycosylated, that is, they are modified with chains of carbohydrates that mediate interactions with other molecules. The two most abundant constituents of the basal lamina are the non-fibrillar collagen IV and laminin (Sanes, 2003). The different structural elements of the basal lamina will be discussed below, with particular emphasis on that of muscle.

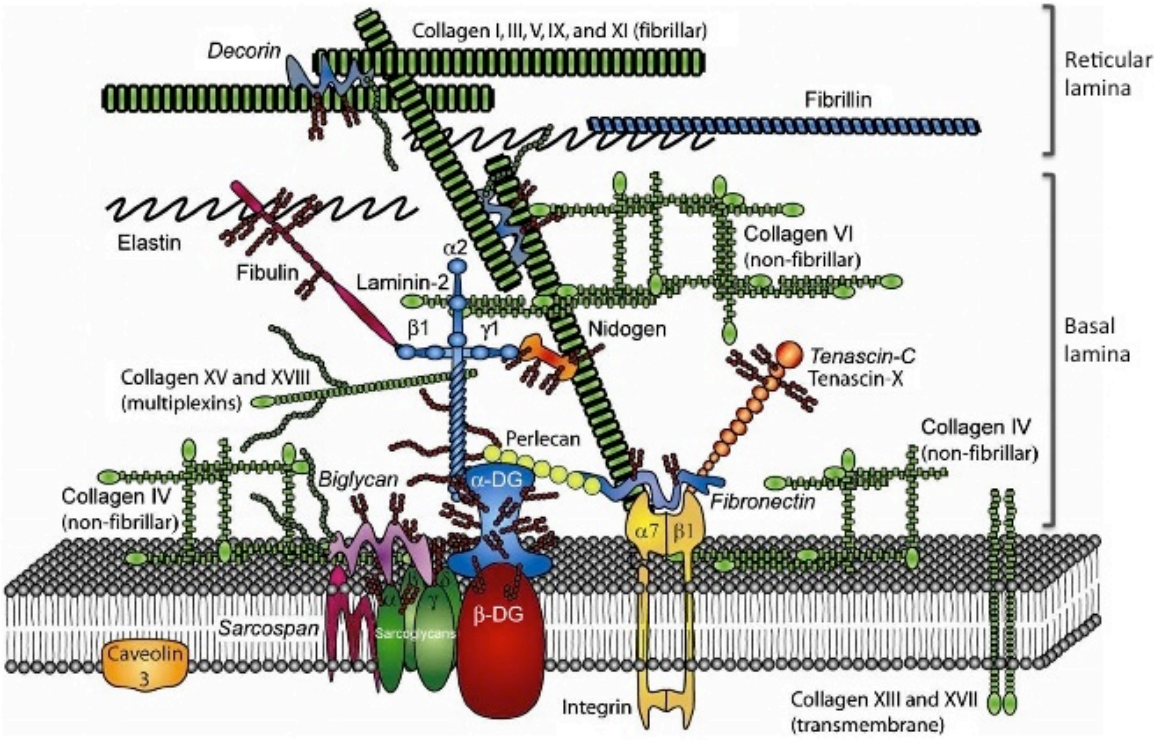

Fig 1.3. Arrangement of the basement membrane in muscle. The outer reticular lamina primarily consists of a network of fibrillar collagens, providing structural support and integrity. The inner basal lamina portion consists of many other proteins, including non-fibrillar collagens and laminin. Collagen IV is the most abundant non-fibrillar collagen, and forms a structural network. Laminin-211 is the major isoform in muscle, and binds to key adhesion receptors on the sarcolemma, thus conferring structural stability on the myofibre. Laminins also arrange into networks, further providing strength to the basal lamina. Collagen VI is another non-fibrillar collagen, and links the basal lamina components to the overlying reticular lamina. Nidogen and perlecan crosslink the collagen and laminin networks. The two key adhesion receptors of muscle are integrin-α7β1 and the α- and β-dystroglycan complex (marked α-DG and β-DG respectively). Adapted from Voermans, NC et al., 2008. Originally published in *Neuromuscular Disorders*, doi: 10.1016/j.nmd.2008.05.017. Rights obtained through Copyright Clearance Centre.

Key basal lamina constituents: collagens and laminins

Collagens make up a large superfamily of proteins, and are a major component of connective tissue, extracellular matrix, tendons and ligaments. They consist of three α chains arranged in a triple helix (Bhattacharjee and Bansal, 2005). In the basement membrane of muscle, the fibrillar collagens are the main structural component of the outer reticular lamina, and can arrange end-to-end to form long fibrils; these include collagens I, II, V, IX and XI (Exposito et al., 2010). In the inner basal lamina, the major collagen isotypes are non-fibrillar, and are arranged into networks rather than long fibrils; these include collagens IV and VI. The most abundant isoform of collagen IV in the basal lamina is collagen IV $(\alpha1)_2(\alpha2)$. Collagen VI, on the other hand, exists at the muscle basal lamina as collagen VI (α1)(α2)(α3) (Lampe and Bushby, 2005).

Along with the non-fibrillar collagens, laminins are another major component of the basal lamina. These are heterotrimeric structures consisting of an α, β and a γ subunit (**Fig 1.4**). There are 5 α, 4 β and 3 γ subunits that are known, forming a total of 15 trimers (Colognato and Yurchenco, 2000). The laminin molecule is arranged into a cross shape, with the α chain forming the long axis, and the β and γ chains forming the short arms. The three chains entwine to form a triple helical region at the bottom leg of the cross; this terminates in a set of ligand binding domains, which allow binding to cell surface receptors including integrins and α-dystroglycan (α-DG) (Aumailley et al., 2005). The laminin-α3 and α4 chains are peculiar in the sense that they are truncated, so that laminins containing these subunits resemble a 'T' more than a cross (possessing the bottom triple helical leg, but no α head region) (Engel et al., 1981; Patton, 2000). At the muscle, the main isoform is laminin-211 (named according to its α2β1γ1 composition) (Holmberg and Durbeej, 2013).

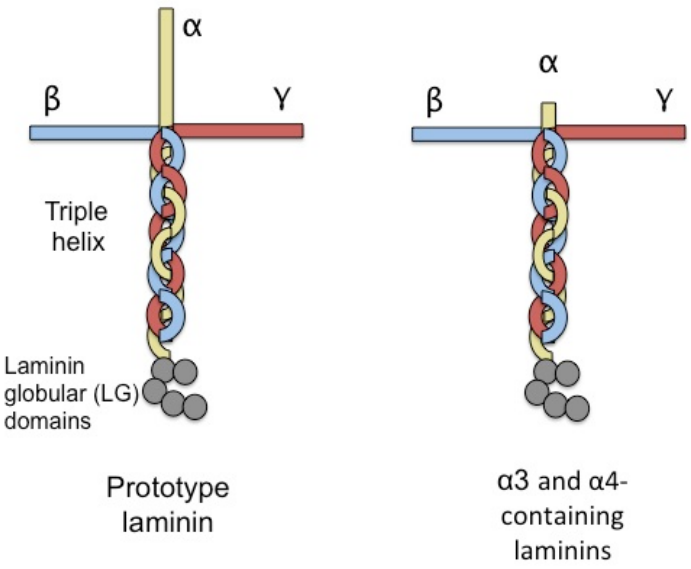

Fig 1.4. Laminin structure. Laminins are composed of three chains (α, β, and γ) which form a cross shape, with an intertwined triple helix region at the base. 5 laminin globular (LG) domains are present at the foot, and these mediate the binding to cell-surface adhesion receptors. Laminins can self-assemble into networks, through ternary interactions between the two arms and the head. The α3 and α4 chains are truncated, and laminins containing these subunits have a much smaller head region, which lack the ability to crosslink with other laminins. Thus these laminins are not able to form networks.

Interactions at the basal lamina

The collagen and laminin molecules are able to polymerise with themselves, to self-assemble as distinct networks in the basal lamina. Although separate, these networks are interlinked by several proteins. Nidogens crosslink the laminin and collagen IV networks, alongside perlecan and agrin. In addition, the latter two contribute to inter-laminin crosslinking (Gillies and Lieber, 2011; Hohenester and Yurchenco, 2013). Fibronectin is also present at the basal lamina, and is able to interact with other constituents such as perlecan and collagens (Pankov and Yamada, 2002). Collagen VI appears to have a role in the linkage of basal lamina components to the overlying reticular lamina (Kuo et al., 1997). Laminin polymerises with itself via ternary interactions between the α head and the β and γ arms; therefore, laminins containing the truncated α3 and α4 chains are unable to polymerise, perhaps reflecting their

different contributions to basal lamina function and organisation (Patton, 2000). Collagen and laminins contribute to the high tensile strength of basal lamina, highlighting its importance in structural support; however, stretch and elasticity are also required during muscle contraction, and elastin is a key component that confers this property (Muiznieks and Keeley, 2013).

Several proteins of the basal lamina are known to form direct interactions with cell surface receptors at the sarcolemma. These include laminin-211 and perlecan, which interact directly with the dystrophin-associated glycoprotein complex (DGC) and integrins. In addition, fibronectin is thought to interact with integrins, and biglycan is able to mediate a connection between non-fibrillar collagens and the DGC (**Fig 1.3**) (Voermans et al., 2008). The particular importance of laminin-211 in skeletal muscle is evidenced by the fact that genetic defects in laminin-α2 cause severe congenital muscular dystrophy in mice and humans (Holmberg and Durbeej, 2013; Vainzof et al., 2008). Laminin-211 is a key ligand for costameric proteins, and in its absence, the axis between basal lamina and the cytoskeleton is perturbed. This results in structural weakness, and leads to contraction-induced damage of muscle fibres, which subsequently undergo degeneration. The tissue is able to regenerate, via the action of myoblasts that can fuse with each other and with damaged fibres for repair (discussed in more detail in *Section 1.3., Development of skeletal muscle*). However, after multiple rounds of degeneration, the capacity for regeneration becomes gradually impaired, and the muscle becomes infiltrated with fibrotic tissue. Pathological hallmarks include excessive deposition of ECM proteins, variability in fibre size, necrosis, inflammation and central nucleation (a characteristic of recently regenerated fibres, as myonuclei are located at the perimeter of the fibre once fully mature) (Iannaccone and Castro, 2013; Wicklund, 2013). Congenital muscular dystrophy is also caused in patients with mutations in collagen VI, and in mouse models with a genetic ablation of this gene (Bonaldo, 1998; Lampe and Bushby, 2005). Other, more ubiquitous basal lamina components such as collagen IV and fibronectin tend to be essential for early development; thus null mutations in mice cause death in embryogenesis (Liu et al., 2010; Pöschl et al., 2004). However, milder mutations in these genes can cause disease in

patients, with defects in multiple systems, but no reported muscle involvement (Castelletti et al., 2008; Savige, 2014).

The basal lamina is linked to the muscle fibre by several adhesion receptors. The primary cellular adhesion system of the sarcolemmal surface is the costamere, which contains two prominent complexes: the DGC, and integrin-α7β1 and its downstream proteins (Ervasti, 2003). The best characterised of these is the DGC, of which the main extracellular ligand is laminin. The MTJs are also rich in adhesion receptors, for the effective mechanical linkage to the tendon. In particular, integrin-α7β1 is important for structural stability at the MTJ, although the DGC is also present here (Charvet et al., 2012). An overview will be given of the DGC and the integrins, below.

1.2.2. The dystrophin-associated glycoprotein complex (DGC)

The DGC is an adhesion complex that primarily binds laminins, and is found in a wide variety of tissues, including skeletal muscle, heart, nerve, brain and eye (Ackroyd et al., 2011; Hoffman et al., 1987; Waite et al., 2012). The DGC component α-dystroglycan, a heavily glycosylated protein, is present on the external leaf of the sarcolemma where it binds to laminin via its glycan chains (Martin, 2003). β-dystroglycan is present in the membrane, binding to α-dystroglycan on the outside of the cell, and dystrophin on the inside (Moore and Winder, 2012). Dystrophin is a very large structural protein (encoded by the largest gene in the genome), which binds to actin filaments of the cytoskeleton, thus forming the last link in the DGC-cytoskeleton axis (Ervasti and Campbell, 1993). Other molecules are associated with the DGC, including the five sarcoglycan proteins (α, β, γ, δ and ε) and sarcospan, which span the membrane together with β-dystroglycan, and stabilise the complex. On the internal leaf of the membrane, α- and β-syntrophins, α-dystrobrevin, and neuronal nitric oxide synthase (nNOS) are found (**Fig 1.5**) (Blake et al., 2002). Apart from laminin-211, agrin and perlecan are also known to interact with the DGC in muscle (Ervasti and Campbell, 1993; Kanagawa et al., 2005). Utrophin is a more widely expressed homolog of dystrophin, and can replace dystrophin to

make the utrophin-associated glycoprotein complex (UGC)(Blake et al., 2002). In muscle, DGC is the most common form, being found in the costameres and the MTJ, while the UGC is found specifically at the MTJ, and the fraction of sarcolemma at the NMJ (Charvet et al., 2012; Deconinck et al., 1997; Grady et al., 1997). In the brain, the DGC and UGC are expressed in various neurons, usually to the exclusion of the other, depending on the brain region or neuronal type (Haenggi and Fritschy, 2006).

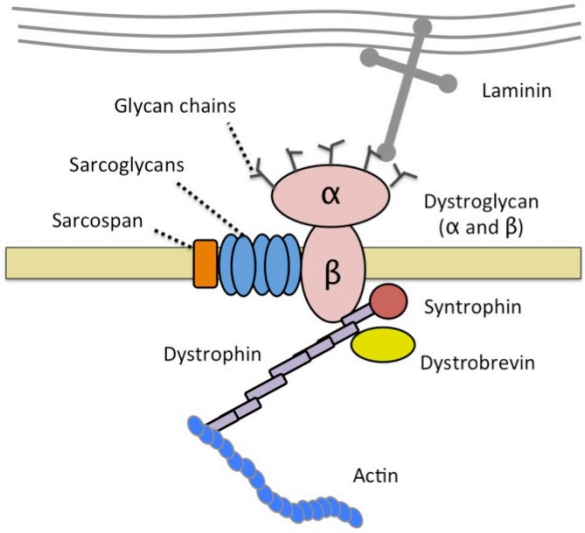

Fig 1.5. The dystrophin-associated glycoprotein complex (DGC). Dystroglycan is a dimer of an α and a β subunit. The α subunit on the external leaf of the sarcolemma is heavily glycosylated, providing a binding site for laminin. The β subunit is a transmembrane protein and is associated with several other molecules: sarcoglycans in the membrane, and dystrophin in the cytoplasm. Sarcospan is a transmembrane protein associated with the sarcoglycans; syntrophin and dystrobrevin are associated with dystrophin on the internal leaf of the sarcolemma. The transmembrane complex provides stability, while the cytoplasmic complex provides a link to actin. Thus the DGC as a whole allows a continuous structural link between the basal lamina and the cytoskeleton.

In addition to their role in maintaining structural stability, the DGC and UGC are also able to mediate a variety of cell signals. In particular, β-dystroglycan phosphorylation can induce cytoskeletal reorganisation, and the activation of the mitogen-activated protein kinase (MAPK) pathway, a key signalling cascade involved in survival, proliferation, migration and differentiation (Spence et al., 2004). In *in vitro* studies using fibroblasts, dystroglycan has been observed to localize to filopodia, structures that are involved in cell migration (Batchelor et al., 2007). In myoblasts, dystroglycan localization has been demonstrated at focal adhesions and podosomes, two structures involved in adhesion and migration (Thompson et al., 2008, 2010). Consistent with this, altered levels of dystroglycan are often associated with cancer, particularly in the facilitation of invasion and migration (Cross et al., 2008). nNOS also appears to have a signalling role, particularly in regulating blood flow to the muscle in response to exercise. Unlike dystrophin, utrophin lacks a binding site for nNOS, so this protein is not present at the UGC (Li et al., 2010). β-dystroglycan can also regulate the clustering of acetylcholine receptors (AChRs), the neurotransmitter receptors in the postsynaptic membrane of the NMJ, through binding to rapsyn (Haenggi and Fritschy, 2006).

As mentioned previously, functional loss of laminin-α2 results in a disruption of the basal lamina-muscle fibre link, leading to dystrophic changes. In a similar way, this axis depends on the DGC, and loss of components of this complex also results in muscle fibre instability. Duchenne muscular dystrophy (DMD) is the most common form of muscular dystrophy, and the most common fatal genetic disorder. It is caused by mutations in dystrophin, and affects 1 in 5000 males, but fewer females (due to an X-linkage of the gene). Less frequently, patients present with a milder form called Becker muscular dystrophy (BMD), generally caused by in-frame deletions or insertions of the dystrophin gene. Defects in dystroglycan are also associated with disease. Both the α and β forms of dystroglycan are encoded by one gene (*DAG1*). In mice, null mutations of *DAG1* are embryonic lethal, although some cases of muscular dystrophy with mutations in this gene have been reported in humans (Geis et al., 2013). More commonly, genetic defects in α-dystroglycan-processing enzymes are causative of congenital muscular dystrophies (Godfrey et al., 2011; Muntoni et al., 2011; Stevens et al., 2013;

Whitmore and Morgan, 2014). These enzymes tend to be involved in the glycosylation of α-dystroglycan, and their deficiency often results in decreased laminin affinity, and thus structural instability. In addition, defects in other components of the DGC can cause muscular dystrophy, including the sarcoglycans (Sandonà and Betto, 2009). Genetic models of utrophin deficiency result in relatively mild structural alterations at the NMJ, associated with impaired neuromuscular transmission, highlighting the role of the UGC at the synaptic portion of the muscle fibre (Deconinck et al., 1997; Grady et al., 1997).

1.2.3. The integrins

The second major adhesion system of skeletal muscle is represented by the integrins. These transmembrane receptors exist as dimers of an α and β subunit, and can bind a diverse array of basal lamina components (Hynes, 2002a). Since their discovery in the mid-1980s, there are now 18 known α and 8 known β subunits in mammals, which can combine to make 24 possible heterodimers (Huhtala et al., 2005; Hynes, 2004). Integrins are widely expressed, and responsible for mediating a variety of cellular events, including adhesion, migration, regulation of cytoskeletal dynamics and cell shape, survival and differentiation (DeSimone et al., 1987; Harburger and Calderwood, 2009; Hynes, 2002b). Although integrins have no catalytic activity by themselves, they are able to interact with a myriad of intracellular adaptor and signalling proteins, which are able to mediate their effects. Approximately 150 proteins are known to interact with integrin complexes (Harburger and Calderwood, 2009). At their position in the membrane, integrins are able to mediate outside-in and inside-out signalling. The ECM is able to transduce chemical and mechanical signals into the cell, to regulate cytoskeletal organisation, cell shape and motility; and the activation and modulation of integrins by intracellular effectors is a key factor driving ECM organisation, and in signalling the internal status of the cell to the outside (Hynes, 2002b).

Integrin structure

Integrins consist of an extracellular region with multiple globular domains, a single transmembrane helix, and a short cytoplasmic tail (**Fig 1.6A**). In the α subunit, the end of the extracellular chain is marked by a β-propeller domain, a structure consisting primarily of β-sheets, arranged in seven spokes (Campbell and Humphries, 2011). This domain is capable of binding divalent cations (Ca^{2+} and Mg^{2+}), which modulate ECM ligand binding. The β-propeller is followed by a thigh and two calf domains, which have immunoglobulin-like structures marked by sandwiches of β sheets. A short region between the thigh and the calf domain called the genu (or knee) confers flexibility on the molecule, together with the thigh itself. The calf domains at the lower end of the extracellular chain link to the transmembrane helix, which in turn links to the internal tail (Xiong et al., 2001).

The smaller β integrin subunit has an I domain at the terminal of the extracellular region (Yang et al., 2004). This has three binding sites for divalent cations. One cation is involved in direct binding to ECM ligands, while the other two can positively or negatively regulate affinity (Chen et al., 2003). Below the I domain are the hybrid domain, and the plexin-semaphorin-integrin (PSI) domain, which are analogous to the genu in the α integrin subunit, allowing flexibility (Mould et al., 2005). These are followed by cysteine-rich repeats, which are important in the folding/unfolding that occurs during activation and inactivation (Beglova et al., 2002). The final extracellular domain of the β integrin subunit is the tail region (not to be confused with the intracellular tail region), which links to the transmembrane helix.

Integrin signalling and interactions

Like the DGC, integrins are anchored to the internal actin cytoskeleton, but via a different set of effectors. Integrins exist in an inactive state, until the binding of talin at the intracellular domain of the integrin β subunit (**Fig 1.6B**). This results in the breakage of a salt bridge between the α and β integrins, and the adoption of an active extracellular domain, with high affinity for ECM proteins (Wegener et al., 2007). Structural studies appear to show that the

extracellular domains of integrins are folded inwards towards the membrane when inactive, but switch to an upright position upon talin binding (Anthis et al., 2009). Kindlin family members have also been shown to be able to activate integrins (Calderwood et al., 2013). Once active, integrins are able to engage with ECM components, and the formation of multiprotein complexes is initiated at the intracellular tail. Talin and vinculin and α-actinin are key proteins that mediate interactions with actin (Burridge and Connell, 1983; Critchley and Gingras, 2008). Many other proteins are able to associate with the complex, including adaptors such as paxillin and integrin-linked kinase (ILK), and signalling proteins including focal adhesion kinase (FAK), Src and Crk (Deakin and Turner, 2009; Turner et al., 1990; Wozniak et al., 2004). Despite its name, ILK appears to lack the catalytic activity of a kinase, instead being a key scaffolding protein for the recruitment of other components (Qin and Wu, 2012). Src activity plays a particular role in mitogenic signalling, including cell survival and proliferation (Playford and Schaller, 2004). In contrast, FAK and Crk tend to mediate signals for motility and cell spreading, acting through pathways involving Rho, Rac and Cdc42, which regulate actin organisation (Allen et al., 1997). However, there is much cross talk between these pathways, allowing for extensive overlap in function in these effectors (Harburger and Calderwood, 2009).

Engagement by internal and external proteins can result in clustering of integrins into larger adhesion complexes. This results in an increase in integrin avidity, that is, the strength of binding associated with local density of receptors (in contrast to the affinity of individual receptors) (Carman and Springer, 2003). Many of these adhesion sites turn over rapidly, so called focal complexes that tend to be associated with cell migration. As such, they are frequently found at the lamellipodia, cell protrusions at leading edges of migrating cells, where they assemble and disassemble to allow new ECM contacts to be made by the cell as it moves (Anderson et al., 2008). Some adhesion sites mature into larger, stronger, more stable contacts called focal adhesions. This allows the bundling and accumulation of many more intracellular molecules and actin filaments. These tend to be associated with cell anchorage rather than

migration, and are marked by the accumulation of particular intracellular components, including vinculin and zyxin (Carisey et al., 2013).

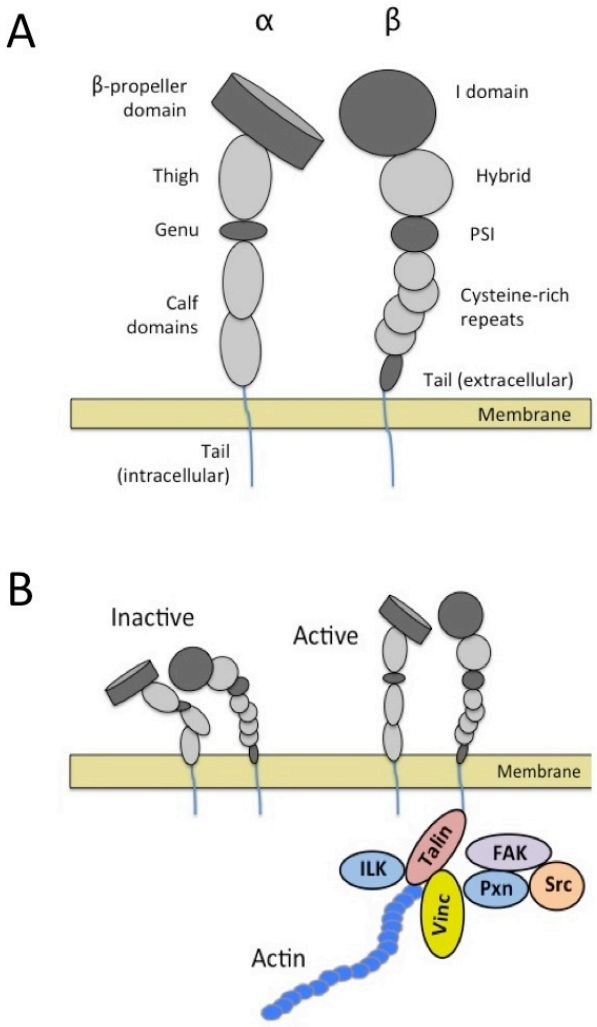

Fig 1.6. The integrins: structure and activation. (A) The integrins exist as a dimer of an α and a β subunit. The domain structure of each subunit is shown here. PSI domain: plexin-semaphorin-integrin domain. (B) The inactive conformation of the integrin dimer is bent towards the membrane. On the binding of talin to the intracellular tail of the integrin β subunit, the complex adopts an upright conformation, with increased affinity for extracellular matrix (ECM) proteins. Many other proteins are able to form complexes at the internal side, including those shown here: adaptor proteins such as vinculin (Vinc), integrin-linked kinase (ILK) and paxillin (Pxn); also signalling proteins including focal adhesion kinase (FAK) and Src. Talin and vinculin are key actin-binding proteins, providing a link to the cytoskeleton.

Larger still are the fibrillar adhesions, which are characterised by adhesion complexes and actin filaments (stress fibres) arranged in a line at the cell surface. Molecular features including the presence of intracellular tensin at the adhesion sites, and the binding to fibronectin in the ECM(Short, 2012). Disassembly of integrin-associated complexes can be achieved through the action of intracellular calpains, which can cleave components such as talins (Harburger and Calderwood, 2009).

Integrins in muscle

A subset of integrins are expressed in mature muscle, with a wide range of others expressed during developmental stages (discussed in *Section 1.3., development of skeletal muscle*, and summarised in **Fig 1.8C** and **Table 1.1**). Integrin-β1 is the predominant β isoform in muscle; thus its dimerisation with different α subunits tends to determine the specificities and functions of the receptor. Integrin-α7β1 is widely expressed in muscle, with a strong binding preference for laminin, and is found at the costameres, the MTJ and the NMJ. Studies in knockout mice have shed light on the functions of integrins in muscle. To date, integrin-β1 mutations have not been associated with human disease, probably due to early embryonic lethality, as observed in mouse knockouts (Fässler and Meyer, 1995; Stephens et al., 1995). However, studies in muscle conditional mutants for integrin-β1 demonstrate its essential roles in the fusion of myoblasts into muscle fibres, and sarcomere assembly (Schwander et al., 2003). In addition, ablation of talin proteins also leads to defects in myoblast fusion, suggesting that integrin-β1 mediates this process via effects on the cytoskeleton and intracellular signalling (Conti et al., 2009). Integrin-β1 in muscle also regulates the patterning of motoneuron innervation, whereas integrin-β1 in motoneurons appears to have no role in this (Schwander et al., 2004). This suggests that integrins in muscle provide cues for developing motoneurons. Innervation of muscle will be discussed in more detail in *Section 1.8., development of the NMJ*.

While integrin-β1 is not required for MTJ formation, various studies indicate that integrins are instrumental for their integrity once developed. Mouse knockouts for integrin-associated proteins including ILK, talin and filamin C display muscle defects primarily at the MTJ (Conti et al., 2008; Fujita et al., 2012; Wang et al., 2008). While integrin-α7β1 is present at both costameres and MTJs, again, its major role in structural stability is at the MTJ rather than the costamere, in contrast to the DGC (Mayer et al., 1997). Mice with ablation of the integrin-α7 gene show myopathic changes that indicate primarily a disruption of MTJ integrity, while hallmarks of a degenerative/dystrophic phenotype such as central nucleation were remarkably minor (Mayer et al., 1997). In agreement with this, patients with integrin-α7 mutations have symptoms of progressive muscle weakness and atrophy, resembling a muscular dystrophy, but with only mild myopathic changes on biopsy (Nakashima et al., 2009).

Despite this, several lines of evidence suggest that integrin-α7β1 is important in costamere function. Integrin-α7β1 is upregulated in dystrophin-deficient *mdx* mice and DMD patients, suggesting that it may be able to partially compensate for the function of the DGC at the costamere (Hodges et al., 1997). Furthermore, when both dystrophin and integrin-α7 are knocked out in mice, a severe pathology ensues which suggests dystrophy associated with costameric weakness; this suggests that integrin-α7β1 contributes to the structural stability at the costamere (Guo et al., 2006). Other studies support a role for integrin-α7β1 in protecting against exercise-induced damage, and in transducing these mechanical signals into downstream muscle injury and hypertrophic pathways (Boppart et al., 2006). In a complementary fashion to this, the DGC is also able to play a partial function in MTJ stabilisation, despite its primary role at the costamere. This is evidenced by the fact that *mdx* mice display morphological defects at the MTJ (Ridge et al., 1994). In addition, when utrophin is knocked out on an integrin-α7-null background, pathology at the MTJ is exacerbated, suggesting that utrophin may normally be able to compensate for integrin-α7 here (Welser et al., 2009).

Several splice variants exist in the α7 and β1 subunits, that contribute to the diversity of expression in muscle. Integrin-β1A is expressed during embryonic development, being replaced by β1D in mature myofibres (Van der Flier et al., 1997). Integrin-α7 can be alternatively spliced to give three intracellular domains (A, B and C), and two extracellular domains (X1 and X2). In adult muscle, α7A is present at the MTJ and NMJ; α7B is at the sarcolemma, MTJ and NMJ; and α7C is at the sarcolemma and NMJ (Martin et al., 1996a; Nawrotzki, 2003; Velling et al., 1996). In terms of the extracellular domains, both X1 and X2 splice variants are present at different stages, with the X2 splice variant being the sole form in adult muscle (Song et al., 1993; Ziober et al., 1993). In addition to integrin-α7β1, evidence suggests that integrin-α5 is present in mature skeletal muscle, presumably in a dimer with β1 (Taverna et al., 1998; Thorsteinsdóttir et al., 2011). Integrin-α5β1, is exclusively a fibronectin receptor, and its localization is not certain; however, mouse studies suggest a requirement for muscle fibre integrity, as mutants present with morphological characteristics of muscular dystrophy (Taverna et al., 1998).

1.2.4. The myofibrils

The adhesion receptors and proteins of the costamere play an important structural role, forming the axis that links the basal lamina to the myofibrils. As mentioned previously (*Section 1.2., structural arrangement of myofibres*), integrins and the DGC at the costamere are precisely in register with the Z-disks of the myofibrils, and remain so during contraction (Peter et al., 2011). Integrins are directly linked to actin and α-actinin at the Z-disk interface, via talins and vinculin; the DGC links to actin via dystrophin (Hoshijima, 2006; Peter et al., 2011). Indeed, the costameres have been shown to play an important role in myofibrillogenesis. During sarcomere formation, electron dense clusters known as Z-bodies appear at the costameres, and these will later become the Z-disks. Integrins are known to be essential mediators in this process, since ablation of integrins and their related proteins in *Drosophila* and mice results in defects in sarcomere assembly (Bloor and Brown, 1998; Sparrow and Schöck, 2009; Volk et al., 1990). In mice, these include integrin-β1 and talins (Conti et al., 2009; Schwander et al., 2003).

Myofibrils assemble first at the periphery of the muscle fibre, where they can contact costameric proteins (Tokuyasu and Maher, 1987). Interestingly, the early myofibril structures resemble stress fibres, the actin bundles that are a characteristic of fibrillar adhesions, perhaps indicative of the role of integrins in their initial organization (Hotulainen and Lappalainen, 2006). The Z-bodies that form at the costameres are rich in α-actinin and titin, and these act as a nucleation site for the recruitment of sarcomeric proteins, including the proteins of the thick and thin filaments (Sparrow and Schöck, 2009).

Major proteins of the Z-disk include α-actinin, titin, desmin, myotilin, ZASP and filamin C (**Fig 1.7**) (Hoshijima, 2006). The proteins are densely packed, giving an electron-dense appearance with EM. The actin filaments are crosslinked by α-actinin at the Z-disk, and from here they extend towards the midline or M-band of the sarcomere. Actin-capping proteins are found at the tips, including tropomodulin near the M-band; these regulate actin length and stability (Gokhin and Fowler, 2011). Titin, the largest known protein, also extends from the Z-disks, parallel with the thin actin filaments; it binds at its furthest end to the M-band, a total distance of around 1 μm (Linke and Hamdani, 2014). Titin has several roles, including regulating sarcomere length, and stabilising the structure and interdigitation of the thick and thin filaments. It also has a spring-like function, conferring flexibility and acting as a shock absorber during contraction.

At the M-line, there is a network of molecules called myomesins. These crosslink the thick myosin filaments and titin molecules, allowing proper alignment of sarcomeric structures (Agarkova and Perriard, 2005). In this respect, myomesin plays a function analogous to that of α-actinin at the Z-disk. The network of myomesin is also elastic in its properties, conferring structural stability on the sarcomere, and allowing even distribution of force (Agarkova et al., 2003). Like the Z-disks, the M-lines are also linked to the cell surface via integrins, presumably offering additional structural integrity and/or force transmission (Qadota and Benian, 2010). Proteins of the Z-disk and M-line are also thought to have roles in mechanosensation. Indeed,

various signalling proteins are associated with sarcomeric proteins, with evidence suggesting they are involved in autophagy, protein turnover, hypertrophy, and stretch-sensitive transcriptional pathways (Gautel, 2008; Hoshijima, 2006; Knöll et al., 2011).

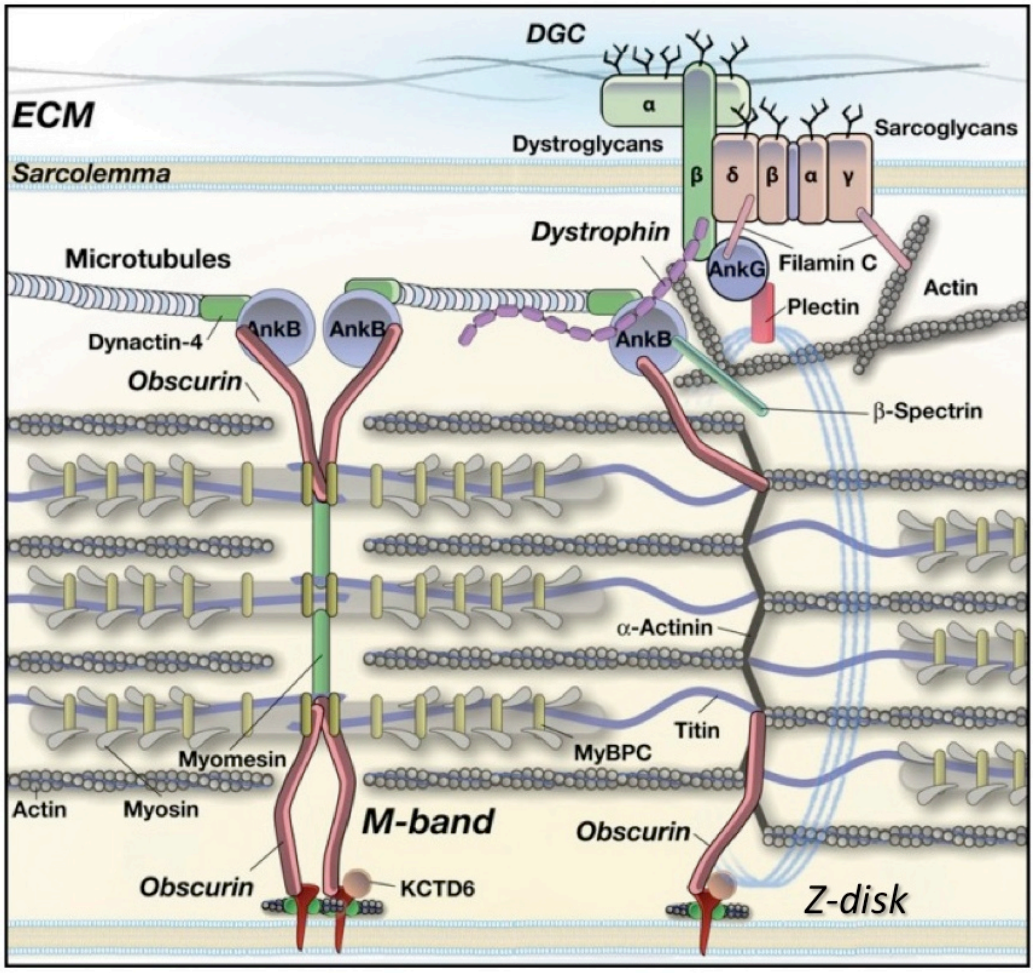

Fig 1.7. Molecular arrangement at the Z-disk and M-band of the sarcomere. The Z-disk is linked to the costamere, of which the dystroglycan/dystrophin complex is a major constituent, although integrin-α7β1 and its associated proteins are also found here. α-actinin is an abundant Z-disk protein which crosslinks actin filaments. Actin and titin extend from the Z-disk towards the M-band, intercalating with myosin filaments. Myomesin is the major protein at the M-band, forming a mesh-like network. Obscurin is at the periphery of the myofibril, associated with both the Z-disk and M-band, where it links to other myofibrils to regulate alignment. Adapted from Randazzo, D et al., 2013. Originally published in *J. Cell Biol.*, doi: 10.1083/jcb.201205118. Material licensed under a Creative Commons Attribution-Noncommercial-Share Alike 3.0 Unported License.

Alignment of sarcomeres with the costameres is important for the transmission of force and structural stability; equally important, however, is the alignment of sarcomeres between different myofibrils. When contraction occurs, all Z-disks remain in register, allowing the forces to be transmitted in an unbroken perpendicular line to the costameres. The T-tubules and sarcoplasmic reticulum are closely associated with the myofibrils, to allow the transmission of action potentials and Ca^{2+} signalling directly to the sarcomeres (Endo, 2009). Uneven forces resulting from disorganised myofibril contraction could potentially damage or rupture these structures (Raeker et al., 2006). Various proteins have been implicated in an inter-Z-disk link that maintains correct myofibril alignment. Genetic disruption of several proteins cause the misalignment of myofibrils, including obscurin, desmin and nebulin (Huang et al., 2002; Ottenheijm and Granzier, 2010; Raeker et al., 2006; Tonino et al., 2010). The first two are known to be found at the peripheries of the Z-disk, a localization which suggests the crosslinking of adjacent myofibrils at this position; obscurin is also found at the M-line, suggesting an additional site of alignment (Granger and Lazarides, 1979; Raeker et al., 2006). Nebulin associates with thin filaments in the sarcomere, and it is believed to maintain the localisation of desmin, suggesting a mechanistic link with the connection of Z-disks across myofibrils (Mainguy et al., 2010).

A group of muscle diseases are associated with mutations in sarcomeric proteins, often termed myofibrillar myopathies. Causative genes include desmin, filamin C, titin, ZASP and myotilin (Selcen, 2011). The heart is also commonly affected in these conditions, due to shared contraction mechanisms in cardiomyocytes. Ultrastructural and histological findings are often characterised by dissolution of Z-disks, aggregations of myofibril components, and abnormal variation in fibre size, including some fibre atrophy. Patients present with progressive muscle weakness, often beginning in the distal muscles of the limbs. Many cases of myofibrillar myopathy have no known genetic mutation, suggesting that defects in other sarcomeric proteins may be responsible for this disease (Selcen, 2011).

1.3. Development of skeletal muscle

Muscle fibre formation depends on multiple fusion events between myoblasts, the precursor cells of the myofibres. During early embryonic patterning, paraxial mesoderm is present along the length of the embryo, on either side of the neural tube. This is organised into discrete segments called somites, visible from around embryonic day 8 (E8) in the mouse, and these will later give rise to a variety of tissues (**Fig 1.8A, C**). The somites develop into two discrete regions: the sclerotome, which will give rise to the skeleton; and the dermomyotome, which will form a variety of tissues, including skeletal muscles, smooth muscles, dermal and endothelial cells (Mootoosamy and Dietrich, 2002). Tendons are formed by an additional layer of cells called the syndetome, which sit between the sclerotome and the dermomyotome (Thorsteinsdóttir et al., 2011). The axial muscles include those of the head and trunk, and of these, the latter are derived from non-migratory cells of the dermomyotome. In contrast, the diaphragm and limb muscles are derived from migratory precursor cells, which reach their target sites from their origins in the dermomyotome. The muscles of the head do not develop from somitic structures. Instead, a separate region of cranial mesoderm gives rise to the majority of these muscles (Mootoosamy and Dietrich, 2002; Sambasivan et al., 2011a).

1.3.1. Overview of myogenesis

In trunk and limb development, the earliest skeletal muscle structures are known as the myotome, which separate from the dermomyotome at around E10 (**Fig 1.8A, C**). Various transcription factors are expressed in the early myotome, and of particular relevance for muscle development are members of the paired box (Pax) family, and the myogenic regulatory factors (MRFs). Pax3 and the MRFs Myf5 and Mrf4 are expressed in the initial formation of the myotome (Kassar-Duchossoy et al., 2004; Sambasivan et al., 2011a; Tajbakhsh et al., 1997). Subsequently, Pax3 and Pax7 expressing cells proliferate in the myotome, and subsequently enter the myogenic programme through the upregulation of MRFs (Buckingham, 2007; Relaix et al., 2005; Seale, 2000). These initially include Myf5 and MyoD for their determination into myoblasts, and later myogenin, for the fusion of myoblasts into myotubes (the early fused

myofibre structures; **Fig 1.8B**). The first round of fusion, occurring between E13 and E16, results in the primary myotubes. Following a second round of fusion between E16 and E18, these act as a scaffold for the formation of secondary myotubes (Bentzinger et al., 2012). Myoblasts continue to differentiate during the late embryonic and postnatal periods, to enable the growth and maturation of myotubes. Many unfused myoblasts will express Pax7 once more, to become the satellite cells, the resident muscle stem cells that are responsible for repair in postnatal life (Collins et al., 2005; Lepper et al., 2011; Montarras et al., 2005; Morgan and Partridge, 2003; Sambasivan et al., 2011b). These cells remain underneath the basal lamina that surrounds each muscle fibre, in a steady state of low turnover and effective dormancy known as quiescence. In response to muscle damage, however, these satellite cells can become activated, expressing MRFs including MyoD, and leaving their niche under the basal lamina. These activated satellite cells give rise to myoblasts which can regenerate the damaged muscle, either by fusing with each other, or with muscle fibres (Cheung and Rando, 2013).

Interestingly, the process of myogenesis in the head is not dependent on the expression of Pax3, perhaps reflecting the distinct evolutionary origins of these muscles (Buckingham, 2007; Relaix et al., 2006). While most of the muscles of the head are derived from the cranial mesoderm, several of the neck muscles and those of the tongue are derived from migratory cells originating in the somites, in a similar way to the limb muscles (Sambasivan et al., 2011a). The neck and tongue musculature is therefore considered to be in some ways a feature of evolutionary transition, since some of the muscles are derived from somitic mesoderm, and some from cranial mesoderm (Gans and Northcutt, 1983).

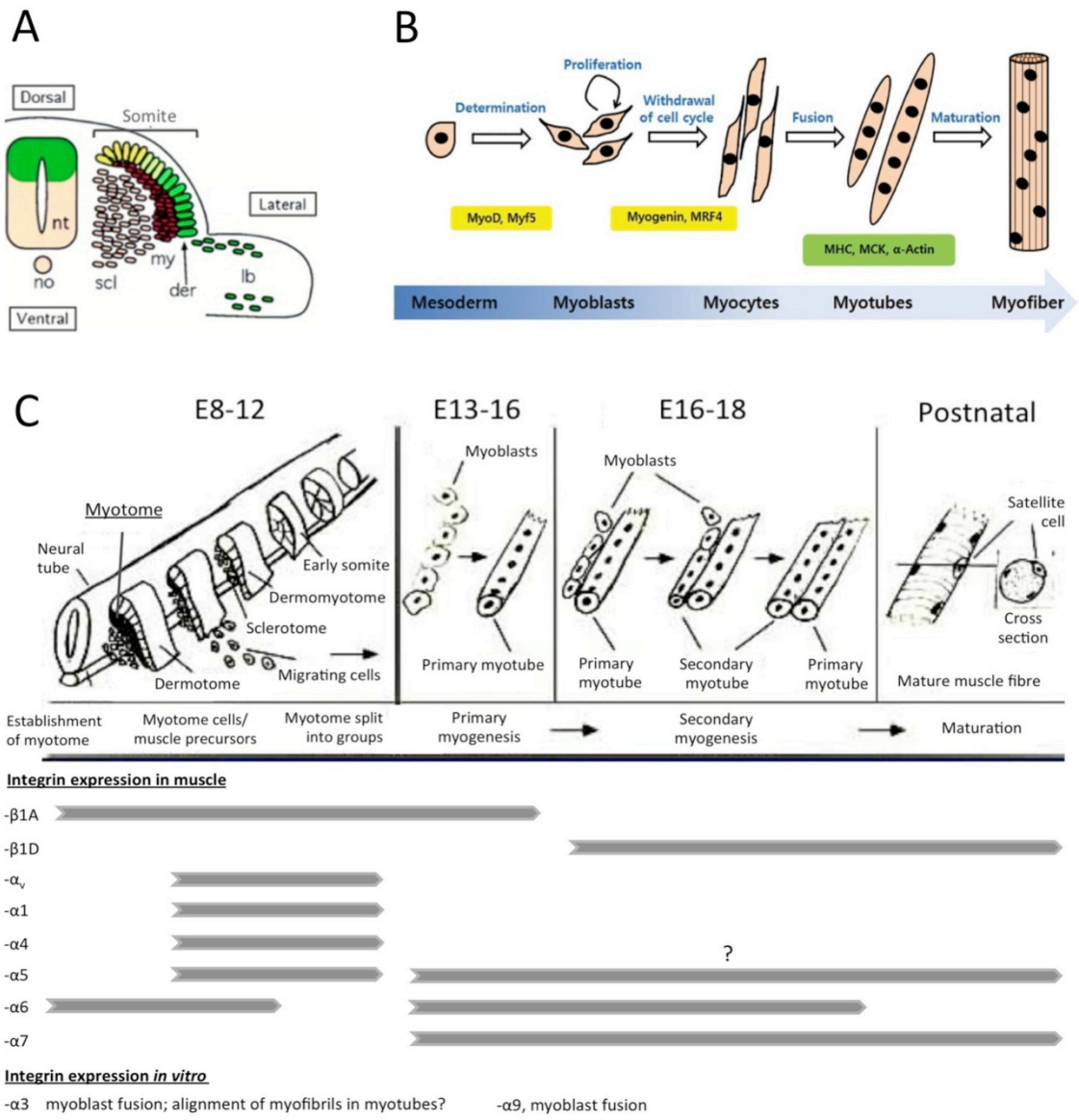

Fig 1.8. Somite formation and myogenesis. (A) Cross section of a developing embryo, showing the structure of the somite, and its positioning at either side of the notochord. der, dermomyotome; lb, limb bud; my, myotome; no, notochord; nt, neural tube; scl, sclerotome. Also shown are myogenic precursor cells migrating into the limb buds to establish early muscle structures. (B) Myoblast fusion in the myotome to create myofibres, and expression patterns of transcription factors (yellow) and key muscle markers (green; MHC, myosin heavy chain; MCK, muscle creatine kinase). (C) Approximate expression patterns of integrin subunits during muscle development. During E8-12, somites differentiate to give rise to the dermotome, myotome and sclerotome layers. The myotome also splits into groups (translocation) to give rise to individual, early muscle structures. During ~E13 – E18, primary and secondary myogenesis proceed. Following this, the myotubes mature into myofibres during late embryogenesis and postnatal life.

(Fig 1.8; continued from previous page) (A) Adapted from Rawls, A and Olsen, EN, 1997. Originally published in Cell, doi: 10.1016/S0092-8674(00)80175-0. Rights obtained through Copyright Clearance Centre. (B) Image from Jang, YN and Baik EJ, 2013. Originally published in *JAK-STAT, doi:* 10.4161/jkst.23282. Material licensed under a Creative Commons Attribution-Non-Commercial 3.0 Unported License. (C) Adapted from Gullberg, D et al., 1998. Originally published in *Front. Biosci*., vol 3 d1039-1050. Material under free use license for academic purposes.

The extraocular muscles (EOMs) that control eye movement also have their own peculiarities. Unlike other mature muscles, which only express the adult myosin heavy chain (MyHC), they also coexpress the embryonic and neonatal forms, as well as an EOM-specific isoform. The patterns of expression of these can vary along the length of the fibre. Secondly, some EOMs are multiply innervated, receiving more than one motoneuron input, unlike the monoinnervated skeletal muscles (Lucas and Hoh, 1997; Wasicky et al., 2000). These striking adaptations probably reflect the diverse and unique features of eye movement.

1.3.2. Integrin expression during myogenesis

In contrast to postnatal muscle, which expresses relatively few types of adhesion receptor, developing muscle displays a wide array of cell surface proteins at different stages, as exemplified by the integrins. The expression patterns of integrins during myogenesis have mostly been studied in the mouse (**Fig 1.8C**). In addition, various basal lamina components appear to be important at different stages of muscle development, corresponding to the appearance of different receptors with their particular specificities. Integrin-β1A is the major β isoform present from the somite to myoblast stage (from around E8 to E15), being replaced by β1D as muscle fibres form (Van der Flier et al., 1997). In addition, integrins α1, α4, α5, α6, α7, α9 and α_v appear to be expressed from somite stages onwards, although at different times

during the process of muscle development (summarised in **Table 1.1**) (Thorsteinsdóttir et al., 2011). Once the somites are established, they become encompassed by basal lamina proteins including fibronectin and laminin-α1 (presumably as a laminin-111 trimer) (Rifes and Thorsteinsdóttir, 2012). Within the somites, a basal lamina forms around the dermomyotomal cells, containing laminin-111 and 511. The interaction of laminin and integrin-α6β1 on the dermomyotomal cells appears to prevent premature differentiation (Bajanca et al., 2006). Integrin-α6β1 is also required for the separation of the myotome from the dermomyotome at around E10, thus marking the first cells determined specifically for skeletal muscle fate.

In the newly formed myotome, muscle precursor cells start to elongate, and at their ends they contact the fibronectin layer that exists round the edges of the myotome. This region at the interface of the myotome boundary and the tips of the cells will later correspond to the MTJ, following cell fusion. The muscle precursor cells express integrins-α4β1 and α5β1, two fibronectin receptors; which presumably allows them to adhere to these boundaries (Bajanca et al., 2004). Knockdown studies in zebrafish corroborate the importance of fibronectin for this elongation and alignment (Snow et al., 2008). Subsequently, laminin-211 is deposited in the basal lamina surrounding these myoblasts at around E11.5, marking the arrival of the first elements of the mature muscle ECM (Cachaço et al., 2005). The elongated cells now start to separate into groups to form the early, individual muscle structures (Deries et al., 2010). Integrins-α4β1 and α5β1 continue to be expressed during this process, and in addition, the collagen receptor integrin-α1β1 and an α_v-containing integrin are upregulated (Hirsch et al., 1994). Interestingly, during this process, laminin receptors such as integrin-α6β1 are downregulated, coinciding with a reduction in the quantity of the laminin matrix. This suggests that the separation of muscle structures depends more on the basal lamina interactions with the fibronectin and collagen receptors (integrins α1β1, α4β1 and α5β1), than with those for laminin (Cachaço et al., 2005; Thorsteinsdóttir et al., 2011). At E13, just prior to myoblast fusion, the laminin receptors integrin-α6β1 and α7β1 are upregulated, and the laminin matrix becomes re-organised (Cachaço et al., 2005).

Itg	Ligands	Tissue distribution	Expression and function in muscle
$\alpha_v\beta1$	Lam, FN, Opn, Vn	Smooth muscle, fibroblasts, osteoclasts	Unspecified α_v-containing integrin ~E11-12; splitting of myotomal cells/muscle precursors into distinct muscle groups?
$\alpha_v\beta3$	Fg, Vn, Tn, Opn, FN	Endothelial cells, smooth muscle, osteoclasts, fibroblasts, epithelia	
$\alpha_v\beta5$	Opn, Fg, Vn, FN	Endothelial cells, smooth muscle, osteoclasts, platelets, epithelia	
$\alpha_v\beta6$	FN, Fg, Vn, Tn	Epithelia	
$\alpha_v\beta8$	Vn	Melanoma, kidney brain, ovary, uterus, placenta	
α1β1	Coll VI, Coll I, Lam	Chondrocytes, endothelial cells	~E11-12; splitting of myotomal cells/muscle precursors into distinct muscle groups? Presynaptic terminus of NMJ
α2β1	Coll I, Coll IV, Lam, Tn	Keratinocytes, chondrocytes, platelets	
α3β1	Lam	Keratinocytes, kidney, lung, brain, NMJ	~E11, brief expression at boundary of sclerotome/myotome Localised at the active zones of NMJs, where it binds to lam-421. Fusion of myoblasts (*in vitro*). Assembly and/or alignment of myofibrils (*in vitro*).
α4β1	FN	Leukocytes, endothelial cells	~E10-11; muscle precursor cells, adherence to FN in myotomal boundaries? Itg-α5β1 expressed at developing MTJs, before replacement by α7β1. Disruption of Itg-α5 causes muscular dystrophy in mice, but role unclear.
α5β1	FN, fibrillin-1	Chondrocytes, endothelial cells	
α6β1	Lam	Chondrocytes, endothelial cells	~E10; formation of myotome from dermomyotome. Re-expressed at ~E13 in myoblasts.
α7β1	Lam	Skeletal muscle, MTJ, NMJ	~E13 onwards, into adulthood. Integrity at MTJ, and to some extent at costamere. Signalling in response to exercise or damage –> hypertrophic response. Role in agrin-induced clustering of AChRs at NMJ (*in vitro*).
α9β1	TN	Keratinocytes,	Fusion of myoblasts (*in vitro*).

Table 1.1. Major integrins and their tissue distribution and functions in muscle. Lam, laminin; FN, fibronectin; Coll, collagen; Fg, fibrinogen; Opn, osteopontin; Tn, tenascin; Vn, vitronectin.

From around E13, the muscle precursor cells start to fuse together to form the first set of myofibres (the beginning of myogenesis). Integrins have an important role in myoblast fusion, as evidenced by the fact that knockout of integrin-β1 and talins severely impairs this process (Conti et al., 2009; Schwander et al., 2003). Knock-in studies with different integrin-β1 splice variants suggest that integrin-β1A is the essential isoform in primary myoblast fusion, with β1D being more important in secondary fusion (Cachaço et al., 2003). Several integrin α subunits have been suggested as binding partners for β1 in the process of myoblast fusion, including α3 and α9 (Abmayr and Pavlath, 2012). Disruption of these integrins *in vitro* markedly diminishes fusion, and in addition integrin-α3 is expressed by myoblasts in regenerating mouse muscle (Brzóska et al., 2006; Lafuste et al., 2005; Przewoźniak et al., 2013). Despite the importance of integrin-α7β1 in later muscle development, knockout mice develop normal muscles (Mayer et al., 1997). In addition, disruption of integrin-α4 or α5 does not affect muscle development, despite their expression in the developing myotome (Taverna et al., 1998; Yang et al., 1996). This might reflect a partial redundancy between these two fibronectin receptors. Aside from the formation of muscle fibres, an additional part of myogenesis is the targeting of motoneurons to the muscle, to create the NMJs. The following sections will discuss in detail the structure, function and development of this synapse.

1.4. The neuromuscular junction (NMJ)

The NMJ is the synapse at the interface of the motoneuron and the muscle fibre. In the vast majority of muscles, with the exception of some of the extraocular muscles, the muscle fibres are each innervated by a single motoneuron axon, forming a single contact site. Vesicles containing the neurotransmitter acetylcholine are present in the presynaptic bouton of the motoneuron. In response to an action potential, P/Q-type VGCCs on the nerve terminal open, resulting in an influx of Ca^{2+}, and the synaptic vesicles fuse with the membrane, releasing the acetylcholine into the synaptic cleft. Acetylcholine receptors (AChRs) on the postsynaptic muscle side are engaged by their ligand, and become activated, allowing Na^{+} and K^{+} ions to flow in through their pore. This triggers a membrane depolarisation in the muscle fibres, and a

subsequent action potential. In response, the muscle contracts, as described in more detail in *Section 1.1., skeletal muscle*. In the next section, the structural elements of the NMJ and their roles will be described in detail.

1.5. Structure of the NMJ

The NMJ is perhaps the best-studied synapse of all, owing to its large size (~1000 times larger than many central synapses), and relative accessibility. Central synapses are often small and densely packed, so that individual analysis *in vivo* or *ex vivo* is challenging. Many of the electrophysiological characteristics of synapses were first determined in the NMJ of the frog (Augustine and Kasai, 2007). There are three major cell types at the NMJ – the motoneuron, the muscle, and the Schwann cell, which caps the motoneuron terminal. Recently, a fourth cell type was discovered, the so-called 'kranocyte' (derived from the ancient Greek word for 'helmet'). This cell surrounds and caps the Schwann cell, and appears to have a role in NMJ regeneration (Court et al., 2008). The motoneuron terminal apposes the muscle cell with a synaptic cleft of ~50 nm, through which a basal lamina traverses, although its composition is distinct from that which covers the extrasynaptic regions of the muscle. The nerve terminal and the corresponding post-synaptic apparatus on the muscle are topologically organised into a pretzel shape, with complete and precise overlap of pre- and postsynaptic structures (**Fig 1.9A**) (Marques et al., 2000). On the nerve terminal, there are many presynaptic structures called active zones. These are the sites of neurotransmitter release, where synaptic vesicles fuse with the presynaptic membrane. Synaptic vesicles are clustered (or 'docked') at these sites, therefore existing in a primed state for rapid fusion with the membrane. In classical synapses, the active zone is a single, plaque like structure; however, in the NMJ, the active zones are arranged as discrete (~50-100 nm) puncta, each with their own cluster of vesicles (Nishimune, 2012) (**Fig 1.9B**).

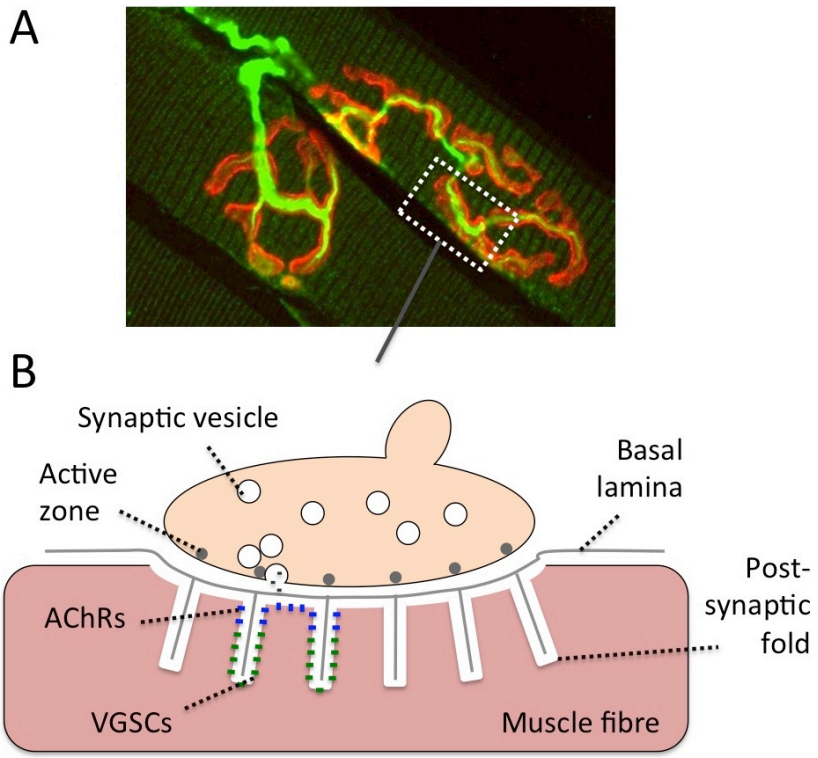

Fig 1.9. Structure of the mature neuromuscular junction (NMJ). (A) Immunofluorescence image of two NMJs innervating muscle fibres, branching from the same axon. Motoneurons are labelled in green, and the postsynaptic acetylcholine receptors (AChRs) are labelled in red with fluorescently conjugated α-bungarotoxin. The pre- and postsynaptic elements overlay each other in a branched pretzel shape. (B) Schematic illustrating the ultrastructure at a small portion of the NMJ. The presynaptic terminus contains many synaptic vesicles. Some of these are docked at the active zones, the sites where they will fuse with the presynaptic membrane to release their neurotransmitter, acetylcholine. On the postsynaptic side, many deep folds are formed in the membrane, and these align with the active zones on the presynaptic side. AChRs are densely packed at the crests and upper portions of the folds, while voltage-gated sodium channels (VGSCs) are concentrated at their depths. The basal lamina runs through the synaptic cleft and into the folds. While the basal lamina of the NMJ is continuous with the basal lamina surrounding the rest of the muscle fibre, the composition differs, with specific isoforms of collagens, laminins and other constituents being present (discussed in detail in *section 1.8., development of the NMJ*). Note that the nerve terminal is slightly embedded into the muscle fibre to form a synaptic gutter.

The postsynaptic membrane is heavily packed with AChRs in a crystalline array, with ~10,000 per μm^2 of membrane (Fertuck and Salpeter, 1976; Matthews-Bellinger and Salpeter, 1983). These receptors are ligand-gated sodium channels, and are categorised into two major classes: nicotinic and muscarinic. As their names suggest, the nicotinic AChRs are responsive to nicotine as well as acetylcholine, while muscarinic AChRs are sensitive to muscarine. The NMJ possesses AChRs of the nicotinic class, while various others systems possess the muscarinic form, including parts of the parasympathetic nervous system and central nervous system (CNS) (Eglen, 2006). The nicotinic AChRs of the NMJ consist of five subunits: the α, β, δ, and ε subunits in a 2:1:1:1 ratio. In development, the ε subunit is replaced by the γ isoform (Giniatullin et al., 2005); this subunit also reappears when muscle is denervated, and in various neuromuscular disorders in which there is muscle atrophy or motoneuron dysfunction (Gattenlohner, 2002). The postsynaptic membrane is also marked by many deep folds, which align with the active zones on the presynaptic terminal. AChRs are found at the crests of the folds, and in the first one-third of the fold nearest the cleft. The depths of the folds (inner two-thirds) are packed with voltage-gated sodium channels (VGSCs), possessing the $Na_v1.4$ α subunit and a β subunit (Awad et al., 2001; Caldwell, 2000). The ligand-induced opening of AChRs results in an influx of Na^+ and K^+ ions; the resulting depolarisation causes the VGSCs in the depths of the folds to open, and the initiation of an action potential in the muscle (Martin, 1994). In the next sections, various components of the NMJ will be discussed in more detail.

1.5.1. The active zone: recruitment, docking and priming of synaptic vesicles

The term 'active zone' was coined in 1970, in studies which used EM to reveal electron dense regions at the nerve terminal membrane (Südhof, 2012). Since then, the various components of the active zone and their functions have been investigated, primarily in central synapses, using *in vitro* and *in vivo* models, although much progress has recently been made in the characterisation of the NMJ active zones. Considerable homology exists between the machinery of the active zones in different synaptic systems, so many of the molecular characteristics are widely applicable. Indeed, the core proteins of the active zone were first

discovered in non-neuronal cells with secretory functions, indicative of the shared mechanisms for vesicle release across systems (Nakata et al., 1999). The active zone consists of a scaffold of different proteins at the nerve terminal membrane. Several of these proteins are transmembrane receptors, including the VGCCs, which initiate synaptic vesicle release. On the internal side, other proteins form a complex, including bassoon, piccolo, spectrin, RIM, RIM-binding protein (RIM-BP), ELKS, α–liprin and Munc13 family members. Together, the molecular assembly is often referred to as the presynaptic cytomatrix, which extends into, and interacts with the actin cytoskeleton (**Fig 1.10**) (Volknandt and Karas, 2012).

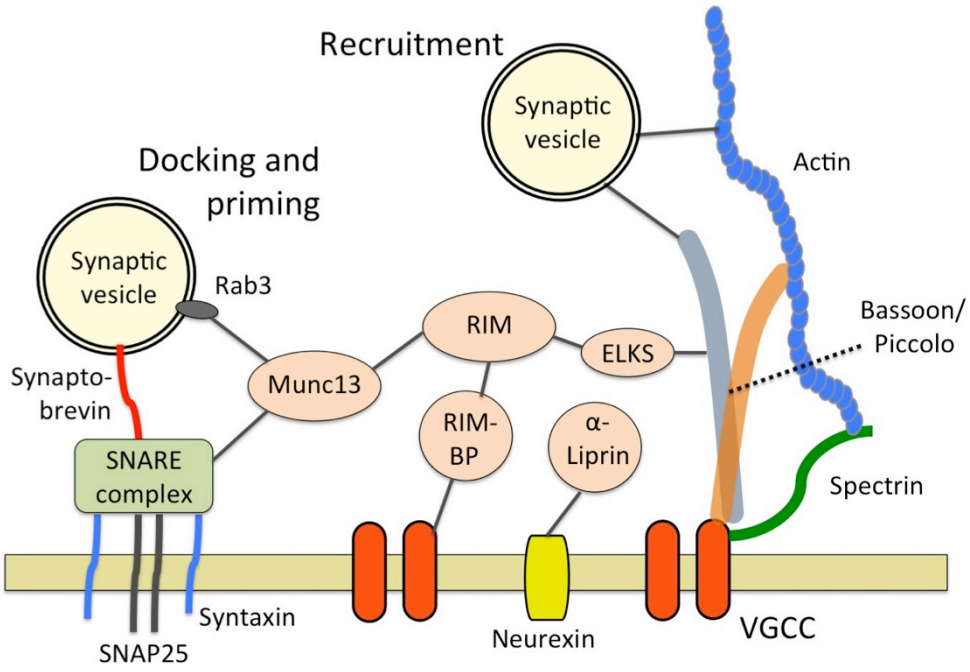

Fig 1.10. Molecular interactions at the active zone. Core proteins of the active zone include RIM, RIM-binding protein (RIM-BP), Munc13, ELKS and α-liprin. RIM-BP is important for the tethering of voltage-gated calcium channels (VGCCs) in the membrane. Munc13 plays a role in the docking of synaptic vesicles, and is able to interact with the SNARE complex, thus mediating vesicle priming. In addition, bassoon and piccolo extend from the VGCCs into the cytoplasm; together with actin, they are involved in the recruitment of synaptic vesicles.

Active zones perform several functions. These include: the docking and priming of synaptic vesicles, ready for release; and the local recruitment of VGCCs, so that the synaptic vesicle release machinery is in close contact with the regions of Ca^{2+} entry, to allow fast coupling between these two entities. They also participate in the precise alignment of pre- and postsynaptic elements. A final function is their ability to regulate the efficiency of synaptic vesicle release, to allow synaptic plasticity and homeostasis; this is particularly important in various central systems, where 'strength' of a synapse plays important roles in information encoding and memory formation. This element of plasticity is also important at the NMJ, so that adjustments can be made to regulate and maintain synaptic efficiency. Plasticity of neuromuscular transmission is therefore a feature of homeostasis during normal activity, in disease, and in adaptation to increased or decreased activity (discussed in *Section 1.9., disorders of the NMJ*, and *Section 1.10., sarcopenia*) (Slater, 2003).

Components of the active zone

Various functions have been ascribed to the different components of the active zone, although the functions of several are elusive. RIM has been identified as a central scaffolding protein, using its multiple domains to recruit a range of other proteins, including VGCCs, RIM-BP and Munc13. Given its role in the localisation of several proteins, RIM is crucial for multiple functions of the active zone, and conditional knockout in mice results in near abolition of synaptic transmission (Dulubova et al., 2005; Kaeser et al., 2011; Wang et al., 1997). Munc13 is understood to be the most important component for the priming of vesicles for release, via its binding to Rab3 on the synaptic vesicle membrane. It exists as an inactive homodimer which is activated through RIM binding (Dulubova et al., 2005). Munc13 is also able to interact with the SNARE (soluble NSF attachment protein receptor) proteins on the synaptic vesicle and in the nerve terminal membrane; these proteins are the final step in vesicle release, triggering membrane fusion (discussed in more detail in *Section 1.5.2., the SNARE complex; priming and fusion of synaptic vesicles*). Through this interaction, Munc13 is able to promote the formation of the active SNARE complex, thus facilitating vesicle priming and fusion (Ma et al., 2011). Disruption of Munc13 in hippocampal neurons and at the NMJ severely impairs

neurotransmitter release (Varoqueaux et al., 2002, 2005). The other major RIM interaction is with RIM-BP. The function of this protein is in the tethering of VGCCs at the active zone, thus ensuring fast excitation-release coupling (Kaeser et al., 2011). Consequently, RIM is a central mediator of vesicle priming and VGCC recruitment, via its binding to Munc13 and RIM-BP respectively.

Two other proteins of the active zone complex are bassoon and piccolo (Cases-Langhoff et al., 1996; tom Dieck et al., 1998; Wang et al., 1999). While the components mentioned above are in close proximity to the membrane, these two large proteins extend further into the cytoplasm, interacting with actin. Although widely studied, the roles of bassoon and piccolo were unclear for some time, and in some model systems appeared to have only minor contributions to neurotransmission. Knockout mice for bassoon suffer from epileptic seizures, decreased postnatal survival rate, and a silencing of a subset of synapses (Altrock et al., 2003). Piccolo-deficient mice are smaller than wild types, have a decreased postnatal survival rate, but exhibit no clear electrophysiological defects in the hippocampus (Mukherjee et al., 2010). However these mice, which had a targeted mutation of piccolo, were still found to express other splice variants, raising the possibility of functional compensation (Waites et al., 2011). Further confusion was created when cultured cortical neurons that were deficient in both bassoon and piccolo displayed no clear defects in neurotransmission, although they had fewer synaptic vesicles docked at active zones (Mukherjee et al., 2010). This was surprising, as the high level of homology between these two proteins suggested that they might function in a partially redundant manner. However, using different synapses as models for study, several functions could be assigned to these molecules, indicating that they are more important in some synapses than in others.

In photoreceptor, auditory and cerebellar synapses, bassoon was required to maintain fast vesicle loading for sustained release, with mutants suffering from synaptic depression during trains of high frequency neural stimulation (Frank et al., 2010; Hallermann et al., 2010; Schulz

et al., 2014). In addition, bassoon and piccolo were found to act together to maintain synaptic integrity. Knockdown of both piccolo and bassoon from glutamatergic neurons resulted in a marked reduction of various synaptic proteins, including RIM, Munc13, synaptic vesicle-associated proteins, and molecules of the SNARE complex. This occurred via a ubiquitin-mediated protein degradation pathway, suggesting that bassoon and piccolo are involved in protein homeostasis (Waites et al., 2013). Bassoon has also been found to interact with P/Q VGCC, with *in vitro* expression studies suggesting that it enhances Ca^{2+} entry by prolonging channel opening times (Nishimune et al., 2012). Bassoon has also been shown to enhance P/Q VGCC recruitment to active zones in central synapses, acting through the VGCC-tethering protein RIM-BP (Davydova et al., 2014).

The functions of α-liprins and ELKS have remained elusive. α-liprin may act as a structural link between transmembrane adhesion receptors such as neurexins, and components of the active zone (Ackley et al., 2005). Genetic studies on ELKS have not revealed any clear function, although neurotransmitter release is partially impaired in *Drosophila* knockouts, but not in mice or *C. elegans* (Südhof, 2012). Additional proteins that interact with active zones are CASK, Velis and Mint, which are also not well characterised. However, CASK may have a similar role to α-liprin, linking active zone components to the nerve terminal membrane, and mutations in the gene encoding CASK cause a decrease in the efficiency of synaptic transmission (Butz et al., 1998; Kaech et al., 1998; Südhof, 2012).

The active zones of the NMJ

As mentioned previously, the active zones of NMJs differ from those of central synapses in that they are punctate rather than arranged in a plaque. However, the molecular characteristics are essentially the same, and they possess all of the molecules described above (with the CASK, Mint and Velis proteins so far identified at the *Drosophila*, but not mammalian NMJ) (Ashley et al., 2005; Bachmann et al., 2004; Juranek et al., 2006; Sanford et al., 2004). Severe defects in neurotransmission have been reported at the NMJs of several mutant mouse models: RIM,

Munc13 and P/Q VGCC (Heeroma et al., 2003; Nishimune, 2012; Schoch et al., 2006; Sons et al., 2005). While RIM-BP and bassoon have been implicated in the recruitment and tethering of VGCCs in the active zones of central synapses, studies at the NMJ suggest a different mechanism of organisation. Here, laminin-β2 in the synaptic cleft binds to the P/Q and/or N-type VGCCs (the latter being a developmental form that is co-expressed with P/Q VGCC during embryonic development). This interaction results in the clustering of VGCCs, and subsequently the recruitment of other active zone proteins to these sites. Knockout of laminin-β2, and dual knockout of P/Q and N-type VGCC results in drastically reduced numbers of active zones at the NMJ (Chen et al., 2011; Noakes et al., 1995). This also occurs in patients with laminin-β2 mutations, or autoantibodies targeted against P/Q VGCC (the cause of Lambert-Eaton myasthenic syndrome or LEMS) (Maselli et al., 2009; Spillane et al., 2010). Whether or not VGCCs act as initiators for active zone assembly in other synapses remains to be seen.

The ultrastructural arrangement of the active zones of the NMJ has been well characterised with various approaches, including freeze-fracture EM, EM tomography and super resolution light microscopy. Freeze-fracture studies in the mouse have revealed two parallel rows of intramembranous particles (IMPs) studied in the presynaptic membrane (**Fig 1.11A**). These are 50-100 nm in length, the approximate diameter of the active zone as a whole (Ellisman et al., 1976). Evidence suggests that some or all of the IMPs are the VGCCs (labelled 'channels' in **Fig 1.11A**) (Fariñas et al., 1993; Pumplin et al., 1981). EM tomography revealed additional structures of the active zone. Two docked vesicles sit at the centre, lined on either side by the rows of IMPs. 'Beam' structures align with the IMPs, marking the edges of the overall active zone arrangement. The synaptic vesicles in the centre are crosslinked to the other components by 'rib' structures (Nagwaney et al., 2009). Although these analyses have given a detailed insight into the arrangement of material at the active zone, the molecular identities of these ultrastructural components remain elusive.

Recent advances in light microscopy have resulted in the ability to resolve objects within less than 100 nm of each other. Using stimulated emission depletion microscopy (STED), which can resolve distances of 30-50 nm, the relative positioning of several active zone components in *Drosophila* NMJs was determined (**Fig 1.11B**) (Maglione and Sigrist, 2013). In transmission EM sections, and in EM tomographs, the active zone of *Drosophila* resembles a T-shape (often referred to as a T-bar), with a central core anchored to the membrane, and extensions at the cytoplasmic end, forming lateral cross bars (Jiao et al., 2010). Based on STED imaging, a model has been proposed whereby the *Drosophila* homolog of RIM-BP makes up the walls of the central core, with VGCCs positioned in the middle. Lateral extensions of Bruchpilot protein (the homolog of ELKS) project from the central core, and are presumed to be the bars of the T-shape. These extensions appear to dock synaptic vesicles (Liu et al., 2011b). The functional significance of this arrangement remains elusive, and studies to allow comparison with the mammalian active zones have not yet been undertaken.

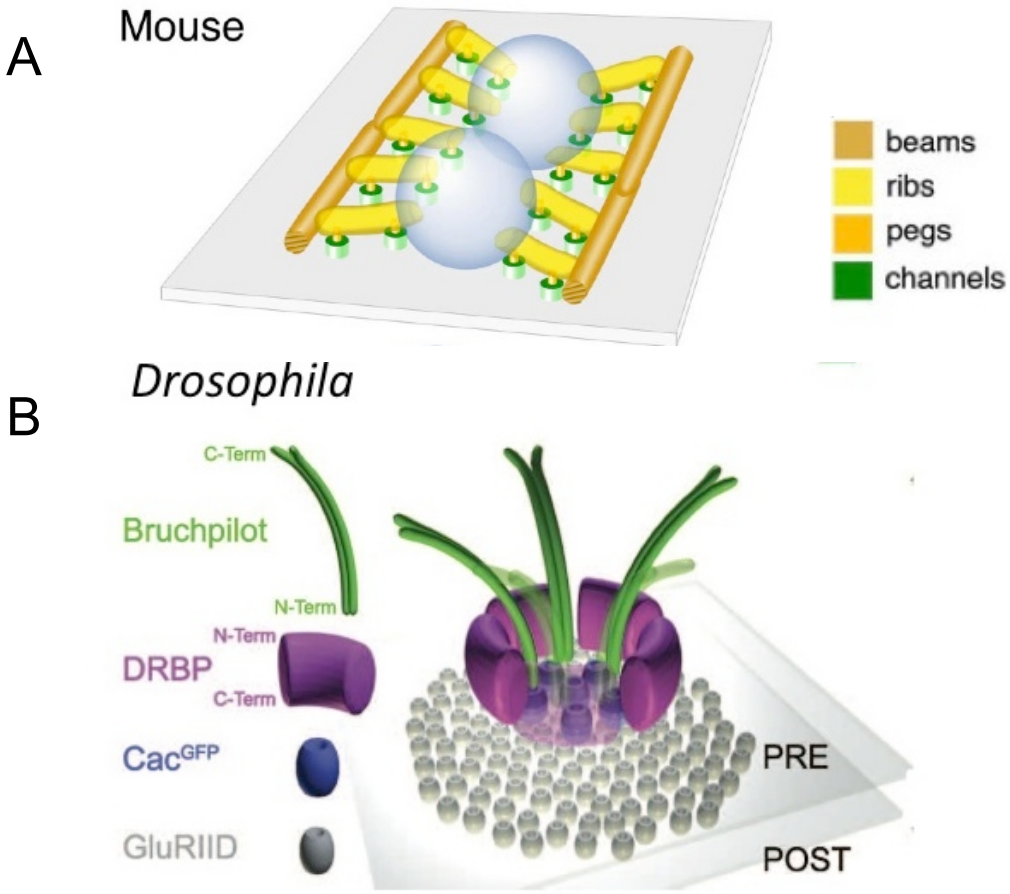

Fig 1.11. Macromolecular structure of the active zones of mouse (A) and *Drosophila* (B) NMJs. Structures for (A) were determined using electron tomography, and that of (B) using super resolution light microscopy. (A) Grey spheres represent synaptic vesicles docked to the active zones. Channels (i.e. VGCCs) are presumed to be equivalent to the intramembranous particles (IMPs), which are observed with freeze-fracture electron microscopy as studs in the presynaptic membrane. Short pegs link the channels to the overlying ribs; one end of the rib (*Fig 1.11; continued from previous page*) contacts the synaptic vesicle, while the other is bound to the beams. (B) The relative positioning of several active zone proteins were determined at the *Drosophila* NMJ. VGCCs (Cac) were found at the centre of the structure, surrounded by DRBP (Drosophila RIM-binding protein). Molecules of Bruchpilot, a protein with homology to ELKS, extend laterally from the central core (presumably the 'T-bars' seen in transmission EM slices). (A) Image from Nagwaney, S et al., 2009. Originally published in *J Comp. Neurol.*, doi: 10.1002/cne.21975. (B) Image adapted from Liu, KSY et al., 2011. Originally published in *Science*, doi: *10.1126/science.1212991.* Rights obtained through Copyright Clearance Centre.

1.5.2. The SNARE complex: priming and fusion of vesicles

While active zones are required for the recruitment, docking and in part, the priming of synaptic vesicles, they cannot mediate their fusion with the presynaptic membrane. Proteins of the SNARE and SM (Sec1/Munc18-like) class are the mediators of vesicle priming and fusion, and are present in homologous forms in many vesicle secretory systems, including those in yeast (Südhof et al., 1993). SNARE proteins are the targets of several toxins, including those from tetanus and botulinum (Schiavo et al., 1992). Somewhat surprisingly, these proteins are distributed throughout the membrane, despite their close functional link to the anchored active zones.

The fusion of phospholipid bilayers is energetically unfavourable, so the fusion complex is specialised to overcome this. SNARE proteins are classed according to their location: v-SNARES (vesicle) or t-SNARES (target membrane, i.e., the presynaptic membrane). Synaptobrevin is the v-SNARE that is present on the synaptic vesicle surface, which complexes with the two t-SNARES on the presynaptic membrane: syntaxin, and SNAP-25 (**Fig 1.12**) (Südhof, 2013). These three proteins are essentially unfolded, but when brought together, they spontaneously fold to form a very stable four-helix bundle (Südhof and Rothman, 2009). One of these helices is derived from the v-SNARE, synaptobrevin, two from SNAP-25, and one from syntaxin. Prior to membrane fusion, two of these complexes form, at either side of the vesicle docked to the membrane. Various isoforms of the SNARE proteins exist, expressed in many different cells with secretory functions. Despite hundreds of possible combinations, only a few of these can form cognate SNARE complexes, lending to the idea of an inherent specificity in the system (Parlati et al., 2000).

Prior to the formation of the active SNARE complex, the SM protein Munc18 is able to bind and clasp to syntaxin, promoting an inactive state; on the formation of the active SNARE complex, Munc18 is able to clasp the four-helix bundle (Dulubova et al., 2007; Shen et al., 2007). Here, it is proposed to act as a facilitator of SNARE-mediated fusion. During this process, the two four-

helix SNARE complexes at either side of the primed vesicle zipper along the membrane towards each other, and towards the centre of the vesicle (where it contacts the presynaptic membrane). In doing so, they propel the vesicle into the terminal membrane with enough mechanical force that the two membranes fuse, allowing a pore to form for neurotransmitter release. Subsequently, the SNARE proteins are converted back to their separated and unfolded conformations, a process which requires ATP hydrolysis by N-ethylmaleimide-sensitive factor (NSF) (Mayer et al., 1996).

Additional studies revealed that this zippering process is carried out essentially in two steps. The first step involves partial zippering, before the process is halted, leaving the vesicle and complex in an intermediate frozen state. This is an important part of fast and synchronous vesicle release, because the zippering process is already partially completed, and the vesicle sits in a primed state. The second step involves the completion of the zippering process, and thus membrane fusion. Two proteins, synaptotagmin and complexin, have been implicated as proteins which halt and maintain partial zippering. The binding of Ca^{2+} to synaptotagmin is the final step which triggers the rest of the fusion process (Melia, 2007; Südhof, 2013; Trimbuch et al., 2014). Munc13, a component of the active zones, is able to bind to the SNARE proteins to promote the formation of the active conformation; this is therefore a structural and functional link between these two parts of the presynaptic machine (Ma et al., 2011). The importance of the process of vesicle release, including that in synapses, was recognised in 2013 with the award of a Nobel Prize to Thomas Südhof, James Rothman and Randy Schekman, for their work on synaptic active zones, SNARE proteins, and secretion in several systems.

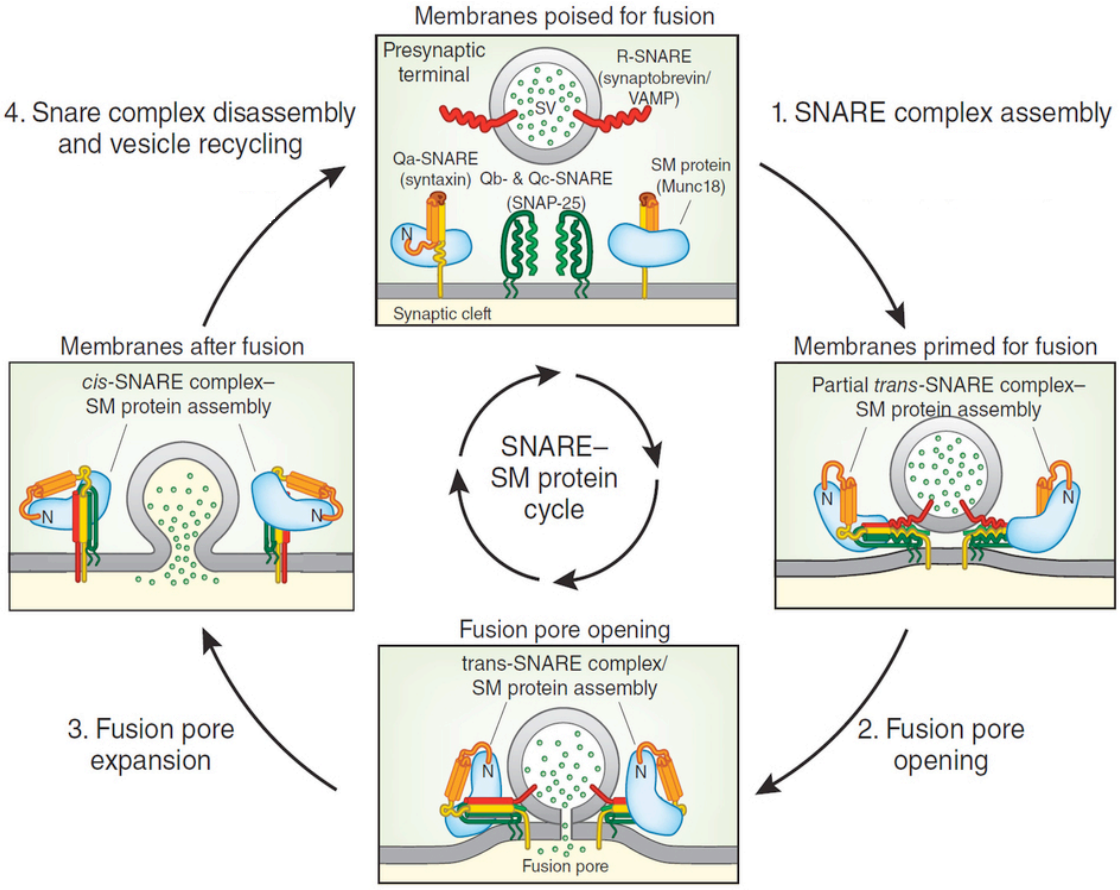

Fig 1.12. The SNARE (soluble NSF attachment protein receptor) proteins and vesicle exocytosis. The SNARE proteins SNAP-25 and syntaxin are present on the presynaptic membrane, while synaptobrevin is present on the synaptic vesicle surface. Munc18, a so-called SM (Sec1/Munc18-like) protein, forms a clasp around syntaxin. When the synaptic vesicles are primed (step 1), the three SNARE proteins form a triple helix (the active SNARE complex), one at each side of the vesicle. On entry of Ca^{2+}, the triple helices zipper along the membrane, forcing the synaptic vesicle to fuse with the presynaptic membrane (step 2). Following this, the fusion pore expands to allow release of neurotransmitter (Step 3). The SNARE proteins are then returned to their original conformations, with the energy provided by ATP hydrolysis (step 4). Adapted from Sudhof TC, 2013. Originally published in *Nature Medicine*, Doi: 10.1038/nm.3338. Rights obtained through Copyright Clearance Centre.

1.5.3. The synaptic basal lamina of the NMJ

The NMJ is unusual for a synapse, in that it has a basal lamina that runs through the synaptic cleft, and into the depths of the folds. On first thought, the basal lamina might be expected to hinder the diffusion of acetylcholine across the synaptic cleft; however, it has been shown that it has little or no effect on this process, owing in part to the small size of the acetylcholine molecule. The basal lamina of the NMJ is truly that, as it has no reticular lamina that is present in many other basement membranes; only the lamina densa in the middle of the cleft, and the lamina lucida on either side, apposing both the pre- and postsynaptic membranes, are present (Sanes, 2003). Thus, the components of the basal lamina are able to interact with both the muscle and the nerve terminal.

Although the basal lamina of the NMJ is continuous with that of the muscle fibre, its composition differs quite markedly. In the mature NMJ, the laminin-β1 subunit that is found in the rest of the basal lamina as laminin-211 is absent. Here, the laminins-221, -421 and -521 are present. In addition to the ubiquitous collagen IV muscle isoform $(\alpha1)_2(\alpha2)$, collagen IV $(\alpha3)(\alpha4)(\alpha5)$ and $(\alpha5)_2(\alpha6)$ specifically localise to the synaptic basal lamina. Other NMJ-specific proteins here include nidogen-2, collagen Q (ColQ), collagen XIII, and neural agrin (Fox et al., 2008; Patton, 2000; Singhal and Martin, 2011). All of these are synthesised and deposited by the muscle fibre, with the exception of the latter, which is released by the nerve terminal (Nishimune et al., 2008). The expression of the different components is developmentally regulated (see **Table 1.2**), and the basal lamina itself has a huge role in the development and function of the NMJ, as discussed in *Section 1.8., development of the NMJ*).

	E18		P21	
	Extrasynaptic	**Synaptic**	**Extrasynaptic**	**Synaptic**
Ubiquitous				
Coll IV $(\alpha1)_2(\alpha2)$	+	+	+	+
Fibronectin	+	+	+	+
Nidogen 1	+	+	+	+
Perlecan	+	+	+	+
Synapse-specific				
Lam-221	-	+	-	+
Lam-421	-	+	-	+
Lam-521	-	+	-	+
Agrin (neural)	-	+	-	+
AChE	-	+	-	+
ColQ	-	+	-	+
Coll IV $(\alpha3)(\alpha4)(\alpha5)$	-	-	-	+
Coll IV $(\alpha5)_2(\alpha6)$	-	-	-	+
Coll XIII	-	-	-	+
Ubiquitous, then restricted to synapse				
Agrin (muscle-derived)	+	+	-	+
Neuregulin	+	+	-	+
Nidogen-2	+	+	-	+
Ubiquitous, then removed from synapse				
Lam-211	+	+	+	-
Lam-411	+	+	+	-
Lam-511	+	+	+	-
Laminins (summary)				
Lam-α2 chain	+	+	+	+
Lam-α4 chain	+	+	-	+
Lam-α5 chain	+	+	-	+
Lam-β1 chain	+	+	+	-
Lam-β2 chain	-	+	-	+

Table 1.2. Summary of synaptic and extrasynaptic basal lamina components in muscle. Newly formed NMJs at E18 and adult/mature stages at P21. Coll, collagen; Lam, laminin; AChE, acetylcholinesterase.

1.6. Basic electrophysiological principles at synapses

As mentioned previously, the influx of Ca^{2+} following the arrival of an action potential into the synaptic bouton results in membrane fusion, and depends on the engagement of Ca^{2+} sensors such as synaptotagmin. On the postsynaptic side, Na^{+} and K^{+} enter the cell in response to neurotransmitter binding to receptors, initiating an action potential. The electrophysiological characteristics of these processes have been characterised in detail, with broad implications for the understanding of synaptic transmission in health and disease. Many of these principles were first established at the frog neuromuscular junction, in studies that began in the 1950s by Bernard Katz and colleagues (Augustine and Kasai, 2007). Katz was awarded a Nobel Prize in 1970, shared with Julius Axelrod and Ulf von Euler, who worked on mechanisms of neurotransmission in other systems (Shafrir, 1994). First, basic principles of electrophysiology will be discussed, before these are applied specifically to the NMJ.

Ex vivo electrophysiological analysis in intact tissue has been largely carried out on acute slices of rodent brain, or in diaphragm muscle preparations, with ribcage, spinal column, and efferent motoneurons intact. *In vitro* analyses on single excitable cells are usually carried out with a patch clamp, a micropipette that allows the isolation and recording of one or a few ion channels. Here, we will focus on analyses made with *ex vivo* preparations, as it is most relevant to our understanding of whole synapses and the NMJ. Two-electrode methods involve one electrode being placed in the axon or cell body of an efferent neuron (e.g. in neurons originating in one part of the brain, or in the neurons of the phrenic nerve which contain the motoneurons for the diaphragm), and one being placed in the postsynaptic cell. Electrical stimulation by the first electrode induces and action potential in the input neuron, resulting synaptic transmission at the terminal; these events are recorded by the second electrode on the receiving cell. This technique allows the recording of synaptic events between a single pre- and postsynaptic cell (e.g. the electrical changes at an NMJ of a single muscle fibre). Although inferences can be made about both pre- and postsynaptic electrical events, the readings are only recorded on the postsynaptic side (Rigoard et al., 2009).

By stimulating the input neuron, evoked neurotransmission can be elicited; the resulting postsynaptic depolarisation is commonly known as an evoked excitatory postsynaptic current (EPSC), or in the case of the NMJ, an evoked endplate potential (EPP). This results from the release of multiple vesicles and the rapid depolarisation of the postsynaptic membrane (a sharp rise in response), followed by a slower decline, as ions are buffered away and the neurotransmission ceases (**Fig 1.13A**) (Billups and Forsythe, 2002). In the absence of stimulation, synaptic events of low amplitude are still able to be recorded. These so-called spontaneous events are widely assumed to be caused by the release of a single vesicle. They are termed miniature EPSCs (MEPSCs) or miniature EPPs (MEPPs) in the case of the NMJ. In the model of synaptic vesicle fusion, the influx of Ca^{2+} is not an absolute trigger for active zone firing; it merely results in an increase in the probability of firing. Thus, even in the absence of an action potential, a vesicle is still capable of being occasionally released at random. Usually, this has no physiological effect, since the depolarisation caused by the contents of a single vesicle is small, and not high enough to reach the threshold required to cause an action potential (Mozrzymas, 2008). However, it is a phenomenon which has implications for the analysis of synaptic parameters, as will be discussed below.

Miniature depolarisations demonstrate the contribution of a single vesicle to neurotransmission, and thus are an approximate correlate of the quantity of neurotransmitter in each vesicle. By using the amplitude of a miniature event, the approximate number of synaptic vesicles released in an evoked event can be determined (amplitude of the evoked event is divided by that of the miniature event). This parameter, the number of vesicles released for a given stimulus, is termed quantal content, and each vesicle is often referred to as a quantum. In addition, the frequency of miniature events under resting conditions can be an indicator of the 'leakiness' of the system. Therefore these events give information about the functional status of the presynaptic machinery (Slater, 2008).

Under normal physiological activity, neuronal stimulation normally does not occur in single events of depolarisation, but in high frequency bursts of stimulation. Action potentials in the brain may fire at more than 300 Hz, and motoneurons may stimulate transmission at around 100 Hz during heavy muscle exertion. The effect of high stimulation in the brain contributes to the complex encoding of signals (Selverston and Moulins, 1985). At the NMJ, it results in sustained muscle contraction (Wood and Slater, 2001). During high frequency stimulation, often two phenomena are observed: short-term facilitation (STF), and short-term depression or decrement (**Fig 1.13B**). In the former, the amplitude of signal builds over the first few stimuli. After the first action potential, VGCCs open then close, and vesicles are released. When the action potential fires for the second time, some of the Ca^{2+} from the first round is still present, and this residual Ca^{2+} contributes to the second response. A gradual build-up of Ca^{2+} results in the increasing signal over time, until an equilibrium of Ca^{2+} concentration and buffering is reached, and the responses are stabilised (Billups and Forsythe, 2002; Katz and Miledi, 1968). The second phenomenon of decrement usually begins after STF has ended. After the first vesicles are released, the replacement of new vesicles (recruitment, docking and priming) takes time, and under high frequency stimulation, becomes a rate-limiting step in neurotransmission. Thus the efficiency of neurotransmission may start to gradually decrease over successive stimuli, resulting in depression, decrement or 'run-down' of the signal. This is particularly apparent when there are defects which impair neurotransmission (commonly seen in patients with myasthenic syndromes, which affect NMJ function and cause neuromuscular weakness, discussed in *Section 1.9., disorders of the NMJ*) (Poage and Meriney, 2002; Spillane et al., 2010).

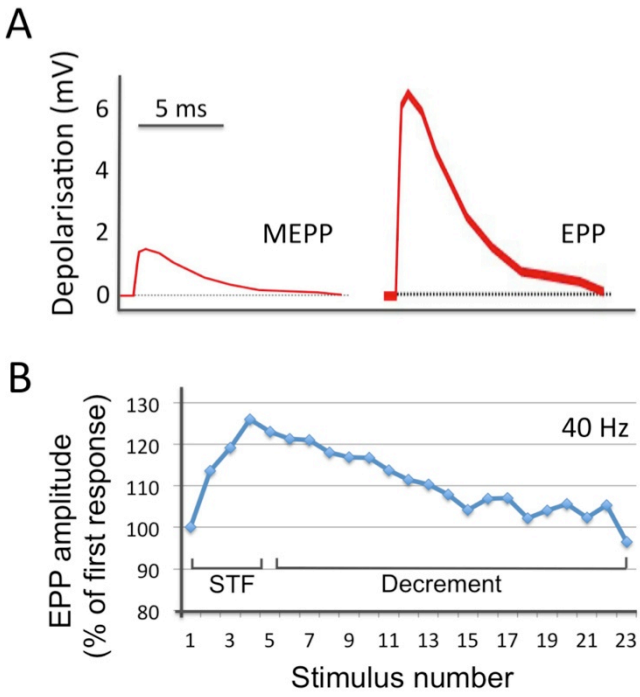

Fig 1.13. Electrophysiological measurements at the NMJ. (A) Depolarisation at the postsynaptic membrane in response to released neurotransmitter. Spontaneous release of a single synaptic vesicle occasionally occurs in the absence of nerve stimulus, and results in a small depolarisation on the postsynaptic membrane. At the NMJ, this is known as a miniature endplate potential (MEPP). These events are below the threshold required for the generation of an action potential in the muscle fibre, and contraction does not occur. When the input nerve is stimulated, an action potential in the axon results in the release of multiple vesicles, and a much larger depolarisation on the postsynaptic side. At the NMJ, this is known as an evoked endplate potential (EPP), and under normal conditions is above the threshold required for muscle contraction. (B) During normal muscle activity, repeated bouts of synaptic activity are required for sustained contraction. In this manner, repetitive stimulation brings about multiple depolarisation events. During the first few stimuli, a phenomenon known as short-term facilitation (STF) occurs, characterised by a gradually increasing EPP amplitude. This is due to the build up of Ca^{2+} in the nerve terminal over successive stimuli, whereby some of the Ca^{2+} from one stimulus remains, and has an additive effect on the next. Under high frequency stimulation, the EPP amplitude then begins to gradually decrease (decrement), as vesicle redocking and fusion cannot sustain itself at a high rate.

1.7. Neurotransmission at the NMJ, and the purpose of structural elements

The function of the NMJ differs from that of central synapses. The NMJ is designed as a highly reliable synapse with one goal: to create a large response capable of stimulating contraction of a muscle fibre much larger than itself. Although the NMJ is around 1000 times larger than many central synapses, it only occupies around 0.1% of the total surface area of the muscle fibre (Sanes and Lichtman, 1999). Therefore it has to be highly efficient and reliable, and its structural characteristics are a key factor in this. In contrast, central synapses are designed to integrate excitatory and inhibitory signals from other neurons, thus encoding information; as such, synaptic transmission has to be tightly regulated, but it does not necessarily have to be large in its output (Gulledge et al., 2005). The main feature of the NMJ that ensures reliability is termed the safety factor. As mentioned previously, an action potential in the muscle cell will only be elicited once a certain threshold of AChR activation is reached. The quantal output of the nerve terminal, and the influx of ions on the postsynaptic side is greater than that required to reach this threshold, thus always ensuring that successful stimulation occurs, even if there are fluctuations in the local environment. This excess in neurotransmission that (usually) prevents the failure of the NMJ is the basis of the safety factor. Experiments on human subjects suggest that even under extreme muscle exertion, failures of neurotransmission are rare (Bigland-Ritchie et al., 1982). The safety factor depends on the characteristics and arrangement of structures in the NMJ, as will be discussed below.

Various studies have shown that the density of active zones at the NMJ is around 2.5 per μm^2 of membrane in mice and humans (Chen et al., 2012; Clarke et al., 2012). Each active zone has primed and docked synaptic vesicles, known as the readily releasable pool (RRP). There is also a reserve pool of vesicles outside of the active zones, which can be recruited into the RRP when necessary (Fdez and Hilfiker, 2006). It is estimated that there are 150,000-300,000 vesicles in a typical NMJ nerve terminal of a frog, mouse or human (Reid et al., 1999). Each vesicle contains 5000-10,000 acetylcholine molecules (Kuffler and Yoshikami, 1975). When an action potential arrives, the rise in Ca^{2+} results in an increased probability of active zone firing. Counter-intuitively, only around 10% of active zones will be activated on nerve stimulation,

each releasing around one vesicle. However, the quantity of acetylcholine released is enough to saturate virtually all of the densely packed AChRs on the postsynaptic side. It has also been shown that the neurotransmitter from one vesicle can diffuse so that it saturates a region of receptors that is ~1 μm^2 in diameter; thus, it reaches the AChRs in and around the adjacent postsynaptic folds as well (Wood and Slater, 2001). There are several benefits to this low probability of firing. During high frequency stimulation, it takes much longer for the RRP to become exhausted, as only a small proportion of active zones are releasing vesicles at any one time. In effect, while one set of active zones are firing, the others can re-dock synaptic vesicles, to allow sustained and reliable transmission over many stimuli. It also means that it is unlikely that two adjacent active zones will fire at once, so that the microdomains of released neurotransmitter do not tend to overlap. As a result, neurotransmitter release is highly efficient, and little excess needs to be released each time to ensure efficient saturation on the postsynaptic side.

The postsynaptic folds are also highly relevant to the function of the NMJ. On first glance, it might seem that the folds function to amplify signal by greatly increasing surface area, and thus availability of AChRs. While this may partly be true, the AChRs only extend into the first one-third of each fold, while the final two-thirds are occupied by VGSCs. Computer modelling suggests an alternative function for the folds. Plasma membranes are very impermeable to current, and the multiple deep invaginations of membrane create a region of high electrical resistance. This results in an increase in the voltage, as current and resistance are linked (voltage = current x resistance). As such, fewer VGCCs need to open to stimulate the VGSCs in the adjacent regions of the folds, and the postsynaptic potential is amplified by around two-fold (and thus the threshold required for activation is approximately halved) (Martin, 1994).

Another feature of the NMJ that appears to play an important role, but is not fully understood, is the alignment of active zones with the mouths of the postsynaptic folds. In central synapses, where there are no folds, the single active zone plaque as a whole aligns with a similar sized

plaque of receptors on the postsynaptic side. The precise alignment of individual active zones in NMJs may allow neurotransmitter to be focused to some extent at the AChR-rich postsynaptic fold regions, enhancing the efficiency of synaptic transmission. However, as mentioned previously, neurotransmitter actually spreads much further afield into the adjacent folds, thus making the purpose of alignment less clear. Laminin-α4 mutant mice, which display few morphological defects in NMJs, but active zone misalignment, showed a trend for reduced motor strength (~30%, but not statistically significant) (Nishimune et al., 2008; Patton et al., 2001).

Another feature of the NMJ that has an unknown purpose is the folding of the nerve terminal and underlying postsynaptic density into a pretzel shape. The branches of the pretzel are embedded into the muscle, forming interconnected gutters. Some investigators have commented that the width of these branches/gutters correspond roughly to the distance that Ca^{2+} can diffuse, during the time frame of a synaptic transmission event (Wood and Slater, 2001). Thus, the shape may allow Ca^{2+} to efficiently reach all parts of the internal nerve terminal, as it can diffuse between the branches of the pretzel. The relevance of the embedding of nerve terminals into the muscle membrane (the gutters) may be to increase the surface area of pre- and postsynaptic contact, when compared to a simple flat interface (Slater, 2008).

The onset of synaptic transmission is synchronous across the different synapses of the muscle, and is elicited on an extremely fast time scale (within a few milliseconds of the initial brain input). Precise regulation is also required to effectively terminate synaptic transmission, and this is largely achieved through the enzyme acetylcholinesterase (AChE). This enzyme is responsible for the rapid breakdown and inactivation of acetylcholine, thus ending the activation of AChRs, all within the time frame of a few milliseconds (Hartzell et al., 1975; Katz and Miledi, 1973). AChE is found in the synaptic cleft, bound by collagen Q (ColQ), which is itself anchored to perlecan in the synaptic basal lamina. Studies have shown that the vast majority of acetylcholine molecules manages to traverse the synaptic cleft and reach the

AChRs before AChE can act on it; the breakdown occurs very shortly after (Slater, 2008). Reuptake of the released components of the vesicles can occur for the purpose of recycling, through endocytosis in the nerve terminal (Purves et al., 2001).

While the basic structural elements of NMJs are present in all the vertebrates that have been studied, there are some major differences in their organisation across species. These influences seem to reflect different strategies in the achievement of muscle cell depolarisation. It is accepted that larger NMJs release more synaptic vesicles, as there is a greater surface area of presynaptic membrane. In the frog, the neuromuscular junction is much larger than in mice or humans, with processes of the pretzel sometimes extending most of the length of the myofibre. This allows it a very large area of synaptic contact with the muscle, and thus the release of a large number of quanta upon nerve stimulation, around 200 vesicles. The extent of postsynaptic folding at the frog NMJ is fairly minimal, however, which may explain the large requirement for neurotransmitter release, in order to overcome the threshold for muscle activation. In contrast, the NMJ of the mouse is much smaller, and with its presynaptic surface area can emit around 50 vesicles on stimulation. However, with many more folds, the response is presumably amplified much more than in the frog, allowing it to reach the threshold with fewer vesicles. In the human, the NMJs are even smaller than in the mouse, and release only 20 quanta. Correspondingly, fewer vesicles released requires more postsynaptic folding, and the density and depth of the folds is greater at the human NMJ (Hartzell et al., 1975; Katz and Miledi, 1979; Slater et al., 1992). These observations in different species have increased to our understanding of the structure-function correlation at the NMJ (Slater, 2003).

1.8. Development of the NMJ

The development of motor innervation occurs alongside myogenesis, which was described in detail earlier (*Section 1.3., development of skeletal muscle*). Innervation has been best described in the mouse diaphragm, a thin, flat muscle which can be readily stained and imaged in whole mount. Motoneuron axons emanating from the spinal cord first reach the muscle during primary myogenesis, when the first set of myofibres form (around E13). Shortly after, they start to branch, and form nascent NMJs with the muscle, and this process continues as secondary fibres form. By E18, when myogenesis has finished, the mature innervation pattern has been established, with one neuronal endplate per fibre. The path of the motoneurons runs through the middle of the muscle, forming NMJs at this midline region (Singhal and Martin, 2011; Witzemann, 2006). Throughout the period of motoneuron branching (E13 up until the first few days of postnatal life), around half the motoneurons undergo programmed cell death, leaving only the motoneurons that have successfully managed to target muscle fibres (Banks et al., 2001, 2003; Sendtner et al., 2000).

In the first two to three weeks after birth, several key developmental processes occur at the NMJ. In neonates, NMJs are usually polyinnervated, that is, they have inputs from several different axons. Over the coming weeks, synaptic elimination ('pruning') occurs, whereby many of the axons withdraw to leave a single input at each NMJ (Buffelli et al., 2003; Fox et al., 2011). The small plaque-shaped endplate also grows, and regions are eliminated to leave the characteristic, mature pretzel shape (Marques et al., 2000). Postsynaptic folds also start to form, and the active zones, which were apparent from around E16.5, become aligned with the folds (Clarke et al., 2012; Sanes and Lichtman, 1999). Several switches in molecular composition occur during the maturation of the NMJ. At the AChRs, the γ subunit is replaced by ε (Sanes and Lichtman, 1999). At the presynaptic active zones, the N- and P/Q VGCCs that are present in embryonic NMJs are gradually replaced, to leave only the P/Q-type (Nishimune, 2012). With the emergence of folds comes the localisation of VGSCs to their depths (Awad et al., 2001). In the basal lamina, NMJ-specific collagen isoforms become upregulated: collagen IV

(α3)(α4)(α5) and $(α5)_2$(α6), and collagen XIII (Singhal and Martin, 2011). The basal lamina proteins of the NMJ and muscle fibre, at developing and mature stages, are summarised in **Table 1.2**. In humans, it has been observed that the maturation of the NMJ finishes several years after birth (compared to several weeks in the mouse), at least at the level of postsynaptic folds (Wood and Slater, 2001).

1.8.1. AChR clustering and the agrin-MuSK-Lrp4 pathway

Many of the proteins that are involved in NMJ development were first isolated from the electric organ of *Torpedo* electric ray fish. These large synapses have very similar structural and molecular homology to NMJs. While NMJs make up a tiny fraction of the total volume in muscle, the electric organs are densely packed with synapses, allowing proteins and complexes to be isolated in bulk (Unwin, 2013). The molecular events that govern the assembly of postsynaptic molecules, in particular the AChRs, have been studied in detail. Small plaques or 'hot spots' of AChRs become apparent before motoneurons arrive, with multiple clusters per muscle fibre, concentrated in the midline region (Bevan and Steinbach, 1977). This process has been described as pre-patterning, as it occurs in the absence of nerve. The initial placement of AChR hot spots at the sarcolemma is known to be dependent on muscle-specific kinase (MuSK) and rapsyn. The former is a receptor tyrosine kinase involved in signal transduction, and the latter a downstream protein that associates with AChRs and stabilises them in clusters at the membrane (DeChiara et al., 1996; Froehner, 1993; Musil et al., 1989; Valenzuela et al., 1995). The expression of the surface receptor MuSK is assumed to be carried out by the midline nuclei of the fibre, thus restricting the accumulation of the AChRs to this region (Witzemann, 2006). When nerve terminals arrive, they form stable contacts with the AChR plaques; the basal lamina protein agrin, which is released by the nerve is a major regulator of this process.

The exact role of agrin in NMJ development was a subject of confusion for some time. When added to cultured myotubes, the *in vitro* equivalent of muscle fibres, neural agrin was able to

induce the surface accumulation of AChR clusters. In contrast, the muscle isoform of agrin was not able to induce clustering to nearly the same extent. This led to the hypothesis that the arrival of nerve terminals, and the release of neural agrin was the essential initiator of postsynaptic assembly (Gesemann et al., 1995; McMahan, 1990). However, neural agrin knockout mice displayed normal pre-patterning of AChRs on muscle fibres, indicating that postsynaptic apparatus could assemble in the absence of agrin (Lin et al., 2001; Yang et al., 2001). Even so, these mice have a severe defect, with motoneurons being unable to terminate and form functional contacts with these endplates (and as a result the mice die at birth). It was not until the characterisation of the MuSK and rapsyn knockout mice that the true mediators of pre-patterning were established; no AChR clusters can form in these mice (Banks et al., 2001; DeChiara et al., 1996).

The current and widely accepted model is that MuSK activity in the nascent myofibres stimulates the initial insertion and aggregation of AChRs in the membrane, before motoneurons arrive. Nerve terminals contact and stabilise individual AChR clusters, through the binding of agrin to MuSK, thus ensuring continuous signalling. Various studies have shown that the release of acetylcholine at these junctions is actually a negative regulator of AChR aggregation, acting to disperse the clusters in the membrane; however, those where the nerve has bound are stabilised through the release of agrin (An et al., 2010). Thus, early neurotransmission removes the AChRs that are extrasynaptic, whilst maintaining those that are opposed by a nerve terminal (Ferraro et al., 2012). Consequently, the maintenance of NMJs involves a balance between the destabilising influence of acetylcholine release, and the stabilising influence of agrin. The agrin-MuSK pathway is now very well characterised. Agrin binds to both MuSK and another transmembrane receptor, Lrp4, bringing about the dimerisation of MuSK. The intracellular domain of MuSK can bind to various adaptor and signalling proteins, and its activity can be enhanced by the binding of Dok7 (Inoue et al., 2009). Downstream signalling pathways include those that regulate actin dynamics (e.g. Rho, ROCK, Arp2/3); these are required for the trafficking and insertion of AChRs into the membrane.

Finally, rapsyn binds AChRs, and has a positive effect on their stabilisation in the membrane (Martínez-Martínez et al., 2009; Wu et al., 2010; Zong and Jin, 2013). β-DG can regulate this process through direct binding to rapsyn. In agreement with this, mice and patients with defects in DG processing have reduced clustering of AChRs (Taniguchi et al., 2006). Integrin-α7β1 also appears to enhance agrin activity in AChR clustering, *in vitro,* although no NMJ defects have been reported in α7 mutant mice (Burkin et al., 2000; Pilgram et al., 2010).

1.8.2. Postnatal maturation of the NMJ

After the formation of nerve-muscle contacts, some of the axons withdraw, leaving one endplate per fibre. Evidence suggests that electrical activity from the input nerves regulate this process, with 'stronger' contacts persisting, and the 'weaker' ones withdrawing (Buffelli et al., 2003). Recently, it was demonstrated that the timing of action potential pulses, as well as the general neural activity has an influence on synaptic elimination. When two inputs were stimulated asynchronously (depolarisation spikes out of sync with each other), the elimination of one axon was promoted. However, when the spikes were synchronous, the two inputs persisted (Favero et al., 2012). Multiply innervated NMJs are likely to have slightly asynchronous patterns of activity, since the two inputs usually originate from different axons (Teriakidis et al., 2012). This is assumed to be unfavourable, as asynchronous stimulation would result in disorderly neurotransmitter release and action potential generation in the muscle. Thus, it may be that when the muscle or NMJ is on the receiving end of asynchronous synaptic activity, it initiates a programme of synapse elimination, and the strongest axon remains. In addition, signalling from Schwann cells has been shown to be a part of the process of elimination (Roche et al., 2014).

The maturation of the endplate into the elaborate pretzel shape occurs alongside axon withdrawal, and continues until the second or third postnatal week in the mouse. This is the result of synaptic area growth, combined with the elimination of certain areas to give the final pattern (Marques et al., 2000). Cleavage of agrin at these sites appears to be the key factor in

this process, suggesting a mechanism whereby loss of agrin results in a destabilisation of the postsynaptic apparatus, and thus elimination of contact areas. Expression of a cleavage-resistant form of agrin resulted in halted maturation, and overexpression of neurotrypsin, an agrin-cleaving enzyme resulted in excessive reorganisation (Bolliger et al., 2010). However, it is likely that in normal development, a different enzyme is responsible, since neurotrypsin is not normally expressed in muscle. Other studies show a role for muscle podosomes in eliminating areas of synaptic contact. These structures are invasive actin-rich processes with ECM-degrading enzymes at their tips. They are related to other actin-containing structures such as focal adhesions and lamellipodia, in that they share many of the same components, including integrins (Badowski et al., 2008; Luxenburg et al., 2006; Murphy and Courtneidge, 2011). Areas of AChR elimination coincide with podosome structures, and depletion of ECM components occurs at these sites, including laminins (Proszynski and Sanes, 2013; Proszynski et al., 2009). Podosomes may therefore displace AChRs, and degrade agrin at local sites, resulting in destabilisation of postsynaptic clustering. To what extent the nerve regulates this remodelling is unknown; however, cultured myotubes in the absence of nerve can form AChR plaques which subsequently reorganise into primitive pretzels, suggesting a major role for the muscle in this process (Kummer et al., 2004).

1.8.3. The role of the synaptic basal lamina in NMJ maturation

In addition to agrin, other basal lamina components play an instrumental part in several aspects of NMJ development. In particular, the laminins have been well characterised. In the first few weeks of postnatal life, laminins-α4, and α5 are present around the muscle membrane, alongside α2. In addition, the β2 subunit is present specifically at the NMJ. By the end of NMJ maturation, laminins-α4 and α5 have disappeared from the bulk of the muscle basal lamina, becoming restricted at the NMJ together with the β2 subunit. As such, the major laminin of the muscle fibre is laminin-211, and those of the NMJ -221, 421 and 521 (Patton, 2000). The interplay between the different laminins at the NMJ is complicated. Ablation of the β2 subunit, thus disabling the formation of all three laminin isoforms at the NMJ, results in a

very severe pathology (and is recapitulated in patients with mutations in this gene). Active zone formation is virtually abolished, as is maturation of the pretzel shape postsynaptic infolding; in addition, Schwann cells are able to invade parts of the synaptic space. These findings indicate a crucial role for synaptic laminins in major aspects of pre- and postsynaptic assembly, and for restricting glial cells to their extrasynaptic location (Maselli et al., 2009; Noakes et al., 1995). A schematic depicting known basal lamina interactions at the NMJ is found in **Fig 1.14**.

Absence of laminin-α2 causes a severe muscular dystrophy pathology, with membrane instability (similar to that seen in patients with mutations in this gene) (Holmberg and Durbeej, 2013). This makes specific NMJ defects hard to dissociate from the general underlying pathology. Analysis does show some decrease in postsynaptic folding in these mice, and EPP decrement during repetitive stimulation (Edwards et al., 1998; Tremblay et al., 1988). Laminin-α4 mutants are largely healthy and are viable. Their NMJs are mostly normal, but display active zones that are misaligned with the postsynaptic folds. The hypothesis is that laminin-α4 binds to active zones and acts as a spacer to regulate their positioning, and consistent with this, α4 is enriched at the interfold zones, and absent at the folds themselves (Patton et al., 2001). In addition, these mice have an accelerated ageing phenotype at the NMJs, with accumulation of degenerative characteristics at earlier ages than expected. These indicators of ageing include the increased fragmentation of the pretzel shape; nerve inputs with bulbous, varicose terminal boutons; terminal sprouting, with extra axons emerging and leaving the endplate; cases of polyneuronal innervation, with multiple inputs; and finally, denervation, characterised by the eventual withdrawal and vacation of nerve terminals at endplates (Samuel et al., 2012).

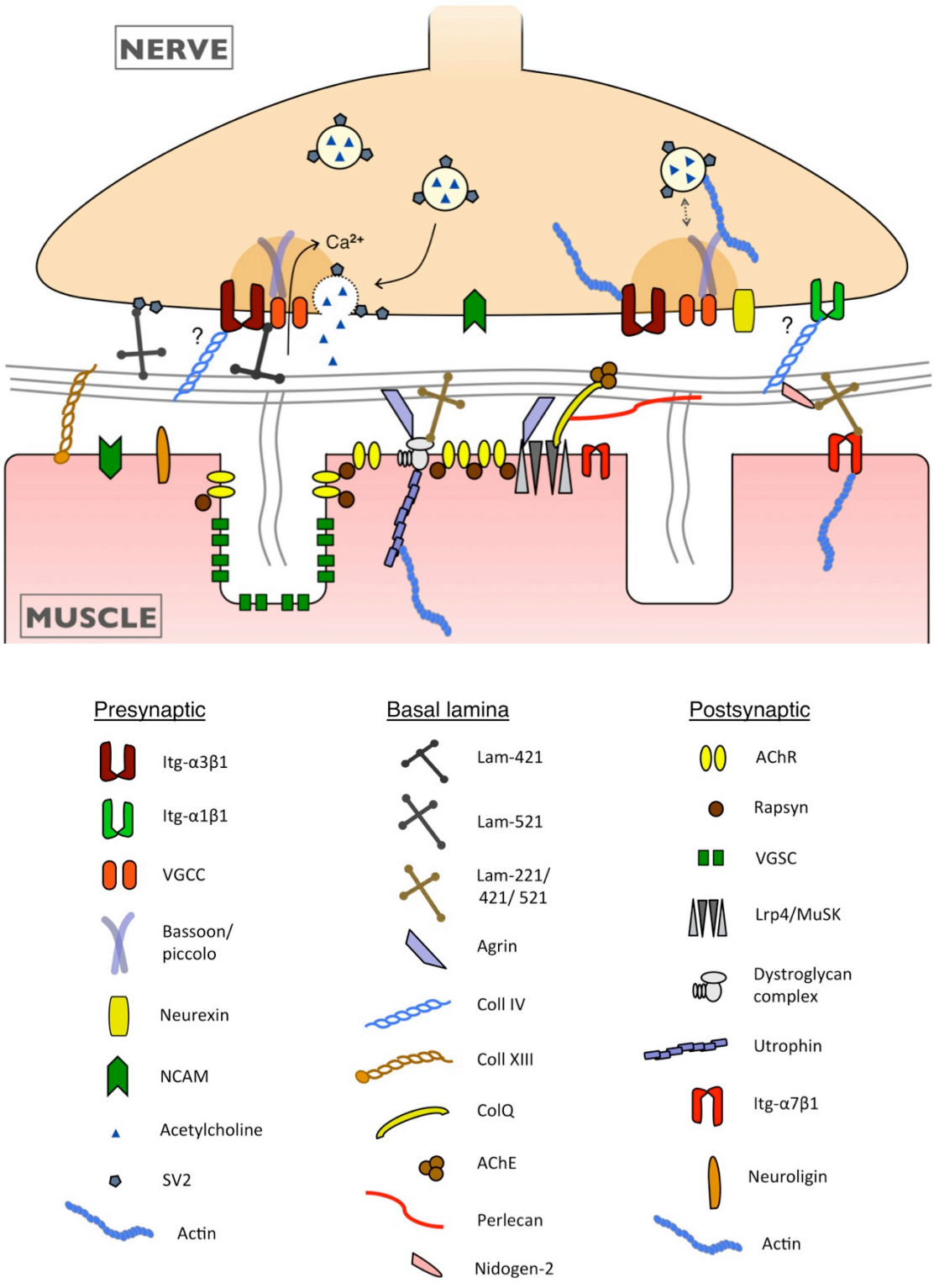

Fig 1.14. Basal lamina-receptor interactions at the NMJ. Hypothesised interactions are marked with question marks, and are based on the known ligand-binding affinities of particular receptors. Itg, integrin; VGCC, voltage-gated calcium channel; NCAM, neural cell adhesion molecule; SV2, synaptic vesicle protein 2; Lam, laminin; Coll, collagen; AChE,

acetylcholinesterase; AChR, acetylcholine receptor; VGSC, voltage-gated sodium channels; MuSK, muscle-specific kinase.

When laminin-α5 is ablated in skeletal muscle, the elaboration of NMJs into pretzels is normal, but delayed by around two weeks. Otherwise, NMJs are indistinguishable from wild types (Nishimune et al., 2008). Laminin-α5 can also form a complex with synaptic vesicle protein 2 (SV2). When vesicles are released, proteins on their surface become incorporated into the presynaptic membrane, and remain there until reuptake and recycling. The functional importance of this interaction is not known (Son et al., 2000). The subtle phenotypes obtained when laminin α subunits are knocked out individually are somewhat surprising, given the severe phenotype of the laminin-β2 mutants. A probable explanation is that the synaptic laminins are partially redundant, and can compensate for each other. Indeed, evidence for this was obtained when both laminin-α4 and α5 were knocked out. Instead of a delay in pretzel formation, a complete arrest of the process was apparent, indicating a functional overlap between these two proteins (Nishimune et al., 2008).

Other molecules of the synaptic basal lamina have been shown to have a role in NMJ development, in addition to the laminins. ColQ, the principle anchor of AChE, is known to interact with MuSK, through which it contributes to both expression and clustering of AChRs (Sigoillot et al., 2010). Nidogen-2, a crosslinking protein between collagen IV and laminin has a role in enhancing the maturation process, and maintaining NMJ integrity, since knockouts have higher proportions of both immature and fragmented endplates (Fox et al., 2008). A very similar phenotype is observed in the collagen XIII mutants. This protein is a collagen with a transmembrane region anchored to the sarcolemma, and like nidogen-2, promotes maturation and subsequent integrity of NMJs. In addition to increased fragmentation, NMJs with terminal sprouting are also observed (suggestive of degeneration), as well as cases of partial detachment of nerve terminal from the synaptic basal lamina, indicating a role in physical adhesion (Latvanlehto et al., 2010). Knockout studies in *Drosophila* have identified other basal lamina components that regulate the physical anchorage of nerve terminal at the NMJ. Partial

detachment was observed when collagen IV or lamininA was ablated (the latter being one of only two laminin trimers that exists in this organism) (Koper et al., 2012; Prokop et al., 1998). Patients with laminin-β2 mutations also display a similar phenotype of partial nerve retraction, suggesting a role for multiple basal lamina proteins in mediating this attachment (Maselli et al., 2009).

1.8.4. The role of adhesion receptors in NMJ maturation

While much is known about the basal lamina components and their roles in NMJ development, less is known about the receptors that mediate their effects. There are several known cell surface receptors through which the synaptic laminins act. Both the N- and P/Q VGCCs have regions which can interact with laminin-β2, and this interaction has been shown to initiate active zone formation, with the VGCCs linking to bassoon and CAST on the internal side (Chen et al., 2011; Nishimune et al., 2004). On the postsynaptic side, dystroglycan has been shown to be a key mediator of topological organisation and junctional folding, as well as AChR clustering. Skeletal muscle-specific knockout of dystroglycan results in an arrest of the formation of the pretzel, a phenotype that is similar to the laminin-α4/α5 double mutant (Nishimune et al., 2008). Mice and patients with defects in dystroglycan processing display a reduced number of folds (Taniguchi et al., 2006). Downstream of dystroglycan, there are various components that appear to mediate different aspects of this receptor's function. Utrophin-deficient mice display a relatively mild reduction in postsynaptic folding, but otherwise develop normally (Deconinck et al., 1997; Grady et al., 1997). Absence of dystrophin leads to muscular dystrophy, and increased fragmentation of endplates; however this is observed in various other models of muscular dystrophy, and also when muscle fibres undergo degeneration/regeneration, and might therefore be caused by fibre turnover (Rudolf et al., 2014). α-dystrobrevin mutants have subtle defects, including altered topology and AChRs that are more evenly distributed throughout the depths of the postsynaptic folds, rather than being concentrated at the crests (Grady et al., 2000). Double knockouts for utrophin and α-dystrobrevin display more severe defects, with almost complete absence of postsynaptic folds,

indicating that α-dystrobrevin must play a redundant function with utrophin for the formation of these structures (Patton et al., 2001).

Other receptors are present at the NMJ, but it is not clear which basal lamina proteins they interact with. Neural cell adhesion molecule (NCAM) is present on both pre- and postsynaptic specialisations. Knockout of this protein in mice results in several NMJ defects, including smaller size, and a delay in both synapse elimination and accumulation of synaptic vesicles. Electrophysiological defects include a greater rate of decrement during repetitive stimulation, and reduced STF (Rafuse et al., 2000). Basal cell adhesion molecule (BCAM) is present on the postsynaptic side, and known to bind to laminins in other systems; however, knockout studies showed that it plays no clear role in gross NMJ development (Nishimune et al., 2008). Neurexin is a neuron-specific adhesion molecule that in central synapses binds to postsynaptic receptors across the cleft. At the NMJ, it is hypothesised to interact with the basal lamina (which is absent in central synapses). On the intracellular side, neurexins interact with synaptotagmin, CASK and Mint (components of the synaptic vesicle release machinery) (Biederer and Südhof, 2000). NMJs of knockout mice display electrophysiological defects including reduced quantal content (Sons et al., 2006). Finally, neuroligin is another receptor, present on the postsynaptic terminus. In central synapses it binds to NCAM across the cleft, although at the NMJ, it is likely to interact with the basal lamina. In *Drosophila*, it is required for the growth and maturation of postsynaptic apparatus at the NMJ (Banovic et al., 2010; Sun et al., 2011).

Integrins are also known to be present at NMJs. Studies show that integrin-α1, which dimerises with the β1 subunit to form a collagen receptor, is present at the presynaptic terminus (Martin et al., 1996b). In addition, integrin-α3β1 is found in the active zones of the NMJ, and in the *Torpedo* electric organ has been shown to complex with laminin-α4 and active zone components, including VGCCs (Carlson et al., 2010a; Cohen et al., 2000a). On the postsynaptic side, integrin-α7β1 is present with all three intracellular (A-C) splice variants of the α7 chain (Martin et al., 1996b). The function of these proteins is not understood, although integrin-α7β1 modulates agrin-induced AChR clustering *in vitro* (Burkin et al., 2000). Studies in *Drosophila*

have revealed roles for integrin homologs at the NMJ. The *Drosophila* genome encodes 5 α and 2 β integrin subunits. Knockout of one of the β subunit homologs resulted in the failure of NMJs to elaborate into the mature topological structure(Beumer et al., 2002). *Volado* mutants (which cannot encode two of the integrin α subunits) display defects in neurotransmission, including reduced STF (Rohrbough et al., 2000).

Other studies demonstrate roles for unknown integrins in various aspects of NMJ function, by using RGD (arginine-glycine-aspartate) sequence-containing peptides to prevent integrin engagement with the basal lamina, or antibodies to block integrin-β1. Studies at the frog NMJ show a role for integrins in the modulation of neurotransmitter release in response to muscle stretch, highlighting the importance of integrins as mechanoreceptors. When the muscle is stretched beyond its resting length, MEPP frequency and quantal content are increased (Chen and Grinnell, 1995; Fatt and Katz, 1952). This effect is immediate but also reversible, and depends on integrins; blockade of integrins markedly reduces the modulation. At the frog NMJ, EPPs are often subthreshold, possibly due to the limited extent of postsynaptic folding, and thus stretch modulation may be a mechanism whereby neurotransmission can be amplified on an activity-dependent basis (Grinnell et al., 2004). In the muscles that have been investigated in mammals (almost entirely performed on the diaphragm), stretch modulation does not appear to be a prominent feature at the NMJ. This may be due to the larger extent of postsynaptic folding compared to NMJs of the frog, rendering further amplification unnecessary (Grinnell et al., 2004; Hutter and Trautwein, 1956).

Whether or not integrins play a role in mammalian stretch modulation at the NMJ, they have been demonstrated to regulate synaptic activity in early postnatal life. At around day 5 in the rat, ChAT is upregulated, coinciding with increased neurotransmitter release. At this time, motoneurons display increased survival in response to nerve crush injury. In support of the link between neurotransmitter release and motoneuron survival, the artificial upregulation of

synaptic activity by aminopyridines renders neonatal motoneurons more resistant to this injury at earlier stages. The effect on ChAT activity and motoneuron survival were both dependent on integrins. This raises the possibility of a mechanical and/or signalling link between integrins, presynaptic neurotransmitter release and motoneuron survival, during the first days of muscle activity (Greensmith et al., 1996; Wong et al., 1999).

1.9. Disorders of the NMJ

Over the last few decades, the molecular mechanisms of NMJ development, neurotransmission and integrity have been well characterised, but there are still many unknowns. Even so, this knowledge has greatly increased our understanding, diagnosis and treatment of NMJ disorders. The spectrum of NMJ disorders includes myasthenic syndromes of both autoimmune and genetic origin, toxicity associated with botulism, and neurodegenerative diseases.

1.9.1. Myasthenic syndromes

Autoimmune myasthenia

A subset of disorders known as myasthenia or myasthenic syndromes are responsible for reduced efficiency of neurotransmission at the NMJ. These usually reduce the synaptic efficiency by lowering the safety factor, thus increasing the likelihood of EPPs being subthreshold; the result is muscle weakness (Wood and Slater, 2001). In addition, there is frequently a greater extent of decrement during repetitive stimulation, resulting in a fatigable weakness phenotype, whereby subthreshold neurotransmission is reached quicker during muscle exertion (Wood and Slater, 2001). There are two known origins for myasthenic disorders, one being autoimmune, and the other being genetic. Of the former category, there are two major types: myasthenia gravis, and Lambert-Eaton myasthenic syndrome (LEMS). Genetic forms of myasthenia usually present at birth, and are commonly known as congenital

myasthenic syndromes (CMS). A wide panel of genes encoding for NMJ proteins are implicated in this form of the disease, with mutations in more and more genes being discovered (Spillane et al., 2010).

Myasthenia gravis is caused by an autoimmune response to a variety of postsynaptic NMJ proteins. The majority of cases (~80%) are caused by autoantibodies to AChRs, but more recently, other targets have been identified: MuSK, Lrp4 and cortactin (the latter being an effector in the actin-mediated trafficking of AChRs to the membrane) (Gallardo et al., 2014; Li et al., 2013). However, a small proportion of patients are seronegative; that is, despite the autoimmune origins of their disease, the targets of the antibodies are not known. Myasthenia gravis has a prevalence of around 15 in 100,000, although it is thought to be underdiagnosed in the elderly. It is more common in females than males in the younger population, with a reverse pattern in the older population. Apart from causing disruption of AChRs and/or its clustering pathways, autoantibodies also cause damage to the postsynaptic membrane, further exacerbating the pathology. Eye muscles are usually the most affected, and often are the first to be involved, with the vast majority of these cases subsequently becoming generalised. Characteristic drooping of the eyelids (ptosis) is a symptom of ocular weakness, and is often an early sign of the disease. Other common diagnostic indicators include decrement on repetitive nerve stimulation, increased jitter (variation in latency between stimulus and response), and sometimes failure of the nerve to depolarise the muscle. The latter two are indicative of decreased reliability of neurotransmission (Spillane et al., 2010).

LEMS is more rare than myasthenia gravis, and has no difference in prevalence between men and women. The vast majority of cases have detectable autoantibodies against P/Q VGCCs at the presynaptic membrane. As a result, neurotransmitter release is greatly reduced, but often increases slightly on repetitive nerve stimulation, in contrast to myasthenia gravis; this is thought to be due to alterations in STF. Muscles are therefore weak, but do not fatigue during

continuous exertion. LEMS is often associated with small cell lung carcinoma, and in these cases, the autoantibodies are thought to arise as an anti-tumour mechanism against channels in the lung cells (Petty, 2007).

Congenital myasthenic syndromes (CMS)

Cases of CMS are rare, but like LEMS, are thought to be underdiagnosed. In Europe, the known prevalence is around 1 in 500,000. The majority of the 19 known causative genes encode for postsynaptic proteins, but 3 encode for basal lamina proteins, and 1 for a presynaptic protein. However, around 40-50% of cases have no known genetic diagnosis, suggesting the involvement of other genes. Mutations that affect postsynaptic proteins have been found in genes that encode several of the AChR subunits, rapsyn, MuSK, DOK7, sodium channels, and plectin 1. CMS-causing mutations have also been found in genes encoding for the basal lamina proteins ColQ, laminin-β2 and agrin. Genes encoding for presynaptic proteins have also been implicated in CMS, with mutations identified in ChAT and synaptotagmin-2 (Abicht et al., 2012; Maselli et al., 2012). Finally several mutations have been found in genes encoding for glycosyltransferases – *DPAGT1*, *GFPT1*, *ALG2* and *ALG14*. These encode proteins that are involved in the glycosylation of targets at the synaptic cleft, including AChRs, and defects in these genes often cause reduced AChR trafficking and membrane insertion (Hantaï et al., 2013; Houlden, 2013; Sumikawa and Miledi, 1989). However, due to the complexity of post-translational modification of cell surface receptors and basal lamina components, it is possible that these proteins are involved in the glycosylation of multiple targets, and that potentially other glycosyltransferases are involved in NMJ disorders.

1.9.2. Treatment of myasthenic syndromes

Therapeutic strategies for myasthenic syndromes vary, depending on the type of disease and the patient's individual response to therapy. Inhibitors of AChE are commonly used to treat

myasthenia gravis, resulting in a potentiation of the acetylcholine signal, and partial recovery of neurotransmission. These drugs include pyridostigmine and neostigmine. Immunosuppression to mitigate the patient's autoimmune response is also a common therapeutic strategy, usually accomplished with corticosteroids. Since respiratory muscles are often affected, ventilatory care may be necessary in many cases. The thymus has a major role in the autoimmune pathogenesis of myasthenia gravis, and abnormalities of the thymus are common. In around 10% of cases, myasthenia gravis is associated with thymoma, and often thymectomy is sought as a treatment for this (Spillane et al., 2010).

LEMS patients usually only respond moderately well to AChE inhibitors, and are usually treated primarily with other drugs, including aminopyridines. These drugs block K^+ channels in motoneuron axons, thus prolonging action potentials and neurotransmitter release (Petty, 2007). Treatment of CMS is often more complex, and depends on the gene involved. In the cases where AChRs or the AChR clustering pathway are affected, aminopyridines and AChE inhibitors can cause improvement, by potentiating the release and persistence of neurotransmitter (Abicht et al., 2012; Hantaï et al., 2013). However, in patients with ColQ mutations, there is a deficiency of AChE, and consequently muscles suffer from overstimulation. This results in excessive influx of ions through AChRs, causing damage and degeneration of endplates. Similar pathology is observed in patients with slow channel mutations of AChRs, which prolong ion entry. Treatment with AChE inhibitors or aminopyridines may therefore worsen the symptoms of these patients, and other treatments should be sought. Ephedrine and salbutamol, two β2-adrenergic receptor agonists, have been shown to improve symptoms in patients with ColQ mutations through unknown mechanisms; however an effect on quantal release or AChR kinetics is suggested (Bestue-Cardiel et al., 2005; Chan et al., 2012). In contrast, patients with slow channel mutations have benefited from drugs that partially block AChRs (often referred to as open channel blockers) such as fluoxetine or quinidine (Finlayson et al., 2013; Webster et al., 2013). While drugs can modulate elements of neurotransmission for therapeutic benefit, the NMJ also exhibits a certain extent of plasticity,

and can partially compensate for loss of efficiency. NMJs affected by myasthenia gravis often display increased quantal content, presumably in an attempt to overcome the defects in the postsynaptic apparatus (Plomp et al., 1995). In AChR-deficient CMS, there is often an increase in the developmental γ subunit, which displays longer opening times, and may provide a compensatory effect (Beeson et al., 1998).

1.9.3. Other disorders affecting the NMJ

In addition to myasthenic syndromes there are other disorders that affect the NMJ, including botulism (caused by the toxin from *Clostridium botulinum*). This is a rare but serious condition, caused by the presence of the bacterium in food, or by its infection of wounds. The botulinum toxin affects the presynaptic termini of NMJs by cleaving SNARE proteins, and neurophysiological symptoms are similar to LEMS (Rossetto et al., 2014; Spillane et al., 2010). Botulism is commonly associated with descending paralysis, and loss of reflexes. Treatment of patients with antitoxin and intensive care management has resulted in a marked decrease in mortality (Spillane et al., 2010). Additionally, some neurodegenerative diseases feature an NMJ involvement. Amyotrophic lateral sclerosis is a degenerative disorder affecting the motoneurons, and evidence suggests that alterations at the NMJs may precede synapse disassembly in the early stages of the disease (Moloney et al., 2014). In spinal muscular atrophy, a genetic disorder which affects infants (except in very mild, adult-onset forms), motoneuron degeneration and eventual denervation occurs. This process again seems to begin with NMJ alterations, including a lack of maturation (Goulet et al., 2013). Another disorder with an NMJ involvement is sarcopenia, the age-related decline in muscle mass and neuromuscular function, which will be discussed in the next section.

1.10. Sarcopenia

Sarcopenia is a disorder that has been hard to define. Its name derives from the Greek, and literally means "poverty of the flesh". A decline in various systems may contribute to poor neuromuscular function associated with ageing, traditionally including the muscle, the motoneuron and the NMJ. However, general frailty and mobility is affected by changes in bone mass and density (osteoporosis), the joints (arthritis), and may also involve the tendons, blood supply and central motor systems. In addition, a decline in muscle mass may be caused by other conditions, including cirrhosis and cancer, the latter phenomenon being termed cachexia. Several working groups have attempted to define sarcopenia, and stress is usually placed on it being the direct result of ageing, rather than any other contributing disease (Cruz-Jentoft et al., 2010). Taken together, sarcopenia may be understood as a major component of the frailty and loss of mobility associated with ageing (Alchin, 2014; Morley et al., 2014).

The impact of sarcopenia on society and the economy is huge, and has been emerging as a major health concern in recent years. This is particularly the case in the developed world, where there is an increasing elderly population. It was estimated that the healthcare costs of sarcopenia in the USA were around $18.5 billion for 2000 (Janssen et al., 2004). In addition to poor mobility, weakness and decreased quality of life, sarcopenia has a major influence on injuries, fractures and death in the elderly. Postural muscles are important for maintaining balance, and muscles of the limbs are important for righting or catching reflexes in response to a loss of balance, and therefore sarcopenia is a large contributor to accidents and falls in later life.

Characteristics of sarcopenia include changes in the muscle: atrophy (reduction in size) and degeneration of muscle fibres, and replacement with fatty or fibrotic tissue. Other histopathological features include increased heterogeneity in fibre size, and the grouping

together of fibres of the same type (in muscles that contain both type I and II fibres) (Andersen, 2003; Berger and Doherty, 2010). These changes are suggestive of rounds of muscle degeneration, regeneration and reinnervation. In addition, changes at the NMJ occur. These often manifest themselves in several ways: increased fragmentation of the endplate pretzel shape; faint AChR staining at NMJs; bulbous, varicose nerve inputs; terminal sprouting; multiple innervation of NMJs; and eventual denervation (Li et al., 2011; Rudolf et al., 2014; Samuel et al., 2012). Subsequent reinnervation of endplates occurs following this, and the gradual remodelling of the nerve patterning leads to a decrease in the number of motor units, as individual motoneurons become responsible for the control of more and more muscle fibres. Since motor units are recruited individually to allow different outputs of force generation, this remodelling may have an impact on the versatility and control of contraction (Ling et al., 2009). This section will focus mostly on the effects of sarcopenia on the NMJ.

Fragmentation, the most commonly occurring characteristic across populations of aged NMJs in mouse models (Li et al., 2011), appears to be brought about by two means. In a study that monitored individual NMJs in living mice over a ~26 month life span, NMJs were mostly found to be very stable over long periods of time, with very little remodelling. However, some underwent fairly sudden transitions from continuous pretzel to fragmented endplate. These changes corresponded with degeneration of the underlying segment of muscle fibre, followed by subsequent regeneration (as observed by central nuclei in the fibres at these locations). The assumption is that when the nerve reinnervates the newly regenerated fibre, the NMJ acquires a different morphology. However, incidents of muscle damage and repair were not able to explain the fragmented appearance of all the NMJs studied (Li et al., 2011). Indeed, in some mouse models, including the laminin-α4 mutant, NMJs accumulate aged characteristics much earlier than their wild type counterparts. However, in these models, there is no underlying muscle pathology or central nucleation, suggesting an alternative mechanism for NMJ degeneration that is not dependent on turnover of the muscle fibre (Patton et al., 2001; Samuel et al., 2012).

The functional significance of NMJ ageing and morphological hallmarks is not very well understood, but is assumed to be indicative of a general progression towards degeneration and eventual denervation. On appearance, endplate fragmentation and faintening of AChRs resembles a 'breaking up' of the synapse, although it is not clear whether this is the case or not in terms of the integrity of the NMJ. Terminal sprouting is probably a sign of NMJ dysfunction, and synaptic terminals attempting to find adjacent sites to innervate; indeed when synapse disassembly is induced via disruption of agrin or MuSK, terminal sprouting occurs (Punga et al., 2011; Samuel et al., 2012). This is also seen in other mutant models with NMJ defects (Latvanlehto et al., 2010; Wang et al., 2005). Multiple innervation is likely to be a sign of recent reinnervation following denervation, resembling the developmental patterning observed when NMJs first form (Teriakidis et al., 2012). Electrophysiological assessment of NMJs in aged animals has resulted in different findings, depending on the muscle studied. This variation may also be in part due to the wide range of morphological changes associated with the different NMJs within a muscle (and perhaps different stages of degeneration). Generally, it is accepted that a reduction in quantal content is the main defect, with some muscles displaying increased rundown during repetitive stimulation (Wood and Slater, 2001).

Recently, it was shown that changes in active zones occur at the NMJs of aged animals. The density of active zones at the NMJs of aged animals was decreased by around 30%; in addition, staining intensity of the active zone protein bassoon was decreased (Chen et al., 2012). In central synapses, bassoon maintains synaptic integrity, by preventing presynaptic proteins from being broken down by the ubiquitin-mediated degradation pathway (discussed previously in *Section 1.5.1., the active zone: recruitment, docking and priming of synaptic vesicles*) (Waites et al., 2013). Speculatively, a partial loss of bassoon may therefore explain or be related to the degeneration/disassembly seen at the NMJs of aged animals. Another more convincing indicator of synapse integrity in aged NMJs is agrin. As has been discussed previously, agrin disruption can induce synapse disassembly and excessive remodelling of endplates (Bolliger et al., 2010; Samuel et al., 2012). When the cleavage and inactivation of

agrin was upregulated in mice, an ageing phenotype was conferred on the NMJs (Bütikofer et al., 2011). Interestingly, it also brought about sarcopenic changes in muscle fibres, indicating that agrin might also play a role outside of the NMJ. Patients with sarcopenia also have increased levels of cleaved agrin fragments in their serum, suggesting that inactivation of agrin may be both a diagnostic marker and a cause of this condition (Drey et al., 2013).

Lack of exercise has long known to be a risk factor for sarcopenia, and increased exercise can ameliorate symptoms (Favier et al., 2008; Rudolf et al., 2014; Valdez et al., 2010). In mouse models, one month of exercise reversed many of the morphological characteristics of aged NMJs: fragmentation, faintening of AChRs, denervation and terminal sprouting. Bassoon immunoreactivity also increased, to similar levels as in young mice (Nishimune et al., 2012, 2014; Valdez et al., 2010). Apart from short-term reversal, physical activity throughout life is particularly effective in mitigating the effects of sarcopenia (Power et al., 2010). High-intensity exercise is well known to have multiple effects on the NMJs of healthy adults (prior to ageing). The size of endplates grows, and this is correlated with an increase in quantal content. In addition, the pretzel shape of the NMJ usually becomes more compact, with more of the AChR-negative areas becoming occupied, and additional complexity being added. Spontaneous neurotransmitter release is reduced in frequency, and repetitive trains of stimuli show a reduced decrement (and thus NMJs are more fatigue-resistant). These electrophysiological effects suggest that exercise brings about plasticity of the synaptic vesicle release and/or recycling machinery (Deschenes et al., 2000, 2011). While exercise can prevent and reverse the ageing-associated changes at the NMJ, so can life-long calorie restriction (in mouse studies), suggesting a role for metabolism in sarcopenia and neuromuscular health (Valdez et al., 2010).

The precise contribution of NMJ defects to the sarcopenic phenotype, versus those of the muscle is not known. Interestingly, although exercise significantly improves neuromuscular

performance in sarcopenia, the increase in muscle mass is only modest. In contrast, the extent of plasticity and remodelling of the NMJ is quite striking. This suggests that the effect of exercise on sarcopenia is mediated in large part through changes at the NMJ (Vandervoort, 2002).

1.11. Rationale and premise of this project

Integrins, as discussed earlier, are a widely expressed and versatile family of cell surface receptors, both in their ability to bind a variety of ECM ligands, and in their range of functions. At the interface of both the ECM and the internal cytoskeleton, they are able to communicate signals from the outside to the inside of the cell, and vice versa. Key functions of integrins on a cellular level include the regulation of cell shape, migration, invasion, survival, differentiation, proliferation, structural integrity and mechanical linkage to the ECM. On the organ and tissue scale, integrins are crucial for many functions: development, including cell organisation and patterning; would healing and repair of tissues; interactions and recognition in immune cells; blood clotting; structural and mechanical stability of tissues; and function and plasticity of synapses (Campbell and Humphries, 2011).

While integrins are widely studied, there is something of a paucity of knowledge regarding their roles in the neuromuscular system. As discussed in detail in *Section 1.3., development of skeletal muscle*, there are various integrins that are developmentally regulated during somitogenesis and myogenesis, often appearing in combination with their preferred ECM ligand(s). Yet, the functional relevance of these interactions is not well understood. This is likely to be caused by two factors: many of the integrin knockout models show very early embryonic lethality, making the study of their functions during and after somitogenesis difficult; and the large number of integrin subunits allows for partial redundancy and compensation of function. In the fully developed neuromuscular system, fewer integrins

appear to be present, with the best characterised being integrin-α7β1. Its major role is in structural integrity at the MTJ, and appears to contribute relatively little to costameric stability, despite its presence there (Hodges et al., 1997). However, evidence suggests that its upregulation can play a compensatory role at the costamere, when other proteins are lost (Guo et al., 2006). An additional role for integrin-α7β1 is in transducing downstream signalling pathways in response to exercise, although whether this is mediated primarily at its position at the MTJ or the costamere (or both) is not known (Boppart et al., 2006).

Integrin-α5 also appears to be crucial for muscle fibre stability, with disruption causing a muscular dystrophy phenotype in mice (Taverna et al., 1998). Localisation of integrin-α5 in adult muscle is unclear, although its expression pattern in early myogenesis would suggest a role in the establishment of the MTJ (Bajanca et al., 2004). However, this structure appears to develop normally in mutant mice (Taverna et al., 1998). The most prominent feature of myogenesis is the fusion of myoblasts to form multinucleated myofibres, and integrins have an essential role in this, since genetic ablation of integrin-β1 or associated proteins markedly impairs this process (Conti et al., 2009; Schwander et al., 2003). *In vitro* studies have implicated two potential integrin α binding partners for integrin-β1 in myoblast fusion: α3 and α9 (Brzóska et al., 2006; Lafuste et al., 2005). In addition, studies in cultured myotubes suggest a role for integrin-α3 in the assembly of myofibrils, based on its alignment with these nascent structures (McDonald et al., 1995).

At the NMJ, integrins have also been shown to have major roles in development and function, although the dissection of individual isoforms has been difficult. In various *in vivo* models, roles for integrins at the NMJ include: maturation, effective STF, stretch-sensitive plasticity, and regulation of synaptic activity and motoneuron survival in early postnatal development (Greensmith et al., 1996; Grinnell et al., 2004; Rohrbough et al., 2000; Wong et al., 1999). At the mammalian NMJ, 3 known integrin α subunits are found: α1 (presynaptic) α3 (presynaptic,

active zone), and α7 (postsynaptic) (Martin et al., 1996a). These are known to specifically dimerise with integrin-β1, which is the main isoform in motoneuron and muscle (Thorsteinsdóttir et al., 2011). The functions of these integrin subunits are not clear, although *in vitro* work suggests that integrin-α7β1 might enhance the agrin-mediated clustering of the AChRs (Burkin et al., 2000). Immunoprecipitation studies in the *Torpedo* electric organ reveal that integrin-α3 binds to laminin-421 and active zone components, including VGCCs (Carlson et al., 2010a). With its suggested roles in myoblast fusion, myofibril assembly, and an as yet unknown aspect of NMJ function, integrin-α3 represents an interesting candidate for study. Ascertaining its role(s) *in vivo* will contribute to the understanding of the regulation and/or development of the neuromuscular system. Integrins are also arguably understudied in this system, with the vast majority of the focus placed on integrin-α7β1; even then, its function is only partially understood, and many of its roles in mechanotransduction, downstream signalling, and its relevance at the costamere and NMJ are unknown.

The generation of an integrin-α3 knockout mouse has allowed investigators to study this protein in various organs and tissues (Kreidberg et al., 1996). The first studies revealed a role for this protein in kidney and lung development, with mutants dying just after birth, presumably due to insufficient respiratory function. Increased stromal content, morphological defects in glomeruli, and lack of microvilli in ducts were the principle findings in the kidney. In lungs, a marked decrease in the branching of bronchioles was observed in mutants, as well as altered morphology of the epithelial cells (Kreidberg et al., 1996). Further studies revealed defects in the skin, including ECM disorganisation and blistering. Skin grafts from newborn integrin-α3 knockouts onto immunodeficient adult mice were performed, to study postnatal development. Marked defects in hair follicles were observed, with poor growth and stability, cytoskeletal abnormalities in keratinocytes, and increased deposition of basal lamina proteins (Conti et al., 2003). Other studies have pointed to roles of integrin-α3 in the brain. Conditional forebrain-specific knockouts have impaired working memory, and defects in long-term potentiation (LTP; a form of plasticity whereby the strength of synaptic transmission is

modulated over long periods of time) in the hippocampus; all other behavioural traits that were tested were normal (Chan et al., 2007). Another study which used mice that were heterozygous for a global integrin-α3 knockout (and were thus viable after birth), concluded that there was also a defect in LTP in the hippocampus, but that animals had no behavioural defects; however they did not use a test of working memory for this study (Chan et al., 2003). Structural alterations have also been observed in forebrain-specific conditional knockouts, which may act as an explanation for the aforementioned defects. These include a decline in dendritic branching size and complexity, and reduction in dendritic synapse number in the hippocampus (Kerrisk et al., 2013).

Recently, three patients with homozygous integrin-α3 mutations were reported, and as in mice, there were signs of severe lung, kidney and skin disease. The patients lived to ages between 2 and 19 months (Has et al., 2012). Normal gross anatomy of the brain was observed, and in the patient that was the most studied (age at death, 7.5 months), cognitive development was normal. However, the study did report 'mild muscular hypotonia' and 'delayed neurological development' in this patient, although no further details were given (Has et al., 2012). To investigate the function(s) of integrin-α3 in the neuromuscular system, I used the integrin-α3 knockout mouse (Kreidberg et al., 1996).

1.12. Aims and scope of this project

Firstly, the role of integrin-α3 in muscle development will be studied. Wild type embryos will be harvested at various stages of development (E13.5 – E18.5, and adult), to assess whether integrin-α3 is expressed in muscle. Embryos of wild type and integrin-$\alpha3^{-/-}$ genotype will then be compared, to determine whether there are differences in muscle structure, morphology and immunoreactivity of key proteins. In addition, ultrastructural analysis using EM will be made.

Secondly, the role of integrin-α3 in NMJ development will be investigated, using E18.5 embryos. Immunohistochemistry of basal lamina and active zone proteins will be carried out to determine whether there are differences in localisation between wild type and integrin-$\alpha3^{-/-}$ NMJs. Innervation patterning in whole mount muscles will be examined, as well as ultrastructural analysis of NMJs using EM. If there are observed differences in NMJ development between wild type and integrin-$\alpha3^{-/-}$ animals, then electrophysiological characterisation may be carried out.

Thirdly, the role of integrin-α3 in adult NMJs will be studied. Again, key basal lamina and active zone proteins will be analysed using immunohistochemistry, comparing wild type and integrin-α3 mutant tissue. Morphological and ultrastructural features will also be examined. Functional tests will then be carried out, to assess electrophysiological parameters under normal and reduced external Ca^{2+} conditions; *in vivo* grip strength tests will then be used to assess overall function of the neuromuscular system in integrin-α3 mutants.

Previous studies have utilised integrin-β1 knockouts to study the role of integrins in a variety of tissues, since these animals lack a broad spectrum of functional integrins. However, these animals die shortly after implantation, making it impossible to assess the contribution of integrin-β1 to organogenesis. Therefore, conditional knockouts of integrin-β1 have been used to study the function of this protein in e.g. muscle and motoneurons (Schwander et al., 2003, 2004). These studies have established muscle-derived integrin-β1 as a key regulator of myoblast fusion, sarcomere assembly and innervation patterning; however, potential roles of integrin-β1 in motoneurons were unclear, as no obvious defects in muscle innervation or expression of key NMJ proteins were observed.

Other studies have utilised knockouts of integrin-α5 and -α7 to study the role of specific α-β1 dimers in muscle (Mayer, 2003; Taverna et al., 1998); however, no such studies have used knockouts of integrin-α3. Due to the technical and logistical difficulties of generating and

maintaining conditional knockouts of integrin-β1, and the comprehensive analyses already carried out on these animals, we chose to utilise integrin-α3 knockouts. This allowed the assessment of a specific integrin in neuromuscular development and function, and represented a candidate that had not yet been studied in this context. However, given that the roles of integrin-β1 in motoneurons have perhaps not been fully addressed, this may offer an interesting avenue for future exploration.

Work excluded from this thesis

I also carried out two additional projects during my PhD, which were taken to partial completion. The first project was concerned with the role of integrins in myoblast fusion. A previous study had utilised *Drosophila* to study the ultrastructural aspects of myoblast fusion *in vivo* (Sens et al., 2010). The investigators found podosome-like processes extending between adjacent myoblasts, which appeared to result in the formation of a fusion pore between the two cell membranes. Podosomes are actin containing cellular processes, normally associated with the degradation of ECM. Integrins are considered to be the master regulators of podosome formation, activating a number of pathways required for the modulation of cytoskeletal dynamics (Murphy and Courtneidge, 2011). Using a myoblast cell line, and primary cultures isolated from mouse embryos, I begun to investigate the role of integrins and podosomes in myoblast fusion. Cells were cultured and differentiated into myotubes, either in the presence or absence of siRNAs targeted to integrin-β1, vinculin, paxillin or Tks5. Vinculin and paxillin are key integrin-associated adaptors that regulate downstream pathways for actin assembly (Hu and Luo, 2013). Tks5 is a large scaffold protein which mediates the final steps of podosome assembly (Seals et al., 2005). Using both the cell line and primary myoblasts, I found that all four proteins were required for cell fusion, with siRNA knockdown of each protein resulting in the near abolition of myotubes. In addition, primary cultures displayed immunoreactivity of integrin-β1, paxillin, actin and Tks5 at the contacting edges of myoblasts. Finally, I began to characterise the signalling pathways that might be involved in myoblast fusion. As integrin-β1 likely represents the key upstream mediator of both podosome assembly and myoblast fusion, I treated the myoblast cell line with siRNA to this protein.

Western blotting revealed alterations in the levels of phosphorylated signalling proteins. Specifically, the phosphorylated forms of Src and FAK, two key kinases downstream of integrins, were markedly reduced in response to integrin-β1 knockdown. Further work might involve ultrastructural and/or super-resolution analysis of fusing myoblasts, to determine whether the structural elements of podosomes are present; also the further dissection of potential signalling pathways to provide mechanistic insight.

A second project aimed to characterise the role of integrin-associated molecules in muscle development, using the zebrafish as a model. Given that paxillin was shown to be required for myoblast fusion *in vitro* (see above), I designed morpholinos to this protein, and injected them into zebrafish oocytes to achieve knockdown. Somewhat surprisingly, myoblast fusion appeared to be unaffected, with somites forming normal myotubes with sarcomeres, as visualised with actin staining. However, fish displayed defects commonly observed when components of the DGC or integrin axis were disrupted, including curved or bent tail, reduced ability to swim, and somite boundaries with curved, rather than chevron shape (Bassett and Currie, 2003; Postel et al., 2008). In addition, somite boundaries of morpholino-treated fish showed almost no immunoreactivity to paxillin. This project was no longer pursued, although I did contribute work towards a collaboration with the Yalda Jamshidi group at St George's University of London. I carried out microinjections of zebrafish oocytes with a morpholino to TCEA3, a novel transcription factor with suspected roles in muscle development. In addition, I carried out EM imaging to reveal detachment between muscle fibre and MTJ in morpholino-treated fish. This work is currently being drafted as a manuscript. With regards to this thesis, I felt that these projects were somewhat unfinished and not contiguous with the rest of the work, so I decided to exclude them.

2. Materials and methods

All work was carried out by the author, except where indicated (named experimenter in bold).

2.1. Materials

Item	Manufacturer
100 bp DNA ladder	Life Technologies, Paisley, UK
2,3-butanedione monoxime	Sigma Aldrich, Poole, UK
α-bungarotoxin, Alexa 488- or 594-conjugated	Life Technologies
# μ-conotoxin GIIIB	Alomone labs, Jerusalem, Israel
Acetone	VWR, Lutterworth, UK
* Acetonitrile	VWR
Agarose	Appleton Woods, Birmingham, UK
^ Automatic syringe pump perfuser	Hugo Sachs Elektronik-Harvard Apparatus, March-Hugstetten, Germany
Autoquant X3 imaging software	Autoquant Imaging Inc, Rockville, MD, USA
# Axoclamp-2A amplifier	Molecular Devices, California, USA
# Borosilicate glass electrode (10–15 MΩ resistance)	Harvard Apparatus, Edenbridge, UK
Bovine serum albumin (BSA)	Sigma Aldrich
* Cacodylic acid	Sigma Aldrich
§ Chatillon Grip Strength Meter	Columbia Instruments, Columbus, OH
Confocal microscope (LSM 710)	Zeiss, Cambridge, UK
Coverslips, 0.2 mm thick, Nunc Thermanox	Thermo Scientific, Loughborough, UK
Coverslips, high precision, 0.17 mm thick	Paul Marienfeld, Lauda-Königshofen, Germany
Cryostat (CM1850)	Leica, Milton Keynes, UK
Custodial HTK (Histidine-tryptophan-ketoglutarate) organ preservation solution	Essential Pharmaceuticals**,** Ewing, NJ, USA
DNA Polymerase from *Thermus Aquaticus* (Taq polymerase)	Life Technologies
dNTP (deoxynucleotide triphosphate) mix	Life Technologies
DPX mounting medium	VWR
Eosin	VWR

Ethanol	VWR
Ethylenediaminetetraacetic acid (EDTA)	Sigma
Fluorescent beads, 1 µm (Alexa 488- and 594-conjugated)	Life Technologies
Fluorescence mounting medium	Dako, Ely, UK
Gatan Microscopy Suite (EM)	Gatan, Abingdon, UK
Gel loading buffer	Thermo Scientific
Gel reader, ultraviolet, GenoSmart	VWR
Glutaraldehyde	Sigma Aldrich
Glycerol	Thermo Scientific
Goat serum	Sigma
Graphpad Prism 5 software	Graphpad Software, La Jolla, CA, USA
Gum tragacanth	Fisher Scientific, Loughborough, UK
Haematoxylin, Harris	Raymond A Lamb, Eastbourne, UK
Histo-Clear	National Diagnostics, Hessle, UK)
Hoechst dye	Life Technologies
Horse serum	GE Healthcare, Little Chalfont, UK
Hydrophobic PAP pen	Abcam, Cambridge, UK
Image J software	National Institutes of Health, Bethesda, MD, USA. Rasband WS, http://imagej.nih.gov/ij/
Isopentane	VWR
# Krebs-Henseleit buffer (Sigma Aldrich)	Sigma Aldrich
Magnesium chloride ($MgCl_2$)	Life Technologies
Metamorph Advanced Acquisition software	Molecular Devices
Methanol	VWR
# Micromanipulation rig	Scientifica, Maidenhead, UK
Microscope slides	VWR
Mouse-on-mouse block	Vector Laboratories, Peterborough, UK
OCT embedding medium	Raymond A Lamb
* Osmium Tetroxide (OsO_4)	Sigma Aldrich
Paraformaldehyde (PFA)	Thermo Scientific
# pCLAMP 9 software	Molecular Devices
PCR reaction buffer	Life Technologies
Phosphate buffered saline (PBS)	Sigma Aldrich
# Potassium chloride (KCl)	Sigma Aldrich

Primers (for details, see *Section 2.4., genotyping of integrin-α3 knockout mice by polymerase chain reaction (PCR)*)	Life Technologies
Prolong Gold Antifade mounting medium (Life Technologies)	Life Technologies
Secondary antibodies, Alexa 488-, 594-, 647-conjugated	Life Technologies
Sodium hydroxide (NaOH)	Sigma Aldrich
# Solid-state square wave pulse generator	Grass Instruments S48, Quincy, MA, USA
* Spurr's resin	Sigma Aldrich
# Stereomicroscope BX51WI	Olympus, Southend, UK
Sucrose	VWR
SYBR Safe	Life Technologies
# Sylgard	Dow Corning Europe, Seneffe, Belgium
* Transmission electron microscope (1010)	Jeol, Welwyn Garden City, UK
Tris/Borate/EDTA (TBE) buffer	Life Technologies
Tris-HCl	Sigma Aldrich
Triton X100	Sigma Aldrich
* Uranyl acetate	Sigma Aldrich
Veriti PCR thermal cycler	Applied Biosystems/Life Technologies
Widefield fluorescence microscope (DM4000)	Leica
Zen Software	Zeiss

Table 2.1. List of materials, reagents, equipment and software. All items were used by the author, with the exception of those marked with the following symbols: (*), used by Mark Turmaine at the UCL Biosciences Electron Microscopy Facility; (^), used by Bruce Williams for cardiac perfusion fixation, at the Barts Cancer Institute, Queen Mary University of London; (§), used by Dr Tanguy Lechertier and Dr Louise Reynolds at the Barts Cancer Institute; and (#), used by Dr Richard Webster for electrophysiology at the Weatherall Institute of Molecular Medicine, John Radcliffe Hospital, University of Oxford.

2.2. Antibodies

Antigen	Clone	Species	Dilution	Fixation	Cat #	Source
Acetylcholinest-erase (AChE)	ZR3	M IgG2b	1:20	PFA	GTX22802	Source Bioscience
Agrin	AF550	Gt	1:200	PFA	AF550	R & D Systems
Bassoon	SAP7 F407	M IgG2a	1:500	PFA	GTX13249	Source Bioscience
Collagen IV	-	Rb	1:400	PFA	ab6586	Abcam
* Dystrophin(Lu et al., 2005)	P7	Rb	1:1000	No fix		Partridge, T (Childrens' National Medical Centre, Washington, USA)
Fibronectin	-	Rb	1:100	PFA	ab23750	Abcam
* Integrin-α3(DiPersio et al., 1995)	8-4	Rb	1:200	MeOH/ PFA	-	Hynes, RO (Massachusetts Institute of Technology, Cambridge, MA, USA)
* Integrin-α7(Nawrotzki, 2003)	U31+	Rb	1:200	MeOH	-	Mayer, U (University of East Anglia, Norwich, UK)
* Integrin-β1(Nawrotzki, 2003)	U49+	Rb	1:400	MeOH	-	Mayer, U
Laminin (pan)	-	Rb	1:1000	PFA	L9393	Sigma Aldrich
Laminin-α4	-	Gt	1:400	Acetone	AF3837	R & D Systems
* Laminin-α5(Miner et al., 1997)	-	Rb	1:200	No fix	-	Miner, JH (Washington University, St Louis, MO, USA; gift from Dr Susan Brown, Royal Veterinary College, London).
Neurofilament 160kD chain	NN18	M IgG1	1:200	MeOH/ PFA	N5264	Sigma Aldrich
Perlecan	A7L6	Rat	1:5000	PFA	1948P	Merck Millipore
Piccolo	-	Rb	1:200	PFA	142 002	Synaptic Systems
Rapsyn	1234	M IgG1	1:200	PFA	GTX11423	Source Bioscience
SV2 (synaptic vesicle marker 2)	-	M IgG1	1:50	PFA	SV2	Developmental Studies Hybridoma Bank

Talin-2	68E7	M IgG2b	1:200	MeOH	ab105458	Abcam
Utrophin	DRP3/ 20C5	M IgG1	1:100	PFA	VP-U579	Vector Laboratories, Peterborough, UK
Vinculin	SPM 227	M IgG1	1:200	PFA	ab18058	Abcam
Voltage-gated calcium channel, P/Q-type (P/Q VGCC)	-	Rb	1:300	PFA	152 203	Synaptic Systems

Table 2.2. Antibodies used in the study, with the clone number (if monoclonal), species in which it was raised (and isotype if monoclonal), working dilution, fixative (5 mins PFA at room temp; 5 mins MeOH at -20°C; 10 mins acetone at -20°C); catalogue number and source. Antibodies marked with (*) are not commercially available, and were gifts from the investigators indicated in the source column. Manufacturer details: Source Bioscience, Nottingham, UK; R & D Systems, Abingdon, UK; Abcam, Cambridge, UK; Sigma Aldrich, Poole, UK; Merck Millipore, Darmstadt, Germany; Synaptic Systems, Goettingen, Germany; Developmental Studies Hybridoma Bank (DSHB), Iowa City, IA, USA. *Abbreviations: M, mouse; Rb; rabbit; Gt, goat.*

2.3. Integrin-α3 knockout mice

Mutant animals were originally generated by Kreidberg et al. (Kreidberg et al., 1996). Colonies had been established using a mixed C57BL6/129 background strain, and maintained under the project license of Prof. **Kairbaan Hodivala-Dilke** (Queen Mary University, London). Animals were housed at the Barts Cancer Institute, Queen Mary University of London, in accordance with the Animals (Scientific Procedures) Act 1986. Breeding and maintenance of the colonies was carried out by Dr. **Tanguy Lechertier**.

2.4. Genotyping of integrin-α3 knockout mice by polymerase chain reaction (PCR)

A protocol for genotyping the integrin-α3 knockout mice was developed by previous investigators (DiPersio et al., 1997). In mutant animals, the integrin-α3 transcript is disrupted by the insertion of a neomycin cassette into exon 7 of the gene. Thus, primers had been designed to distinguish between wild type and mutant genes, through the detection of the neomycin cassette. **Fig 2.1A** illustrates the strategy employed for the PCR reaction. There are two forward primers: one recognising a sequence of the integrin-α3 gene (the wild type primer), and another recognising a sequence in the neomycin cassette, further downstream (the mutant primer). There is one reverse primer, recognising a sequence in the integrin-α3 gene (the common primer). This is downstream of the forward primers, and thus downstream of the neomycin cassette inserted in the mutant gene. The sequences for the primers are as follows: wild type, 5'-CCGTCTATGTCTTCATGAACC-3'; mutant, 5'-GGGGAACTTCCTGACTAG-3'; common, 5'-GGAATCCATCCTGGTTGATGTC (Life Technologies, Paisley, UK). In the presence of the wild type gene, the wild type and common primers amplify a 130 bp sequence. In the presence of the mutant gene, this region of amplification is greatly lengthened, by the insertion of the ~1700 bp neomycin cassette. The extension phase of the PCR cycle (30 secs) does not allow adequate time for the detectable amplification of this product, due to its length. Instead, a different fragment is amplified in the presence of the mutant gene. The mutant forward primer recognises a sequence towards the 3' end of the neomycin cassette; together with the common primer, it amplifies a 285 bp sequence, consisting of part of the cassette and part of the integrin-α3 gene. When the amplified PCR products are separated by gel electrophoresis, wild type and mutant tissue produce bands at 130 and 285 bp, respectively. Heterozygous tissue possesses one of each gene, and thus produces both bands (**Fig 2.1B**).

To obtain genomic DNA for the purpose of genotyping, 4-5 mm snips were taken from the ends of the tails of embryos or adult mice. Tissue was lysed using the "hot sodium hydroxide and Tris" (HotSHOT) method (Truett et al., 2000). Buffer A, the alkaline lysis reagent, consists of 25

mM NaOH, and 0.2 mM Ethylenediaminetetraacetic acid (EDTA) in water. Buffer N, the neutralisation reagent, consists of 40 mM Tris-HCl in water. The pH is 12 for buffer A, and 5 for buffer N. Tail snips were placed in 0.2 ml PCR tubes, and 75 µl of buffer A was added. Following this, tubes were heated in a PCR thermal cycler machine for 30 mins at 95°C, to partially lyse the tissue. Neutralisation of the alkaline lysate was carried out after cooling, with the addition of 75 µl of buffer N. For the PCR reaction, 1 µl of this solution (containing the template DNA), was added to 19 µl of PCR mastermix, the recipe for which is below (**Table 2.3**):

	Stock concentration	Volume to use per reaction	Final concentration
Water	-	11.3 µl	-
PCR reaction buffer	10x	2 µl	1x
$MgCl_2$ solution	50 mM	0.6 µl	1.5 mM
dNTP (deoxynucleotide triphosphate) mix	2 mM	2 µl	0.2 mM
WT primer	100 µM	1 µl	5 µM
Mutant primer	100 µM	1 µl	5 µM
Common primer	100 µM	2 µl	10 µM
DNA Polymerase from *Thermus Aquaticus* (Taq polymerase)	5 U/µl	0.1 µl	0.025 U/ul (25 U/ml)

Table 2.3. Components of the PCR mastermix for amplification of genomic DNA. Quantities represent the amount required for one reaction (i.e. one extraction of genomic DNA).

After denaturation at 94°C for 2 mins, 30 cycles were performed, each consisting of: 30 secs at 94°C (denaturation), 40 secs at 55°C (annealing), and 30 secs at 72°C (extension). A 1.5% agarose gel was made in 1 x TBE buffer, and solubilised by heating at high power in the microwave for 1.5-2 mins. SYBR Safe DNA Gel Stain was added at 1:10,000, and the mixture

added to a gel tank with teeth etchers to form wells. After cooling and solidifying for 20 mins, 1x TBE buffer was added to cover the gel. 4 µl of glycerol/loading buffer was added to each tube of PCR product. 4 µl of 100bp DNA ladder was added to the first well of the gel, and the PCR products were added to each of the subsequent wells. A water only control was used (consisting of the PCR mastermix, but with no genomic DNA added). In addition, a positive control was used, consisting of DNA from a previously genotyped heterozygous animal, to allow both of the bands to be observed. Gels were imaged and photographed under UV light.

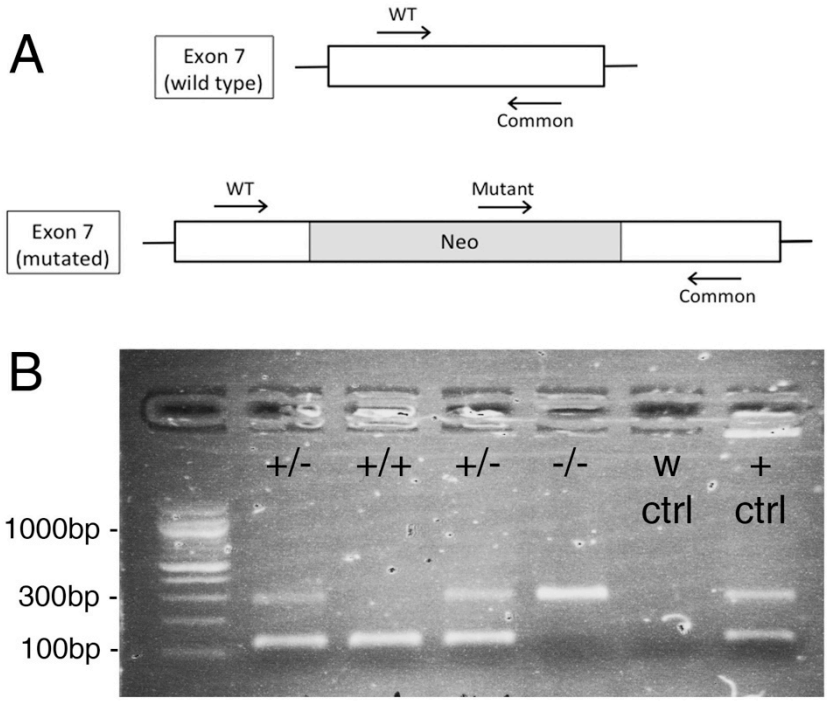

Fig 2.1. Genotyping integrin-α3 mice by polymerase chain reaction (PCR). (A) Schematic of exon 7 of wild type (top) and mutant (bottom) alleles of the integrin-α3 gene. Mutated genes have a ~1700 bp neomycin (Neo) cassette inserted into exon 7. PCR reactions were carried out as described previously (DiPersio et al., 1997), with three primers: wild type (WT), mutant and common. (B) primers amplify a 130 bp fragment from the wild type gene, and a 285 bp fragment from the mutant gene. +/+, +/- and -/- refer to PCR results from wild type, heterozygous and mutant animals, respectively. Water controls (w ctrl) containing no genomic DNA, and positive controls (+ ctrl) containing DNA from known heterozygotes, were included in each experiment.

2.5. Harvesting of tissue for immunohistochemistry (E13.5 – E18.5)

After sacrificing by decapitation, various tissues were taken for immunohistochemical analysis. Tissues were mounted on corks in 6% gum tragacanth in water. A plastic beaker was filled to ~3 cm with isopentane, and floated in liquid nitrogen until about half of the liquid had frozen. Mounted tissues were then frozen in the liquid phase for ~1.5 mins, before being transferred to -80°C.

For transverse sections of intercostal muscle, skin and lung, whole thoraxes were mounted with neck facing upwards. Sectioning was carried out at 50 μm intervals until the lung and ribcage were exposed. Cryosections were then taken and collected at 10 μm intervals, allowing all three tissues to be observed. For transverse sections of the right hemisphere of the diaphragm, thoraxes were mounted sideways, with the right flank facing upwards (i.e. with the spinal cord and sternum facing sideways, and ribs facing upwards). This orientation was necessary, as the muscle fibres of the diaphragm extend radially from the centre, outwards to the lateral parts of the ribcage. Sectioning was carried out at 50 μm intervals until the diaphragm was exposed. Cryosections were then taken and collected at 10 μm intervals.

Longitudinal sections of sternomastoid muscles were also prepared for immunostaining of integrin-α3 and other active zone proteins at the NMJ. These muscles run from the skull region at the side of the jaw, to the top of the sternum (one at each side of the jaw). This muscle is often used to study the morphology of NMJs, as it is accessible, relatively flat, and can therefore be easily mounted longitudinally; in addition, the NMJs are relatively large, making them easy to locate and image. Fixation of muscles soon after death, and cryoprotection with sucrose are necessary steps for the preservation of active zones (Chen et al., 2012). Animals were sacrificed by decapitation at the level of the brain, so as to maintain the morphology and integrity at the neck muscles. Skin was removed, and the whole neck region fixed in 4% PFA/PBS for 2 hours fixation. Following this, sternomastoid muscles were dissected from the neck, and washed in PBS, 4 times over a total of 2 hours, in 2 ml Eppendorf tubes. Tissue was

then placed in a 30% sucrose/PBS solution for cryoprotection, until it sank to the bottom of the tube (indicating that the dense sucrose solution had fully permeated the tissue, ~1 hour). Muscle was then blotted briefly on paper towel, before being mounted and frozen in liquid nitrogen-cooled isopentane, as described at the beginning of this section. Sectioning was carried out at 25 μm, to increase the chance of including whole NMJs within each section.

Diaphragms were also collected for whole mount immunohistochemistry. The diaphragm muscle of embryonic mice serves as a good model to study innervation patterning, as it is relatively thin (~200 μm at E18.5), allowing for imaging through the entire tissue depth (An et al., 2010; Banks et al., 2001, 2003; Fu et al., 2005; Schwander et al., 2004). Embryos were cut in half below the rib cage, and at the level of the lungs, to leave intact the part of the ribcage with the diaphragm. Skin and organs (e.g. liver, heart and lungs) were removed. The thoraxes were then fixed in methanol cooled to -20°C for 5 mins, and washed 3 times in PBS over a total time of 20 mins. Diaphragms were dissected from the rib cage, by careful trimming at the edges, for subsequent staining.

2.6. Harvesting of tissue for immunohistochemistry (8 week adults)

Tissue was generally processed as for embryos. For transverse sections, *Tibialis anterior* (TA) muscles were taken from the lower leg, mounted and sectioned at 10 μm. For sternomastoid muscles, animals were fixed by cardiac perfusion with 4% PFA/PBS, to maintain active zone integrity. This procedure was carried out by **Bruce Williams** at the Barts Cancer Institute, Queen Mary University, London. Animals were anaesthetised under isoflurane gas, until unresponsive to toe pinch. The rib cage was cut away, first by an incision at the sternum, and then at either side of the ribs, to expose the heart. A perfusion needle was inserted into the left ventricle, and a small incision made in the right atrium as an outlet. 4% PFA/PBS was then perfused into the heart using a Hugo Sachs Elektronik-Harvard Apparatus automatic syringe pump perfuser, at 80 mm Hg^2. The pump was run until the animal became rigid, with the exposed liver being a good indicator of this (~2 mins, ~80 ml PFA/PBS solution used in total).

Sternomastoid muscles were removed under a fume hood, processed and sectioned in the same manner as those from the embryos (*Section 2.5., harvesting of tissue for immunohistochemistry (E13.5 - E18.5)*).

Teased fibres were also prepared from adult diaphragms, to assess whether fibres were singly or multiply innervated. Diaphragms were fixed for 1 hour in 4% PFA, washed 3 times in PBS over a total of 20 mins, and fibres teased apart with forceps.

2.7. Immunohistochemistry on transverse muscle sections

A hydrophobic PAP pen was used to draw a barrier around the sections (10 μm sections from whole mounted thoraxes (E13.5-E18.5) or adult TA muscles (8 week adults)). Sections were rehydrated in PBS for 5 mins, and fixed according to the antibody to be used (*Section 2.2., antibodies*): 5 mins for 4% PFA/PBS, 5 mins for methanol, and 10 mins for acetone. All subsequent steps were carried out at room temperature, and all wash steps were 3 x 5 mins in PBS, unless otherwise specified. After washes in PBS, sections were permeabilised in 0.1% Triton X100/PBS for 5 mins, followed by washes. If primary antibodies raised in mouse were to be used, sections were blocked for 1 hour with Mouse-on-Mouse reagent (1:40 in PBS). This product is designed to block endogenous immunoglobulins in the mouse tissue, so that reactivity with anti-mouse secondary antibodies is reduced. Following this, sections were washed once for 5 mins in PBS, and then blocked for 30 mins in 10% goat serum/PBS (except in the cases where primary antibodies raised in goat were to be used; in this case horse serum was substituted). Primary antibodies were diluted in 10% goat or horse serum/PBS, at the dilutions specified in *Section 2.2., antibodies*, then incubated with the sections for 1 hour. After washes, Alexa dye-conjugated secondary antibodies (1:400) and Hoechst 33342 dye (1:1000) were applied in PBS for 1 hour. In the cases involving monoclonal mouse antibodies, isotype-specific secondary antibodies were used where possible. Fluorescently conjugated α-bungarotoxin diluted 1:1000 in PBS was added to the secondary antibody solution, to mark

AChRs when necessary. Sections were washed, mounted in Prolong Gold Antifade, and covered with Nunc Thermanox coverslips.

2.8. Immunohistochemistry on longitudinal sternomastoid muscle sections

Due to the thickness of the sections (25 µm compared to 10 µm for the transverse sections), all incubation and wash times were increased. A hydrophobic PAP pen was used to draw a barrier around the sections. All steps were carried out at room temperature, and all wash steps were 3 times over a total of 40 mins in PBS (unless otherwise specified). Fixation in 4% PFA/PBS had already occurred during the harvesting of the muscles *(Section 2.5., harvesting of tissue for immunohistochemistry (E13.5 – E18.5); Section 2.6., harvesting of tissue for immunohistochemistry (8 week adults))***.** After hydration in PBS for 15 mins, sections were permeabilised in 0.1% Triton X100/PBS for 40 mins. Washes were carried out, and sections incubated with Mouse-on-Mouse block for 2.5 hours (1:40 in PBS). After 1 wash for 15 mins, sections were blocked in 10% goat serum/PBS for 1.5 hours. Primary antibodies were diluted in goat or horse serum blocking buffer, at the concentrations specified in *Section 2.2., antibodies*, then incubated with the sections overnight at 4°C. After washes, Alexa-conjugated secondary antibodies (1:400), Alexa 594-conjugated α-bungarotoxin (1:1000) and Hoechst 33342 dye (1:1000) were applied in PBS for 3 hours. For detection of bassoon, an IgG2a isotype-specific secondary antibody was used. Sections were washed, and mounted in Prolong Gold Antifade with high-precision, thin coverslips (0.17 mm), for optimal imaging at high power.

2.9. Immunohistochemistry on whole mount diaphragms

Immunostaining of diaphragms was performed as described previously (Schwander et al., 2004). Diaphragms were methanol fixed and dissected, as described in *Section 2.5., harvesting of tissue for immunohistochemistry (E13.5 - E18.5)*. Permeabilisation and blocking were carried out simultaneously, in PBS/1% Triton/5% horse serum (HS)/1% bovine serum albumin (BSA)

for 2 hours. Mouse anti-neurofilament 160kD chain (1:200) and mouse anti-SV2 (1:50) were diluted in permeabilisation/blocking buffer, and incubated with the tissue for 2 days at 4°C. Following this, 5 washes in 0.2% Triton/PBS were carried out over 8 hours. Samples were then incubated with Alexa 594-conjugated secondary antibody (anti-mouse IgG1; 1:400), Alexa 488-conjugated α-bungarotoxin (1:1000) and Hoechst 33342 dye (1:1000), diluted in 0.2% Triton/PBS. After 5 washes in 0.2% Triton/PBS over 8 hours, diaphragms were mounted flat in Dako fluorescence mounting medium, and covered with Nunc Thermanox coverslips.

2.10. Haematoxylin and Eosin (H & E) staining

Sections of E18.5 thoraxes, displaying intercostal muscles in transverse, were placed in Coplin staining jars. Slides were first stained with Harris haematoxylin (1:1 in distilled water) for 2 mins. Washing was carried out in running tap water for 1 min, before staining with eosin (1% in distilled water) for 20 secs, followed by another wash step. Slides were then progressed through increasing ethanol concentrations for 10 secs each: 70%, 100%, and 100% again, the last step to fully remove any residual water. Histo-Clear was used to clarify the sections, improving the brightness of the stains. Following this, slides were mounted with Nunc Thermanox coverslips and DPX (distyrene plasticiser and xylene) mounting medium.

2.11. Collection of tissue for EM

Collection of E18.5 diaphragms. Rapid fixation after death is essential for the preservation of tissue morphology, and to prevent hypoxic/ischemic damage. After decapitation, embryos were cut in half below the thorax, and fixed immediately in 2% PFA/1.5% glutaraldehyde/0.1M cacodylate buffer. Diaphragms were harvested as above (*Section 2.5., harvesting of tissue for immunohistochemistry (E13.5 - E18.5)*), and kept in fixative until processing (below).

Collection of 8 week adult diaphragms. Animals were cardiac perfused by **Bruce Williams** as above (*Section 2.6., harvesting of tissue for immunohistochemistry (8 week adults)*), but with 2% PFA/1.5% glutaraldehyde/0.1M cacodylate buffer as the fixative. Diaphragms were excised under fume hood, and kept in fixative until processing (below).

2.12. Processing and imaging of tissue for EM

After collection and fixation, muscles were processed and sectioned for EM by **Mark Turmaine**, at the UCL Biosciences Electron Microscopy Facility. I performed all scanning and imaging of sections. The following steps were carried out, all with 0.1M cacodylate buffer as the diluent: 3 washes in 4% sucrose; secondary fixation in 1% OsO_4; 3 washes, buffer alone. Staining was carried out in 1% uranyl acetate/25% ethanol. Dehydration was carried out in increasing concentrations of EM-grade ethanol in acetonitrile (50 – 100%). Samples were infiltrated in 1:1 acetonitrile/Spurr's resin for 1 hour, and embedded in 100% resin, followed by incubation at 60°C for 24 hours. 75 nm ultrathin sections were cut. A Jeol 1010 transmission electron microscope was used by the author to scan sections at x8000 magnification, and to image located areas at x12 - 100,000. Images were acquired using Gatan Microscopy Suite software.

2.13. *Ex vivo* electrophysiology (E18.5 embryos, 20 week adults)

Experimental procedures were performed by Dr **Richard Webster**, in the laboratory of Prof **David Beeson**, Weatherall Institute of Molecular Medicine, John Radcliffe Hospital, University of Oxford, as described previously (Webster et al., 2013). I played crucial roles in the design of the experiments, and carried out most of the data analysis, and much of the interpretation. Thoraxes were dissected to expose phrenic nerve and hemidiaphragms, and bathed in Krebs-Henseleit buffer, aerated with 95%O_2/5%CO_2. A petri dish coated with a soft substrate (Sylgard) was used to house the preparations, and pins used for fastening. Material was analysed at room temperature (20–22 °C) in a Faraday enclosure to minimise external

influences. Stimulation of the phrenic nerve was carried out via a suction electrode, coupled to a Grass Instruments solid-state square wave pulse generator. An Axoclamp-2A amplifier was used to increase the signal. Muscle contraction was blocked using 2.5 μM μ-conotoxin GIIIB, prior to recording. EPPs and MEPPs were recorded from individual muscle fibres, using borosilicate glass electrodes (10–15 MΩ resistance) filled with 3 M KCl. Electrodes were positioned as close to the endplate region as possible using a Scientifica micromanipulation rig and BX51WI Olympus stereomicroscope. Recordings were made and analysed using pCLAMP 9 software, and normalised to a baseline of -80 mV, to correct for differences in resting membrane potential. Quantal content was calculated according to the following formula:

$$\text{Quantal content} = \text{mean}(AMP_{EPP}) / \text{mean}(AMP_{MEPP})$$

Where AMP_{EPP} and AMP_{MEPP} are respectively the amplitudes of the EPP and MEPP, corrected to -80 mV resting potential. Prior to use with this formula, AMP_{EPP} values had an additional correction factor for species (mouse):

$$AMP_{EPP} = AMP_{EPP(measured)} / [1 - 0.8\ AMP_{EPP(measured)} / E]$$

Where 0.8 is the correction factor for mouse endplates, and E is the resting membrane potential of -80 mV.

Stimulation of the phrenic nerve for the assessment of evoked neurotransmission was not possible in E18.5 embryos, due to technical impracticalities, but recordings of MEPPs at the postsynaptic electrode could be made.

For recordings in adult hemidiaphragm preparations, $CaCl_2$ in the Krebs-Henseleit buffer was altered over a range, to artificially modulate the probability of synaptic vesicle release (and thus efficiency of neurotransmission) at the motor terminals. 2.5 mM $CaCl_2$ was considered the standard physiological concentration; in addition, concentrations of 0.75, 0.5, 0.3 and 0.2 mM were employed.

2.14. Transportation/preservation of tissue for electrophysiology

Electrophysiology is normally carried out on freshly dissected muscle, as soon as possible after death. Experiments on adult mice were arranged by live transportation, followed by sacrifice on the day of analysis. However, for E18.5 embryos, transportation of live pregnant mothers was not possible. Embryos were therefore harvested, decapitated and immediately transported on ice. Initially, embryos were kept in standard electrophysiological buffer; however, on arrival, the tissue quality had degraded, to the extent where the recording of MEPPs could not be made. Other investigators have used standard organ preservation solutions (normally used for surgical transplants), with the addition of 20 mM 2,3-butanedione monoxime to maintain muscle quality, for non-electrophysiological applications (van der Heijden et al., 2000; Norden et al., 1997). Organ preservation solutions generally protect against hypoxia, and maintain correct osmolarity. 2,3-butanedione monoxime was shown to have additional beneficial effects for muscle storage, apparently by preserving balance of Na^+ and K^+ electrolytes, preventing cell swelling, and partially inhibiting myosin ATPases, so that ATP depletion and rigor does not occur. Therefore we used a combination of Custodiol HTK organ preservation solution and 20 mM 2,3-butanedione monoxime for the transportation of muscles on ice. Preliminary tests aimed to compare tissue quality of muscle stored at 4°C overnight in this solution, versus muscle that was freshly dissected. The two groups (n=2) displayed no apparent differences in basic electrophysiological recordings, indicating that this solution was able to maintain muscle quality over a period of several hours. (Dr **Richard Webster**, data not shown).

2.15. Forelimb grip strength (adults, 16 week adults)

Measurements of forelimb grip strength were expressed in grams, using a Chatillon Grip Strength Meter, and carried out by Dr **Tanguy Lechertier** and Dr **Louise Reynolds** at the Barts Cancer Institute. Animals were held and suspended by the base of the tail, and presented with the grip bar of the meter. The instinct of the animal is to hold on to the bar; with steady and continuous pulling back by the tail, the animal will strengthen its grip, until the force

exerted by the experimenter is too great for the animal to sustain it. The meter records this maximum peak of force. Animals were tested on two occasions (5 days apart, at around 3pm). On each occasion, the animals were tested 5 times each, with several minutes pause in between each attempt, during which the other animals were tested. After the complete series was performed, the best three attempts for each animal were taken and averaged. This was designed to filter out any failed attempts, where the animal might have slipped, or incorrectly grasped the bar from the outset. Following this, these scores were averaged for each mouse across the two different experiments, and statistical significance analysed as described in *Section 2.18., data analysis*.

2.16. Fluorescence microscopy (widefield and confocal)

Sections were imaged using a Leica DM4000 widefield fluorescence microscope connected to Metamorph advanced acquisition software, or a Zeiss LSM 710 confocal microscope connected to Zeiss Zen software. For the imaging of muscle, skin and lung in transverse sections, widefield microscopy was employed. Here, tissue histology was imaged at x20 or x40 magnification, and NMJs at x63 with an oil immersion objective. Whole mount diaphragms were imaged using both widefield (x5 - x10 magnification) and confocal (x40) imaging, the latter carried out with Z-stacks at 1 μm intervals. Reconstruction of whole right diaphragm hemispheres was carried out using the automated XY stage of the widefield microscope, followed by image stitching in Metamorph software.

For confocal reconstruction of whole *en face* NMJs in the adult, 0.4 μm slices were taken and projected as a Z-stack by maximal pixel intensity, as described previously (Chen et al., 2012). For imaging of bassoon and integrin-α3 stains in NMJs at E18.5, individual confocal slices were used. At E18.5, stains for piccolo and P/Q VGCC suffered from low signal to background ratio; therefore image restoration was carried out on widefield images, using 3D deconvolution (described below).

2.17. 3D deconvolution of widefield microscope images

Laser scanning confocal microscopy has significant benefits over standard widefield microscopy, allowing images to be captured at specific planes in a sample, excluding the scattered light from the other planes. Thus, highly focused images can be obtained, without the confounding factor of 'out-of-focus' light. The acquisition of multiple planes (or slices) in a sample also allows for 3D reconstruction, so that whole structures can be examined in more detail. In both widefield and confocal microscopes, the objective lens magnifies and focuses the light onto a detector. However, in a confocal microscope, a barrier with a small pinhole is placed just before the detector. The result is that only the in-plane (or 'in-focus') light is allowed through, while all other light is obstructed (Biggs, 2010).

However, there are disadvantages associated with confocal microscopy. The pinhole only allows a small percentage of the light to reach the detector. Thus the signal suffers from a loss of intensity, and so confocal imaging is best suited for samples with strong labelling. When the molecule(s) of interest are low in abundance, or labelling is sub-optimal, this imaging approach may not be ideal. In contrast, widefield microscopes capture much more of the emitted signal, making them more sensitive (although the image contains both in-focus and out-of-focus 'blur'). Immunolabelling of piccolo and P/Q VGCC in the active zones of E18.5 NMJs produced a faint signal that was only slightly higher than the background, giving an indistinct signal by confocal micrograph (data not shown). In addition, the active zones of NMJs are very small structures (50-100 nm), which are difficult to resolve by light microscopy. This combination of weak intensity and small size led me to an approach based on 3D deconvolution of widefield images, with the advice and assistance of Dr **Bertrand Vernay** at the UCL Institute of Child Health.

3D deconvolution is a form of image restoration, which attempts to reassign scattered light back to its original source in the sample, or to eliminate it where necessary. The result is the removal of out-of-focus 'blur' caused by light scatter, and the strengthening of signal of the

light sources themselves (including those of interest to the experimenter). Many widefield microscopes, including the Leica DM4000 are capable of automatically acquiring images at different planes through the sample. This allows 3D reconstructions to be made; subsequent deconvolution techniques can then restore the image to resolutions similar to (or sometimes better than) that of a confocal micrograph. However, unlike confocal imaging, very little signal is lost (Biggs, 2010).

3D deconvolution requires knowledge of how the light is scattered in a sample. This can be determined experimentally, using fluorescently tagged beads (in this case, a diameter of 1 μm was used). Just like individual points of signal in a sample, these beads scatter light in a pattern referred to as a point spread function (PSF; **Fig 2.2A**). This pattern is usually characterised by concentric rings that widen as the distance from the original light source increases (**Fig 2.2D**). To obtain an experimental characterisation of the PSF, Z-stacks of Alexa 488- and -594-tagged beads were taken using the widefield microscope under x63 oil immersion objective, with slices at 0.4 μm intervals. A full series of 200 μm (~500 slices in total) allowed the acquisition of a large proportion of the scattered light above and below the sample; this series is shown in **Fig 2.2B-D**.

This experimentally determined PSF was then used to deconvolve Z-stacks of NMJs taken under the same conditions. Autoquant X3 software was used for this process, relying on a combination of the PSF images and its own algorithms. Certain input variables are required: the refractive index of the immersion oil, coverslip and glass of the slide (all matched at 1.515), and the numerical aperture of the objective (1.25; this value corresponds to the range of angles of light that the lens can collect). Prolong Gold Antifade mountant was chosen for this analysis, as its refractive index is closely matched to that of the immersion oil and glass (~1.46); this minimises artefacts and aberrations. The optimal Z-slice interval used for this analysis (0.4 μm) was determined using the Nyquist calculator (http://www.svi.nl/NyquistCalculator), which relies on the known values for refractive index and numerical aperture. Autoquant X3 is

also capable of running 3D deconvolution without an experimentally derived PSF; instead it uses its own theoretical PSFs. This so-called 'blind' deconvolution yielded images with a similar appearance to those that had used the experimentally derived PSFs. This indicates that the experimental PSFs acquired in our system were close approximates of those derived by standard theory. Single slices of deconvolved stacks were used for the figures, and had a greatly improved signal-to-noise ratio than the unprocessed images. **Fig 2.3** shows single Z-slices of NMJs stained with antibodies to P/Q VGCC, before (A) and after (B) 3D deconvolution.

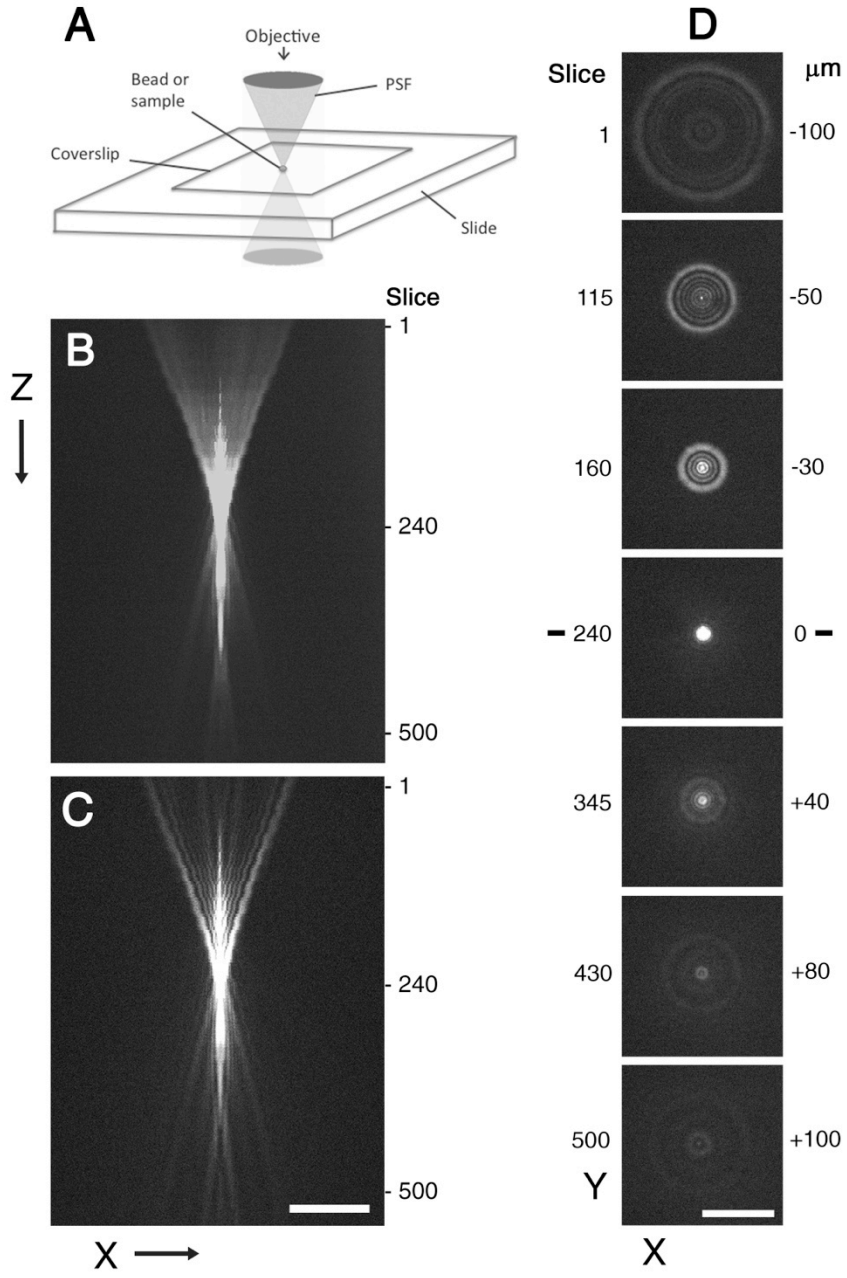

Fig 2.2. (*Legend on next page*).

Fig 2.2. *(Previous page).* Obtaining experimental point spread functions (PSFs) for 3D deconvolution**.** Immunostains of piccolo and P/Q voltage-gated calcium channel (P/Q VGCC) in E18.5 sections suffered from a low signal to background ratio. An approach using 3D deconvolution of widefield images, rather than confocal microscopy was sought, allowing signal capture to be maximised. (A) Illustration of the PSF of a single point of fluorescence in a sample. (B, C) Reconstructed Z-stacks of the PSF of an Alexa-488-conjugated bead (1µm diameter), acquired using the Leica DM4000 widefield microscope. The PSF for a 594-conjugated bead was also acquired. 500 serial Z-slices were taken, at intervals of 0.4 µm; slice number 240 marks the approximate centre of the bead, while the surrounding slices mark the pattern of scattered light. A fully 3D reconstruction is shown in (B), while a central slice through the Y-plane of the PSF is shown in (C). Individual Z-slices at different planes are shown in (D). These PSFs were used to deconvolve Z-stacks of neuromuscular junctions (NMJs), acquired under the same conditions. Scale bars, 20 µm.

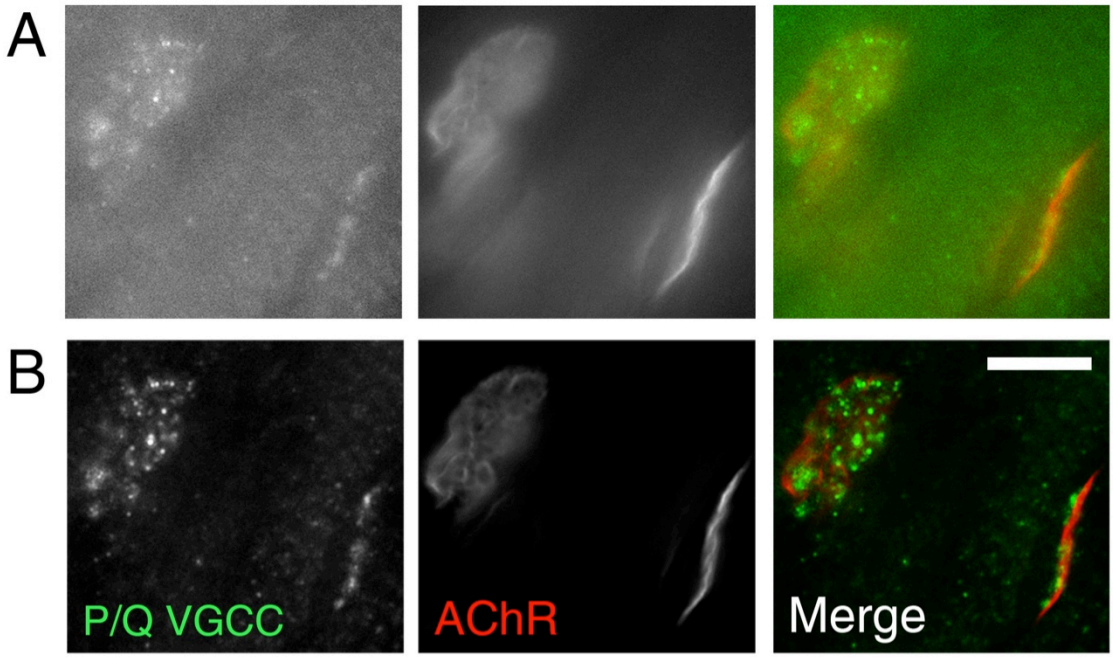

Fig 2.3. Widefield images of E18.5 NMJs – before and after 3D deconvolution. Using the Leica DM4000 widefield microscope, a Z-series of NMJs was acquired. NMJs were stained with antibody to P/Q-type voltage-gated calcium channel (P/Q VGCC) and α-bungarotoxin, to mark acetylcholine receptors (AChRs). Single slices before (A) and after (B) 3D deconvolution, using the point spread functions (PSFs) displayed in **Fig 2.2.** Scale bar, 5 µm.

2.18. Data analysis

I carried out the following data analysis: scanning, acquisition, processing and quantification of all images (immunohistochemical and EM) and analysis of forelimb grip strength data. Electrophysiological data were initially assembled, corrected and tabulated by Dr **Richard Webster**; I carried out further numerical and statistical analysis, conversion into graphical format, and interpretation.

ImageJ was used for the quantification of all images. Diaphragm width was assessed in transverse sections from E18.5 embryos, as an average of 20 random measurements throughout the muscle (**Fig 3.2F**). Measurements were made by drawing a perpendicular line between the two outer surfaces of the muscle. Fibre diameter was measured in 50 random fibres per diaphragm (10 fibres in each of 5 images taken at x20 magnification; **Fig 3.2G**). The minimum Feret's diameter was used; this relies on parallel tangents drawn on the outside of the object, to find the closest possible distance between them. This measurement has been shown to be robust against variability in tissue orientation (Briguet et al., 2004). Fibres were outlined manually, before calculation of the Feret's diameter using an inbuilt algorithm in ImageJ.

Nerve branching in the diaphragm was quantified at the central 2mm region of the phrenic nerve fork which supplies the right hemisphere (**Fig 4.6**). This half of the diaphragm was used for consistency, as the phrenic nerve input of the left hemisphere assumes a slightly different pattern at the gross scale. Primary branches were defined as those furcating from the main trunk; secondary branches as those diverging from primary branches; tertiary branches from secondary branches; and quaternary branches from tertiary branches. In the same area, the number of AChR-positive NMJs (labelled with fluorescently conjugated α-bungarotoxin) were counted. Endplate zone width was measured at >25 random points along the right hemisphere, as the distance between the two furthest NMJs perpendicular to the axis of the phrenic nerve. Values were then averaged for each diaphragm.

For measurements of adult NMJ morphology in ImageJ, only junctions in *en face* orientation were assessed (**Fig 5.5**). Total spread area was measured by tracing the circumference of each NMJ, using the AChR+ components as boundaries, and encompassing any negative (i.e. black) space. Thresholding of the image by pixel intensity allowed the measurement of the AChR+ area (i.e. that labelled with α-bungarotoxin) Fragmentation was measured as the number of discrete AChR+ clusters per NMJ. At the boundary of the AChR+ areas of the NMJ, a bright rim is observed, corresponding to the positivity at the edges of the synaptic gutter. This rim helped to distinguish individual fragments. NMJs that were considered to have faint, fragmented AChR+ regions with varicose nerve terminals were identified first by the appearance of the α-bungarotoxin stain ('ghost-like' in comparison to the others). The nerve terminals of these NMJs always had the same appearance, with the swelling of the parts that were in direct contact with the endplate fragments. NMJs were considered to be undergoing terminal sprouting, when two nerve processes were found projecting from the endplate; one was assumed to be the efferent nerve, and the other a sprout exiting the endplate. Finally, NMJs with excessive prejunctional branching were defined as those where the input axon underwent splitting into three or more branches, shortly before entering the endplate region.

The fluorescence intensity of integrin-α3 at NMJs was assessed (**Fig 4.1; Fig 5.2**). Areas of interest were traced using rectangle selections, and average pixel intensity calculated. In sections at E18.5, fluorescence intensity was assessed using >5 selections to cover the length of the NMJ; in the larger adult NMJs, >20 random selections were used. Measurements were then averaged to give a single intensity value for each NMJ. Values were corrected for the background fluorescence, by subtracting the average pixel intensity of the regions immediately surrounding the NMJs. Final data was then normalised to the wild type values, which were set at 100%.

In EM sections, the number of synaptic vesicles was expressed per μm^2 of nerve terminal (**Fig 4.7**). This area was measured by tracing round the entire nerve terminal in ImageJ, and

excluding any surrounding cells (e.g. Schwann cells). Alignment of active zones (**Fig 5.6**) was defined as follows. A line was drawn as the trajectory from the walls of the folds to the nerve terminal. If this line crossed an active zone, it was considered aligned.

For spontaneous events of neurotransmission in E18.5 diaphragms (**Fig 4.7A-D**), MEPP frequency was presented in raw format, as well as that normalised to the number of NMJs. The quantification of NMJs in diaphragm muscles was carried out as above (and results presented in **Fig 4.6F**), with an additional normalisation to the wild type value, set at '1', i.e. one endplate per fibre. MEPP frequency was then divided by the normalised number of NMJs for that genotype (**Fig 4.7D**). For single stimulation experiments (EPP and quantal content) in adult hemidiaphragm preparations (**Fig 5.10**), 4 measurements were evoked for each endplate. Measurements were then averaged as a mean to give the final value for that endplate. Several endplates (4-6) were selected per animal, and a number of animals assessed (4–11 in total, depending on the buffer type/$CaCl_2$ concentration), to give an $n > 20$ endplates. For repetitive stimulation experiments in adult preparations (**Fig 5.11**), a train of 50 Hz was evoked once at each endplate, and the resulting EPPs in the series recorded for amplitude. 4-6 endplates were assessed per animal, over a total of 5-6 animals per genotype (depending on the buffer type/$CaCl_2$ concentration). An averaged trace was plotted in graphical format, by pooling the individual traces, and calculating a mean for each stimulation point in the series. Traces were presented in two ways. (1) Stimulation points were normalised and expressed as an average of the first point, as per convention (Hallermann et al., 2010; Rafuse et al., 2000; Ruiz et al., 2008; Webster et al., 2013). This allows the traces to be compared alongside each other, making effects of STF and/or decrement more apparent, while ignoring potential differences in the initial EPP in the train. (2) Traces were presented as raw values, without normalisation to the first EPP in the series, so that absolute EPP outputs throughout the train could be compared.

Graphpad Prism 5 was used for representing the data in graphical format, and for analysing for statistical significance. When data are normally distributed, parametric tests such as the t-test

and ANOVA (analysis of variance) may be used. These tests may also be used when data are non-normally distributed, but the n value is ≥20. When the data sets are small (n<20), testing for normal distribution is not possible (unless the parameter is known to be normal, for instance human height). Therefore, non-parametric tests should be used, including the Mann-Whitney U and Kruskal-Wallis ANOVA tests. Parametric data are usually represented as mean +/- range, standard deviation, or standard error. Non-parametric data are usually represented as median +/- range or interquartile range (IQR). In this study, for data where n<20, median +/- IQR were plotted, and the Mann-Whitney U test used. For data where n≥20, mean +/- standard deviation (SD) or standard error of the mean (SEM) was plotted (depending on the experiment, see figure legends for details), and the Students' t-test used. For grip strength measurements (**Fig 5.9**), an F-test was used to confirm that the data sets were normally distributed, and thus suitable for analysis with t-test. No significant difference in grip strength was observed between males and females, although a slight downward trend for females was noted. Because of this, the readings were normalised to body weight, which more or less eliminated sex differences. However, it should be noted that significant differences in grip strength between wild type and integrin-$\alpha 3^{+/-}$ mice were observed, whether the results were normalised or not. Significance thresholds for all experiments were set as $P<0.05$ (*), $P<0.01$ (**) and $P<0.001$ (***).

3. Integrin-α3 is not required for myogenesis

3.1. Introduction

Several studies have investigated the expression and functions of integrin-α3 in the neuromuscular system. The first report found brief transient localization of integrin-α3 at the MTJ in the E11 chick, after the onset of myogenesis; the functional significance of this was not explored (Bao et al., 1993). Other studies have reported roles for integrin-α3 *in vitro*. Disruption of integrin-α3 with siRNA or blocking antibodies abrogated the fusion of primary myoblasts. In addition, integrin-α3 was upregulated in regenerating muscle following injury, as evidenced by immunohistochemistry, western blot and quantitative real time PCR. This suggested a role for integrin-α3 in myoblast fusion *in vivo* (Brzóska et al., 2006; Przewoźniak et al., 2013). Other studies revealed integrin-α3 immunoreactivity at the ends of cultured myotubes, and along their lengths, appearing to be aligned with assembling myofibrils (McDonald et al., 1995). The authors hypothesised that integrin-α3 might mediate myofibril assembly and/or alignment. To investigate the role of this protein in muscle development, I used the integrin-α3 knockout mouse (Kreidberg et al., 1996).

3.2. Integrin-α3 expression is not detectable during myogenesis or in adult muscle

To assess whether integrin-α3 is expressed during myogenesis, immunohistochemistry was carried out on wild type mice. Sections from the trunk were used to study intercostal muscles in transverse, at stages between E13.5 (unfused myoblasts) and E18.5 (differentiated myotubes). In addition, sections of 8 week adult TA muscle were processed. No immunoreactivity was observed in muscles at any stage, using an antibody to integrin-α3 (**Fig 3.1A-E**). Areas adjacent to the ribs (corresponding to MTJs) also failed to show any positivity at any stage (examples in **Fig 3.1A, B**). Lung and skin tissue were found in the trunk sections, and served as positive controls (**Fig 3.1F, G**). Integrin-$\alpha3^{-/-}$ tissue was used as a negative control, with no integrin-α3 staining observed in lung, skin and muscle tissue (E18.5 trunk

sections, lung in **Fig 3.1H**, and intercostal muscle in **Fig 3.1I**). Although no clear immunoreactivity was observed for integrin-α3 in developing or adult muscles, one cannot rule out the possibility that it is expressed at low levels, below the threshold for immunohistochemical detection. Therefore, additional analysis was carried out to determine whether integrin-α3 has a role in myogenesis.

3.3. Muscle morphology is normal in E18.5 integrin-α3 mutant mice

To assess the gross muscle morphology of muscles after myogenesis had occurred, H & E stains were carried out on trunk sections of wild type and integrin-$\alpha3^{-/-}$ mice at E18.5. Structure and morphology of intercostal muscles was similar in both genotypes, with formation of muscle fibres with nuclei that were mostly peripheral (**Fig 3.2A, B**). Regions of muscle surrounding the ribs (corresponding to MTJs, marked 'R') displayed a similar appearance between the two genotypes. Diaphragm muscles were also sectioned in transverse, and stained with an antibody to laminin, to more clearly demarcate the boundaries of myofibres. The structural organisation of the tissue was comparable in wild type, integrin-$\alpha3^{+/-}$ and $^{-/-}$ diaphragms (**Fig 3.2C-E**). Virtually all myonuclei were peripherally located in all three genotypes. In addition, diaphragms were morphologically similar on both the whole tissue and cellular scales, with no significant differences in diaphragm width or myofibre diameter (**Fig 3.2F, G**; diaphragm width, P=0.82 and 0.86 for integrin-$\alpha3^{+/-}$ and $^{-/-}$ muscles respectively, compared to wild type; muscle fibre diameter, P=0.22 and 0.24 for integrin-$\alpha3^{+/-}$ and $^{-/-}$ muscles respectively, compared to wild type). These results indicate that integrin-α3 is not required for the formation of muscle fibres or the MTJ during development.

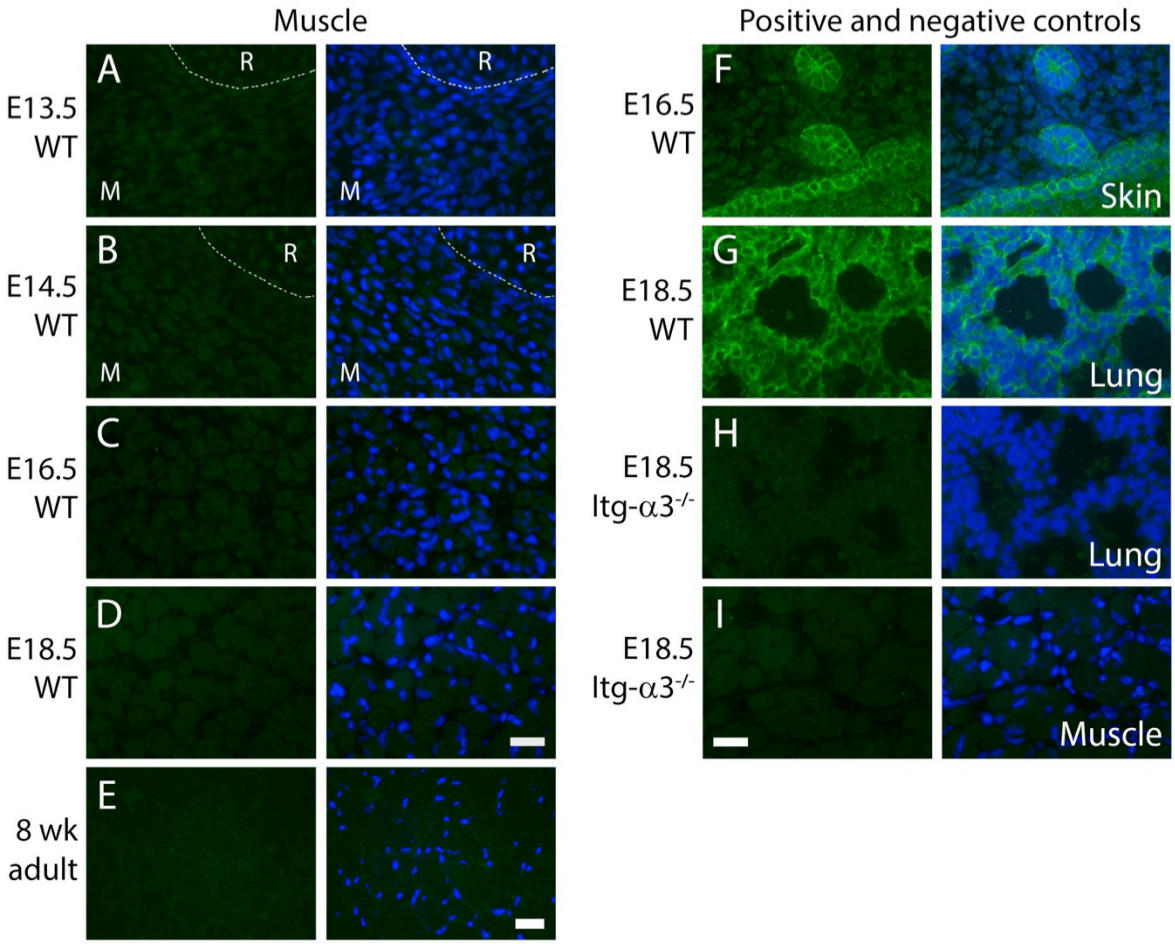

Fig 3.1. Integrin-α3 is not detectable in developing or adult muscle. Sections of trunk from embryos, or *tibialis anterior* (TA) muscle from 8 week adults, were stained with antibody to integrin-α3 (green) and DAPI (blue). No immunoreactivity was observed in developing muscle between E13.5 and E18.5 (A-D), or in the adult (E). In addition, no immunoreactivity was found at the muscle/rib interface in E13.5 – E18.5 embryos, examples shown in (A) and (B) with dotted line to indicate this boundary. Positive controls of skin (F) and lung (G) were observed within the same trunk sections; clear staining of integrin-α3 was observed here, as previously reported(DiPersio et al., 1997; Kreidberg et al., 1996). Trunk sections from integrin-$\alpha3^{-/-}$ mice were used as negative controls; no staining was observed in lung (H) or muscle (I) tissue. *Abbreviations: WT, wild type; Itg-α3, integrin-α3; M, muscle; R, rib. Similar results observed in 3 animals per time point. Scale bars: 50 μm, (A-D, F-I); 20 μm (E).*

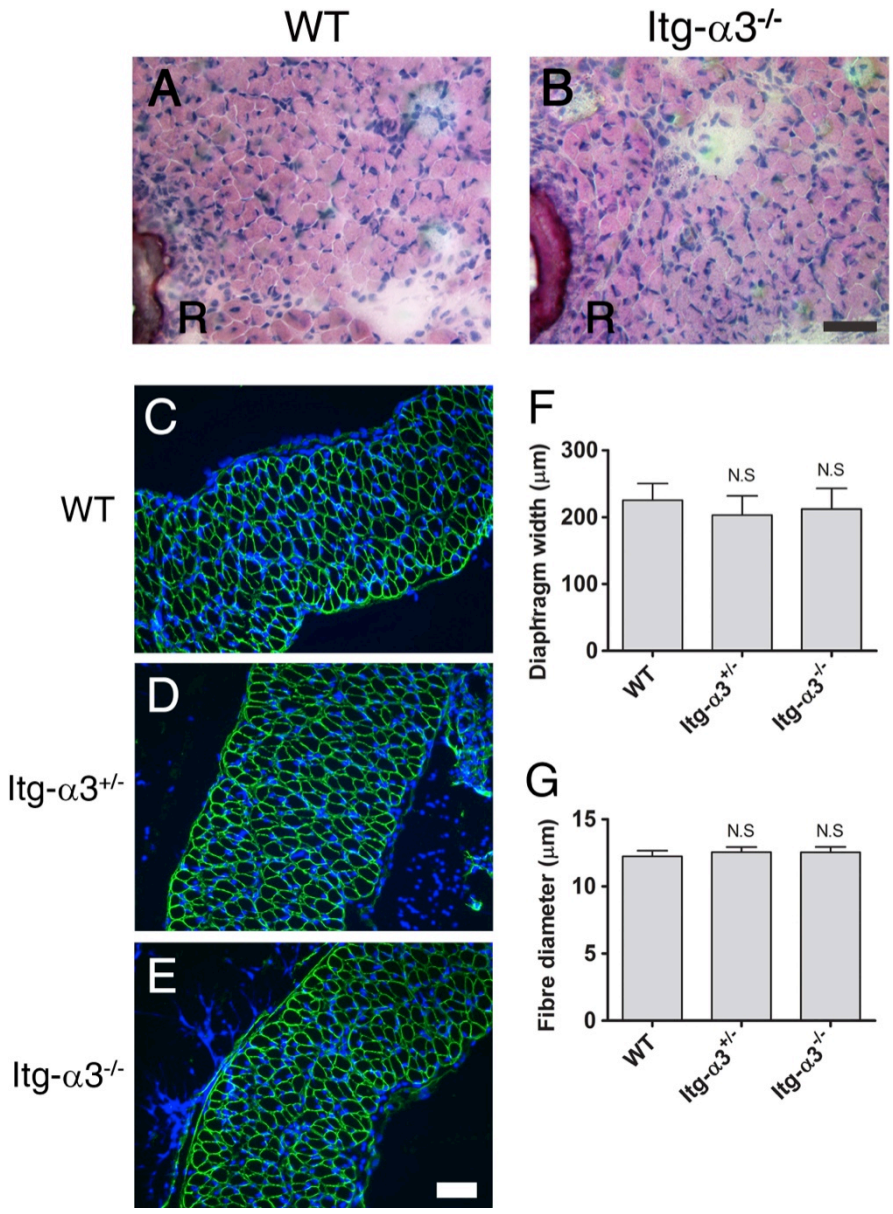

Fig 3.2. Normal muscle morphology in E18.5 integrin- $\alpha3^{-/-}$ mice**.** Sections of trunk were stained with haematoxylin and eosin (H & E), to observe general morphology of intercostal muscles in transverse orientation (A, B). Muscle fibres were apparent in both wild type (A) and integrin-$\alpha3^{-/-}$ (B) mice. Myotendinous junction (MTJ) regions surrounding the ribs (marked 'R') had a similar appearance in both genotypes. Trunks were orientated for transverse sectioning of diaphragm muscles, and stained with antibody to laminin (green) and DAPI (blue; C-E). Similar muscle morphology was observed in wild type (C), integrin-$\alpha3^{+/-}$ (D), and integrin-$\alpha3^{-/-}$ (E) mice. Almost all fibres were peripherally nucleated in each genotype. No significant differences were observed in width of the diaphragm muscle (F), or in fibre diameter (G). *Abbreviations: WT, wild type; Itg-α3, integrin-α3; R, rib. Similar results observed in 4 animals per genotype (F, median +/- IQR, n=4; G, mean +/- SEM, n = 50 fibres per animal). Scale bars: 50 μm.*

3.4. Integrin-α3 is not required for basement membrane organisation in muscle

Integrins are cell surface receptors that bind to ECM components, mediating a diverse array of downstream events within the cell. They are also capable of influencing the external environment, instructing the deposition and organisation of the ECM. To assess whether integrin-α3 influences the composition of the muscle basement membrane/ECM, immunohistochemistry was carried out on trunk sections of E18.5 wild type and integrin-α3$^{-/-}$ mice. No differences were observed in both the staining intensity and localisation of laminin, collagen IV and fibronectin (**Fig 3.3A-C**). To assess whether integrin-α3$^{-/-}$ muscles displayed alterations in the major adhesion complexes at the sarcolemma, staining was carried out for dystrophin (of the DGC), and talin-2 and vinculin (intracellular integrin-associated molecules). Again, no difference in immunoreactivity was observed between wild type and integrin-α3$^{-/-}$ muscles (**Fig 3.3D-F**). To assess basement membrane organisation at the ultrastructural scale, longitudinal sections of diaphragm muscle were imaged using EM. Processing and sectioning of tissue was carried out by **Mark Turmaine**; all scanning and imaging was carried out myself. The basement membrane was observed between adjacent myofibres; in both genotypes, the sarcolemma was lined with a wispy layer of material, with a similar electron density and appearance (**Fig 3.3G, H**). These results indicate that integrin-α3 is not required for ECM organisation in muscle.

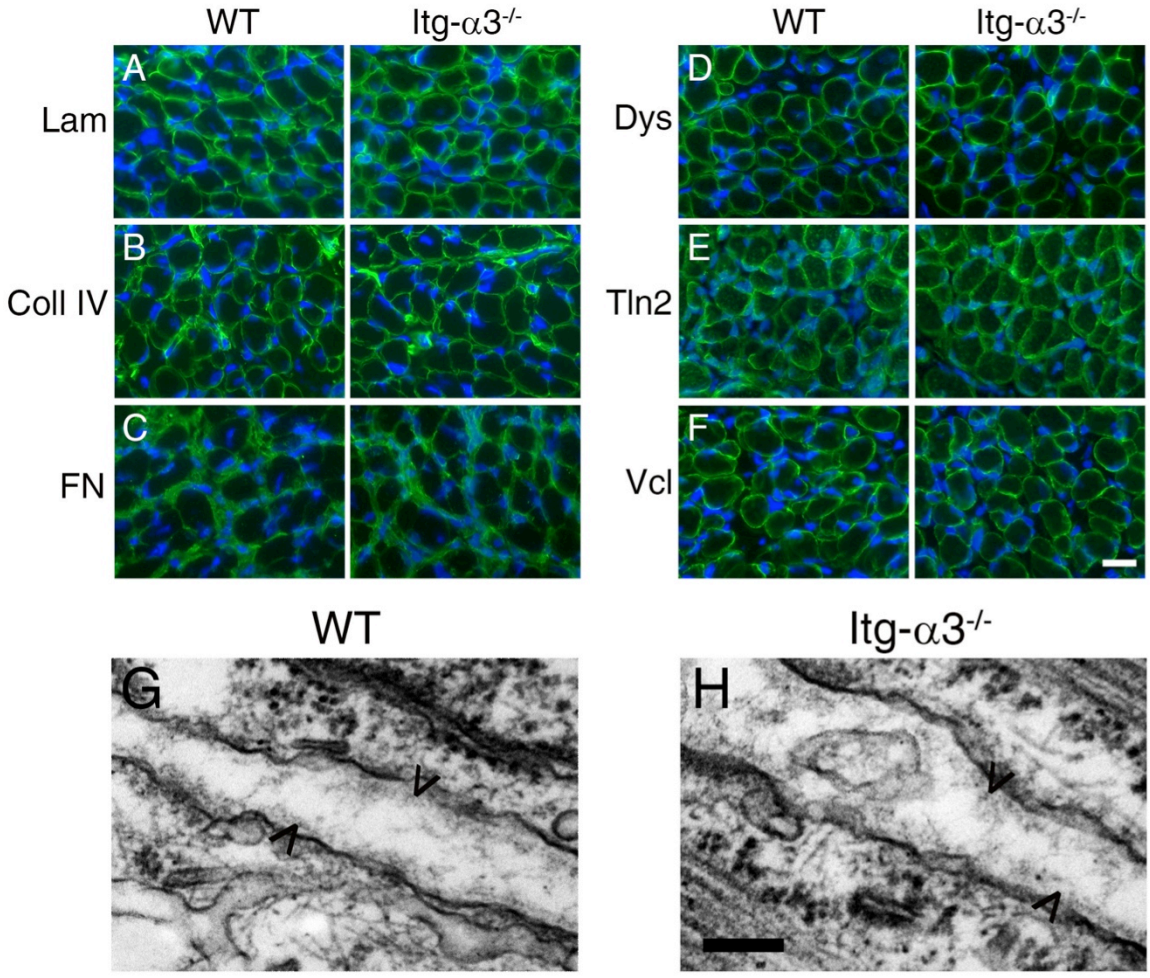

Fig 3.3. Normal deposition of basement membrane in integrin- $\alpha3^{-/-}$ muscle. Sections of trunk were stained with antibodies to several ECM and adhesion proteins (green) and DAPI (blue). Intercostal muscles from wild type and integrin-$\alpha3^{-/-}$ mice displayed similar staining results for laminin (A), collagen IV (B), fibronectin (C), dystrophin (D), talin-2 (E) and vinculin (F). Longitudinal ultrathin sections of diaphragm were used to observe the basement membrane of muscle at the ultrastructural level. The cleft between two muscle fibres was observed in wild type (G) or integrin-$\alpha3^{-/-}$ (H) tissue, at x100,000 magnification. In both genotypes, the basement membrane appeared as a wispy layer lining the sarcolemma (arrowheads), with a similar appearance and electron density. *Abbreviations: WT, wild type; Itg-α3, integrin-α3; Lam, laminin; coll IV, collagen IV; FN, fibronectin; Dys, dystrophin; Tln2, talin-2; Vcl, vinculin. Similar results observed in 3 animals per genotype. Scale bars: 20 μm, (A-F); 200 nm (G,H).*

3.5. Integrin-α3 is not required for myofibril assembly or alignment

The process of sarcomere formation is known to start at the costamere, with the formation of Z-bodies, the nascent structures that will become the Z-disks. Integrins are known to play a role in the formation of these sites and the subsequent assembly of sarcomeric components (Schwander et al., 2003; Sparrow and Schöck, 2009). The costameres remain a key factor in myofibril alignment in developing and mature muscle, with integrins and the DGC being closely associated with the Z-disks. Previous studies have reported that integrin-α3 is aligned at the cell surface with assembling myofibrils. These experiments were carried out in cultured myotubes, and suggested that integrin-α3 might play a role in myofibril assembly and/or organisation (McDonald et al., 1995). To ascertain whether integrin-α3 is involved in this process *in vivo*, electron micrographs of longitudinal diaphragm muscle were obtained at E18.5 (**Fig 3.4**). Processing and sectioning of tissue was carried out by **Mark Turmaine**; all scanning and imaging was carried out myself. At this developmental stage, myofibrils were mostly in register with each other, with some minor misalignments; this has been reported before in developing muscle, prior to maturity (Nelson et al., 2013a). The extent of Z-disk alignment was similar in both wild type and integrin-$\alpha3^{-/-}$ muscles (**Fig 3.4A**). Higher power magnification revealed no discernible differences in sarcomeric organisation, between the two genotypes (**Fig 3.4B, C**). These results indicate that integrin-α3 does not have a role in myofibril formation or organisation.

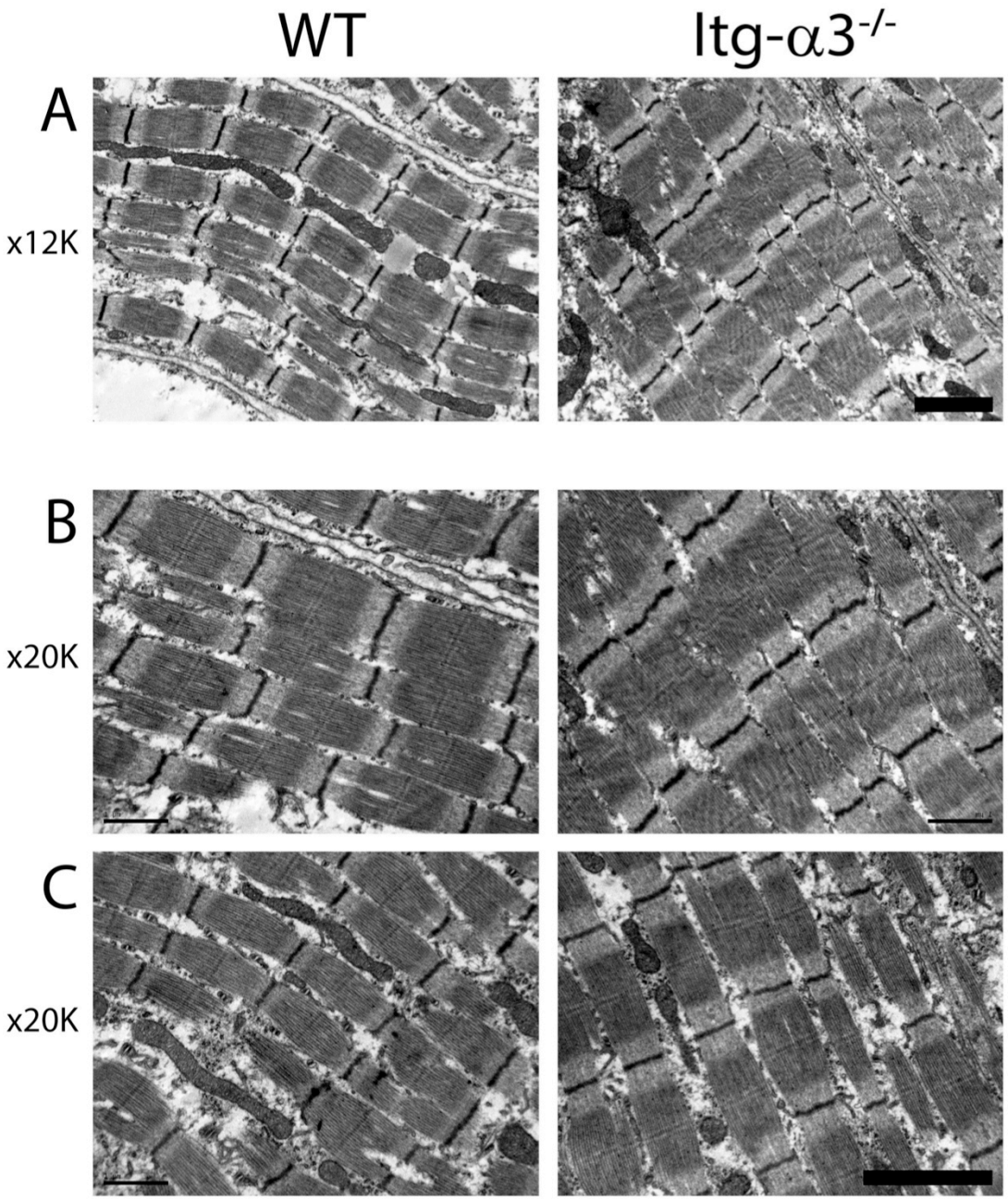

Fig 3.4. Normal assembly and organisation of myofibrils in integrin- $\alpha3^{-/-}$ muscle. Longitudinal ultrathin sections of diaphragm were used to observe the ultrastructure of muscle. Muscles were found to contain myofibrils with similar extent of alignment in both wild type and integrin-$\alpha3^{-/-}$ mice (A; x12,000 magnification). Sarcomeric structure was similar in both genotypes (B, C; x20,000 magnification). *Abbreviations: WT, wild type; Itg-α3, integrin-α3. Similar results observed in 3 animals per genotype. Scale bars: 2 μm.*

3.6. Discussion

The first set of analyses aimed to determine whether integrin-α3 plays a role in myogenesis. The results of chapter 3 demonstrate that integrin-α3 is not expressed in any significant quantity in muscle, either during embryonic development (E13.5 - E18.5) or in the adult (**Fig 3.1A-E**). Consistent with this, myofibres developed normally in integrin-α3 mutant mice, and were peripherally nucleated at E18.5 (**Fig 3.2, Fig 3.4**). At the periphery of myofibres, there were no defects in the deposition of basal lamina, on the ultrastructural or immunohistochemical level (**Fig 3.3A-C, G, H**). In addition, the sarcolemma of integrin-α3 mutants displayed a normal localisation and expression of key adhesion proteins, including dystrophin, and the integrin-associated proteins talin-2 and vinculin (**Fig 3.3D-F**). Taken together, these data demonstrate that integrin-α3 is not required for myogenesis.

A lack of involvement for integrin-α3 in muscle is somewhat surprising, given the results of previous studies which suggested that it might participate in several aspects of myogenesis. Integrin-α3 was found to be expressed in primary myoblasts, and was required for their fusion (as demonstrated with siRNA-mediated knockdown and blocking antibodies) (Brzóska et al., 2006). In addition, myoblasts stained positively for integrin-α3 in regenerating adult tissue following injury, and it was also detectable by western blot and quantitative PCR (Przewoźniak et al., 2013). There are several possible reasons for the discrepancy between the previously published results and those presented here. Firstly, the previous studies used an *in vitro* model to assess the role of integrin-α3 in fusion, and this system may not perfectly mimic that of the *in vivo* environment. Secondly, myoblasts were derived from adult mice; while embryonic myoblasts do not depend on integrin-α3 for fusion (**Fig 3.2**), it is possible that those of the adult rely on a different set of molecules for their regenerative function. Indeed, evidence shows that integrin-β3 is required for myoblast fusion in regenerating adult tissue, but not during development (Liu et al., 2011a).

Another study reported a punctate staining pattern of integrin-α3 at the MTJ of the chick embryo, during a transient period between E11 and E14. Myogenesis begins slightly earlier in the chick, from around E9, and this timeframe coincides with the formation of myotubes (Bao et al., 1993). No immunoreactivity for integrin-α3 was observed at the mouse MTJ, as assessed throughout myogenesis (**Fig 3.1A-D**; E13.5, E14.5, E16.5 and E18.5). In addition, previous studies failed to detect integrin-α3 at the MTJ of the adult mouse (Nawrotzki, 2003). This result may reflect a species difference between mouse and chick. It is also possible that integrin-α3 is expressed during a short period of time, in between the stages analysed in this study. However, a fairly comprehensive set of time points were taken, to increase the chances of detecting transient expression of the protein.

Finally, a previous study suggested that integrin-α3 might have a role in the assembly and/or alignment of myofibrils. The investigators used cultured myotubes as a model, which were differentiated from chick myoblasts. Integrin-α3 immunoreactivity was observed at both the terminal ends of the myotubes and in lateral striations along their lengths, in register with nascent myofibrils. The appearance of integrin-α3 was transient, and was not associated with mature myofibrils (those that had obtained striations) (McDonald et al., 1995). However, in integrin-$\alpha3^{-/-}$ mice, no apparent defects in myofibril structure and organisation were observed (**Fig 3.4**). The lack of agreement between these results may reflect differences in species, and/or the environment associated with an *in vitro* system. Together, these data demonstrate that integrin-α3 performs no major role in myogenesis in the mouse. The remainder of the study focused on the roles of integrin-α3 at the NMJ.

4. Integrin-α3 regulates active zone assembly at the NMJ, and innervation patterning in embryonic muscles

4.1. Introduction

Several studies have reported that integrin-α3 is localised at the active zones of the NMJ. Martin et al. found weak immunoreactivity of integrin-α3 at the NMJ of the mouse (Martin et al., 1996b). Using a different antibody, Cohen et al. found that active zones of the frog NMJ were positive for integrin-α3, which colocalised with VGCCs, and was apposed to the mouths of the synaptic folds. They also found that denervation or collagenase treatment resulted in the detachment of synaptic nerve terminals, and also the disappearance of integrin-α3 staining, suggesting a presynaptic localisation. Using a cell line derived from the *Xenopus* neural tube during early development, the investigators showed that integrin-α3 immunoprecipitated with integrin-β1 (Cohen et al., 2000b); indeed, this is the only dimer that integrin-α3 is known to form (Thorsteinsdóttir et al., 2011).

More recent studies by Carlson et al. have focused on the *Torpedo* electric organ, which possesses synapses with a high degree of homology to the NMJ. Unlike muscle tissue, electric synapses make up a much larger proportion of this organ (by ~100-fold), and synaptic proteins can be isolated in bulk. Synaptosomes (isolated cellular fractions of the synaptic nerve terminal) were obtained from the electric organ, and were found to be positive for integrin-α3 by western blot. Further, integrin-α3 could be immunoprecipitated with VGCCs (suggesting an active zone localisation), laminin-421, as well as the cytoskeletal protein spectrin (Carlson et al., 2010a). This finding is consistent with the fact that integrins form a transmembrane link between the ECM and the cytoskeleton. The investigators noted several previous findings, with particular relevance to these molecular interactions: (1) that in other systems, laminin-421 binds to integrin-α3 via the LG domains found in the laminin-α4 subunit (Suzuki et al., 2005); (2) that synaptic laminins of the NMJ can also bind to VGCCs, but via the laminin-β2 subunit, an interaction that initiates active zone formation (Nishimune et al., 2004). Thus they speculated that different sites within synaptic laminin molecules may bind to

different receptors, thus mediating different downstream effects. The previous finding that laminin-α4 is required for the alignment of active zones with postsynaptic folds suggests that it may do this in association with integrin-α3 (and/or VGCCs). In addition, with its ability to bind to VGCCs and cytoskeletal components, integrin-α3 may play a role in aspects of active zone formation and/or function. Thus, we used the integrin-α3 knockout mouse to investigate the role of this protein at the NMJ. First, we investigated embryos at E18.5, recently after the formation of the NMJ and its active zones (Clarke et al., 2012).

4.2. Integrin-α3 is localised at the active zones of mouse NMJs at E18.5

To assess whether integrin-α3 is localised at the active zones of mouse NMJs, immunohistochemistry was carried out on longitudinal sections of sternomastoid muscle, as described previously (Chen et al., 2012). α-bungarotoxin was used to label the AChRs at the postsynaptic membrane, and NMJs were identified and imaged using the x40 objective of the confocal microscope. Immunoreactivity of integrin-α3 was observed at NMJs, in close apposition to the AChRs (**Fig 4.1A**). To determine whether it was enriched at the active zones, NMJs were colabelled with an antibody to bassoon, and a higher magnification was used (x63 objective, oil immersion). Both bassoon and integrin-α3 were observed to colocalise in discrete puncta, which on the basis of previous analysis, corresponds to individual active zones (**Fig 4.1B**) (Nishimune et al., 2012). To confirm the specificity of the antibody to integrin-α3, immunohistochemistry was performed on tissue from integrin-$\alpha3^{-/-}$ mice. As expected, no signal for integrin-α3 was detected at the NMJ (**Fig 4.1D**). Additionally, tissue from integrin-$\alpha3^{+/-}$ mice was included in the analysis; a marked reduction of immunoreactivity for integrin-α3 was observed at NMJs. Analysis of fluorescence intensity, normalised to that of wild type, revealed the following mean values for each genotype: wild type, 100% (SD 20.0, n=10 NMJs across 3 animals); integrin-$\alpha3^{+/-}$, 43.4% (SD 14.5, n=18 NMJs across 3 animals); integrin-$\alpha3^{-/-}$, 2.5% (SD 4.6, n=8 NMJs across 3 animals). Statistical analysis demonstrated that $P<0.0001$ for each mutant genotype, in comparison to wild type (Mann-Whitney U test). The finding of decreased immunoreactivity of integrin-α3 at integrin-$\alpha3^{+/-}$ NMJs suggests that gene dosage is

important for the regulation of integrin-α3 protein copy number in this system. The following experiments aimed to investigate the role of this protein at the NMJ.

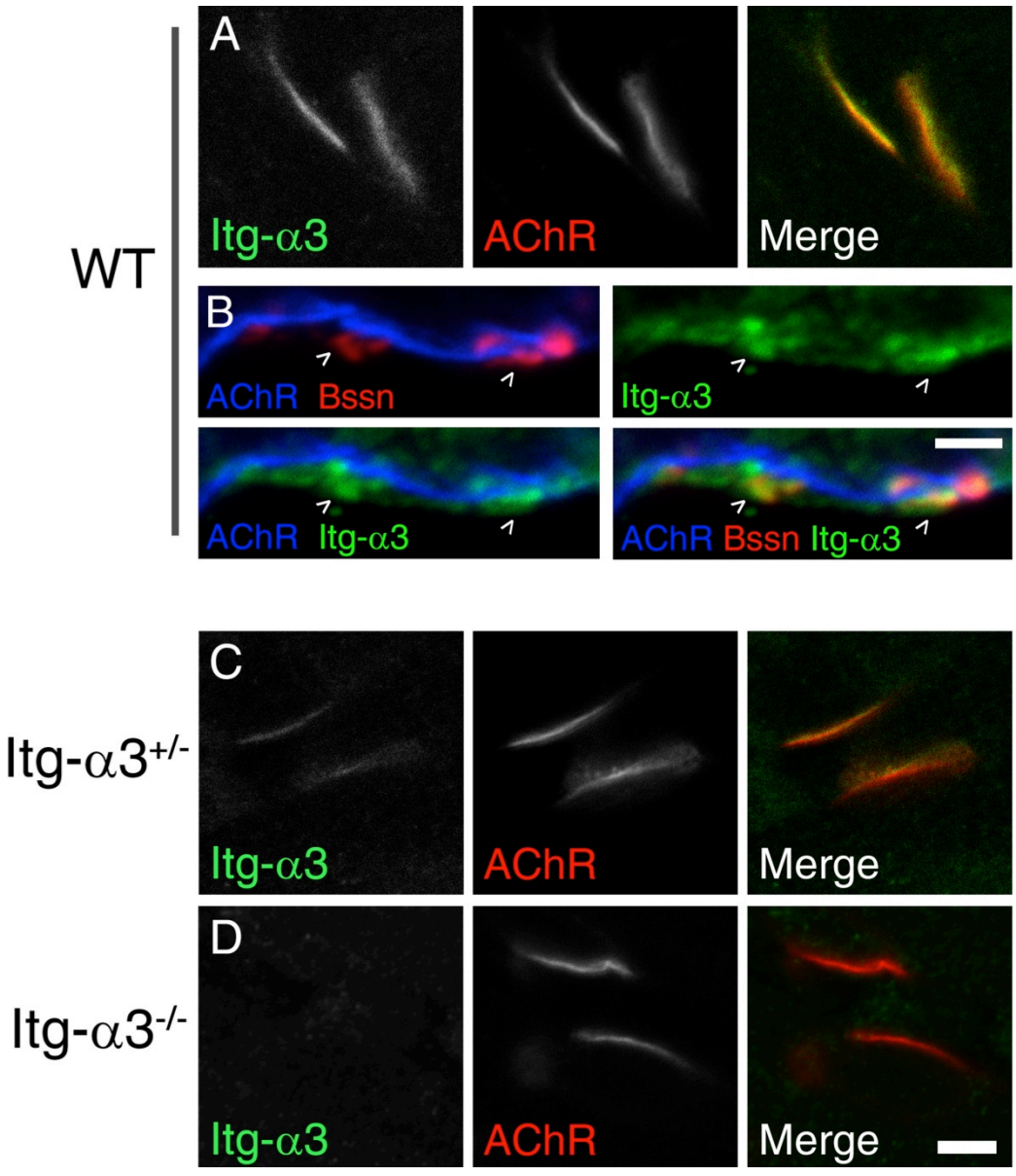

Fig 4.1. Localisation of integrin-α3 at the active zones of the NMJ. Immunohistochemistry for integrin-α3 in E18.5 NMJs. Sternomastoid muscles from wild type (A), integrin-α3$^{+/-}$ (C), and $^{-/-}$ (D) mice. Postsynaptic acetylcholine receptors (AChRs) were counterstained with fluorescently conjugated α-bungarotoxin. (B) Integrin-α3 colocalises with active zone marker bassoon in wild type NMJs. Single confocal slices at x40 magnification (A, C, D); Z-stack of three confocal slices 0.4 μm apart, at high (x63 oil immersion) magnification (B). *Abbreviations: WT, wild type; Itg-α3, integrin-α3; Bssn, bassoon. Similar results observed across three animals per genotype. Scale bars: 5 μm (A, C, D) and 2 μm (B).*

4.3. Integrin-α3 does not have a role in gross development of the NMJ

To assess whether the NMJs of integrin-α3$^{-/-}$ mice form basic pre- and postsynaptic apparatus, immunohistochemistry was carried out on sections of trunk from E18.5 embryos. AChR-positive NMJs were found in the intercostal muscles of wild type (**Fig 4.2A-C**) and integrin-α3 $^{-/-}$ (**Fig 4.2D-F**) mice. Antibodies were used to label SV2 (**Fig 4.2A, D**), rapsyn (**Fig 4.2B, E**) and utrophin (**Fig 4.2C, F**). SV2 is a presynaptic protein found on synaptic vesicles; rapsyn is a postsynaptic effector of the AChR clustering pathway; and utrophin is a component of the UGC on the postsynaptic membrane, and promotes postsynaptic folding. Similar localisation and staining intensity were observed in wild type and integrin-α3$^{-/-}$ NMJs, for all labelled proteins. In addition, NMJs appeared to be approximately similar sizes in both genotypes, as judged by lengths of AChR+ plaques, and the three associated markers that were tested. Similar lengths of AChR plaques was also observed in the NMJs of sternomastoid muscles (**Fig 4.1**). These results suggest that integrin-α3 is not required for the assembly of basic pre- and postsynaptic elements. Further work was carried out to assess whether integrin-α3 is required for the formation of active zones and ultrastructural features.

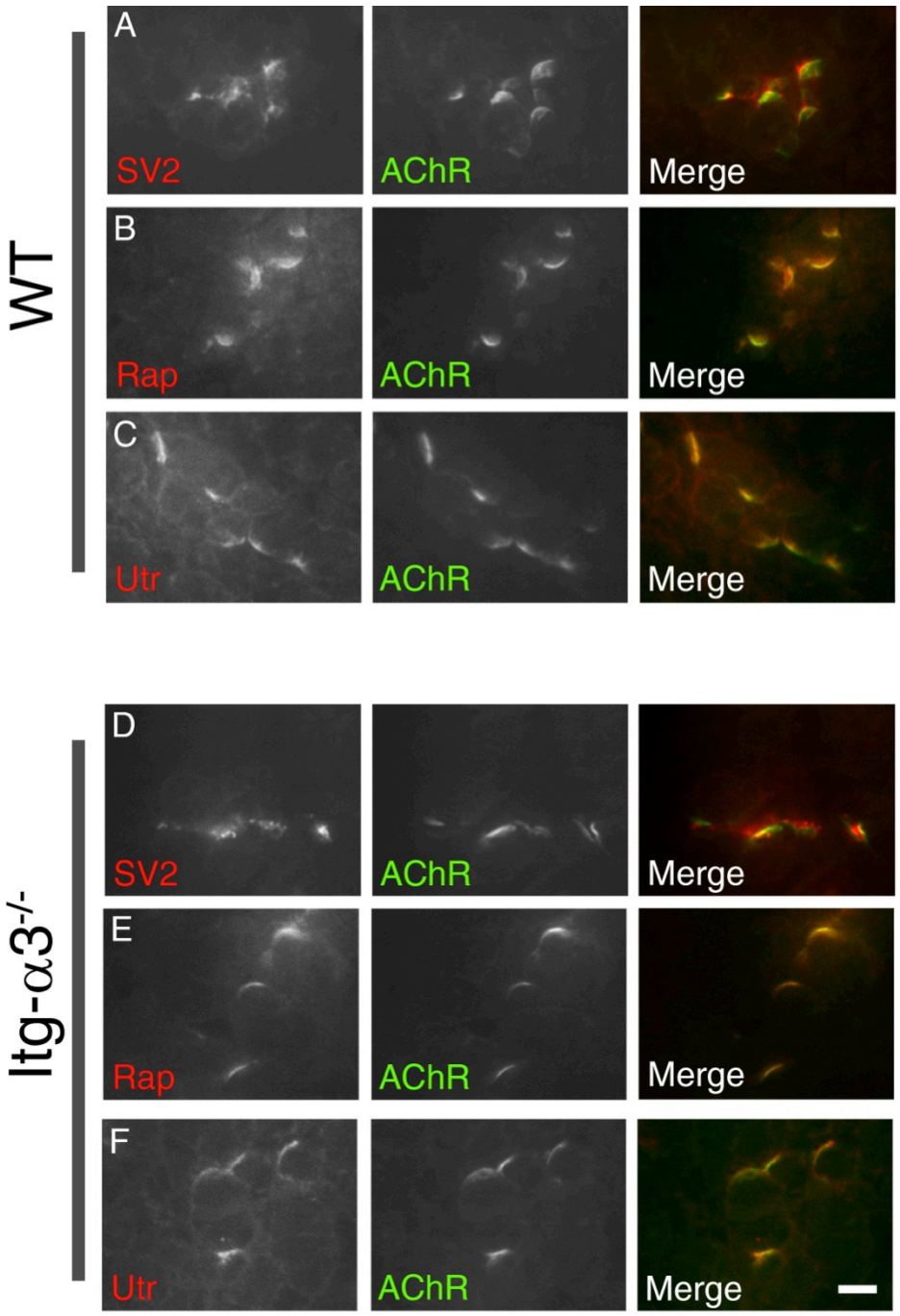

Fig 4.2. Normal localisation of pre- and postsynaptic markers in integrin- $\alpha3^{-/-}$ NMJs. Immunohistochemistry for pre- and postsynaptic markers at E18.5 NMJs. Sternomastoid muscles from wild type (A-C) and integrin-$\alpha3^{+/-}$ (D-F) mice were stained with antibodies to the following: synaptic vesicle protein 2 (SV2), a marker of the presynaptic terminus (A, D); rapsyn, an effector in the clustering of postsynaptic acetylcholine receptors (B, E); and utrophin, a component of the utrophin-dystroglycan complex (UGC), found on the postsynaptic membrane (C, F). AChRs were counterstained with fluorescently conjugated α-bungarotoxin. *Abbreviations: WT, wild type; Itg-α3, integrin-α3; SV2 (synaptic vesicle protein 2); Rap, rapsyn; Utr, utrophin. Similar results observed across three animals per genotype. Scale bar: 10 μm.*

4.4. Integrin-α3 is required for the localisation of key active zone components at the E18.5 NMJ

As mentioned previously, active zones of the NMJ are visible by immunohistochemistry from E16.5 (Chen et al., 2012). To assess whether or not active zones assembly was normal in integrin-α3 mutant NMJs, immunohistochemistry was carried out on E18.5 sternomastoid muscles. Integrin-$\alpha3^{+/-}$ tissue was included in this experiment, as immunoreactivity for integrin-α3 was markedly reduced in NMJs from these animals (**Fig 4.1C**). In wild type mice, the active zone markers bassoon, piccolo and P/Q VGCC were observed to localise in a punctate pattern, in close apposition to the AChRs (**Fig 4.3A-C**). However, the staining intensity of these proteins was markedly reduced in both integrin-$\alpha3^{+/-}$ (**Fig 4.3D-F**) and $^{-/-}$ (**Fig 4.3G-I**) NMJs. These results demonstrate that integrin-α3 has a major role in the initial assembly of active zones at the NMJ.

Although the staining intensity of bassoon, piccolo and P/Q VGCC was markedly reduced in integrin-$\alpha3^{+/-}$ and $^{-/-}$ NMJs, a residual level of immunoreactivity was present, particularly in the case of bassoon. This suggests that some localisation of these active zone proteins occurs even in the absence of integrin-α3, perhaps in reduced copy number, or in a more diffuse pattern in the membrane. In addition, the active zone complex contains various other proteins that were not addressed in this experiment (Südhof, 2012). Therefore, EM was carried out to determine whether structural alterations occur in active zones of integrin-$\alpha3^{+/-}$ and $^{-/-}$ NMJs.

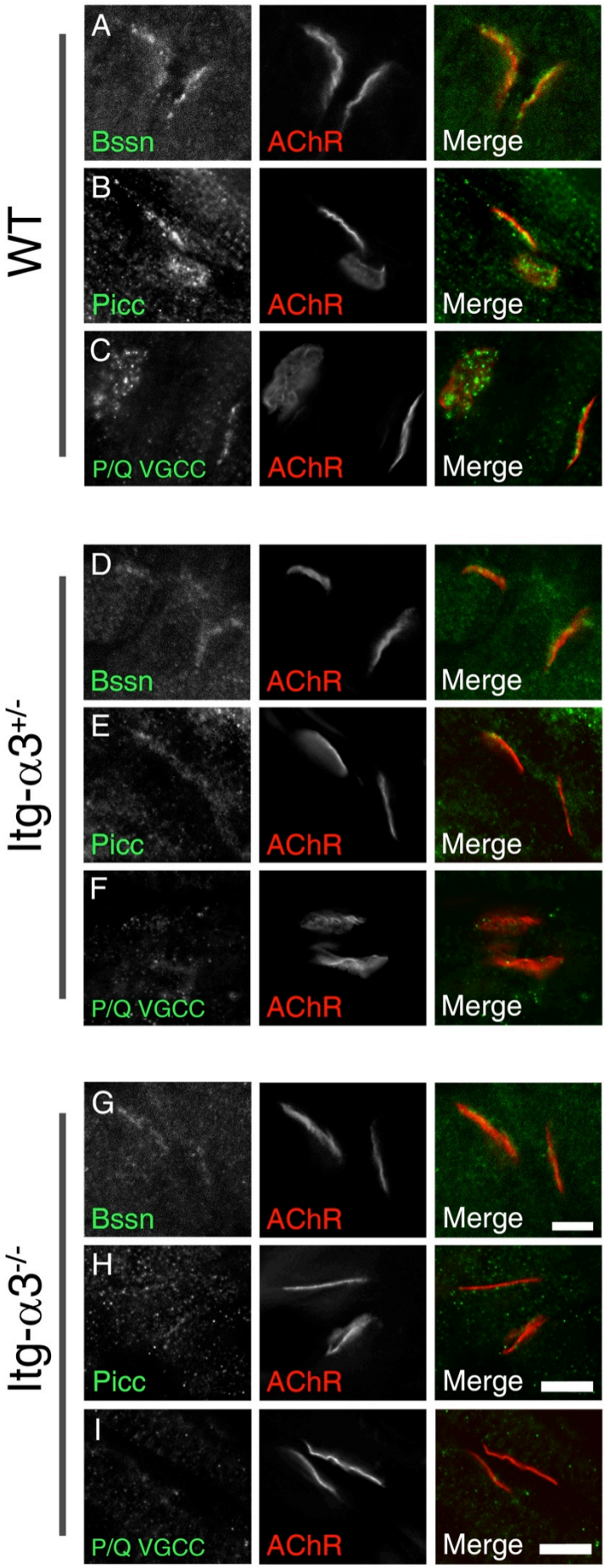

Fig 4.3. *(Legend on next page)*

Fig 4.3. *(Previous page)* Altered assembly of active zones in integrin-α3 mutant NMJs at E18.5. Immunohistochemistry for active zone proteins, in wild type (A-C), integrin-$\alpha3^{+/-}$ (D-F), and $^{-/-}$ (G-I) sternomastoid muscles at E18.5. NMJs were labelled with antibodies to bassoon (A, D, G), piccolo (B, E, H) and P/Q-type voltage gated calcium channel (C, F, I). Postsynaptic acetylcholine receptors (AChRs) were counterstained with fluorescently conjugated α-bungarotoxin. *Abbreviations: WT, wild type; Itg-α3, integrin-α3; Bssn, bassoon; Picc, piccolo; P/Q VGCC, P/Q-type voltage-gated calcium channel. Similar results observed across three animals per genotype. Scale bar: 5 μm.*

4.5. Integrin-α3 is dispensable for gross active zone formation and vesicle docking

Ultrastructural analysis was carried out on longitudinal ultrathin sections of E18.5 diaphragm. Tissue processing and sectioning was carried out by **Mark Turmaine**; scanning and imaging was carried out myself. Active zones of the NMJ are normally visible on EM sections as small (50-100 nm), electron-dense puncta on the inner leaf of the presynaptic membrane, with clusters of docked vesicles (Chen et al., 2011; Patton et al., 2001). NMJs appeared grossly similar in wild type, integrin-$\alpha3^{+/-}$ and $^{-/-}$ tissue: nerve terminals contained synaptic vesicles, and were in apposition with muscle fibres (**Fig 4.4A**). Postsynaptic folding occurs during postnatal development, and was not observed at this stage (Witzemann, 2006). Active zones of similar size and appearance were visible in all three genotypes (**Fig 4.4A, B**; asterisks in B); and were surrounded by clusters of docked vesicles. These results suggest that even though the recruitment of bassoon, piccolo and P/Q VGCC is impaired in integrin-$\alpha3^{+/-}$ and $^{-/-}$ NMJs, other core active zone proteins are still able to assemble and dock vesicles. Thus, integrin-α3 is not required for the formation of active zones, but for the proper localisation of some (at least three) of the components. In addition, it may have roles in the structural arrangement of the active zone; however, EM at this resolution does not reveal the macromolecular elements of the complex.

4.6. Integrin-α3 is required for the correct organisation and/or deposition of synaptic basal lamina at E18.5

In addition to the active zones, electron micrographs allowed other ultrastructural details of the NMJ to be examined. **Mark Turmaine** carried out tissue processing and sectioning; I carried out all image scanning and acquisition. Although the pre- and postsynaptic elements of integrin-$\alpha3^{+/-}$ and $^{-/-}$ NMJs developed normally on the gross scale, alterations in the structure of the synaptic basal lamina were observed in both of these genotypes. In electron micrographs, the basal lamina often consists of an electron-dense layer (lamina densa) and an electron-lucent layer (the lamina lucida) that lines the cell membrane. The former is assumed to be mesh-like in structure, and the latter to be comprised of regions of ligand-receptor interactions. At the basal lamina of the NMJ, the lamina densa occupies the centre of the cleft, with lamina lucida portions on either side lining both the muscle and nerve membranes (Chen et al., 2011; Sanes, 2003). This is apparent in wild type NMJs at E18.5 (**Fig 4.4B**, arrows mark the basal lamina). In integrin-$\alpha3^{+/-}$ and $^{-/-}$ NMJs, the lamina densa was observed to fill the entire width of the synaptic cleft. This result suggests that the basal lamina of mutant NMJs is disorganised, either through the loss of integrin binding, or through increased deposition of its components. The apparent increase in the quantity of electron-dense material present at mutant NMJs would suggest the latter; indeed, the deposition of extra layers of ECM components is observed in other tissues of integrin mutant mice (e.g. the epidermis of integrin-$\alpha3^{-/-}$ mice) (Conti et al., 2003).

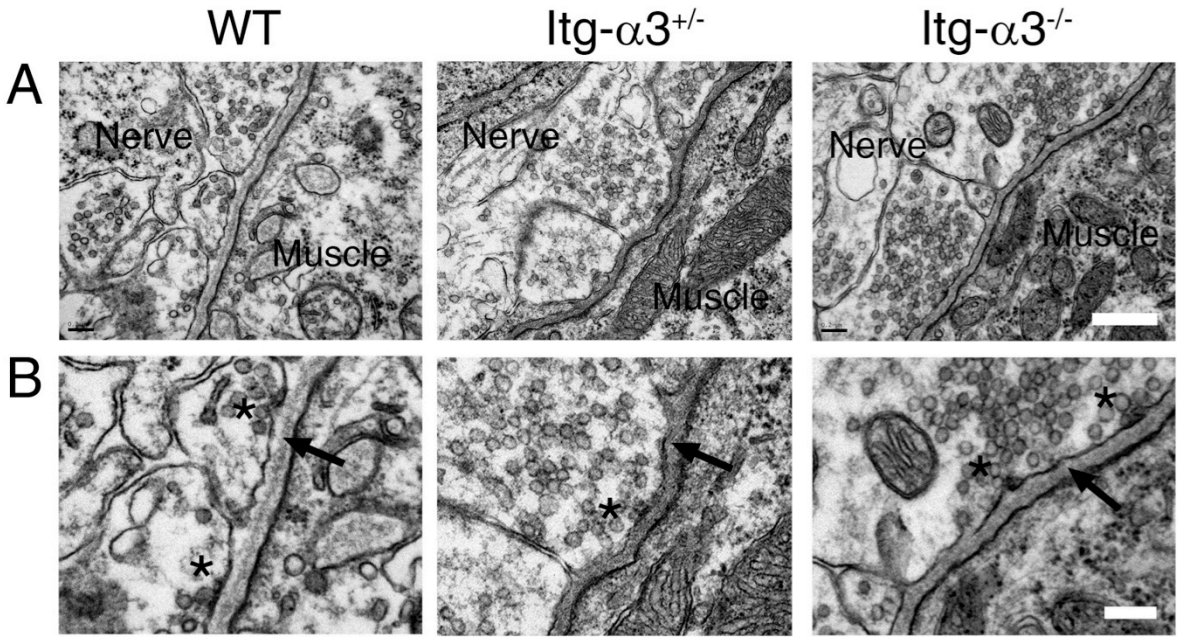

Fig 4.4. Grossly normal active zone structure, but aberrant deposition of synaptic basal lamina in E18.5 integrin-α3 mutants. Electron micrographs of wild type, integrin-α3$^{+/-}$ and $^{-/-}$ NMJs in E18.5 diaphragm muscles. Magnification at x30,000 (A) or x50,000 (B). Synaptic vesicles and active zones (asterisks) were visible in all three genotypes. The deposition of the synaptic basal lamina was abnormal in integrin-α3$^{+/-}$ and $^{-/-}$ NMJs, with electron dense material filling the entire width of the cleft, unlike that of wild type (arrows in B). *Abbreviations: WT, wild type; Itg-α3, integrin-α3. Similar results observed across three animals per genotype. Scale bars: 500 nm (A) and 200 nm (B).*

4.7. Integrin-α3 is not required for the localisation of agrin and synaptic laminins at E18.5 NMJs

While the basal lamina displayed an altered ultrastructural organisation in integrin-α3$^{+/-}$ and $^{-/-}$ NMJs (**Fig 4.4B**), it remained to be determined whether this change was associated with changes at the molecular level. To assess whether the localisation of key basal lamina proteins was altered in mutant NMJs, immunohistochemistry was carried out for three constituents with major roles in NMJ development: agrin, and laminins-α4 and α5 (Jaworski and Burden, 2006; Samuel et al., 2012). As integrin-α3 is known to bind to laminin-α4 at the *Torpedo* electric synapse, its deposition might be altered at the NMJ (Carlson et al., 2010b). E18.5 trunk sections were labelled with antibodies to the aforementioned proteins, and intercostal muscles examined. While in adult muscle these proteins are NMJ-specific, during late embryogenesis and early postnatal life these proteins are also associated with the extrasynaptic portions of the muscle fibre (Singhal and Martin, 2011). All three proteins were found to localise at the NMJs (marked with fluorescently-conjugated α-bungarotoxin), and at the rest of the sarcolemma. Staining intensity and localisation were similar in wild type (**Fig 4.5A-C**), integrin-α3$^{+/-}$ (**Fig 4.5D-F**) and $^{-/-}$ (**Fig 4.5G-I**) NMJs. These results suggest that at the gross level, integrin-α3 does not have a major influence on the localisation of these proteins, despite the defect in deposition/organisation of the basal lamina as a whole (**Fig 4.4B**).

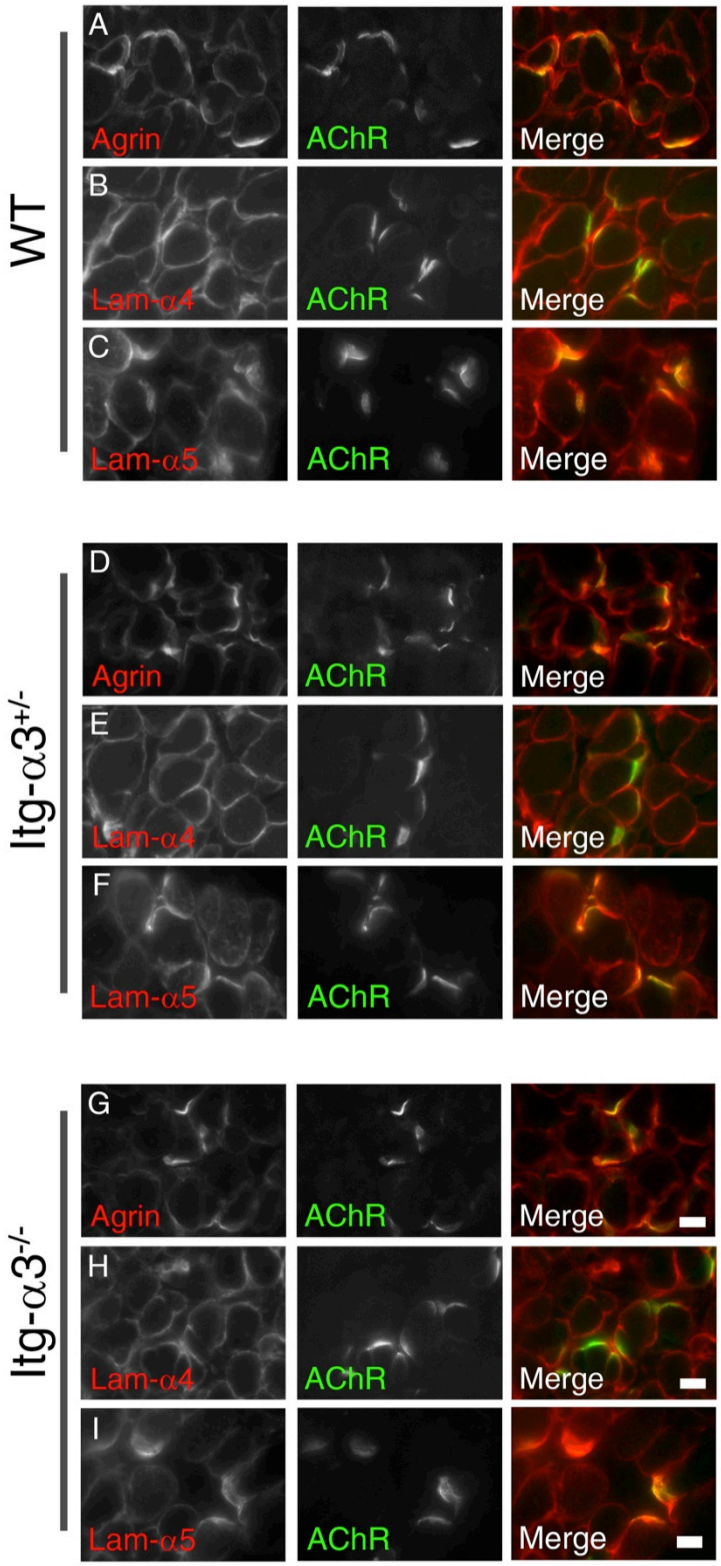

Fig 4.5. Normal deposition of agrin and synaptic laminins at integrin-α3 mutant NMJs at E18.5. Immunohistochemistry on wild type (A-C), integrin-α3$^{+/-}$ (D-F), and $^{-/-}$ (G-I) intercostal muscles at E18.5. Antibodies to agrin (A, D, G), laminin-α4 (B, E, H) and laminin-α5 (C, F, I). Postsynaptic acetylcholine receptors (AChRs) were counterstained with fluorescently conjugated α-bungarotoxin. *Abbreviations: WT, wild type; Itg-α3, integrin-α3; Lam, laminin. Similar results observed across three animals per genotype. Scale bar: 10 μm.*

4.8. The number of NMJs per muscle fibre is increased in integrin-α3 mice at E18.5

In typical muscles, motoneuron axons form a band across the central region of the myofibres, innervating the muscle at the midline. This region is often referred to as the endplate zone. Many experimental models with defects in NMJ proteins, such as rapsyn, agrin, MuSK, ChAT and Munc13 present with altered innervation patterning (An et al., 2010; Banks et al., 2001, 2003; Fu et al., 2005; Schwander et al., 2004). The endplate zone is frequently widened, with innervation sites straying further from the centre. This is assumed to be due to nerve terminals failing to form fully functional NMJs, and sprouting further away in an attempt to find new innervation sites. To assess whether the innervation pattern was altered in integrin-α3 mutant muscles, whole mount diaphragms were immunostained with antibodies to neurofilament and SV2 (labelled as one colour to mark nerves and nerve terminals together), and fluorescently-conjugated α-bungarotoxin to mark AChRs. The diaphragm muscle at late embryogenesis/early postnatal stages serves as a good system to analyse motoneuron patterning, as it is a thin muscle that allows imaging through its entire depth. For consistency, the right hemisphere of the diaphragm was used for analysis in all animals.

Fig 4.6A shows an example right hemisphere, stained for neurofilament, and in this case from an integrin-$\alpha3^{+/-}$ mouse. Here, the phrenic nerve is shown entering the hemisphere from the left hand side, before splitting into a fork, to supply all the muscle fibres along the length. A similar gross morphology was observed at this innervation fork in wild type, integrin-$\alpha3^{+/-}$ and $^{-/-}$ diaphragms (**Fig 4.6B**). To analyse the patterning of innervation in more detail, numbers of branches were quantified. Primary branching was defined as the single nerve entering the hemidiaphragm; subsequent divergences were defined as secondary, tertiary and quaternary branches (as described in *Section 2.18., data analysis*). There was a significant increase in the highest order, quaternary branching in integrin-$\alpha3^{+/-}$ and $^{-/-}$ diaphragms, in comparison to wild type (**Fig 4.6C, E**: 4° branching; integrin-$\alpha3^{+/-}$, 119% increase over wild type, P=0.0089; integrin-$\alpha3^{-/-}$, 138% increase over wild type, P=0.0079).

To determine whether the increase in motoneuron branches in integrin-α3$^{+/-}$ and $^{-/-}$ diaphragms was associated with an increase in the number of NMJs, images were merged to display both AChRs and nerves. In all three genotypes, almost every AChR cluster (>95%) was apposed by a neurofilament/SV2^{+} nerve terminal, indicating that they were innervated. A significant increase in the number of NMJs was observed in integrin-α3$^{+/-}$ and $^{-/-}$ diaphragms, compared to wild type (**Fig 4.6C, F**; integrin-α3$^{+/-}$, 49% increase over wild type, P=0.010; integrin-α3$^{-/-}$, 77% increase over wild type, P= 0.019). In muscle histological analyses of diaphragms (**Fig 3.2C-G**; *Section 3.3., muscle morphology is normal in E18.5 integrin-α3 mutant mice*), similar numbers of muscle fibres were observed in all three genotypes. Thus, these findings demonstrate that there are more NMJs per muscle fibre in integrin-α3 mutant muscles compared to wild type.

As NMJ defects are often accompanied by an increase in the endplate zone width, we analysed the motoneuron patterning further. No significant differences in endplate zone width were observed between wild type, integrin-α3$^{+/-}$ and $^{-/-}$ diaphragms (**Fig 4.6D, G**; P=0.43 and 0.73 for integrin-α3$^{+/-}$ and $^{-/-}$ diaphragms respectively, compared to wild type). Together, these results indicate a role for integrin-α3 in the regulation of NMJ number, but not in gross innervation patterning.

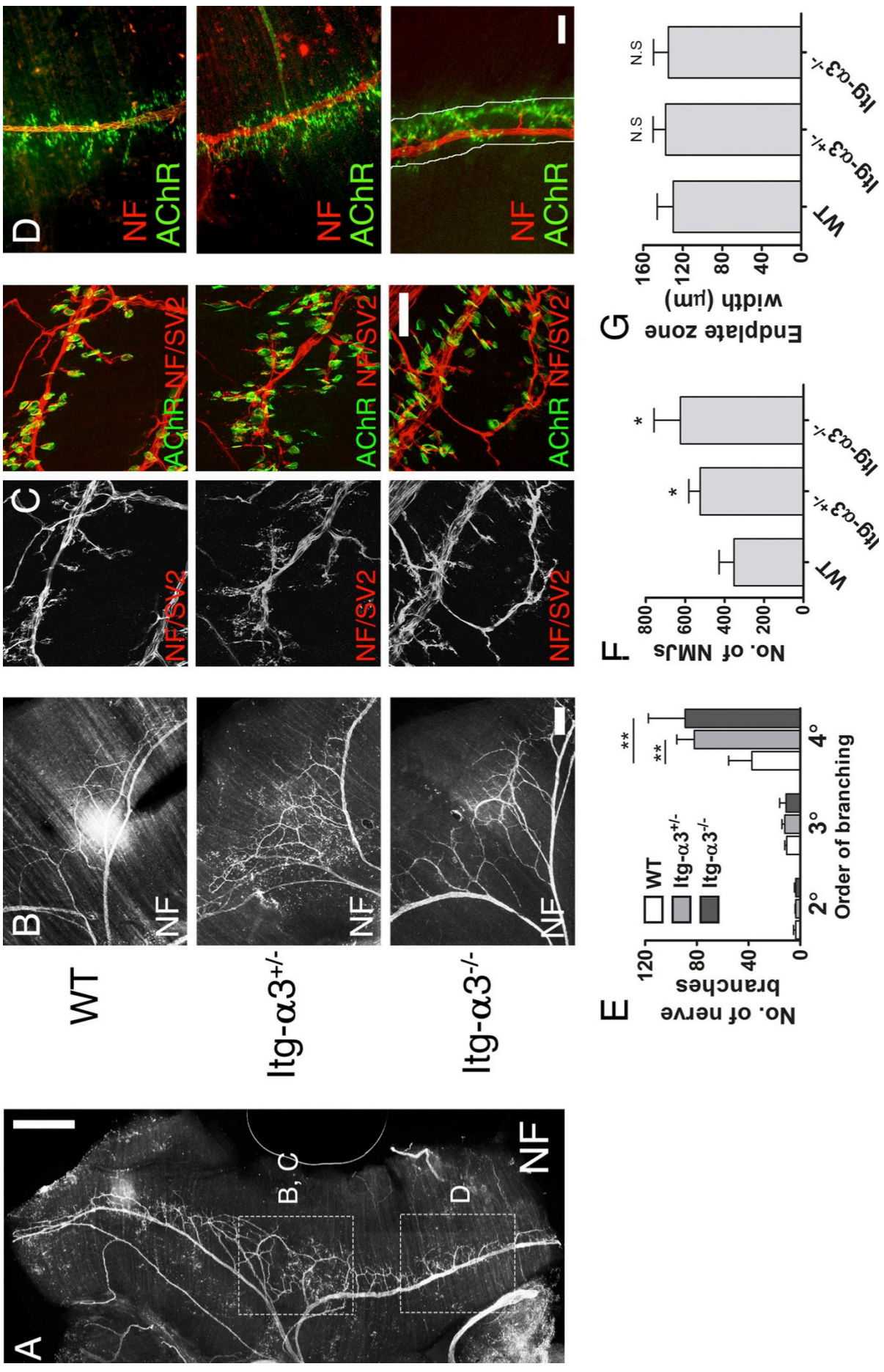

Fig 4.6. *(Legend on next page)*

Fig 4.6. *(Previous page)* Increased number of NMJs per muscle fibre in E18.5 integrin-α3 mutants. Right-hand hemidiaphragms from wild type, integrin-$\alpha3^{+/-}$ and $^{-/-}$ mice at E18.5. Whole mount tissue was stained with anti-neurofilament and anti-synaptic vesicle protein 2 (SV2) to mark axons and presynaptic termini respectively. Postsynaptic acetylcholine receptors (AChRs) were counterstained with fluorescently conjugated α-bungarotoxin. As an example, a low power image from an integrin-$\alpha3^{+/-}$ diaphragm, to show gross innervation pattern (A). Phrenic nerve forks at low (B) and high (C) power, and area of innervation at distal portions of the hemisphere (D). Marked areas on (A) correspond roughly to the sites imaged in (B), (C) and (D). >95% of AChR clusters were innervated in each genotype, being associated with a nerve input and $SV2^{+}$ terminal (C). The central 2 mm of the phrenic nerve fork was quantified for 2°, 3°, and 4° nerve branches and AChR+ NMJs (E, F respectively). Previous analysis had confirmed that there were similar numbers of muscle fibres in diaphragms from all three genotypes (**Fig 3.2**); thus these data imply that there is an increase in NMJs per muscle fibre in integrin-$\alpha3^{+/-}$ and $^{-/-}$ mice, compared to wild type. Quantification of endplate zone width across whole hemispheres (G), with boundaries illustrated by white lines in (D). *Abbreviations: WT; wild type; Itg-α3, integrin-α3; NF, neurofilament. n = 4-7 diaphragms per genotype (median +/- IQR, Mann-Whitney U test). Scale bars: 500 μm (A), 100 μm (B), 50 μm (C, D).*

4.9. Integrin-α3 regulates efficient synaptic vesicle release at E18.5 NMJs

So far, defects identified in integrin-α3 mutants include the aberrant assembly of active zones (**Fig 4.3**), and increased number of NMJs per muscle fibre (**Fig 4.6**). One would expect that neurotransmission is impaired in NMJs that have defects in active zone composition, in this case an apparent decrease in quantity of bassoon, piccolo and P/Q VGCC in mutant terminals. VGCCs are known to be particularly important for active zone function, as it controls Ca^{2+} influx, and thus synaptic vesicle release. An increase in the number of NMJs per muscle fibre may be a compensatory mechanism when neurotransmission is impaired, with the neuromuscular system responding to a lack of electrical activity by forming more innervation sites (Misgeld et al., 2002; Pacifici et al., 2011). Therefore, further studies were carried out to

investigate the hypothesis that exuberant innervation in mutants is an attempt to compensate for reduced synaptic transmission.

Ex vivo electrophysiology was carried out on E18.5 diaphragms, by **Richard Webster**. Data analysis and interpretation was performed myself. The measurement of evoked neurotransmission was technically very difficult in the small thoraxes at perinatal stages, as it requires manipulation of the phrenic nerve. Therefore only spontaneous events of synaptic vesicle release (MEPPs) were recorded. These are visible as single spikes in electrophysiological recordings, and each is assumed to represent a signal deriving from the release of a single synaptic vesicle. Four overlaid traces from an integrin-$\alpha3^{+/-}$ endplate are shown in **Fig 4.7A** as an example. The amplitude and frequency of MEPPs were similar in wild type, integrin-$\alpha3^{+/-}$ and $^{-/-}$ diaphragms (**Fig 4.7B, C**; MEPP amplitude, P=0.28 and 0.19 for integrin-$\alpha3^{+/-}$ and $^{-/-}$ diaphragms respectively, compared to wild type; MEPP frequency, P=0.11 and 0.80 for integrin-$\alpha3^{+/-}$ and $^{-/-}$ fibres respectively, compared to wild type). However, as MEPPs are measured on a single muscle fibre, any events of depolarisation could be caused by activity from any of the synapses that innervate it. In the case of wild types, there should be one endplate per fibre (Witzemann, 2006). In integrin-$\alpha3^{+/-}$ and $^{-/-}$ diaphragms, it was estimated that each muscle fibre was innervated by more than one NMJ. Therefore, MEPP frequency values were normalised to the number of NMJs (**Fig 4.6F**), with the wild type number set at '1' (for one endplate per muscle fibre). Thus a measurement of MEPP frequency per NMJ was obtained. Integrin-$\alpha3^{+/-}$ and $^{-/-}$ diaphragms displayed a significantly reduced MEPP frequency per NMJ, compared to wild type (**Fig 4.7D**; integrin-$\alpha3^{+/-}$, 52% decrease from wild type, P=0.012; integrin-$\alpha3^{-/-}$, 44% decrease from wild type, P=0.040).

Further evidence of a presynaptic defect was found in electron micrographs of E18.5 NMJs. A significant increase in synaptic vesicle accumulation was observed in nerve terminals of integrin-$\alpha3^{-/-}$ mice, compared to wild type (**Fig 4.7E-H**; 26% more synaptic vesicles per μm^2 compared to wild type, P=0.027). The density of synaptic vesicles in integrin-$\alpha3^{+/-}$ NMJs was

slightly higher than that of wild type, but did not reach significance (17% increase over wild type, P=0.14). An increase in the number of synaptic vesicles is often indicative of a defect in neurotransmitter release, as vesicles accumulate in greater numbers due to a decrease in the rate of their fusion. Taken together, these results suggest the possibility that the increase in NMJ number per muscle fibre in integrin-α3 mutants is a result of impaired neurotransmitter release. The average probability of vesicle release is reduced per NMJ in integrin-α3 mutants (**Fig 4.7D**), but the increase in NMJ number compensates and restores this value to approximately that of wild type (**Fig 4.7C**).

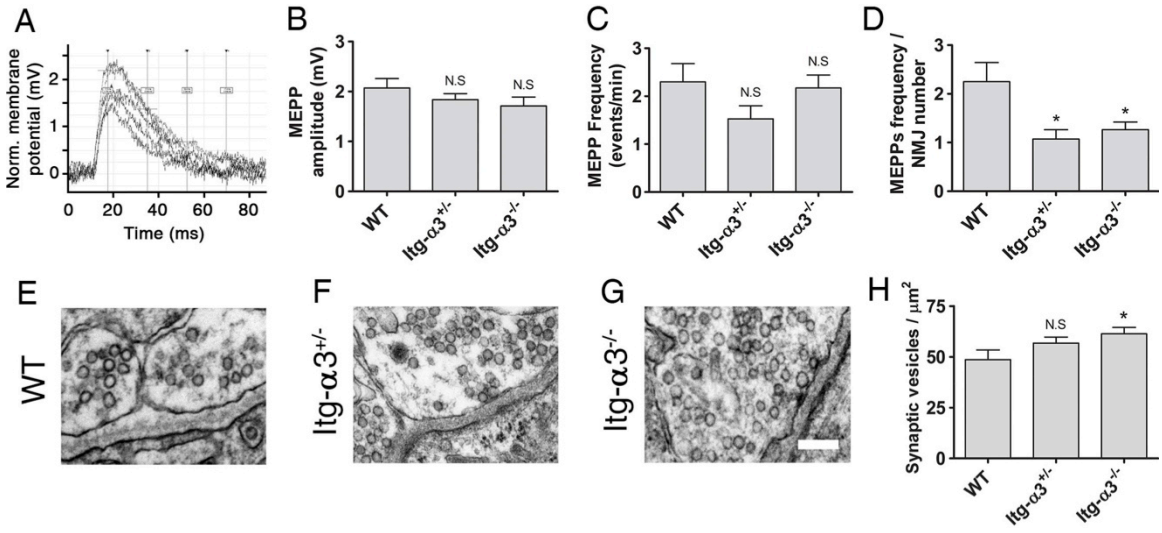

Fig 4.7. Reduced synaptic vesicle release probability in E18.5 integrin-α3 mutant NMJs. Four overlaid, representative traces of miniature endplate potentials (MEPPs) from an integrin-α3$^{+/-}$ diaphragm (A). Quantification of MEPPs: amplitude (B), frequency (C) and frequency normalised per NMJ number (D). NMJ number was previously quantified in whole mount diaphragms (**see Fig 4.6**), and treated as in *Section 2.18., data analysis*. Representative images of synaptic vesicles in nerve terminals by electron microscopy (E-G), and their quantification per μm of presynaptic bouton (H). *Abbreviations: WT; wild type; Itg-α3, integrin-α3. n = 19-24 MEPPs across 3 animals per genotype in panels A-D (mean +/- SEM, t-test); n = 14-32 boutons across 3 animals per genotype in panels E-H (mean +/- SEM, t-test). Scale bar: 200 nm.*

4.10. Discussion

The results of this chapter demonstrate that both integrin-α3$^{+/-}$ and $^{-/-}$ mice serve as a good model to study the role of integrin-α3 at the NMJ. The data, showing a comparable impairment of synaptic transmission in integrin-α3$^{+/-}$ and $^{-/-}$ mice, suggest that there is haploinsufficiency for this protein at the NMJ, with gene dosage being an important factor for maintaining its function. Integrin-α3 is required for the proper assembly of active zones, in particular the localisation of bassoon, piccolo and P/Q VGCC (**Fig 4.3**). However, active zones are still able to form and recruit vesicles in integrin-α3 mutants, suggesting that other members of the core complex are not dependent on integrin-α3 for localisation (**Fig 4.4**). The organisation/deposition of basal lamina on the ultrastructural scale is also directed by integrin-α3 (**Fig 4.4**). However, the general localisation of key synaptic basal lamina proteins is unperturbed by loss of integrin-α3, suggesting that it does not regulate the molecular composition of the ECM on the gross scale (**Fig 4.5**). Finally, an impairment in spontaneous vesicle release was observed in integrin-α3 mutants (**Fig 4.7**); however, a corresponding increase in NMJ number per muscle fibre may be a mechanism to compensate for this loss of activity (**Fig 4.6**).

As integrins are key receptors for ECM proteins, the role of integrin-α3 in the deposition and organisation of the synaptic basal lamina was investigated. The synaptic basal lamina is largely deposited by the muscle fibre, with the exception of neural agrin which is produced by the nerve terminal. While integrin-α3 does not regulate the gross localisation of laminins-α4, α5 and agrin to the synaptic cleft (**Fig 4.5**), the ultrastructural observations suggest that it plays a role in the deposition/organisation of the basal lamina (**Fig 4.4**). The lamina densa, the electron-dense portion of the basal lamina, normally runs through the centre of the cleft, with a structure that is thought to be mesh-like. On either side of this are electron-lucent regions, one lining the nerve terminal, and one the muscle sarcolemma. These portions are known as the lamina lucida, and are assumed to contain the interacting regions of basal lamina proteins and their cell surface receptors (Sanes, 2003). This structural arrangement of the basal lamina is illustrated in **Fig 4.4B**, in the electron micrograph of a wild type NMJ at E18.5. However, in

the integrin-α3$^{+/-}$ and $^{-/-}$ mice, the lamina densa is observed to fill the entire cleft, with no lamina lucida evident.

It should be noted that there is some controversy surrounding the interpretation of electron micrographs, in terms of basal lamina structure. Evidence suggests that the lamina lucida may be an artefact, due to a slight 'shrinking away' of the plasma membrane during tissue preparation (Chan and Inoue, 1994). Even if the lamina lucida is an artefact, the difference in basal lamina appearance was consistent across all NMJs studied. In this respect, the difference between wild type and mutant animals could reflect an altered arrangement of the basal lamina itself, or alternatively alterations in its adhesive properties with the cell membrane. Another explanation is that there is an increase in the overall deposition of basal lamina proteins in integrin-α3 mutants, such that the electron-dense material fills the entire space. This would be consistent with findings in other tissues; for instance, loss of integrin-α3 in the epidermis leads to the deposition of extra layers of basal lamina, extending tens of micrometres from the membrane (Conti et al., 2003). This is also evident by light microscopy, where multiple layers of laminin-α5, collagens and nidogens are observed. However, unlike in the epidermis, the deposition of distinct layers of ECM may not be visible by light or electron microscopy in the narrow (~ 50 nm) space of the NMJ synaptic cleft. This may explain why the lamina densa of integrin-α3 mutants appears to completely fill the available synaptic space. In support of this, the width of the cleft is well below the resolution limit of light microscopy (~200 nm). Finally, we cannot exclude the possibility that other ECM proteins, not tested in this panel, are specifically altered.

Because integrin-α3 is localised at the active zones of the NMJ (**Fig 4.1** and previous studies (Carlson et al., 2010b; Cohen et al., 2000a), immunohistochemistry was carried out for bassoon, piccolo and P/Q VGCC at E18.5. Active zones become visible at the newly formed NMJs from around E16.5 (Clarke et al., 2012), although the timing of integrin-α3 localisation before E18.5 was not investigated in this study. Immunoreactivity for these three proteins was

markedly reduced in integrin-α3$^{+/-}$ and $^{-/-}$ NMJs; in contrast, those from wild type displayed clear, punctate staining for each of these markers (**Fig 4.3**). This result demonstrates that integrin-α3 is required for the initial assembly of active zones at the NMJ. As active zones of perinatal NMJs contain both P/Q and N-type VGCCs, immunohistochemistry for the latter was also carried out. However, no fluorescence signal was observed for any of the antibodies tested. VGCCs are notoriously difficult to detect by immunohistochemistry (personal communication, Prof Annette Dolphin, UCL). Another approach is the use of conotoxins, which bind to different subtypes of VGCC with high specificity (Robinson and Norton, 2014), although the commercial availability of these in fluorescently-conjugated form is limited. Despite this, the data show that the localisation of at least one of the two developmental VGCCs is perturbed at the integrin-α3 mutant NMJ.

Analysis of electron micrographs demonstrated that despite the near loss of several active zone components, electron-dense puncta were still observed at the presynaptic membrane of integrin-α3$^{+/-}$ and $^{-/-}$ NMJs at E18.5. These active zones resembled those of wild type NMJs, in appearance and the presence of docked vesicles (**Fig 4.4**). This suggests that other core active zone components are still able to assemble, as well as recruit vesicles, in the absence of integrin-α3. It would therefore be of interest to assess a range of other active zone proteins such as Munc13, RIM and RIM-BP. In light of the basal lamina defects in integrin-α3 mutants, there are several possible explanations for integrin-α3's precise role in active zone assembly: (1) It recruits active zone components directly; (2) it organises the basal lamina, which in turn ensures correct initiation of active zones, since laminin-VGCC interactions are known to be crucial for this process (Chen et al., 2011; Nishimune et al., 2004); (3) it engages cytoskeletal components such as actin, which is also known to be important for bassoon/piccolo localisation, at least in central synapses (Zhang and Benson, 2001).

A number of mouse models with mutations in NMJ proteins present with innervation defects (e.g. rapsyn, agrin, MuSK, ChAT and Munc13 (An et al., 2010; Banks et al., 2001, 2003; Fu et al.,

2005; Schwander et al., 2004)). A widening of the endplate zone is frequently observed, with motoneuron terminals straying further than usual from the central band of muscle fibre innervation. In all of the above models, this is the most immediately apparent phenotype. In contrast, integrin-α3$^{+/-}$ and $^{-/-}$ mice display no widening of the endplate region at E18.5 (**Fig 4.6D, G**). Instead, there is a significant increase in the number of terminal motoneuron branches, such that there are more innervated NMJ sites per muscle fibre, compared to wild type (**Fig 4.6B, C, E, F**). Taken together, the integrin-α3 mutant mouse appears to have a mixed phenotype, sharing several features with other models: it displays no widened endplate zone, like the Munc18 and N/P/Q VGCC mutants (Chen et al., 2011; Heeroma et al., 2003); but multiple NMJs per muscle fibre, like the ChAT and AChRγ mutants (Misgeld et al., 2002; Pacifici et al., 2011). These data suggest that integrin-α3 is not required for the gross patterning of the endplate zone, and that the increased terminal innervation may rather be an attempt at compensation; this is consistent with the defects in active zone formation and neurotransmission in integrin-α3 mutants. Indeed, the upregulation of NMJ number has previously been suggested as a compensatory mechanism for defects in neurotransmission (Misgeld et al., 2002; Pacifici et al., 2011).

The reason(s) for the occurrence of a widened endplate zone in some mutant models, but not others, is not understood. Most current interpretations point to the fact that the NMJs that are formed are not fully functional, and that there may be subsequent growth in an attempt to establish new contact sites further away (Misgeld et al., 2002; Pacifici et al., 2011). Excessive NMJ formation may stem from an increase in axonal branching, or in the number of efferent axons in the phrenic nerve. Insights could be gained by the quantification of motoneuron bodies in the spinal column, or numbers of axons in the phrenic nerve cross section. Motoneuron survival at different stages of maturation has a major influence on the number of available axonal inputs at the muscle (Banks et al., 2001, 2003).

Of particular relevance to the integrin-α3 mutant model is a study that utilised conditional knockout mice for integrin-β1 (Schwander et al., 2004). When this subunit was ablated specifically in skeletal muscle, AChR clusters were unable to form (highlighting a role for postsynaptic integrins in AChR clustering), and motoneuron axons failed to terminate at the right location, extending far from the central band of the muscle. However, when integrin-β1 was knocked out specifically in motoneurons, NMJs formed normally, and there was no aberration in endplate zone width. These mice would lack a functional integrin-α3β1 dimer in the motoneurons, and as such, they resemble the integrin-α3 mutant in that the axons terminate at the right location in the central muscle region. It may thus be expected that the motoneuron-specific integrin-β1 knockouts would display similar defects to the integrin-α3 mutants in active zone assembly, terminal branching, and synaptic transmission; however the authors did not assess these phenotypic aspects (personal communication, Dr Martin Schwander, Rutgers University, New Jersey, USA).

Ex vivo electrophysiology was carried out on integrin-$\alpha3^{+/-}$ and $^{-/-}$ muscles at E18.5, and provided support to the notion that an increase in NMJ number is indeed a compensatory mechanism for reduced neurotransmitter release. Both MEPP amplitude and frequency were similar in wild type and integrin-α3 mutants (**Fig 4.7B, C**). However, when normalised to NMJ number, there was a significant reduction in MEPP frequency in both mutant genotypes, compared to wild type (**Fig 4.7D**). One implication of this result is that spontaneous release per NMJ is reduced. This is consistent with the marked reduction in immunoreactivity of bassoon, piccolo and P/Q VGCCs at mutant NMJs (**Fig 4.3**). An accumulation of synaptic vesicles in the presynaptic termini of integrin-α3 mutants provides further evidence of impaired neurotransmitter release (**Fig 4.7E-H**) (Martínez-Hernández et al., 2013). The overall consequence is that in mutants, the reduced activity of each synapse is overcome by an increase in their number, thus restoring MEPP frequency to that of wild type. In the next chapter, the functions of integrin-α3 at the adult NMJ are explored.

5. Integrin-α3 drives active zone assembly, synaptic integrity and nerve terminal adhesion in adult NMJs

5.1. Introduction

During the first 2 - 3 weeks of postnatal life in the mouse, NMJs undergo major structural and molecular reorganisation. NMJs initially receive multiple axonal inputs, which are then eliminated to leave one axon per endplate (pruning) (Sanes and Lichtman, 1999). The simple plaque shape of the NMJ elaborates into a complex, branched 'pretzel' structure, with both nerve terminal and postsynaptic apparatus coordinating to precisely overlap with one another (Kummer et al., 2004; Marques et al., 2000). Lastly, deep invaginations in the postsynaptic membrane form, and the active zones become aligned with the mouths of these folds (Hirokawa and Heuser, 1982; Patton et al., 2001).

The basal lamina plays a key role in the development of the NMJ (reviewed in more detail in *Section 1.8., development of the NMJ*). The roles of synaptic laminins (-221, -421 and -521) are particularly well characterised, and participate in active zone formation and alignment, topological branching, and postsynaptic fold formation (Chen et al., 2011; Nishimune et al., 2004, 2008; Noakes et al., 1995; Patton et al., 2001). Several cell surface receptors are known to mediate these effects. Dystroglycan and the UGC proteins on the postsynaptic side have been implicated in the formation of the branched structure and the postsynaptic folds (Adams et al., 2000; Deconinck et al., 1997; Grady et al., 1997; Nishimune et al., 2008). NCAM, thought to be present on the presynaptic side, has a role in regulating topological maturation and neurotransmission (Rafuse et al., 2000). VGCCs on the presynaptic side have been demonstrated to initiate active zone formation, on binding to the laminin-β2 subunit (Chen et al., 2011).

As mentioned previously, integrin-α3 was found to bind to laminin-421 and active zone components at the *Torpedo* electric synapse (Patton et al., 2001). The functional significance of

this interaction remains unknown. As laminin-421 is responsible for the alignment of active zones with postsynaptic folds, a possible function of integrin-α3 is in mediating this effect. Mutants for laminin-α4 also display NMJs with an apparent phenotype of accelerated ageing. Morphological features included increased fragmentation, terminal sprouting, multiple innervation, and denervation; these changes occurred at much earlier time points in mutants, compared to wild types (Samuel et al., 2012). Therefore, to investigate the role of integrin-α3 in adult NMJs, integrin-$\alpha3^{+/-}$ mice, as these are viable after birth, unlike those with an integrin-$\alpha3^{-/-}$ genotype. In the previous chapter (*4. Integrin-α3 regulates active zone assembly at the NMJ, and innervation patterning in embryonic muscles*), it was found that integrin-$\alpha3^{+/-}$ NMJs were similar in most respects to those from integrin-$\alpha3^{-/-}$ animals, displaying comparable defects in active zone assembly, basal lamina organisation, motoneuron branching and probability of synaptic vesicle release. Therefore, I used these heterozygous mice to study integrin-α3 function in mature NMJs (8 weeks of age).

5.2. Muscle morphology is normal in adult integrin-$\alpha3^{+/-}$ mice

Previous experiments in integrin-α3 mutants at E18.5 revealed apparently normal muscle development, with the formation of myofibres with similar diameters to those of wild type, normal ECM deposition, and assembly of myofibrils (**Figs 3.2, 3.3, 3.4**). Further, no detectable immunoreactivity of integrin-α3 was found in the developing myotome between E13.5 and E18.5, or in adult muscle. It cannot be ruled out however, that integrin-α3 is expressed at a low level in muscle tissue. It is also possible that integrin-α3 expression outside of the myofibre (e.g. in the NMJ) may influence muscle function; for instance denervation results in muscle atrophy (Bongers et al., 2013). To assess whether integrin-α3 is required for the maintenance of muscle integrity in adulthood, sections of TA muscle from adult mice were stained with antibodies to several basal lamina proteins and adhesion receptors (**Fig 5.1**). Muscle fibres had an apparently similar morphology in wild type and integrin-$\alpha3^{+/-}$ tissue, and virtually all were peripherally nucleated in both (**Fig 5.1A-E**). Localisation and staining intensity of laminin (**Fig 5.1A**), perlecan (**Fig 5.1B**) and collagen IV (**Fig 5.1C**) were similar in both genotypes,

indicating that there were no major defects in basal lamina constitution. Additionally, integrin-α7 (**Fig 5.1D**) and -β1 (**Fig 5.1E**) immunoreactivity displayed no differences between genotypes, indicating that the major integrin axis at the muscle sarcolemma was not perturbed in integrin-$\alpha3^{+/-}$ mice.

These data demonstrate that the muscles of integrin-$\alpha3^{+/-}$ mice are qualitatively normal in several aspects, with no obvious signs of pathology or morphological defect. As the model system is a heterozygote and not a knockout, it is difficult to conclude whether or not integrin-α3 has a role in adult muscle. However, the absence of integrin-α3 in muscle at the immunohistochemical level, during both embryonic development and adulthood, would likely point to a lack of involvement in muscle (**Fig 3.1A-E**). Analysis of MTJs was not carried out in this experiment. While integrin-α3 localisation was observed transiently at the MTJ during myogenesis in the chick (Bao et al., 1993), no immunoreactivity was apparent at the rib/intercostal muscle interface in this study (**Fig 3.1A-D**; E13.5, E14.5, E16.5, E18.5). Furthermore, a previous study failed to detect integrin-α3 at the adult mouse MTJ (Nawrotzki, 2003). Therefore, MTJs were not taken into consideration.

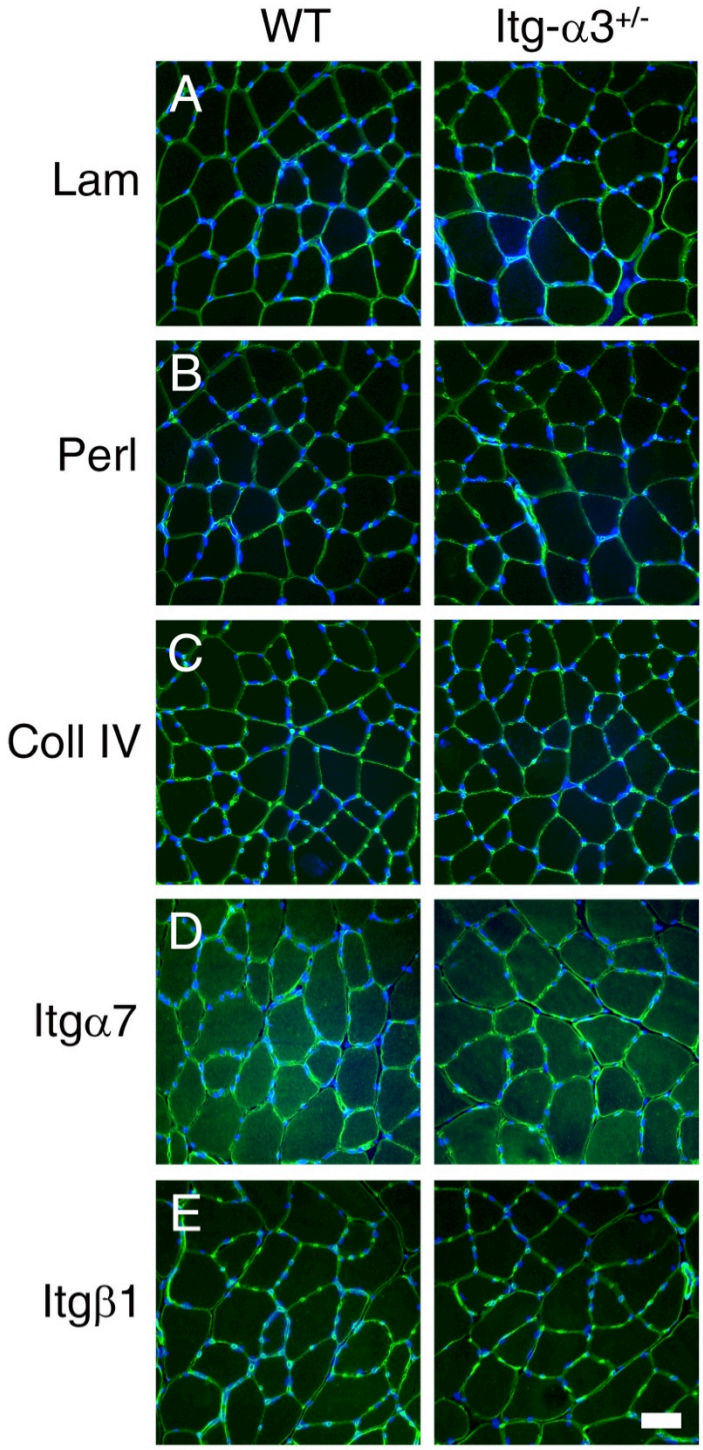

Fig 5.1. Normal muscle histology in adult integrin-α3$^{+/-}$ mice. Transverse sections of *Tibialis anterior* muscle from wild type and integrin-α3$^{+/-}$ mice at 8 weeks. Sections were stained with antibodies to laminin (A), perlecan (B), collagen IV (C), integrin-α7 (D) and integrin-β1 (E), all displayed in green; DAPI was used to label nuclei (blue). *Abbreviations: WT, wild type; Itg, integrin; Lam, laminin; Perl, perlecan; Coll IV, collagen IV. Similar results observed across three animals per genotype. Scale bar: 50 μm.*

5.3. Immunoreactivity of integrin-α3 is reduced at adult integrin-α3$^{+/-}$ NMJs

Previous experiments in E18.5 integrin-α3$^{+/-}$ NMJs had revealed a decrease in integrin-α3 staining intensity, when compared to those of wild type (**Fig 4.1A, C**). To confirm whether adult NMJs displayed a similar decrease, immunohistochemistry was carried out on longitudinal sternomastoid muscles, with fluorescently conjugated α-bungarotoxin to mark AChRs (**Fig 5.2**). Integrin-α3 staining was observed to overlay with the AChR+ postsynaptic endplate (**Fig 5.2A**). However, in integrin-α3$^{+/-}$ NMJs, the labelling intensity of integrin-α3 was markedly reduced (**Fig 5.2B**). Analysis of fluorescence intensity, normalised to that of wild type, revealed the following mean values: wild type, 100% (SD 16.4, n=6 NMJs across 3 animals); integrin-α3$^{+/-}$, 45.9% (SD 16.3, n=13 NMJs across 3 animals; P=0.0007 in comparison to wild type, Mann Whitney U test). These results are in close agreement with those obtained from integrin-α3$^{+/-}$ embryos, where integrin-α3 immunoreactivity at the NMJ was 43.4% of wild type (*Section 4.2., integrin-α3 is localised at the active zones of mouse NMJs at E18.5*).

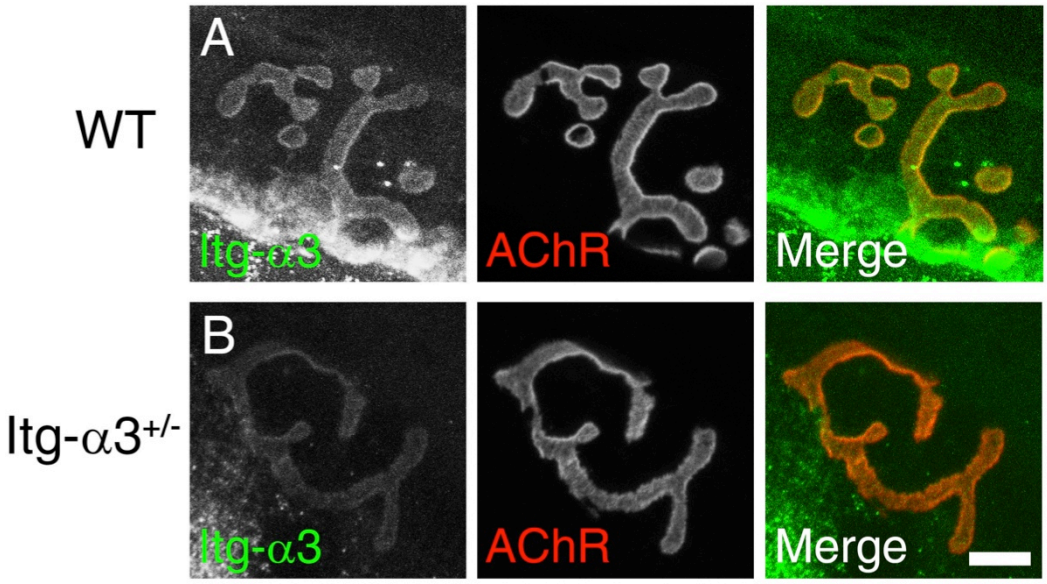

Fig 5.2. Reduced expression of integrin-α3 at adult integrin-α3$^{+/-}$ NMJs. Immunohistochemistry for integrin-α3 in wild type (A) and integrin-α3$^{+/-}$ (B) sternomastoid muscles at 8 weeks of age. Postsynaptic acetylcholine receptors (AChRs) were counterstained with fluorescently conjugated α-bungarotoxin. *Abbreviations: WT, wild type; Itg-α3, integrin-α3. Similar results observed across three animals per genotype. Scale bar: 10 μm.*

5.4. Muscle fibres of integrin-α3$^{+/-}$ mice are innervated at a single NMJ

At E18.5, integrin-α3$^{+/-}$ and $^{-/-}$ diaphragms were observed to have an increase in the number of NMJs per muscle fibre, compared to wild type (**Fig 4.6C, F**). At E18.5, muscle fibres of the diaphragm are normally innervated by a single NMJ (**Fig 5.3**) (Witzemann, 2006). To determine whether muscle fibres of adult integrin-α3$^{+/-}$ mice were singly or multiply innervated, fibres were teased apart from the diaphragm, and AChRs marked with fluorescently conjugated α-bungarotoxin. All observed fibres were singly innervated, in both wild type and integrin-α3$^{+/-}$ mice. This implies that in perinatal and/or postnatal life, the synapse number in integrin-α3$^{+/-}$ muscle is corrected for. During this time, individual NMJs undergo 'pruning', with efferent axons being eliminated to leave a single input; in this process, axons are selected based on activity (Buffelli et al., 2003; Favero et al., 2012); the elimination of entire endplates, as in integrin-α3$^{+/-}$ muscle, might possibly proceed by a similar mechanism.

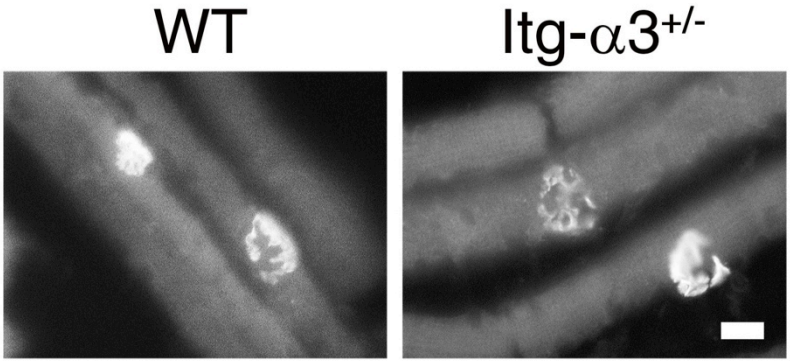

Fig 5.3. One NMJ per muscle fibre in adult integrin-α3$^{+/-}$ mice. Teased muscle fibres from wild type and integrin-α3$^{+/-}$ diaphragms at 8 weeks. Postsynaptic acetylcholine receptors (AChRs) were counterstained with fluorescently conjugated α-bungarotoxin. *Abbreviations: WT, wild type; Itg-α3, integrin-α3. Similar results observed across three animals per genotype (~100 fibres in total per genotype). Scale bar: 50 μm.*

5.5. Integrin-α3 is required for the localisation of key active zone components at adult NMJs

At E18.5, integrin-α3$^{+/-}$ and $^{-/-}$ NMJs had markedly reduced immunoreactivity of bassoon, piccolo and P/Q VGCC at active zones (**Fig 4.3**). However, despite the near loss of these proteins, active zones were able to form, and could recruit vesicles for docking (**Fig 4.4**). To confirm whether similar defects in active zone composition were apparent in adult integrin-α3$^{+/-}$ NMJs, immunohistochemistry was carried out on longitudinal sternomastoid muscles (**Fig 5.4**). Fluorescently conjugated α-bungarotoxin was used to label AChRs. In wild types, immunoreactivity for bassoon, piccolo and P/Q VGCC presented with a generally punctate pattern, overlaying with the AChR+ postsynaptic endplates (**Fig 5.4A-C**). However, in integrin-α3$^{+/-}$ mice, labelling intensity for bassoon was reduced (**Fig 5.4D**), while that for piccolo was virtually absent (**Fig 5.4E**). In contrast, P/Q VGCC staining displayed no discernible difference from that of wild type (**Fig 5.4F**). These results suggest that in adult life as in embryonic development, integrin-α3 is required for the correct assembly of active zones. However, there are some differences in localisation of proteins at the adult, compared to embryonic NMJ. Integrin-α3$^{+/-}$ mice at E18.5 displayed a very similar defect as the $^{-/-}$ mice, with marked reduction of bassoon, piccolo and P/Q VGCC at the NMJs. However, at adult stages, integrin-α3$^{+/-}$ NMJs display no defects in P/Q VGCC localisation. This implies that for the integrin-α3$^{+/-}$ mice, P/Q VGCC accumulation is delayed until postnatal stages.

Fig 5.4. *(Next page)* Altered assembly of active zones in adult integrin-α3$^{+/-}$ NMJs. Immunohistochemistry for active zone proteins in wild type (A-C) and integrin-α3$^{+/-}$ (D-F) sternomastoid muscles at 8 weeks. NMJs labelled with antibodies to bassoon (A, D), piccolo (B, E) and P/Q-type voltage gated calcium channel (C, F). Postsynaptic acetylcholine receptors (AChRs) were counterstained with fluorescently conjugated α-bungarotoxin. *Abbreviations: WT, wild type; Itg-α3, integrin-α3; Bssn, bassoon; Picc, piccolo; P/Q VGCC, P/Q-type voltage-gated calcium channel. Similar results observed across three animals per genotype. Scale bars: 10 μm.*

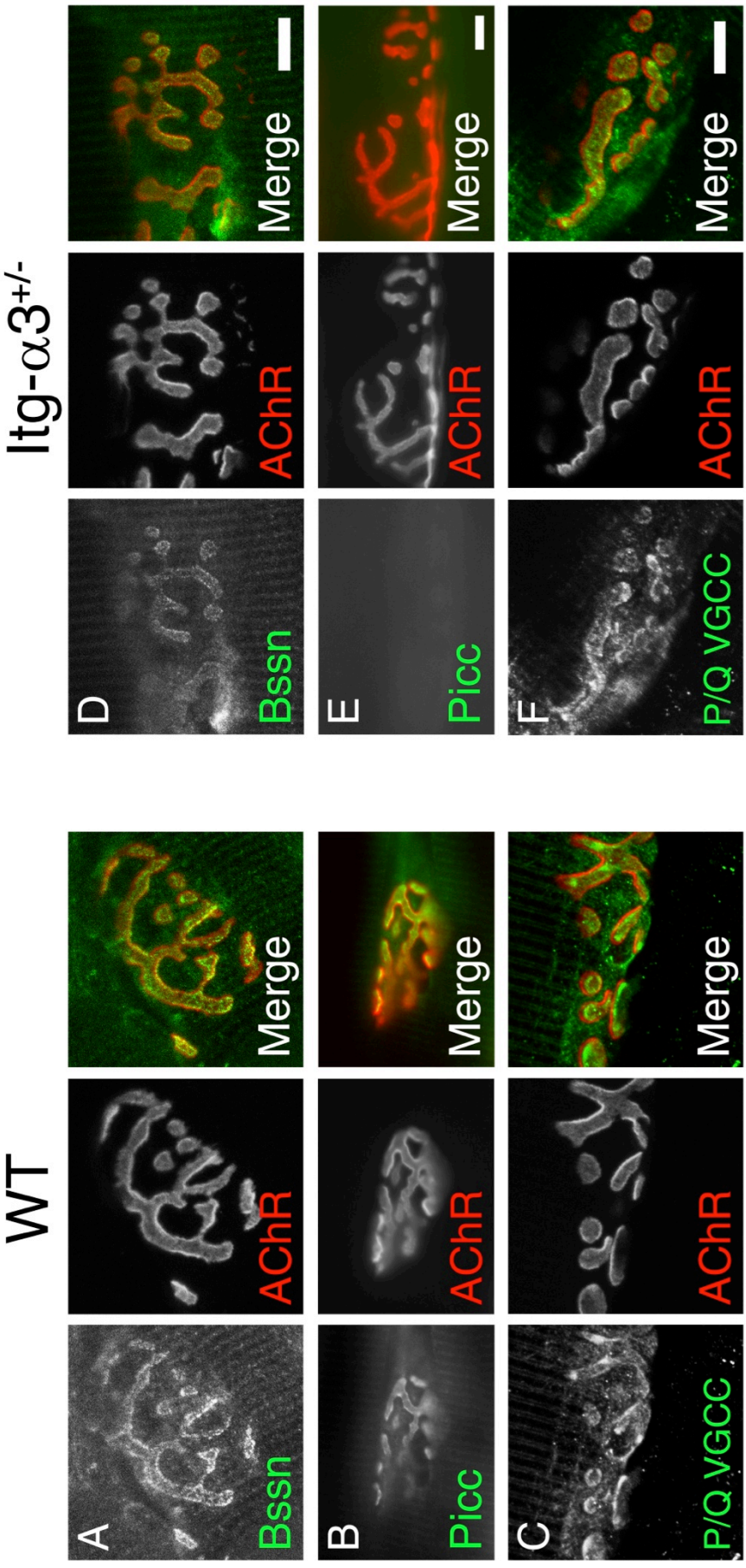

Fig 5.4. *(Legend on previous page)*

5.6. Integrin-α3 is required for synaptic integrity at adult NMJs

Previously studied models with NMJ defects often present with alterations to the general morphology of the endplate (Fox et al., 2008; Latvanlehto et al., 2010; Samuel et al., 2012). To assess morphological aspects of the NMJs of integrin-$\alpha3^{+/-}$ mice, longitudinal sternomastoid muscles were stained with antibodies to neurofilament and SV2 in one colour, to label the nerve and the terminal together, and α-bungarotoxin to mark AChRs. Both wild type and integrin-$\alpha3^{+/-}$ NMJs were arranged in a pretzel shape, with a complete overlap of nerve terminal (**Fig 5.5A-F**). However, a large proportion of integrin-$\alpha3^{+/-}$ NMJs displayed striking morphological alterations. The pretzel arrangement of the endplate was frequently spread out over a larger area, with AChR+ gutters and being further apart (**Fig 5.5B**). By tracing round the entire perimeter, NMJs of integrin-$\alpha3^{+/-}$ mice were observed to occupy a significantly larger total spread area, compared to wild type (**Fig 5.5G**; 27% increase over wild type, $P<0.0001$). However, the total area of AChR+ gutters was similar in both wild type and integrin-$\alpha3^{+/-}$ NMJs, indicating no difference in the total area of contact between nerve and muscle (**Fig 5.5H**; $P=0.40$).

Many endplates of integrin-$\alpha3^{+/-}$ mice were fragmented, tending to form small islands of AChR positivity, rather than continuous gutters (**Fig 5.5C**); the average number of fragments was significantly higher in these mice, compared to wild type (**Fig 5.5I**; 36% increase over wild type, $P<0.0001$). Also evident were NMJs with a characteristic, faint staining intensity of AChRs, which were always contacted by varicose, bulbous nerve terminal ends (**Fig 5.5D**); There were significantly more instances of this type of NMJ in integrin-$\alpha3^{+/-}$ mice, compared to wild type (**Fig 5.5J**; 70% increase over wild type, $P=0.016$). Instances of terminal sprouting, with extra nerve termini leaving the endplates were also observed (**Fig 5.5E**); there were significantly more NMJs with this characteristic in integrin-$\alpha3^{+/-}$ mice, compared to wild type (**Fig 5.5K**; 92% increase over wild type, $P=0.029$). Finally, there was a proportion of NMJs with excessive (3-way or more) axonal branching immediately prior to endplate entry (**Fig 5.5F**); there were significantly more instances of this in integrin-$\alpha3^{+/-}$ mice, compared to wild type (**Fig 5.5L**; 670% increase over wild type, $P=0.027$).

All of the above morphological characteristics, with the exception of an increased spread area, have been reported in mice that are aged (20-26 months) (Nishimune et al., 2014; Rudolf et al., 2014; Samuel et al., 2012; Valdez et al., 2010). The assumption is that these changes are indicative of a general progression towards degeneration, and eventual denervation. The results described here demonstrate that integrin-α3 maintains synaptic integrity at the NMJ. The additional finding that integrin-$\alpha3^{+/-}$ endplates frequently spread themselves over a larger area may be evidence for a role in their morphological maturation.

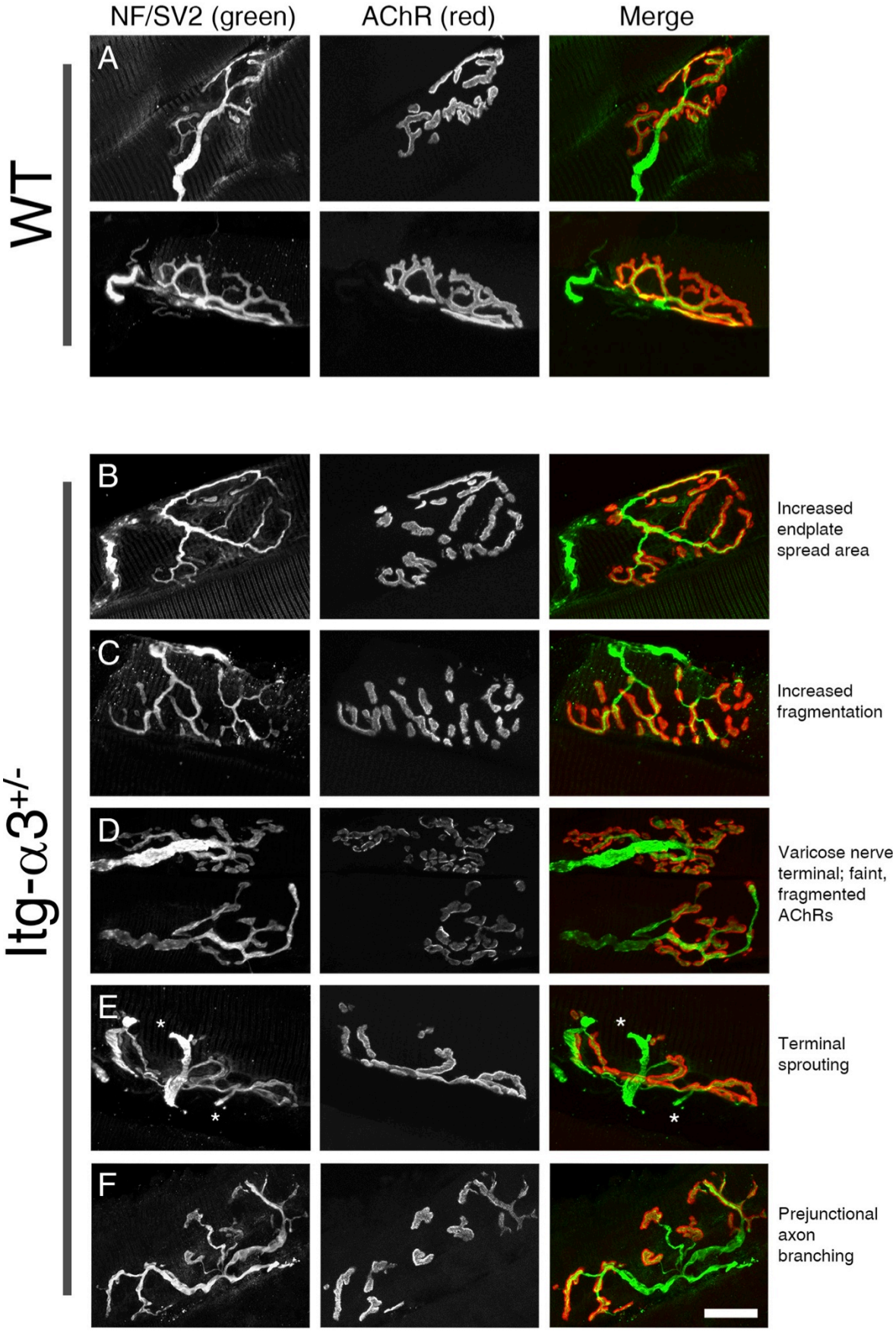

Fig 5.5. Part A. *(continued on next page; legend on next page).*

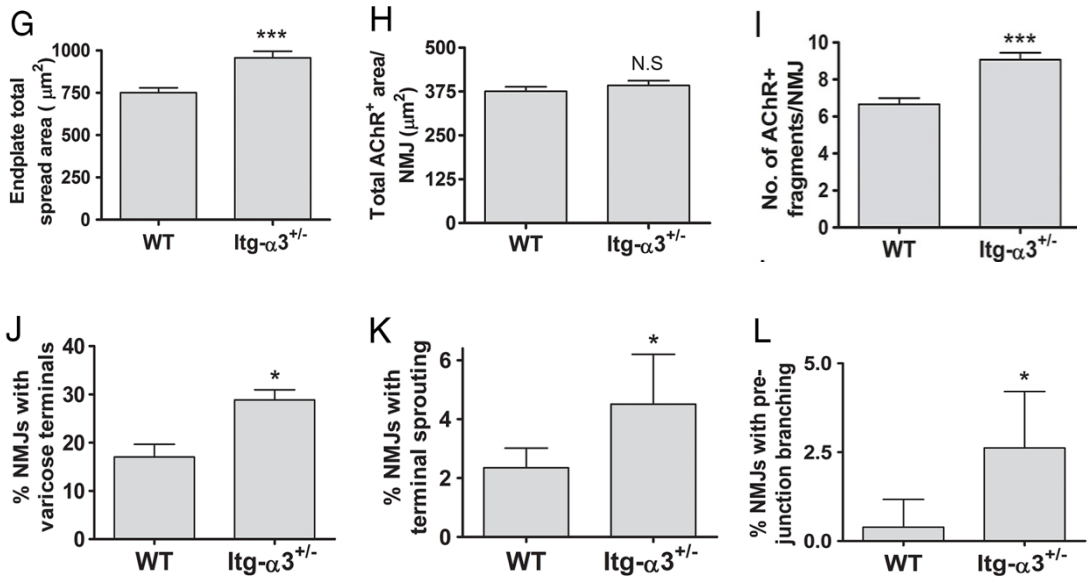

Fig 5.5. Part B. *(continued from previous page).*

Fig 5.5. Altered morphology and degenerative characteristics in NMJs of adult integrin-α3$^{+/-}$ mice. NMJs from wild type (A) and integrin-α3$^{+/-}$ (B-F) sternomastoid muscles at 8 weeks. Tissue was stained with anti-neurofilament and anti-SV2; postsynaptic acetylcholine receptors (AChRs) were counterstained with fluorescently conjugated α-bungarotoxin. Panels depict various morphological characteristics of integrin-α3$^{+/-}$ NMJs, and their quantification in corresponding graphs, as follows. Endplate shape spread out over a larger area than in wild type, but with similar area of nerve-muscle contact (B, G, H). Increased fragmentation of endplates (C, I). NMJs with bulbous, varicose nerve inputs and faint staining for AChRs (D, J). Terminal sprouting, with extra nerve termini leaving the NMJ (E, K; asterisks mark terminal sprouts. Excessive (3-way or more) axonal branching prior to entry into the endplate (F, L). *Abbreviations: WT, wild type; Itg-α3, integrin-α3. n = 101-124 NMJs across 4-5 animals per genotype in panels G-I (mean +/- SEM, t test); >300 NMJs per genotype across 4-5 animals per genotype in panels J-L (median +/- IQR, Mann-Whitney U test). Scale bars: 20 μm.*

5.7. Integrin-α3 is required for adhesion of nerve terminal at the adult NMJ

To assess whether ultrastructural alterations occur in integrin-α3$^{+/-}$ NMJs, EM was carried out on longitudinal diaphragm muscle sections at 8 weeks (**Fig 5.6**). **Mark Turmaine** carried out tissue processing and sectioning; I carried out scanning and imaging. Gross morphology of NMJs was similar in wild type and integrin-α3$^{+/-}$ mice, with the formation of pre- and postsynaptic specialisations, including junctional folds (**Fig 5.6A, B**). Similar numbers of junctional folds and active zones were observed per μm of nerve-muscle apposition (**Fig 5.6E, F**; P=0.14 for junctional folds and 0.76 for active zones). At E18.5, integrin-α3$^{+/-}$ and $^{-/-}$ NMJs had increased deposition and/or disorganisation of the synaptic basal lamina (**Fig 4.4**); however, in adults, a similar electron density and organisation was apparent in both wild type and integrin-α3$^{+/-}$ basal lamina (**Fig 5.6A', B'**). As laminin-α4 has been shown to regulate the alignment of active zones with junctional folds, and to bind to integrin-α3 at the *Torpedo* electric synapse (Carlson et al., 2010b), analysis was carried out to assess the apposition of these two features. No significant difference in the alignment of active zones with postsynaptic folds was observed between wild type and integrin-α3$^{+/-}$ NMJs (**Fig 5.6G**; 85.1% of active zones correctly aligned in wild type, vs 73.2% in integrin-α3$^{+/-}$ NMJs; P=0.30).

A striking observation was the occurrence of nerve terminal detachment in NMJs of the integrin-α3$^{+/-}$ mouse (**Fig 5.6C, D**). The detachment of nerve terminal was observed in 14.3% of integrin-α3$^{+/-}$ NMJs (n=63 boutons across 2 animals): 4/30 boutons in animal 1, or 13.3%; 5/33 boutons in animal 2, or 15.2%. None of the 56 boutons across 2 wild type mice displayed any dissociation of nerve and muscle. Detached nerve regions were usually found to be encased with Schwann cell processes (marked SP in **Fig 5.6C'** and **D'**), a finding that has been reported in mouse mutants for collagen XIII and patients with mutations in the gene for laminin-β2, both of which display a partial detachment phenotype (Latvanlehto et al., 2010; Maselli et al., 2009). The basal lamina was always observed to be largely intact on the postsynaptic side of detached NMJs. Regions of nerve terminal that were left exposed and without Schwann cell processes were always devoid of basal lamina (BL in **Fig 5.6C'** and **D'**; # marks an exposed region of nerve terminal in **D'**). These data demonstrate that integrin-α3

mediates the physical attachment of nerve terminal to the synaptic basal lamina. Consistent with this, integrin-$\alpha 3^{+/-}$ NMJs appear to have mechanical failure at the nerve terminal side, leaving the basal lamina attached to the muscle. To my knowledge, this is the first identified cell surface adhesion receptor that mediates physical anchorage at the NMJ.

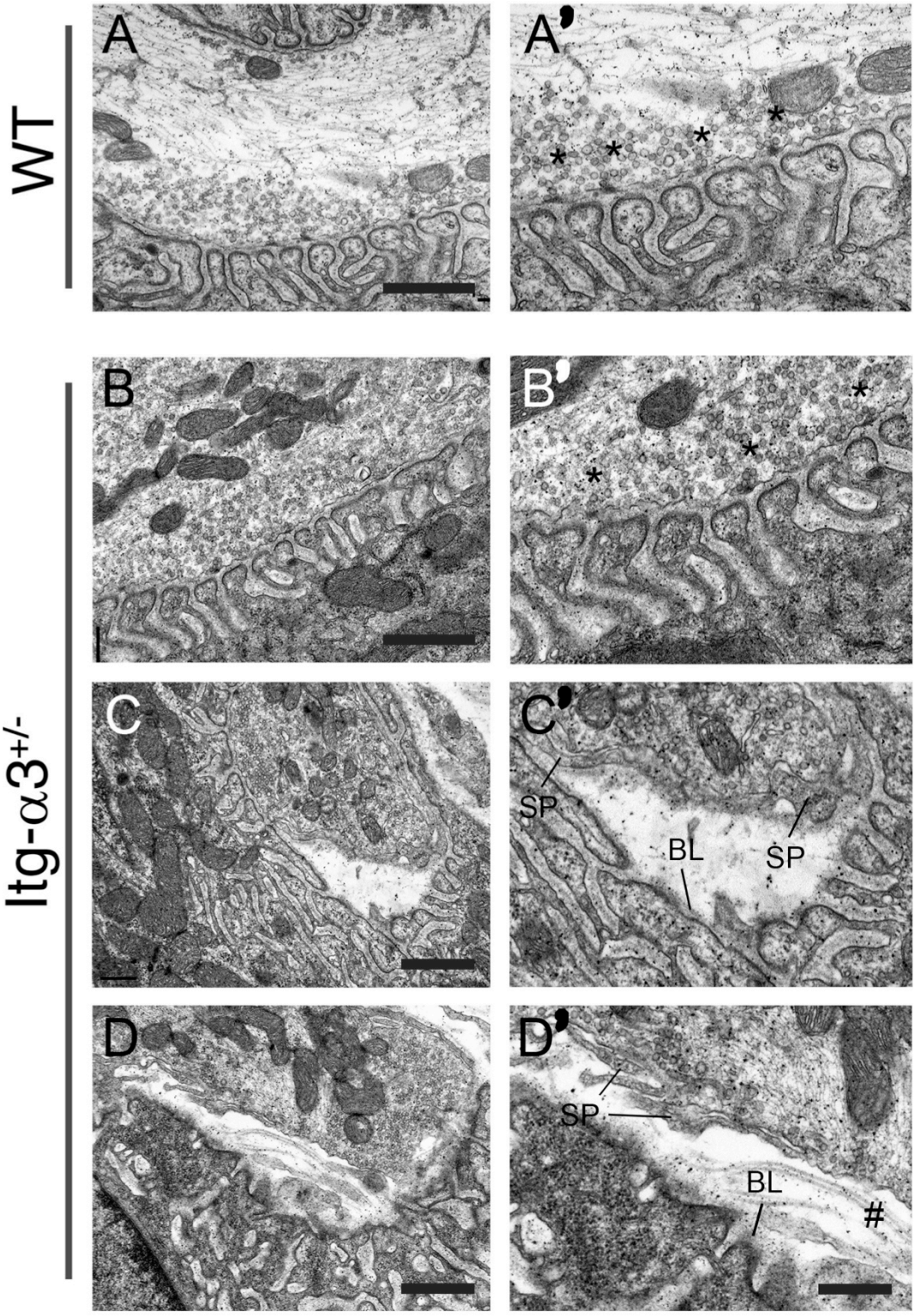

Fig 5.6. Part A. *(continued on next page; legend on next page).*

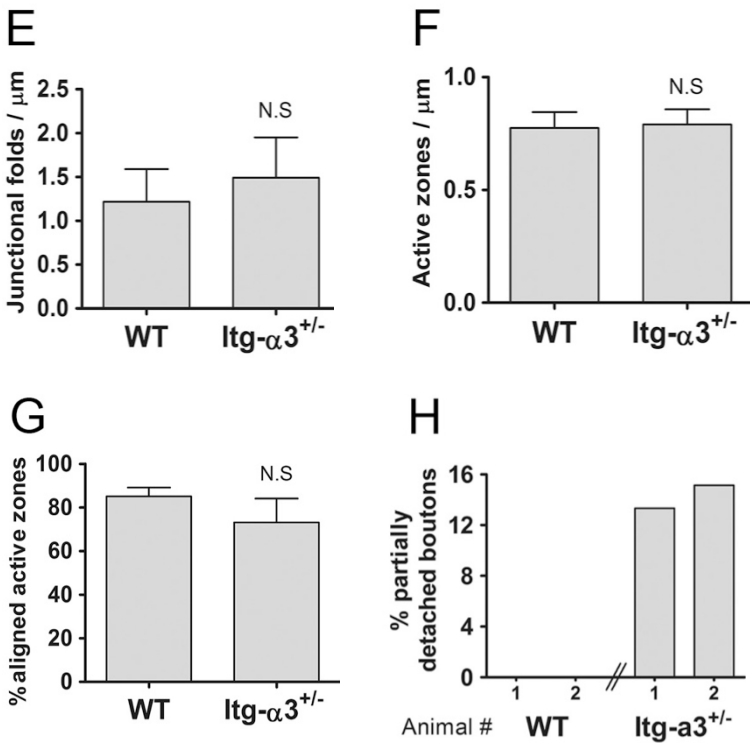

Fig 5.6. Part B. *(continued from previous page).*

Fig 5.6. Nerve terminal detachment in integrin-α3$^{+/-}$ NMJs. Electron micrographs of NMJs in wild type (A) and integrin-α3$^{+/-}$ (B, C, D) diaphragms at 8 weeks. (A-D), low power images at x30,000; (A'-D'), high power regions of A-D at x50,000 magnification. Similar ultrastructural characteristics were observed in NMJs of wild type and integrin-α3$^{+/-}$ mice; numbers of junctional folds and active zones per µm of nerve terminal were similar in both (A and B; high power regions in A' and B', asterisks mark active zones; quantification displayed in graphs E and F). Active zones of both genotypes were largely aligned with the postsynaptic folds (G). The synaptic basal lamina had a similar electron density and structural appearance in both genotypes (A', B'). Instances of nerve terminal detachment were observed in integrin-α3$^{+/-}$ mice, comprising 14.3% of all boutons analysed, compared with none in wild type (C, D, H). Detached regions of nerve were usually encased with Schwann cell processes (SP in C', D'). The basal lamina remains largely intact on the postsynaptic membrane; some regions of detached nerve terminal were left exposed and without Schwann cell protrusions; these parts were not associated with a basal lamina (# in D'). *Abbreviations: WT, wild type; Itg-α3, integrin-α3. n= 56 synaptic boutons in wild type, and 63 in integrin-α3$^{+/-}$ diaphragms, across 2 animals per genotype (mean +/- SEM, t test). Scale bars: 1 µm (A-D) and 500 nm (A'-D').*

5.8. Integrin-α3 is required for the localisation of AChE at adult NMJs

AChE plays a key role in neurotransmission at the NMJ, catalysing the breakdown of acetylcholine, thus terminating neurotransmission. The ColQ subunit of AChE tethers the complex to the synaptic basal lamina (Guerra et al., 2005). Given the well-known role of integrins in directing the organisation of ECM components, experiments were carried out to assess the localisation of AChE at integrin-α3$^{+/-}$ NMJs. Longitudinal sternomastoid muscles at 8 weeks were stained with antibodies targeted against AChE (**Fig 5.7**). In wild type muscles, AChE immunoreactivity was observed as a bright signal overlapping with endplates, as visualised with fluorescently conjugated α-bungarotoxin (**Fig 5.7A**). However, in integrin-α3$^{+/-}$ NMJs, the signal intensity of AChE was markedly reduced (**Fig 5.7B**). This result suggests that integrin-α3 is required for the proper localisation of AChE at the NMJ.

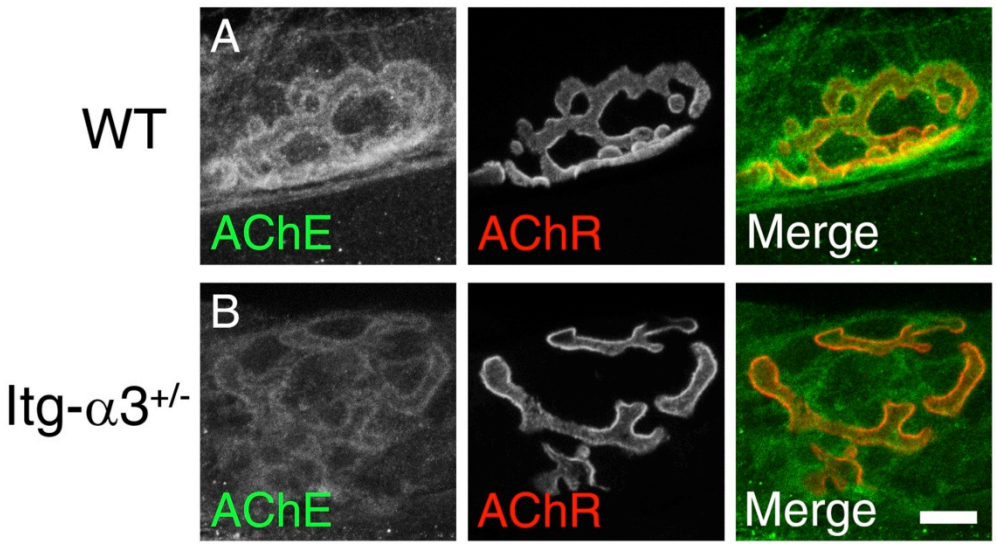

Fig 5.7. Aberrant localisation of acetylcholinesterase in adult integrin-α3$^{+/-}$ NMJs. Immunohistochemistry for acetylcholinesterase in wild type (A) and integrin-α3$^{+/-}$ (B) sternomastoid muscles at 8 weeks. Postsynaptic acetylcholine receptors (AChRs) were counterstained with fluorescently conjugated α-bungarotoxin. *Abbreviations: WT, wild type; Itg-α3, integrin-α3; AChE, acetylcholinesterase. Similar results observed across three animals per genotype. Scale bar: 10 μm.*

5.9. Normal localisation of synaptic basal lamina proteins at NMJs of adult integrin-α3$^{+/-}$ mice

Ultrastructural analysis of the synaptic basal lamina of integrin-α3$^{+/-}$ NMJs revealed no gross changes in deposition, compared to wild type (**Fig 5.6A', B'**). However, the basal lamina-associated protein AChE displayed a clear reduction in immunoreactivity at integrin-α3$^{+/-}$ NMJs (**Fig 5.7**). AChE is tethered in the synaptic cleft by its ColQ subunit; this is known to bind to perlecan in the synaptic basal lamina, and MuSK on the postsynaptic membrane (Guerra et al., 2005). To assess whether the localisation of other synaptic basal lamina proteins was altered in integrin-α3$^{+/-}$ mice, immunohistochemistry was carried out on transverse TA muscles at 8 weeks. Furthermore, alterations to the composition of the synaptic basal lamina might be a possible explanation for the AChE deficiency in these mice. Antibodies were used to label a variety of basal lamina proteins, and fluorescently conjugated α-bungarotoxin used to co-label AChRs (**Fig 5.8**). No differences in gross localisation or staining intensity were observed for any basal lamina protein, between wild type and integrin-α3$^{+/-}$ NMJs. These included agrin (**Fig 5.8A, I**), laminin-α4 (**Fig 5.8B, J**), laminin-α5 (**Fig 5.8C, K**), pan-laminin (**Fig 5.8D, L**), perlecan (**Fig 5.8E, M**), and collagen IV (**Fig 5.8F, N**). In addition, muscles were stained with antibodies against integrin-α7 (postsynaptic; **Fig 5.8G, O**) and integrin-β1 (the binding partner for both integrin-α7 and integrin-α3; **Fig 5.8H, P**). No differences in localisation or staining intensity were observed for either protein, in wild type or integrin-α3$^{+/-}$ NMJs.

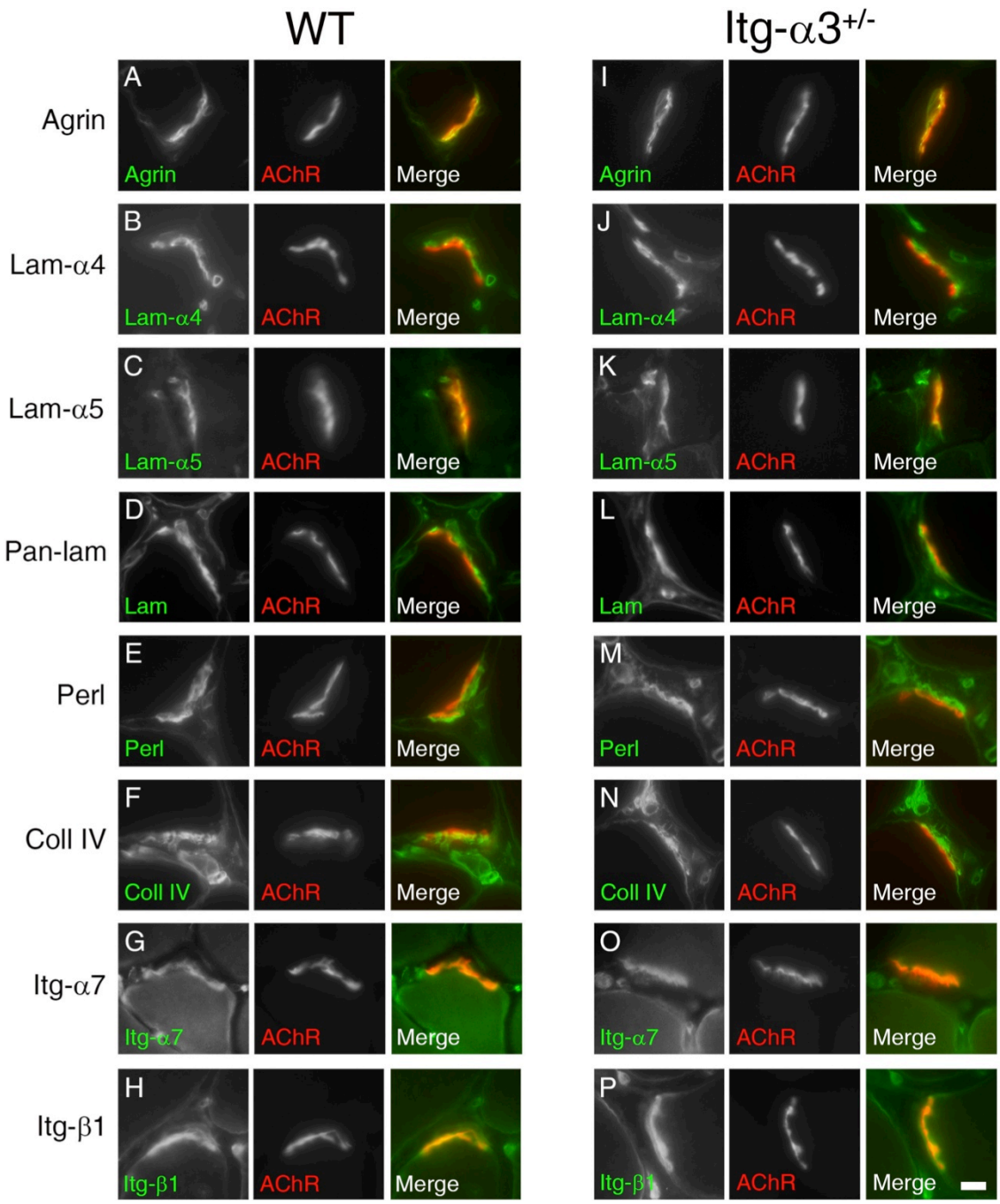

Fig 5.8. Normal deposition of synaptic basal lamina proteins at adult integrin-α3$^{+/-}$ NMJs. Immunohistochemistry for basal lamina proteins in wild type (A-H), integrin-α3$^{+/-}$ (I-P) *Tibialis Anterior* muscles at 8 weeks. Antibodies were used to label the following: agrin (A, I); laminin-α4 (B, J); laminin-α5 (C, K); pan-laminin (D, L); perlecan (E, M); collagen IV (F, N); integrin-α7 (G, O) and integrin-β1 (H, P). Postsynaptic acetylcholine receptors (AChRs) were counterstained with fluorescently conjugated α-bungarotoxin. *Abbreviations: WT, wild type; Itg, integrin; Lam, laminin; Perl, perlecan; Coll, collagen. Similar results observed across three animals per genotype. Scale bar: 10 μm.*

5.10. Impaired grip strength in adult integrin-α3$^{+/-}$ mice

To determine whether the defects at integrin-α3$^{+/-}$ NMJs have an impact on neuromuscular function, forelimb grip strength was assessed. Cohorts of 11 wild type and 11 integrin-α3$^{+/-}$ mice were used, at an age of 16 weeks (4 male and 7 female wild type mice; 6 male and 5 female integrin-α3$^{+/-}$ mice). No significant difference in body mass was observed between wild type and integrin-α3$^{+/-}$ mice (**Fig 5.9A**; P=0.914 for male groups; P=0.639 for female groups). However, body mass of females was significantly lower than that of males (**Fig 5.9A**; 12.7% reduction from males for wild type groups, P=0.0106; 17.2% reduction from males for integrin-α3$^{+/-}$ groups, P=0.0087). Grip strength values were therefore normalised to body mass, a common approach for the elimination of factors relating to size and sex (Brooks and Dunnett, 2009). Integrin-α3$^{+/-}$ mice were significantly weaker than their wild type littermates (**Fig 5.9B**; 13.9% reduction from wild type, P = 0.0154).

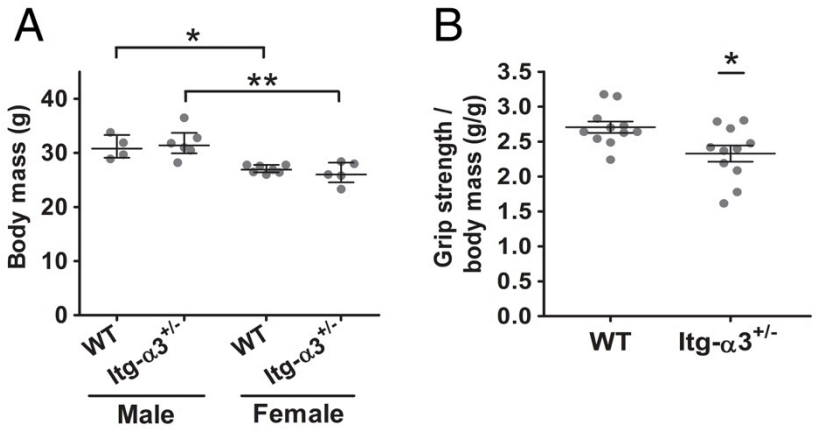

Fig 5.9. Impaired forelimb grip strength in adult integrin-α3$^{+/-}$ mice. 16 week old mice were assessed for body mass (A) and forelimb grip strength (B). No significant difference in body mass was observed between the two genotypes, although females were smaller than males (A). Grip strength was significantly reduced in integrin-α3$^{+/-}$ mice compared to wild types (B). *Abbreviations: WT, wild type; Itg-α3, integrin-α3. n= 11 wild type (4 males and 7 females) and 11 integrin-α3$^{+/-}$ (6 males and 5 females) mice. (A) median +/- IQR, Mann-Whitney U test; (B) mean +/- SEM, F test to ascertain that data sets were normally distributed, followed by t test.*

5.11. Integrin-α3 is required for efficient synaptic vesicle release at the adult NMJ

In order to further examine the consequences of NMJ defects on neuromuscular function in integrin-$\alpha3^{+/-}$ mice, *ex vivo* electrophysiology was carried out on diaphragm muscles. **Richard Webster** carried out the experiments; I played a large part in the experimental design, and carried out most of the data analysis and interpretation. The same cohorts of mice that were assessed for grip strength were used in this analysis (see *Section 5.10., impaired grip strength in adult integrin-$\alpha3^{+/-}$ mice*), this time at the age of 20 weeks. In the first analyses, the basic parameters of MEPP amplitude, MEPP frequency, EPP amplitude and quantal content were determined. MEPPs are postsynaptic depolarisations that derive from the release of a single synaptic vesicle, a process that occurs spontaneously. The MEPP amplitude provides an indication of the response of the muscle membrane to neurotransmitter, and assuming there are similar numbers of acetylcholine molecules in each vesicle, can reveal if there are any defects in the postsynaptic apparatus. The MEPP frequency is a correlate of the probability of vesicle release, and therefore can be an indication of the efficiency of the presynaptic machinery. The two parameters of evoked neurotransmission, EPP amplitude (depolarisation of the muscle membrane in response to evoked release) and the related quantal content (number of vesicles released) are used to assess the efficiency of the system when the nerve is stimulated (Slater, 2003; Wood and Slater, 2001).

In standard Krebs-Henseleit buffer with physiological concentration of Ca^{2+} (2.5 mM), there were no significant differences in any of these parameters between wild type and integrin-$\alpha3^{+/-}$ mice (**Fig 5.10A-F**; P values displayed with graphs for ease of reference). To investigate whether integrin-$\alpha3^{+/-}$ NMJs are associated with more subtle defects in basic neurotransmission, the concentration of Ca^{2+} in the external buffer was reduced to 0.3 mM. The fusion of synaptic vesicles depends on the influx of Ca^{2+} into the nerve terminal; under conditions of reduced free Ca^{2+}, the efficiency of this process is impaired, due to a decrease in release probability at the active zones (Slater, 2008). Therefore, the modulation of Ca^{2+} in the

external environment may serve to exacerbate any subtle dysfunction in vesicle exocytosis. This is a common approach for the full characterisation of functional defects at the NMJ and other synapses (Chand et al., 2015; Rafuse et al., 2000; Ruiz et al., 2008). At 0.3 mM Ca^{2+}, the EPP amplitude and quantal content of both wild type and integrin-$\alpha3^{+/-}$ NMJs were reduced, compared to those at physiological concentration (compare *y*-axis of **Fig 5.10D** and **G**), due to the decrease in basal release probability. However, these two parameters were significantly lower in integrin-$\alpha3^{+/-}$ NMJs compared to those of wild type (**Fig 5.10G-I**; 51.4% reduction from wild type for EPP amplitude, P=0.0017; 52.2% for quantal content, P=0.0079). These results indicate that there are defects in the efficiency of synaptic vesicle exocytosis in integrin-$\alpha3^{+/-}$ NMJs, that are exposed at low concentrations of free Ca^{2+}.

To further characterise the relationship between external Ca^{2+} concentration and synaptic vesicle release, the two parameters of MEPP frequency and quantal content (*y*-axis, linear) were plotted against the Ca^{2+} concentration (*x*-axis, logarithmic), as described previously (Chand et al., 2015; Urbano et al., 2003) (**Fig 5.10J, K**). During the analysis of these data, it was revealed that MEPP frequency was significantly reduced in integrin-$\alpha3^{+/-}$ NMJs at 0.5 mM Ca^{2+}, compared to wild type (**Fig 5.10J**; 22.1% reduction from wild type, P=0.0211). Over the range of Ca^{2+} concentrations, typical sigmoidal dose response curves were apparent for wild type and integrin-$\alpha3^{+/-}$ NMJs, in both parameters of neurotransmission. However, there was a small trend for the integrin-$\alpha3^{+/-}$ curves to be shifted towards the right (towards higher concentrations of Ca^{2+}). In previous studies, this has been interpreted as a decrease in sensitivity to Ca^{2+} at the nerve terminal (Chand et al., 2015; Ruiz et al., 2008). Therefore, two pieces of evidence suggest that Ca^{2+} sensitivity is regulated by integrin-α3 at the NMJ: (1) that there is a shift towards higher concentrations of Ca^{2+} in integrin-$\alpha3^{+/-}$ dose response curves, although subtle; and (2) that nerve terminals of these mice are less responsive to low concentrations of Ca^{2+}, as they display a significant impairment in MEPP frequency at 0.5 mM, and quantal content at 0.3 mM. Together, these results suggest that integrin-α3 regulates the efficient release of synaptic vesicles at the NMJ, by modulating the sensitivity of the presynaptic terminus to external Ca^{2+}.

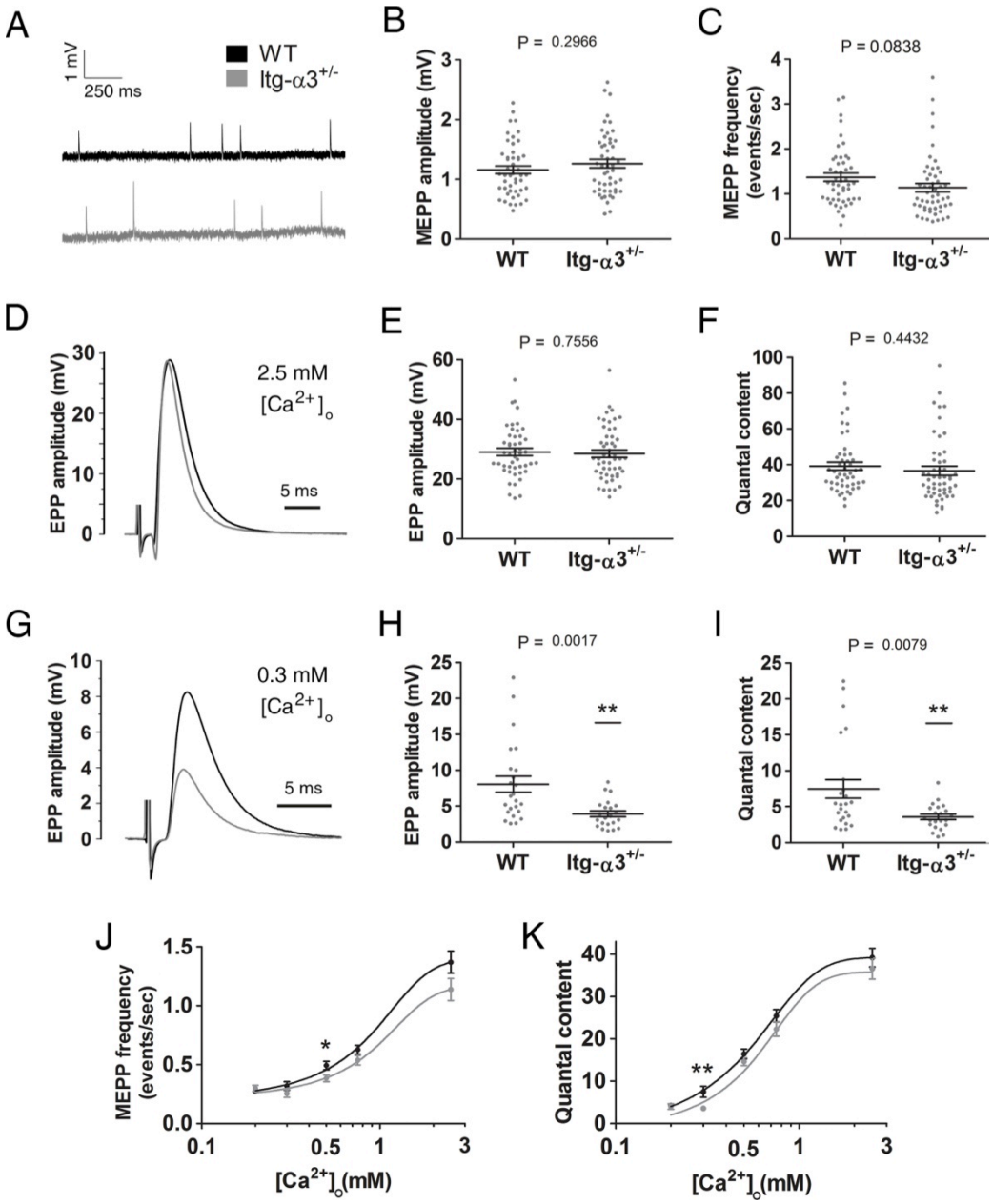

Fig 5.10. Impaired synaptic vesicle release at adult integrin-α3$^{+/-}$ NMJs. *Ex vivo* diaphragm preparations were obtained from adults at 20 weeks, and used for the assessment of 4 basic electrophysiological parameters: MEPP amplitude (A, B); MEPP frequency (A, C); EPP amplitude (D, E, G, H); and quantal content (F, I). Recordings were made in Krebs-Henseleit buffer with $CaCl_2$ at a standard concentration of 2.5 mM (A-F), or at a reduced concentration of 0.3 mM (G-I). Synaptic vesicle release depends critically on free Ca^{2+}; thus, the efficiency of this process is impaired at lower concentrations. Dose response curves of MEPP frequency (J) and quantal content (K) at varying concentrations of Ca^{2+}. *Abbreviations: WT, wild type; Itg-α3, integrin-α3; MEPP, miniature endplate potential; EPP, (evoked) endplate potential. n = 49-53 endplate recordings across 11 animals per genotype in panels A-F; n = 22-24 recordings across 4 animals per genotype in panels G-I; (mean +/- SEM, t-test; P values displayed with graphs).*

5.12. Sustained neurotransmission is unaffected at integrin-α3$^{+/-}$ NMJs, but short-term facilitation is enhanced at low Ca^{2+} conditions

Next, phrenic nerves of diaphragm preparations were stimulated at 50 Hz, to assess the role of integrin-α3 during repetitive neurotransmission. Again, **Richard Webster** carried out the experiments; I played a large part in the experimental design, and carried out most of the data analysis and interpretation. EPPs generated at each stimulus were recorded, and the traces plotted in two different ways. In the first analyses, the EPPs in the traces were plotted as absolute EPP values, to assess the raw output of neurotransmission at the NMJ (**Fig 5.11B, E, H**). In the second method of representation, all EPP values were normalised to the first pulse in the train, as is the conventional approach for representing repetitive stimulation data (**Fig 5.11C, F, I**) (Hallermann et al., 2010; Ruiz et al., 2008; Sons et al., 2006; Webster et al., 2013). This method eliminates any differences in basic neurotransmission, by bringing the first pulses in the train to the same value of 100%. Thus, any differences in STF and decrement can be compared in parallel.

At physiological Ca^{2+} conditions (2.5 mM), traces from wild type and integrin-α3$^{+/-}$ NMJs resembled each other very closely, displaying a similar extent of decrement during stimulation (**Fig 5.11A-C**). This was the case when EPPs were expressed as raw values (**Fig 5.11B**), or when normalised to the first stimulus in the train (**Fig 5.11C**). Next, repetitive stimulation was carried out under reduced Ca^{2+} conditions of 0.75 mM (**Fig 5.11D-F**). Under these conditions, the EPPs throughout the train remained slightly lower in integrin-α3$^{+/-}$ compared to wild type NMJs (**Fig 5.11D, E**). Despite this reduction, there was a slight enhancement of STF in integrin-α3$^{+/-}$ NMJs over that of wild type (apparent over the first ~5 pulses; **Fig 5.11F**). The concentration of external Ca^{2+} was reduced further to 0.3 mM (**Fig 5.11G-I**). Here, the trends that were observed at 0.75 mM were more marked, with a dramatic reduction in EPP amplitudes at integrin-α3$^{+/-}$ compared to wild type NMJs (**Fig 5.11G, H**). Again, integrin-α3$^{+/-}$ endplates were associated with an enhancement of STF compared to wild type (apparent over the first~7 pulses; **Fig 5.11I**).

In summary, these results demonstrate that at standard concentrations of external Ca^{2+}, partial loss of integrin-α3 does not have an impact on sustained synaptic vesicle release during high frequency stimulation, as similar extents of decrement were observed in both wild type and integrin-$\alpha3^{+/-}$ NMJs. This suggests that the kinetics of mobilisation, redocking and fusion of vesicles is unaffected in these mice. However, at low Ca^{2+} conditions, several alterations in function were observed. An enhancement of STF was observed at integrin-$\alpha3^{+/-}$ NMJs, demonstrating that integrin-α3 regulates this process. However, under these conditions the absolute amplitudes of EPPs always remained lower in integrin-$\alpha3^{+/-}$ compared to wild type NMJs. This reflects the previous result presented in **Fig 5.10G-I**, which demonstrated that there was an impairment in basal transmission in integrin-$\alpha3^{+/-}$ NMJs compared to wild type, at low availability of Ca^{2+}.

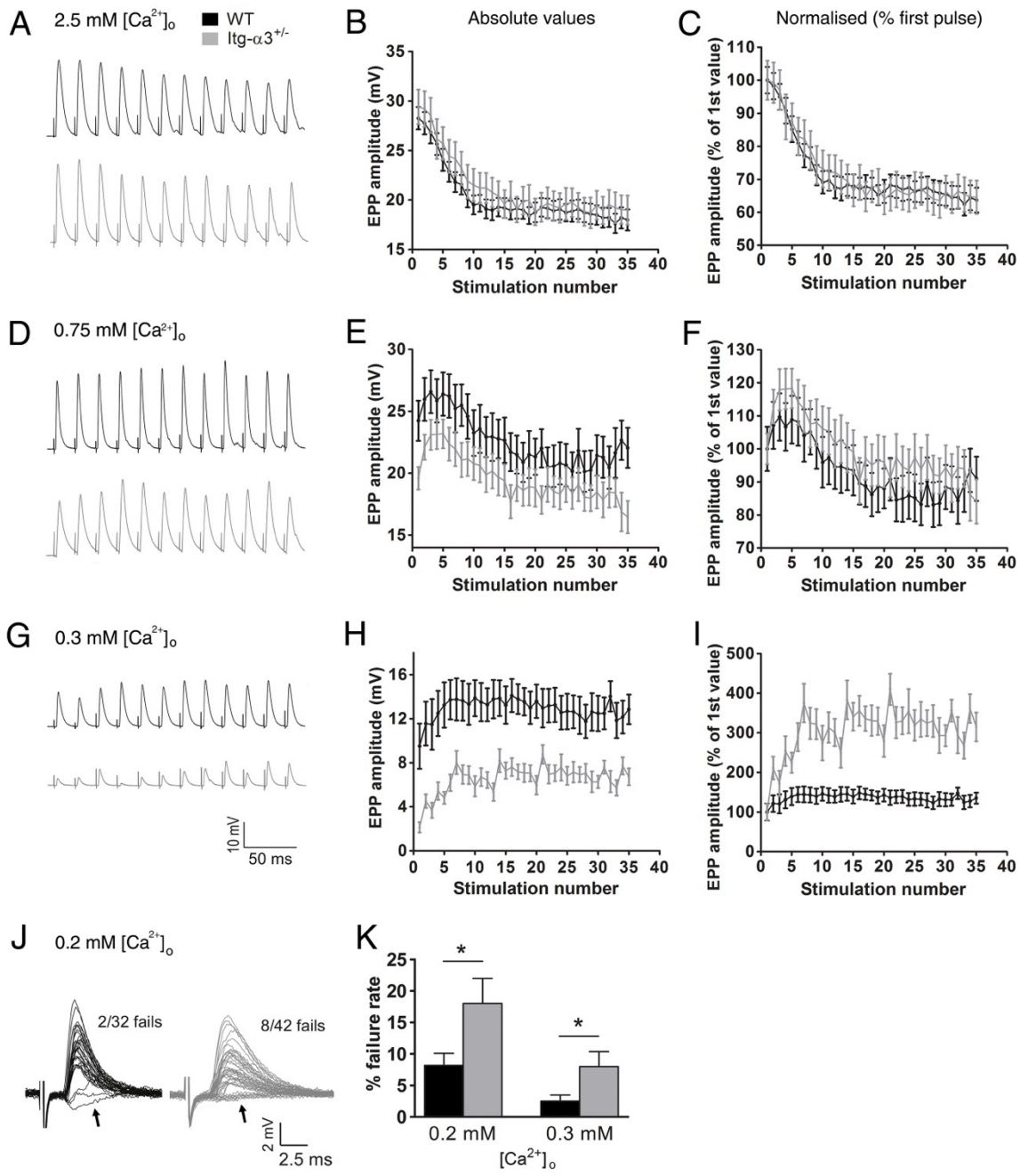

Fig 5.11. Repetitive stimulation at adult integrin-α3$^{+/-}$ NMJs. Phrenic nerves of *ex vivo* diaphragm preparations were stimulated at 50 Hz, in Krebs-Henseleit buffer containing a standard $CaCl_2$ concentration of 2.5 mM (A-C), or reduced concentrations of 0.75 mM (D-F) or 0.3 mM (G-I). Amplitudes of EPPs were recorded with each stimulus in the series. Representative traces of the first 12 pulses are shown in (A, D, G). Data are presented in graphical format with absolute EPP amplitudes (B, E, H), or with values normalised to that of the first EPP in the series (C, F, I). No obvious differences in the rate of decrement were observed between the two genotypes under any of the conditions (A-I). At 0.3 mM Ca^{2+}, absolute EPP values in the series were markedly reduced in integrin-α3$^{+/-}$ NMJs compared to

(*Fig 5.11; continued from previous page*) wild type (G, H). However, at 0.3 mM Ca^{2+}, integrin-$\alpha3^{+/-}$ NMJs displayed an increase in short-term facilitation compared to those of wild type, as demonstrated in (I), where EPPs are normalised to the first in the series. A trend for lower EPPs, but enhanced facilitation in integrin-$\alpha3^{+/-}$ NMJs was also observed at 0.75 mM (D-F). 32-42 overlaid traces of individual EPPs, recorded at 1 Hz with 0.2 mM Ca^{2+} (J). There is an increased neurotransmission failure rate at 0.2 mM and 0.3 mM Ca^{2+}, whereby some EPPs fail to generate (K). These events are marked with arrows in (J), with some traces remaining at baseline. *Abbreviations: WT, wild type; Itg-α3, integrin-α3; EPP, (evoked) endplate potential. n =24-27 endplate recordings across 5-6 animals per genotype in panels A-C; n = 15 endplate recordings across 3 animals per genotype in panels D-F; n = 12-15 endplate recordings across 3 animals per genotype in panels G-I; n = 32-42 endplate recordings across 6 animals per genotype (0.2 mM $CaCl_2$ buffer), and 22-24 endplate recordings across 4 animals per genotype (0.3 mM $CaCl_2$ buffer) in panel K. (mean +/- SEM, t-test).*

5.13. Integrin-$\alpha3^{+/-}$ NMJs display an increased failure rate under low Ca^{2+} conditions

During stimulation at very low external Ca^{2+} concentrations (0.2 and 0.3 mM), another phenomenon was observed: failures of neurotransmission. At certain points in the train, EPPs failed to be generated at all (**Fig 5.11J**; arrows mark EPPs that remain at baseline). There were significantly more failures in integrin-$\alpha3^{+/-}$ NMJs compared to wild type (**Fig 5.11K**; 139% over wild type, P=0.0287 for 0.2 mM Ca^{2+}; 219% over wild type, P=0.0328, for 0.3 mM Ca^{2+}). At very low Ca^{2+} concentrations, the probability of vesicle release is reduced to the extent that sometimes all active zones fail to fire. In mutants, these failures were probably more likely to occur, due to the decreased efficiency of synaptic vesicle release, below that of wild type.

5.14. Discussion

The experiments in this chapter explore the various roles of integrin-α3 at the fully developed NMJ. Firstly, integrin-α3 has a crucial role in the assembly of the active zones (**Fig 5.4**). A similar observation was made in the embryo, with active zones of integrin-$\alpha3^{+/-}$ and $^{-/-}$ NMJs failing to recruit significant quantities of bassoon, piccolo and P/Q VGCC (**Fig 4.3**). However, a less severe phenotype is observed in adult integrin $\alpha3^{+/-}$ NMJs, as P/Q VGCC is able to accumulate at the active zones. Secondly, integrin-α3 plays an essential role in two aspects of synaptic integrity. NMJs of 8 week integrin-$\alpha3^{+/-}$ mice display morphological characteristics that resemble those of aged animals (**Fig 5.5**). In addition, motoneuron terminals of these mice are frequently detached from the synaptic basal lamina (**Fig 5.6**). Thus integrin-α3 appears to protect against degenerative processes, and to physically anchor the nerve terminal at the NMJ. Thirdly, integrin-α3 is required for the localisation of AChE at the synaptic cleft, although it is unclear whether this is dependent on the structure/composition of the synaptic basal lamina to which it is tethered (**Fig 5.7**). Fourthly, integrin-α3 regulates efficient neuromuscular function and neurotransmission, with impairment in the efficiency of synaptic vesicle release, altered STF, and increased failure rate at low Ca^{2+} conditions (**Fig 5.9, Fig 5.10, Fig 5.11**). To my knowledge, this study identifies for the first time a cell surface receptor that anchors the nerve terminal at the NMJ.

At E18.5, integrin-α3 mutants displayed alterations in the deposition of basal lamina in the synaptic cleft of NMJs (**Fig 4.4B**). No obvious defect in ultrastructural organisation or electron density was observed at the NMJs of adult integrin-$\alpha3^{+/-}$ mice (**Fig 5.6A', B'**). In addition, a wide-ranging panel of immunohistochemical stains revealed no obvious differences in basal lamina composition between wild type and integrin-$\alpha3^{+/-}$ NMJs (**Fig 5.8**). While the deposition of synaptic basal lamina is affected in integrin-$\alpha3^{+/-}$ mice at E18.5, the results suggest that a recovery has occurred by the time these mice reach adulthood. As the model used at this adult stage is a heterozygote, it may be that the residual expression of integrin-α3 is able to compensate during later development. Another explanation is that the recovery may be due to compositional changes that occur in the basal lamina, upon NMJ maturation. In addition to the

ubiquitous collagen IV $(\alpha1)_2(\alpha2)$, two other isoforms are upregulated in the adult: $(\alpha3)(\alpha4)(\alpha5)$ and $(\alpha5)_2(\alpha6)$. The expression of collagen XIII also coincides with the formation of the mature NMJ structure (Singhal and Martin, 2011). These changes may have an impact on overall basal lamina structure, and possibly adhesion to integrin-α3. Indeed, evidence suggests that *in vitro*, integrin-α3 binds more specifically to collagen IV (α3) than (α1), two subunits which are developmentally regulated at the NMJ (Aggeli et al., 2009). In order to more clearly address the effects of integrin-α3 on the basal lamina, a motoneuron-specific conditional knockout would be very useful, as it would result in a complete absence of this protein at the adult NMJ.

The role of integrin-α3 at the active zone was also explored at the adult NMJ, again by immunohistochemical detection of bassoon, piccolo and P/Q VGCC. In integrin-$\alpha3^{+/-}$ NMJs, the signal intensity of bassoon was reduced, and that of piccolo virtually absent, when compared to wild type (**Fig 5.4**). However, the staining intensity of P/Q VGCC was unaltered in integrin-$\alpha3^{+/-}$ NMJs, in contrast to the findings at E18.5 in these mice (**Fig 4.3**). These data suggest that in integrin-$\alpha3^{+/-}$ NMJs there is a delay in the recruitment of P/Q VGCC, since it is virtually absent at E18.5, but normally localised in 8 week adults. There are several possible reasons for this finding. Firstly, as this is a heterozygous model, the partial expression of integrin-α3 may allow the recruitment of P/Q VGCC to be restored by the time adulthood is reached. Secondly, there are likely to be a different set of molecular interactions at adult and developmental synapses. As detailed in the previous paragraph, various changes occur to the basal lamina composition during NMJ maturation, including in the collagen IV isoforms that are known to have differential affinities for integrin-α3 (Aggeli et al., 2009). This is evidenced by ultrastructural analysis in integrin-α3 mutants, in that the deposition of synaptic basal lamina is aberrant at E18.5, but apparently normal by adulthood (**Fig 4.4, Fig 5.6A', B'**). This recovery of basal lamina integrity in adulthood may lead to the concurrent recovery of P/Q VGCC localisation. Thirdly, the composition of active zones also changes once the mature NMJ structure is acquired, with a loss of the N-type, but persistence of P/Q VGCC (Nishimune, 2012; Urbano et al., 2003). Therefore it may be that integrin-α3 has different interacting partners in

adult and developmental NMJs, and that it fulfils a slightly different role in the recruitment of active zone components at these two stages.

Morphological elements of wild type and integrin-α3$^{+/-}$ NMJs were also examined. Endplates were found to have a branched, pretzel-shaped endplate, with a complete and precise overlap of nerve terminal (**Fig 5.5A-F**). However, integrin-α3$^{+/-}$ NMJs displayed various characteristics commonly observed in aged (~2 year old) animals (Gonzalez-Freire et al., 2014; Nishimune et al., 2014; Rudolf et al., 2014; Samuel et al., 2012; Valdez et al., 2010)(**Fig 5.5C-L**). The functional significance of these features is not well understood. Commonly, the assumption is that they are symptomatic of a general degenerative phenotype. Terminal sprouting is presumed to be a compensatory mechanism, with axons attempting to establish new sites when the existing NMJ fails (Hesser et al., 2006). The observation of integrin-α3 mutant NMJs with varicose terminal inputs and faint AChR staining suggests both nerve terminal degeneration (sometimes referred to as axonal dystrophy) and disassembly of the postsynaptic apparatus (Li et al., 2011; Samuel et al., 2012). One study aimed to determine the mechanisms by which synaptic gutters become fragmented during ageing. They found that a frequent cause was the degeneration and subsequent regeneration of the underlying muscle fibre. When the nerve reinnervated the fibre following regeneration, the resulting NMJ was often fragmented. However, many of the NMJs underwent fragmentation even without underlying muscle damage (Li et al., 2011). Indeed, in the integrin-α3$^{+/-}$ mice, a lack of overt muscle pathology rules this out as a likely mechanism (**Fig 3.2, Fig 3.3, Fig 3.4, Fig 5.1**).

The eventual end stage of NMJ degeneration is complete denervation; however no clear instances of this were seen in integrin-α3$^{+/-}$ muscles. If the observations in integrin-α3$^{+/-}$ NMJs are truly indicative of an on-going degenerative program, then an absence of denervation may be explained by the young age of the mice, as at only 8 weeks of age, the phenotype may not have fully progressed. Interestingly, laminin-α4 mutant NMJs display very similar characteristics to those of integrin-α3$^{+/-}$ mice. However, the denervation that was observed in

these mice was not apparent until 200 days of age (~2.5% of total NMJs), much later than the time point analysed in this study (Samuel et al., 2012). As laminin-α4 and integrin-α3 are likely interacting partners at the NMJ (Carlson et al., 2010b), it is possible that they maintain synaptic integrity in a shared pathway. This is a tempting conclusion, supported in part by the similar phenotypes observed in both mutant models. The overall picture may however be more complicated, as there are several other mutants that display fragmentation at the NMJ. These include mutants for the postsynaptic protein ephexin-1, and the basal lamina proteins nidogen-2, collagen IV(α5) and collagen XIII (Fox et al., 2007, 2008; Latvanlehto et al., 2010; Shi et al., 2010). Therefore, it seems likely that multiple interactions regulate the maintenance of synaptic integrity, and that laminin-α4 and integrin-α3 may represent only part of the picture.

Previous studies on the aforementioned laminin-α4 mutant had found that active zones were misaligned with the postsynaptic folds at the NMJ (Patton et al., 2001). Although integrin-α3 is a likely interacting partner of laminin-α4, no such defect was found in integrin-$\alpha3^{+/-}$ mice, as observed with EM (**Fig. 5.6A, A', B, B'**). As the model is a heterozygote, rather than a complete knockout, it would be interesting to see if a motoneuron-specific ablation of integrin-α3 would result in active zone misalignment. If not integrin-α3, then other receptors at the active zone might mediate this interaction; these might include VGCCs and/or neurexins (Dean et al., 2003; Nishimune et al., 2004).

While there were no obvious defects in maturation on the ultrastructural scale at integrin-$\alpha3^{+/-}$ NMJs, a striking and unexpected observation was the partial detachment of nerve terminals from a proportion of NMJs. (**Fig 5.6C, C', D, D', H**). The synaptic basal lamina remained localised at the postsynaptic side; this suggests that mechanical failure occurs between the nerve and the basal lamina, and the role of integrin-α3 is consistent with its presence at the presynaptic terminus. Large parts of the exposed nerve terminals were also enwrapped by Schwann cell processes. Laminin-β2 has previously been shown to restrict the

Schwann cell to the extrasynaptic regions (Noakes et al., 1995); therefore this phenotype is likely explained by the absence of basal lamina at the detached nerve terminal, thus allowing the Schwann cell to encroach. Overall, this result demonstrates that integrin-α3 is required for physical adhesion of nerve terminal at the synaptic cleft.

To my knowledge, this is the first report of a receptor that mediates the anchorage of pre- and postsynaptic elements at the NMJ. Despite several extensive studies, particularly at the *Drosophila* NMJ, receptor(s) could not be identified for this function (Koper et al., 2012; Prokop et al., 1998). The investigators ablated various candidate receptors using genetic means, including neurexins, cadherins and integrin-βPS, but no detachment of nerve terminals was observed. However, these studies were able to identify collagen IV and lamininA (one of two laminin trimers in *Drosophila*) as mediators of nerve-muscle adhesion. Collagen XIII in the mouse, and laminin-β2 in humans have also been implicated in adhesion at the NMJ (Latvanlehto et al., 2010; Maselli et al., 2009). While several basal lamina proteins are critical in this process, it seems surprising that no receptors were implicated until now. It has been postulated that this may be due to a large extent of redundancy in this system (Koper et al., 2012; Prokop et al., 1998). Strong attachment is a prerequisite at the NMJ, where small synaptic contacts must withstand the large forces generated in muscle. Efficient adhesion would therefore ideally depend on multiple interactions between basal lamina and cell surface. Despite the likely redundancy, the implication of integrin-α3 in this study is clear, and detachment still occurs even though the model is a heterozygote (with only partial reduction of expression). This probably marks it as one of the more important mediators of adhesion at the NMJ.

Finally, functional assessments were undertaken to determine whether there were defects in synaptic transmission at integrin-$\alpha3^{+/-}$ NMJs. No electrophysiological defects were observed at physiological (2.5 mM) Ca^{2+}; however, upon lowering the concentration of Ca^{2+}, alterations in synaptic transmission could be observed in integrin-$\alpha3^{+/-}$ NMJs (**Fig 5.10**). The modulation of

external Ca^{2+} is a common technique to fully interrogate aspects of synaptic physiology in various systems (Chand et al., 2015; Rafuse et al., 2000; Ruiz et al., 2008). The results indicate that the efficiency of synaptic vesicle release is impaired in integrin-$\alpha3^{+/-}$ NMJs (**Fig 5.10G-I**). Further experiments investigating the relationship between Ca^{2+} concentration and vesicle release suggest that this defect is likely caused by a decrease in Ca^{2+} sensitivity at the nerve terminal (**Fig 5.10J, K**). This could arise through several possible mechanisms. Within the presynaptic machinery, synaptotagmin acts as a key Ca^{2+} sensor, triggering the fusion of docked vesicles with the terminal membrane (Südhof, 2013). This protein is found on the surface of synaptic vesicles, and is known to interact with the SNARE complex and components of the active zones, including VGCCs (Melia, 2007). Bassoon and piccolo also harbour Ca^{2+}-binding regions, and thus have putative roles in mediating the response to Ca^{2+} (tom Dieck et al., 1998; Wang et al., 1999). At the NMJs of integrin-$\alpha3^{+/-}$ mice, the decrease in Ca^{2+} sensitivity may therefore be explained by the concurrent decrease in the levels of bassoon and piccolo (**Fig 5.4**). Alternatively, integrin-α3 may establish direct or indirect interactions with other Ca^{2+}-sensing proteins such as synaptotagmin, to modulate their sensitivity.

Another possibility is that integrin-α3 regulates Ca^{2+} influx into the nerve terminal, rather than the Ca^{2+} sensitivity at the exocytosis machinery. Integrins have been shown to interact with VGCCs in other systems, where they regulate their activity through direct binding or through intracellular signalling pathways (Gui et al., 2006; Sheng et al., 2013). In addition, *in vitro* patch clamp studies have demonstrated that in the presence of bassoon, the opening times of P/Q VGCCs were prolonged, resulting in increased flow of ions (Nishimune et al., 2012). Given the partial loss of bassoon in integrin-$\alpha3^{+/-}$ NMJs, it is possible that VGCC function is altered, with decreased opening times, and thus a decrease in Ca^{2+} influx into the nerve terminal. This would suggest a model whereby at high concentrations of external Ca^{2+}, influx is sufficient to saturate the presynaptic machinery, eliciting efficient vesicle release in both wild type and integrin-$\alpha3^{+/-}$ nerve terminals. However, when free external Ca^{2+} is reduced, influx through the VGCCs of integrin-$\alpha3^{+/-}$ NMJs is not sufficient to saturate the exocytosis machinery, and fewer vesicles are released compared to wild type.

As muscle contraction requires repetitive bouts of neurotransmitter release at the NMJ, phrenic nerves were stimulated at 50 Hz. Analysis of integrin-$\alpha3^{+/-}$ diaphragms revealed no defects in the decrement of EPP amplitudes, at standard 2.5 mM Ca^{2+}, and reduced conditions of 0.75 and 0.3 mM (**Fig 5.11A-I**). This indicates that the kinetics of vesicle mobilisation, docking and exocytosis are unaffected at 50 Hz stimulation. It would be interesting to determine if mutant NMJs show defects in sustained neurotransmission at higher rates of stimulation (e.g. 100 Hz), since bassoon has been shown to mediate high-rate neurotransmission in very fast synapses of the central nervous system, such as those found in the auditory, photoreceptor and cerebellar systems (Frank et al., 2010; Hallermann et al., 2010; Schulz et al., 2014). This might be relevant to the integrin-$\alpha3^{+/-}$ model, since the immunoreactivity of bassoon and piccolo was shown to be reduced (**Fig 5.4**). Further, a complete inactivation of integrin-α3 (via the generation of a conditional knockout) might be useful for a more definitive assessment of the roles of this protein in vesicle exocytosis.

Interestingly, an overall observation was that the decrement of EPPs occurred to the greatest extent at 2.5 mM, and was essentially absent at 0.3 mM. In the latter, vesicle release is already occurring at very low efficiency, and perhaps cannot decrease any further (**Fig 5.11A-I**). Finally, an additional piece of evidence was found, that is consistent with a role of integrin-α3 in regulating the efficiency of neurotransmitter release. Despite the quantal content of individual EPPs being dramatically impaired in integrin-$\alpha3^{+/-}$ NMJs throughout the course of a 50 Hz train, there was an enhancement of STF over the first few stimuli. A likely explanation for this is that since the basal probability/efficiency of exocytosis is more severely impaired in mutant terminals compared to wild type, there is a greater capacity to increase the synaptic output over subsequent stimuli. Enhanced STF is also observed in other mutant models that display an impaired baseline level of vesicle release, including mouse mutants of CSP-α and models of SMA (Kong et al., 2009; Ruiz et al., 2008). All in all, the data in this chapter explore the functions of integrin-α3 in postnatal NMJ function: in active zone assembly and synaptic vesicle release; and in the maintenance of synaptic integrity and adhesion. These results establish the multiple roles of integrin-α3 in NMJ development and maintenance.

6. Discussion

6.1. Summary of results

This study aimed to explore the various roles of integrin-α3 in the neuromuscular system, using the integrin-α3 knockout mouse. Previous reports had suggested that it might have functions in muscle development, including myoblast fusion, myofibril assembly and/or organisation, and MTJ formation (Bao et al., 1993; Brzóska et al., 2006; McDonald et al., 1995; Przewoźniak et al., 2013). However, a comprehensive analysis in the mouse revealed no detectable expression of this protein in muscle, and no major role in myogenesis (**Fig 3.1, Fig 3.2, Fig 3.3, Fig 3.4**). Other investigators had reported integrin-α3 localisation at the active zones of frog NMJs and the *Torpedo* electric synapse; this study confirmed that this was also the case in the mouse (**Fig 4.1A, B**) (Carlson et al., 2010b; Cohen et al., 2000b). Initially, the role of integrin-α3 in embryonic development was studied, as the integrin-$\alpha3^{-/-}$ mouse dies at birth (Kreidberg et al., 1996). However, the expression of integrin-α3 was markedly reduced at NMJs of the integrin-$\alpha3^{+/-}$ mouse (**Fig 4.1C, D**), which survive into adulthood. Therefore, both integrin-$\alpha3^{+/-}$ and $^{-/-}$ mice were used to study the role of this protein during embryogenesis, and the integrin-$\alpha3^{+/-}$ mice to study postnatal development and maintenance.

Integrin-α3 plays a crucial role in the assembly of the active zones, in particular the recruitment of certain proteins (bassoon, piccolo and P/Q VGCC; **Fig 4.3, Fig 5.4**). It is also important for the structural organisation and/or deposition of the synaptic basal lamina, particularly at embryonic stages (**Fig 4.4**); however, it does not regulate its molecular composition (**Fig 4.5, Fig 5.8**). The basal lamina is responsible for the tethering of AChE at the synaptic cleft; the results demonstrate that integrin-α3 directs its accumulation here (**Fig 5.7**). Correct innervation of developing muscles is also dependent on integrin-α3, with multiple NMJs forming per myofibre in integrin-$\alpha3^{+/-}$ and $^{-/-}$ mice at E18.5 (**Fig 4.6**). Despite this, innervation patterning is amended in postnatal life, at least in the heterozygous model studied at this stage (**Fig 5.3**). Exuberant formation of innervation sites may be a compensatory mechanism, as mutant NMJs display several electrophysiological defects. These include the

reduced probability of synaptic vesicle release at E18.5, and reduced quantal content and increased rate of neurotransmission failure at low concentrations of external Ca^{2+}, in adulthood (**Fig 4.7, Fig 5.10, Fig 5.11**). Further analysis in adult mice revealed that the defects are likely to be caused by a reduction in sensitivity of the nerve terminal to Ca^{2+}. Neuromuscular function as assessed by grip strength is compromised in adult integrin-$\alpha3^{+/-}$ mice, a feature which likely originates from the defects in synaptic transmission (**Fig 5.9**).

Several aspects of synaptic integrity are also dependent on integrin-α3. At 8 weeks, integrin-$\alpha3^{+/-}$ mice display NMJs with various characteristics normally observed in aged animals. These include: fragmentation of endplate morphology; faint staining of AChRs, which are opposed by bulbous, varicose nerve terminals; excessive axonal branching prior to entry into the NMJ; and terminal sprouting (**Fig 5.5**). Additionally, nerve terminals were sometimes observed to be detached from the synaptic cleft, indicating a role for integrin-α3 in the adhesion of the presynaptic membrane to the basal lamina (**Fig 5.6**). To my knowledge, this report is the first to identify a cell surface receptor for the physical anchorage of the nerve terminal at the NMJ. Overall, these results demonstrate multiple roles for integrin-α3 in the development and maintenance of the NMJ.

6.2. Integrin-α3 has an essential role in active zone assembly at the NMJ

The results of chapters 4 and 5 indicate that integrin-α3 recruits the active zone proteins bassoon, piccolo and P/Q VGCC (**Fig 5.4; Fig 4.3**). However, there appears to be a differential role in active zone assembly during embryonic development and in adulthood. While both integrin-$\alpha3^{+/-}$ and $^{-/-}$ NMJs display a lack of P/Q VGCC immunoreactivity at E18.5, this protein is normally localized in adult integrin-$\alpha3^{+/-}$ mice. As discussed in *Section 5.14., Discussion*, there may be several possible reasons for this. Firstly, in the heterozygote, the residual expression of integrin-α3 is sufficient to compensate by the time adulthood is reached, and VGCC localisation occurs normally. Secondly, the differences in basal lamina deposition at E18.5 and in adulthood result in different effects on active assembly. The basal lamina shows

ultrastructural changes in mutants at E18.5, but is apparently normal in composition and arrangement in adulthood (**Fig 4.4, Fig 5.6A', B', Fig 5.8**), and this might explain the concurrent recovery in VGCC localisation. This is particularly relevant, given the known dependence of VGCC-laminin interactions in active zone assembly (Chen et al., 2011; Nishimune et al., 2004).

If both integrin-α3 and VGCCs are required for correct active zone assembly, then the question remains of what their specific contributions might be. Based on the known interactions between synaptic laminins, VGCC and integrin-α3, a model might be envisaged as shown in **Fig 6.1**. The striking observation from the mutant in adulthood is that bassoon and piccolo are still perturbed, despite the proper localisation of P/Q VGCC. The previous studies concluded that VGCCs are the central mediators of active zone formation, essential for the initiation of the complex (Chen et al., 2011; Nishimune et al., 2004). However the results in this thesis demonstrate that even in the presence of P/Q VGCC, there is still a requirement for integrin-α3 in the recruitment of downstream proteins. Therefore, combining all the models, the clustering of active zone proteins is jointly dependent on both P/Q VGCC and integrin-α3. The presence of P/Q VGCC in integrin-$\alpha3^{+/-}$ NMJs (despite perturbation of bassoon and piccolo) suggests that the two pathways act in an independent manner.

On the intracellular side of the nerve terminal, integrin-α3 might interact with multiple other proteins to bring about active zone formation. At the *Torpedo* electric synapse integrin-α3 is part of a complex with VGCCs, and a range of cytoskeletal proteins including presynaptic dystrophin, spectrin, myosin and plectin and AHNAK/desmoyokin. Dystrophin has previously been observed in the synaptic bouton of the motor nerve (Huard et al., 1991); in central synapses it has been shown to influence synaptic vesicle release, possibly through interaction with SNARE proteins (Parames et al., 2014; Tozawa et al., 2012). Spectrin is associated with synapse stability and nerve terminal attachment, and myosin with mobility of synaptic vesicles at the NMJs of *Drosophila* (Massaro et al., 2009; Seabrooke et al., 2010). The role of plectin at

the synapse is unclear, although it enhances electrical conductance in motoneuron axons (Fuchs et al., 2009). Another likely candidate for downstream signalling of integrin-α3 is the actin cytoskeleton. Indeed, several lines of evidence suggest that actin plays an important role in the clustering of active zone proteins in central synapses, via interactions with components including bassoon and piccolo (Nelson et al., 2013b). The cytoskeleton may therefore be a key axis through which integrin-α3 directs active zone assembly.

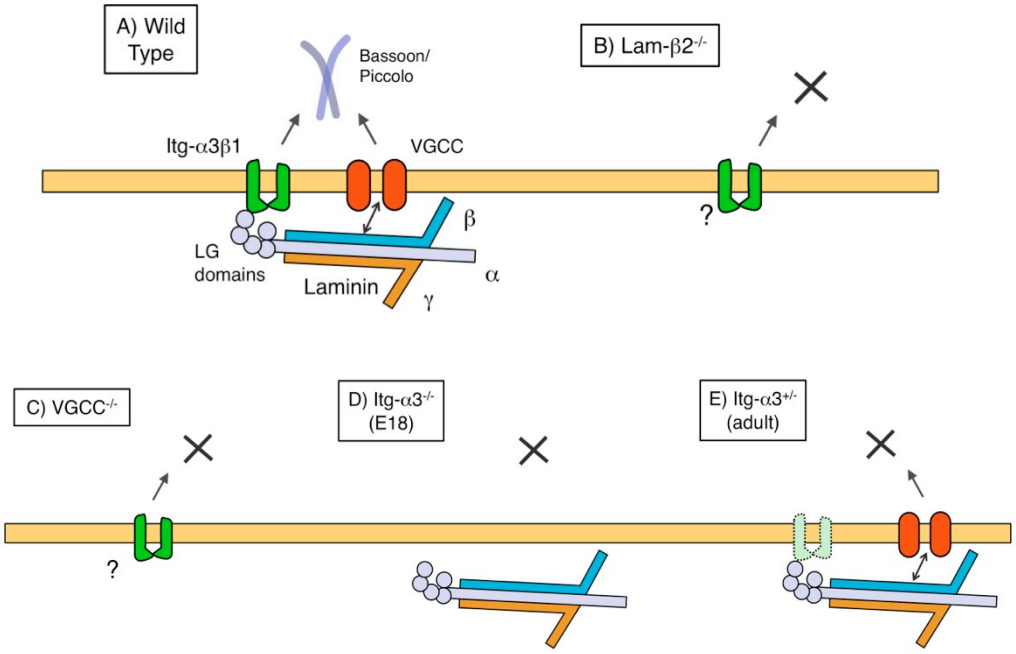

Fig 6.1. Models of active zone assembly at the NMJ. (A) In wild type mice, localisation of bassoon and piccolo depends on both integrin-α3β1 and VGCCs (this study, and (Chen et al., 2011; Nishimune et al., 2004)). (B) In laminin-β2 knockouts, active zones do not assemble, and synaptic laminins fail to localise (Noakes et al., 1995). The expression of integrin-α3 was not assessed. (C) In N- and P/Q VGCC double knockout mice, a similar phenotype is observed, with failure of active zone assembly and laminin localisation (Chen et al., 2011). (D) In integrin-α3$^{-/-}$ NMJs at E18.5, bassoon, piccolo and P/Q VGCC do not localise, suggesting that the clustering of these three proteins is dependent on integrin-α3 at this stage. Synaptic laminins localise normally at E18.5, indicating that integrin-α3 does not direct the gross deposition of these proteins. (E) In integrin-α3$^{+/-}$ NMJs at adult stages, despite the normal patterning of P/Q VGCC,

bassoon and piccolo are still unable to localise; this suggests that integrin-α3 regulates aspects of active zone assembly independently of P/Q VGCC.

6.3. Integrin-α3 is required for efficient synaptic vesicle release at the NMJ

Given that the composition of active zones is altered in integrin-α3 mutants, it might be expected that there are impairments in synaptic transmission. At E18.5, the innervation patterning in mutants was also aberrant, such that there were more NMJs per muscle fibre (**Fig 4.6**). However, the frequency of MEPPs per endplate was markedly reduced in both mutants (**Fig 4.7**). A phenotype of increased numbers of NMJs has been previously observed in e.g. ChAT and AChRγ mutants, and has been interpreted as a compensatory mechanism for a reduction of electrical activity (Misgeld et al., 2002; Pacifici et al., 2011); this hypothesis could also fit the observations in integrin-α3 mutants.

Electrophysiological experiments on adult integrin-$\alpha3^{+/-}$ NMJs revealed a reduction in the efficiency of quantal release and in the sensitivity of nerve terminals to Ca^{2+} (**Fig 5.10**). As explored in *Section 5.14., Discussion*, there are several possible explanations for the defects in neurotransmission. Binding of Ca^{2+} occurs in several proteins of the release sites, e.g. synaptotagmin, bassoon and piccolo (tom Dieck et al., 1998; Wang et al., 1999), and integrin-α3 may directly or indirectly modulate the dynamics and/or affinity of these associations. Alternatively, the kinetics of VGCC opening and closing may be altered. Possible evidence for the latter explanation is derived from *in vitro* studies, which showed that bassoon positively regulates P/Q VGCC by prolonging opening times, allowing more ions to enter the cell (Nishimune et al., 2012). The partial loss of bassoon at integrin-$\alpha3^{+/-}$ NMJs (**Fig 5.4**) could therefore render the presynaptic terminals less permanent to Ca^{2+} during stimulation.

Given the loss of bassoon and piccolo at integrin-$\alpha3^{+/-}$ NMJs, one might expect there to be more severe effects on neurotransmission. However, the roles of bassoon and piccolo have been unclear for some time. Piccolo mutant mice failed to show any defects in neurotransmission in the hippocampus, although the targeted mutation still allowed additional splice variants to be

expressed, potentially allowing some compensation (Mukherjee et al., 2010; Waites et al., 2011). Neurotransmission defects in bassoon-deficient mice were also difficult to uncover initially, although later studies found that bassoon was important for very high-rate neurotransmitter release at particular synapses, including those of the photoreceptor, auditory and cerebellar systems (Frank et al., 2010; Hallermann et al., 2010; Schulz et al., 2014). Surprisingly, the simultaneous disruption of both bassoon and piccolo in cultured cortical neurons failed to yield any clear electrophysiological phenotype (Mukherjee et al., 2010), perhaps owing to the varying requirement for these proteins across different neuronal populations. An analysis of bassoon and/or piccolo function at the NMJ has not been carried out to my knowledge, and so their functions here remain unknown. Although mild, the electrophysiological defects of adult mutant integrin-α3$^{+/-}$ mice were associated with a modest reduction in grip strength (**Fig 5.9**). Given that the muscles of mutants appeared to develop normally, with no differences in histological or ultrastructural aspects (**Fig 3.1, Fig 3.2, Fig 3.3, Fig 3.4, Fig 5.1**), it is likely that deficits in synaptic transmission are responsible for an impairment in neuromuscular function.

6.4. Integrin-α3 is required for synaptic integrity at the mature NMJ

During the analysis of adult tissue, NMJ morphology was also examined. Integrin-α3$^{+/-}$ NMJs displayed various characteristics normally observed in aged (~2 year old) animals (Gonzalez-Freire et al., 2014; Nishimune et al., 2014; Rudolf et al., 2014; Samuel et al., 2012; Valdez et al., 2010)(**Fig 5.5C-L**). Other mouse models also display hallmarks of ageing at the NMJ, including mutants for ephexin-1, laminin-α4, nidogen-2, collagen IV(α5) and collagen XIII (Fox et al., 2007, 2008; Latvanlehto et al., 2010; Shi et al., 2010). Integrin-α3 therefore joins a group of known proteins involved in maintaining these aspects of synaptic integrity. Given that many of these are basal lamina proteins, including laminin-α4 (the hypothetical ligand of integrin-α3), it appears that interactions between the synaptic cleft and cell surface receptors are important for synaptic maintenance.

Interestingly, 'true' ageing at the NMJ is accompanied by defects at the active zone. Immunoreactivity of bassoon has been found to decrease at aged NMJs, although other proteins were not analysed (Nishimune et al., 2012; Valdez et al., 2010). Similar defects in bassoon and piccolo immunoreactivity are found at integrin-α3$^{+/-}$ NMJs (**Fig 5.4**). Based on previous findings in cultured cortical neurons, it is possible that there is a link between active zone defects and synaptic integrity. When bassoon and piccolo were knocked down, protein degradation pathways were activated, resulting in turnover of key proteins and synaptic degeneration (Waites et al., 2013). If the same is true at the NMJ, then bassoon may also provide a positive role in synaptic maintenance. Therefore, it is possible that integrin-α3 and bassoon are linked in a pathway that regulates integrity at the NMJ. Alternatively, integrin-α3 may protect NMJs from degeneration by promoting motoneuron survival, since integrins have been implicated in this process in neonatal animals (Wong et al., 1999).

To gain further insight into these processes, it would be interesting to determine how the morphological features at integrin-α3 mutant NMJs change over the lifespan of the mice. Laminin-α4 mutant mice show a phenotype that seems to resemble premature ageing at the NMJ, since these animals acquire the morphological characteristics of degeneration more rapidly over time than wild type mice (Samuel et al., 2012). Even so, instances of denervation (the endstage of degeneration at the NMJ) were only observed from around 6 months in laminin-α4 mutants, and in the integrin-α3$^{+/-}$ mice, this was not observed at the younger age of 2 months. Therefore, longer time periods might be useful to fully assess aspects of a progressive phenotype. Another study showed that the morphological characteristics at aged NMJs were reversible when the mice were exercised (Valdez et al., 2010). Further, this regime had a local effect, only acting on NMJs in exercised muscles. This process may be at least partially dependent on mechanical signals, since increased exercise is associated with increased transmission of forces. Given that integrins are well known to act as mechanotransducers (Ross et al., 2013), it may be that integrin-α3 acts in a pathway to maintain synaptic activity though the sensing of force. It would be interesting to observe

whether increased exercise can ameliorate the morphological defects at integrin-α3 mutant NMJs, as it does in aged animals.

6.5. Integrin-α3 is required for nerve terminal adhesion at the mature NMJ

The morphological observations described above were visible using light microscopy. To carry out an ultrastructural comparison of wild type and integrin-$\alpha3^{+/-}$ NMJs, EM was employed. No obvious differences were observed between the two genotypes in the majority of synapses that were examined; however, there were regions of nerve terminals that were detached from the synaptic cleft in around 14% of mutant NMJs (**Fig 5.6**). Previous investigators had studied a panel of adhesion receptors in *Drosophila*, ablating them individually or in combination, and had failed to identify any that mediate physical anchorage (Koper et al., 2012; Prokop et al., 1998). Therefore, they speculated that multiple receptors/ECM proteins maintain stability, providing a well-buffered system. In the case of the integrin-$\alpha3^{+/-}$ mutants, even the partial loss of this protein was sufficient to cause clear detachment; this marks it out as perhaps one of the more important adhesion receptors for nerve terminal anchorage, since this phenotype was not observed when other receptors were disrupted in mice (Chen et al., 2011; Dean et al., 2003; Moscoso et al., 1998; Nishimune et al., 2008; Rafuse et al., 2000).

The partial detachment phenotype in integrin-$\alpha3^{+/-}$ mice might be expected to have an effect on neurotransmission (**Fig 5.6**). The withdrawal of nerve terminal results in a dramatic widening of the synaptic cleft, which would result in the dilution of acetylcholine, and presumably a failure to saturate the AChRs on the endplate. No defects in EPP amplitude were observed at physiological Ca^{2+} conditions, although integrin-$\alpha3^{+/-}$ NMJs displayed reduced EPPs at low Ca^{2+}, compared to wild type. However, this can be explained by the concomitant reduction in quantal content (**Fig 5.10**). Perhaps it is unlikely that nerve terminal detachment would cause an obvious difference in neurotransmission, since (a) only a fraction (~14%) of terminals displayed this phenotype, and (b) only parts of individual gutters were displaced.

6.6. Integrin-α3 in the central nervous system

Integrin-α3 has been implicated in aspects of neurotransmission at central synapses. It would therefore be of interest to see if there are parallels or insights that could be gained, in order to better understand its function at the NMJ. One study found a synaptic localisation of integrin-α3 in the cortex and hippocampus, although they did not determine whether it was associated with pre- or postsynaptic fractions. In the absence of a conditional knockout, the investigators used integrin-$\alpha3^{+/-}$ mice. In the hippocampus, no defects in gross synaptic ultrastructure were observed. However, a deficit in LTP (the capacity to modulate synaptic activity over minutes or hours) was revealed. This form of plasticity is often associated with memory formation, yet animals had no such defects (Chan et al., 2003). In more recent studies, forebrain-specific knockouts of integrin-α3 were generated, and hippocampal plasticity analysed. There was a stronger deficit in LTP, this time associated with defects in working memory (Chan et al., 2007). Interestingly, the amplitudes of evoked release were slightly reduced in these mice, findings that are analogous to those at the NMJ of integrin-$\alpha3^{+/-}$ mice. In contrast to central synapses, LTP does not occur at the NMJ, so this particular function of integrin-α3 is not directly relevant to the present study. Aside from its roles in synaptic physiology, integrin-α3 also plays a part in the structural development of the brain. In the hippocampus, conditional knockouts of integrin-α3 were found to have a decreased extent of branching complexity within the dendrites; this was associated with a decrease in synapse number (Kerrisk et al., 2013).

6.7. Conclusions and future perspectives

As we have seen, integrin-α3 is important for several aspect of NMJ development. This opens a number of avenues for further investigation into how the interaction between the basal lamina and presynaptic receptors drives the molecular composition and organisation of the NMJ. Nishimune et al. induced the formation of active zones in primary motoneurons, using beads coated with laminin-β2 (Nishimune et al., 2004). The role of integrin-α3 could be explored

using a similar method, since the immunolabelling of key integrin-associated proteins is difficult at the NMJ, as these are expressed in the neighbouring muscle, nerve and Schwann cell membranes (Schmidt et al., 2012). Similarly, western blot and immunoprecipitation of NMJ proteins is difficult, as the quantity of these molecules in whole muscle extract is very minimal. Molecules downstream of integrins could also be investigated. Interestingly, actin has been shown to promote the formation of active zones in cultured neurons, and thus integrin-α3 might act by regulating cytoskeletal dynamics (Nelson et al., 2013b; Waites et al., 2011).

The results presented here constitute the first functional characterisation of integrin-α3 at the NMJ. Most crucially, integrin-α3 provides a signal for the induction of active zone assembly, providing a parallel pathway to the previously identified laminin-VGCC axis (Chen et al., 2011; Nishimune et al., 2004). Additionally, it mediates the physical adhesion of nerve terminal at the synaptic cleft, apparently the first receptor to be identified for this process. The basal lamina is essential for multiple aspects of NMJ function, including active zone assembly, maintenance of integrity, and adhesion at the synaptic cleft. It is therefore likely that integrin-α3 is a key receptor for the transduction of basal lamina signals in these processes. This work raises the possibility of the involvement of integrin-α3 in human disorders of the NMJ. Three recently reported patients with homozygous mutations in integrin-α3 presented with severe kidney, lung and skin disease, and did not live beyond early infancy (Has et al., 2012). In the most studied patient, it was noted that there were signs of 'mild muscular hypotonia' and 'delayed neurological development'. Currently, only 40-50% of CMS cases have a genetic diagnosis (Hantaï et al., 2013), and it may be that mutations which partially disrupt integrin-α3 function are causative in a subset of these disorders. Therefore, future diagnostic efforts should consider the possibility of integrin-α3 mutations in congenital disorders of the NMJ.

7. References

Abicht, A., Juliane Müller, S., and Lochmüller, H. (2012). Congenital Myasthenic Syndromes.

Abmayr, S.M., and Pavlath, G.K. (2012). Myoblast fusion: lessons from flies and mice. Development *139*, 641–656.

Ackley, B.D., Harrington, R.J., Hudson, M.L., Williams, L., Kenyon, C.J., Chisholm, A.D., and Jin, Y. (2005). The two isoforms of the Caenorhabditis elegans leukocyte-common antigen related receptor tyrosine phosphatase PTP-3 function independently in axon guidance and synapse formation. J. Neurosci. *25*, 7517–7528.

Ackroyd, M.R., Whitmore, C., Prior, S., Kaluarachchi, M., Nikolic, M., Mayer, U., Muntoni, F., and Brown, S.C. (2011). Fukutin-related protein alters the deposition of laminin in the eye and brain. J. Neurosci. *31*, 12927–12935.

Adams, M.E., Kramarcy, N., Krall, S.P., Rossi, S.G., Rotundo, R.L., Sealock, R., and Froehner, S.C. (2000). Absence of alpha-syntrophin leads to structurally aberrant neuromuscular synapses deficient in utrophin. J. Cell Biol. *150*, 1385–1398.

Agarkova, I., and Perriard, J.-C. (2005). The M-band: an elastic web that crosslinks thick filaments in the center of the sarcomere. Trends Cell Biol. *15*, 477–485.

Agarkova, I., Ehler, E., Lange, S., Schoenauer, R., and Perriard, J.-C. (2003). M-band: a safeguard for sarcomere stability? J. Muscle Res. Cell Motil. *24*, 191–203.

Aggeli, A.S., Kitsiou, P. V, Tzinia, A.K., Boutaud, A., Hudson, B.G., and Tsilibary, E.C. (2009). Selective binding of integrins from different renal cell types to the NC1 domain of alpha3 and alpha1 chains of type IV collagen. J. Nephrol. *22*, 130–136.

Alchin, D.R. (2014). Sarcopenia: describing rather than defining a condition. J. Cachexia. Sarcopenia Muscle.

Allen, W.E., Jones, G.E., Pollard, J.W., and Ridley, A.J. (1997). Rho, Rac and Cdc42 regulate actin organization and cell adhesion in macrophages. J. Cell Sci. *110 (Pt 6*, 707–720.

Altrock, W.D., Tom Dieck, S., Sokolov, M., Meyer, A.C., Sigler, A., Brakebusch, C., Fässler, R., Richter, K., Boeckers, T.M., Potschka, H., et al. (2003). Functional inactivation of a fraction of excitatory synapses in mice deficient for the active zone protein bassoon. Neuron *37*, 787–800.

An, M.C., Lin, W., Yang, J., Dominguez, B., Padgett, D., Sugiura, Y., Aryal, P., Gould, T.W., Oppenheim, R.W., Hester, M.E., et al. (2010). Acetylcholine negatively regulates development of the neuromuscular junction through distinct cellular mechanisms. Proc. Natl. Acad. Sci. U. S. A. *107*, 10702–10707.

Andersen, J.L. (2003). Muscle fibre type adaptation in the elderly human muscle. Scand. J. Med. Sci. Sports *13*, 40–47.

Anderson, T.W., Vaughan, A.N., and Cramer, L.P. (2008). Retrograde flow and myosin II activity within the leading cell edge deliver F-actin to the lamella to seed the formation of graded polarity actomyosin II filament bundles in migrating fibroblasts. Mol. Biol. Cell *19*, 5006–5018.

Anthis, N.J., Wegener, K.L., Ye, F., Kim, C., Goult, B.T., Lowe, E.D., Vakonakis, I., Bate, N., Critchley, D.R., Ginsberg, M.H., et al. (2009). The structure of an integrin/talin complex reveals the basis of inside-out signal transduction. EMBO J. *28*, 3623–3632.

Ashley, J., Packard, M., Ataman, B., and Budnik, V. (2005). Fasciclin II signals new synapse formation through amyloid precursor protein and the scaffolding protein dX11/Mint. J. Neurosci. *25*, 5943–5955.

Augustine, G.J., and Kasai, H. (2007). Bernard Katz, quantal transmitter release and the foundations of presynaptic physiology. J. Physiol. *578*, 623–625.

Aumailley, M., Bruckner-Tuderman, L., Carter, W.G., Deutzmann, R., Edgar, D., Ekblom, P., Engel, J., Engvall, E., Hohenester, E., Jones, J.C.R., et al. (2005). A simplified laminin nomenclature. Matrix Biol. *24*, 326–332.

Awad, S.S., Lightowlers, R.N., Young, C., Chrzanowska-Lightowlers, Z.M.A., Lomo, T., and Slater, C.R. (2001). Sodium Channel mRNAs at the Neuromuscular Junction: Distinct Patterns of Accumulation and Effects of Muscle Activity. J. Neurosci. *21*, 8456–8463.

Bachmann, A., Timmer, M., Sierralta, J., Pietrini, G., Gundelfinger, E.D., Knust, E., and Thomas, U. (2004). Cell type-specific recruitment of Drosophila Lin-7 to distinct MAGUK-based protein complexes defines novel roles for Sdt and Dlg-S97. J. Cell Sci. *117*, 1899–1909.

Badowski, C., Pawlak, G., Grichine, A., Chabadel, A., Oddou, C., Jurdic, P., Pfaff, M., Albiges-Rizo, C., and Block, M.R. (2008). Paxillin phosphorylation controls invadopodia/podosomes spatiotemporal organization. Mol. Biol. Cell *19*, 633–645.

Bajanca, F., Luz, M., Duxson, M.J., and Thorsteinsdóttir, S. (2004). Integrins in the mouse myotome: developmental changes and differences between the epaxial and hypaxial lineage. Dev. Dyn. *231*, 402–415.

Bajanca, F., Luz, M., Raymond, K., Martins, G.G., Sonnenberg, A., Tajbakhsh, S., Buckingham, M., and Thorsteinsdottir, S. (2006). Integrin alpha6beta1-laminin interactions regulate early myotome formation in the mouse embryo. Development *133*, 1635–1644.

Banks, G.B., Chau, T.N.P., Bartlett, S.E., and Noakes, P.G. (2001). Promotion of motoneuron survival and branching in rapsyn-deficient mice. J. Comp. Neurol. *429*, 156–165.

Banks, G.B., Choy, P.T., Lavidis, N.A., and Noakes, P.G. (2003). Neuromuscular synapses mediate motor axon branching and motoneuron survival during the embryonic period of programmed cell death. Dev. Biol. *257*, 71–84.

Banovic, D., Khorramshahi, O., Owald, D., Wichmann, C., Riedt, T., Fouquet, W., Tian, R., Sigrist, S.J., and Aberle, H. (2010). Drosophila neuroligin 1 promotes growth and postsynaptic differentiation at glutamatergic neuromuscular junctions. Neuron *66*, 724–738.

Bao, Z.Z., Lakonishok, M., Kaufman, S., and Horwitz, A.F. (1993). Alpha 7 beta 1 integrin is a component of the myotendinous junction on skeletal muscle. J. Cell Sci. *106 (Pt 2*, 579–589.

Bárány, M. (1967). ATPase activity of myosin correlated with speed of muscle shortening. J. Gen. Physiol. *50*, Suppl:197–218.

Bassett, D.I., and Currie, P.D. (2003). The zebrafish as a model for muscular dystrophy and congenital myopathy. Hum. Mol. Genet. *12 Spec No*, R265–R270.

Batchelor, C.L., and Winder, S.J. (2006). Sparks, signals and shock absorbers: how dystrophin loss causes muscular dystrophy. Trends Cell Biol. *16*, 198–205.

Batchelor, C.L., Higginson, J.R., Chen, Y.-J., Vanni, C., Eva, A., and Winder, S.J. (2007). Recruitment of Dbl by ezrin and dystroglycan drives membrane proximal Cdc42 activation and filopodia formation. Cell Cycle *6*, 353–363.

Batters, C., Veigel, C., Homsher, E., and Sellers, J.R. (2014). To understand muscle you must take it apart. Front. Physiol. *5*, 90.

Beeson, D., Newland, C., Croxen, R., Buckel, A., Li, F.Y., Larsson, C., Tariq, M., Vincent, A., and Newsom-Davis, J. (1998). Congenital myasthenic syndromes. Studies of the AChR and other candidate genes. Ann. N. Y. Acad. Sci. *841*, 181–183.

Beglova, N., Blacklow, S.C., Takagi, J., and Springer, T.A. (2002). Cysteine-rich module structure reveals a fulcrum for integrin rearrangement upon activation. Nat. Struct. Biol. *9*, 282–287.

Bentzinger, C.F., Wang, Y.X., and Rudnicki, M.A. (2012). Building muscle: molecular regulation of myogenesis. Cold Spring Harb. Perspect. Biol. *4*.

Berger, M.J., and Doherty, T.J. (2010). Sarcopenia: prevalence, mechanisms, and functional consequences. Interdiscip. Top. Gerontol. *37*, 94–114.

Bestue-Cardiel, M., Sáenz de Cabezón-Alvarez, A., Capablo-Liesa, J.L., López-Pisón, J., Peña-Segura, J.L., Martin-Martinez, J., and Engel, A.G. (2005). Congenital endplate acetylcholinesterase deficiency responsive to ephedrine. Neurology *65*, 144–146.

Beumer, K., Matthies, H.J.G., Bradshaw, A., and Broadie, K. (2002). Integrins regulate DLG/FAS2 via a CaM kinase II-dependent pathway to mediate synapse elaboration and stabilization during postembryonic development. Development *129*, 3381–3391.

Bevan, S., and Steinbach, J.H. (1977). The distribution of alpha-bungarotoxin binding sites of mammalian skeletal muscle developing in vivo. J. Physiol. *267*, 195–213.

Bhattacharjee, A., and Bansal, M. (2005). Collagen structure: the Madras triple helix and the current scenario. IUBMB Life *57*, 161–172.

Biederer, T., and Südhof, T.C. (2000). Mints as adaptors. Direct binding to neurexins and recruitment of munc18. J. Biol. Chem. *275*, 39803–39806.

Biggs, D.S.C. (2010). 3D deconvolution microscopy. Curr. Protoc. Cytom. *Chapter 12*, Unit 12.19.1–20.

Bigland-Ritchie, B., Kukulka, C.G., Lippold, O.C., and Woods, J.J. (1982). The absence of neuromuscular transmission failure in sustained maximal voluntary contractions. J. Physiol. *330*, 265–278.

Billups, B., and Forsythe, I.D. (2002). Presynaptic mitochondrial calcium sequestration influences transmission at mammalian central synapses. J. Neurosci. *22*, 5840–5847.

Blake, D.J., Weir, A., Newey, S.E., and Davies, K.E. (2002). Function and genetics of dystrophin and dystrophin-related proteins in muscle. Physiol. Rev. *82*, 291–329.

Bloor, J.W., and Brown, N.H. (1998). Genetic analysis of the Drosophila alphaPS2 integrin subunit reveals discrete adhesive, morphogenetic and sarcomeric functions. Genetics *148*, 1127–1142.

Bolliger, M.F., Zurlinden, A., Lüscher, D., Bütikofer, L., Shakhova, O., Francolini, M., Kozlov, S. V, Cinelli, P., Stephan, A., Kistler, A.D., et al. (2010). Specific proteolytic cleavage of agrin regulates maturation of the neuromuscular junction. J. Cell Sci. *123*, 3944–3955.

Bonaldo, P. (1998). Collagen VI deficiency induces early onset myopathy in the mouse: an animal model for Bethlem myopathy. Hum. Mol. Genet. *7*, 2135–2140.

Bongers, K.S., Fox, D.K., Ebert, S.M., Kunkel, S.D., Dyle, M.C., Bullard, S. a, Dierdorff, J.M., and Adams, C.M. (2013). Skeletal muscle denervation causes skeletal muscle atrophy through a pathway that involves both Gadd45a and HDAC4. Am. J. Physiol. Endocrinol. Metab. *305*, E907–E915.

Boppart, M.D., Burkin, D.J., and Kaufman, S.J. (2006). Alpha7beta1-integrin regulates mechanotransduction and prevents skeletal muscle injury. Am. J. Physiol. Cell Physiol. *290*, C1660–C1665.

Briguet, A., Courdier-Fruh, I., Foster, M., Meier, T., and Magyar, J.P. (2004). Histological parameters for the quantitative assessment of muscular dystrophy in the mdx-mouse. Neuromuscul. Disord. *14*, 675–682.

Brooks, S.P., and Dunnett, S.B. (2009). Tests to assess motor phenotype in mice: a user's guide. Nat. Rev. Neurosci. *10*, 519–529.

Brzóska, E., Bello, V., Darribère, T., Moraczewski, J., Brzoska, E., and Darribere, T. (2006). Integrin alpha3 subunit participates in myoblast adhesion and fusion in vitro. Differentiation. *74*, 105–118.

Buckingham, M. (2007). Skeletal muscle progenitor cells and the role of Pax genes. C. R. Biol. *330*, 530–533.

Buffelli, M., Burgess, R.W., Feng, G., Lobe, C.G., Lichtman, J.W., and Sanes, J.R. (2003). Genetic evidence that relative synaptic efficacy biases the outcome of synaptic competition. Nature *424*, 430–434.

Burkin, D.J., Kim, J.E., Gu, M., and Kaufman, S.J. (2000). Laminin and α 7 β 1 integrin regulate agrin-induced clustering of acetylcholine receptors. *2886*, 2877–2886.

Burridge, K., and Connell, L. (1983). Talin: a cytoskeletal component concentrated in adhesion plaques and other sites of actin-membrane interaction. Cell Motil. *3*, 405–417.

Bütikofer, L., Zurlinden, A., Bolliger, M.F., Kunz, B., and Sonderegger, P. (2011). Destabilization of the neuromuscular junction by proteolytic cleavage of agrin results in precocious sarcopenia. FASEB J. *25*, 4378–4393.

Butz, S., Okamoto, M., and Südhof, T.C. (1998). A tripartite protein complex with the potential to couple synaptic vesicle exocytosis to cell adhesion in brain. Cell *94*, 773–782.

Cachaço, A.S., Chuva de Sousa Lopes, S.M., Kuikman, I., Bajanca, F., Abe, K., Baudoin, C., Sonnenberg, A., Mummery, C.L., and Thorsteinsdóttir, S. (2003). Knock-in of integrin beta 1D affects primary but not secondary myogenesis in mice. Development *130*, 1659–1671.

Cachaço, A.S., Pereira, C.S., Pardal, R.G., Bajanca, F., and Thorsteinsdóttir, S. (2005). Integrin repertoire on myogenic cells changes during the course of primary myogenesis in the mouse. Dev. Dyn. *232*, 1069–1078.

Calderwood, D.A., Campbell, I.D., and Critchley, D.R. (2013). Talins and kindlins: partners in integrin-mediated adhesion. Nat. Rev. Mol. Cell Biol. *14*, 503–517.

Caldwell, J.H. (2000). Clustering of sodium channels at the neuromuscular junction. Microsc. Res. Tech. *49*, 84–89.

Campbell, I.D., and Humphries, M.J. (2011). Integrin structure, activation, and interactions. Cold Spring Harb. Perspect. Biol. *3*, a004994.

Carisey, A., Tsang, R., Greiner, A.M., Nijenhuis, N., Heath, N., Nazgiewicz, A., Kemkemer, R., Derby, B., Spatz, J., and Ballestrem, C. (2013). Vinculin regulates the recruitment and release of core focal adhesion proteins in a force-dependent manner. Curr. Biol. *23*, 271–281.

Carlson, S.S., Valdez, G., and Sanes, J.R. (2010a). Presynaptic calcium channels and alpha3-integrins are complexed with synaptic cleft laminins, cytoskeletal elements and active zone components. J. Neurochem. *115*, 654–666.

Carlson, S.S., Valdez, G., and Sanes, J.R. (2010b). Presynaptic calcium channels and α3-integrins are complexed with synaptic cleft laminins, cytoskeletal elements and active zone components. J. Neurochem. *115*, 654–666.

Carman, C. V, and Springer, T.A. (2003). Integrin avidity regulation: are changes in affinity and conformation underemphasized? Curr. Opin. Cell Biol. *15*, 547–556.

Cases-Langhoff, C., Voss, B., Garner, A.M., Appeltauer, U., Takei, K., Kindler, S., Veh, R.W., De Camilli, P., Gundelfinger, E.D., and Garner, C.C. (1996). Piccolo, a novel 420 kDa protein associated with the presynaptic cytomatrix. Eur. J. Cell Biol. *69*, 214–223.

Castelletti, F., Donadelli, R., Banterla, F., Hildebrandt, F., Zipfel, P.F., Bresin, E., Otto, E., Skerka, C., Renieri, A., Todeschini, M., et al. (2008). Mutations in FN1 cause glomerulopathy with fibronectin deposits. Proc. Natl. Acad. Sci. U. S. A. *105*, 2538–2543.

Chan, F.L., and Inoue, S. (1994). Lamina lucida of basement membrane: an artefact. Microsc. Res. Tech. *28*, 48–59.

Chan, C.-S., Weeber, E.J., Kurup, S., Sweatt, J.D., and Davis, R.L. (2003). Integrin requirement for hippocampal synaptic plasticity and spatial memory. J. Neurosci. *23*, 7107–7116.

Chan, C.-S.S., Levenson, J.M., Mukhopadhyay, P.S., Zong, L., Bradley, A., Sweatt, J.D., and Davis, R.L. (2007). Alpha3-integrins are required for hippocampal long-term potentiation and working memory. Learn. Mem. *14*, 606–615.

Chan, S.H.S., Wong, V.C.N., and Engel, A.G. (2012). Neuromuscular junction acetylcholinesterase deficiency responsive to albuterol. Pediatr. Neurol. *47*, 137–140.

Chand, K.K., Lee, K.M., Schenning, M.P., Lavidis, N.A., and Noakes, P.G. (2015). Loss of β2-laminin alters calcium sensitivity and voltage-gated calcium channel maturation of neurotransmission at the neuromuscular junction. J. Physiol. *593*, 245–265.

Charvet, B., Ruggiero, F., and Le Guellec, D. (2012). The development of the myotendinous junction. A review. Muscles. Ligaments Tendons J. *2*, 53–63.

Chen, B.M., and Grinnell, A.D. (1995). Integrins and modulation of transmitter release from motor nerve terminals by stretch. Science *269*, 1578–1580.

Chen, J., Salas, A., and Springer, T.A. (2003). Bistable regulation of integrin adhesiveness by a bipolar metal ion cluster. Nat. Struct. Biol. *10*, 995–1001.

Chen, J., Billings, S.E., and Nishimune, H. (2011). Calcium channels link the muscle-derived synapse organizer laminin β2 to Bassoon and CAST/Erc2 to organize presynaptic active zones. J. Neurosci. *31*, 512–525.

Chen, J., Mizushige, T., and Nishimune, H. (2012). Active zone density is conserved during synaptic growth but impaired in aged mice. J. Comp. Neurol. *520*, 434–452.

Cheung, T.H., and Rando, T.A. (2013). Molecular regulation of stem cell quiescence. Nat. Rev. Mol. Cell Biol. *14*, 329–340.

Clarke, G.L., Chen, J., and Nishimune, H. (2012). Presynaptic Active Zone Density during Development and Synaptic Plasticity. Front. Mol. Neurosci. *5*, 12.

Cohen, M.W., Hoffstrom, B.G., and Desimone, D.W. (2000a). Active Zones on Motor Nerve Terminals Contain a3b1 Integrin. Dev. Biol. *20*, 4912–4921.

Cohen, M.W., Hoffstrom, B.G., and DeSimone, D.W. (2000b). Active zones on motor nerve terminals contain alpha3beta1 integrin. J. Neurosci. *20*, 4912–4921.

Collins, C.A., Olsen, I., Zammit, P.S., Heslop, L., Petrie, A., Partridge, T.A., and Morgan, J.E. (2005). Stem cell function, self-renewal, and behavioral heterogeneity of cells from the adult muscle satellite cell niche. Cell *122*, 289–301.

Colognato, H., and Yurchenco, P.D. (2000). Form and function: the laminin family of heterotrimers. Dev. Dyn. *218*, 213–234.

Conti, F.J., Felder, A., Monkley, S., Schwander, M., Wood, M.R., Lieber, R., Critchley, D., and Muller, U. (2008). Progressive myopathy and defects in the maintenance of myotendinous junctions in mice that lack talin 1 in skeletal muscle. Development *135*, 2043–2053.

Conti, F.J., Monkley, S.J., Wood, M.R., Critchley, D.R., and Muller, U. (2009). Talin 1 and 2 are required for myoblast fusion, sarcomere assembly and the maintenance of myotendinous junctions. Development *136*, 3597–3606.

Conti, F.J.A., Rudling, R.J., Robson, A., and Hodivala-Dilke, K.M. (2003). Alpha3beta1 integrin regulates hair follicle but not interfollicular morphogenesis in adult epidermis. J. Cell Sci. *116*, 2737–2747.

Court, F. a, Gillingwater, T.H., Melrose, S., Sherman, D.L., Greenshields, K.N., Morton, a J., Harris, J.B., Willison, H.J., and Ribchester, R.R. (2008). Identity, developmental restriction and reactivity of extralaminar cells capping mammalian neuromuscular junctions. J. Cell Sci. *121*, 3901–3911.

Critchley, D.R., and Gingras, A.R. (2008). Talin at a glance. J. Cell Sci. *121*, 1345–1347.

Cross, S.S., Lippitt, J., Mitchell, A., Hollingsbury, F., Balasubramanian, S.P., Reed, M.W.R., Eaton, C., Catto, J.W., Hamdy, F., and Winder, S.J. (2008). Expression of beta-dystroglycan is reduced or absent in many human carcinomas. Histopathology *53*, 561–566.

Cruz-Jentoft, A.J., Baeyens, J.P., Bauer, J.M., Boirie, Y., Cederholm, T., Landi, F., Martin, F.C., Michel, J.-P., Rolland, Y., Schneider, S.M., et al. (2010). Sarcopenia: European consensus on definition and diagnosis: Report of the European Working Group on Sarcopenia in Older People. Age Ageing *39*, 412–423.

Daugaard, J.R., and Richter, E.A. (2001). Relationship between muscle fibre composition, glucose transporter protein 4 and exercise training: possible consequences in non-insulin-dependent diabetes mellitus. Acta Physiol. Scand. *171*, 267–276.

Davydova, D., Marini, C., King, C., Klueva, J., Bischof, F., Romorini, S., Montenegro-Venegas, C., Heine, M., Schneider, R., Schröder, M.S., et al. (2014). Bassoon specifically controls presynaptic P/Q-type Ca(2+) channels via RIM-binding protein. Neuron *82*, 181–194.

Deakin, N.O., and Turner, C.E. (2009). Paxillin comes of age. Cell *121*, 2435–2444.

Dean, C., Scholl, F.G., Choih, J., DeMaria, S., Berger, J., Isacoff, E., and Scheiffele, P. (2003). Neurexin mediates the assembly of presynaptic terminals. Nat. Neurosci. *6*, 708–716.

DeChiara, T.M., Bowen, D.C., Valenzuela, D.M., Simmons, M. V, Poueymirou, W.T., Thomas, S., Kinetz, E., Compton, D.L., Rojas, E., Park, J.S., et al. (1996). The receptor tyrosine kinase MuSK is required for neuromuscular junction formation in vivo. Cell *85*, 501–512.

Deconinck, A.E., Potter, A.C., Tinsley, J.M., Wood, S.J., Vater, R., Young, C., Metzinger, L., Vincent, A., Slater, C.R., and Davies, K.E. (1997). Postsynaptic abnormalities at the neuromuscular junctions of utrophin-deficient mice. J. Cell Biol. *136*, 883–894.

Deries, M., Schweitzer, R., and Duxson, M.J. (2010). Developmental fate of the mammalian myotome. Dev. Dyn. *239*, 2898–2910.

Deschenes, M.R., Judelson, D.A., Kraemer, W.J., Meskaitis, V.J., Volek, J.S., Nindl, B.C., Harman, F.S., and Deaver, D.R. (2000). Effects of resistance training on neuromuscular junction morphology. Muscle Nerve *23*, 1576–1581.

Deschenes, M.R., Roby, M.A., and Glass, E.K. (2011). Aging influences adaptations of the neuromuscular junction to endurance training. Neuroscience *190*, 56–66.

DeSimone, D.W., Stepp, M.A., Patel, R.S., and Hynes, R.O. (1987). The integrin family of cell surface receptors. Biochem. Soc. Trans. *15*, 789–791.

DiPersio, C.M., Shah, S., and Hynes, R.O. (1995). Alpha3A beta1 integrin localizes to focal contacts in response to diverse extracellular matrix proteins. J. Cell Sci. *108*, 2321–2336.

DiPersio, C.M., Hodivala-Dilke, K.M., Jaenisch, R., Kreidberg, J.A., and Hynes, R.O. (1997). Alpha3beta1 integrin is required for normal development of the epidermal basement membrane. JCB *137*, 729–742.

Le Douarin, N.M., and Smith, J. (1988). Development of the peripheral nervous system from the neural crest. Annu. Rev. Cell Biol. *4*, 375–404.

Drey, M., Sieber, C.C., Bauer, J.M., Uter, W., Dahinden, P., Fariello, R.G., and Vrijbloed, J.W. (2013). C-terminal Agrin Fragment as a potential marker for sarcopenia caused by degeneration of the neuromuscular junction. Exp. Gerontol. *48*, 76–80.

Dulubova, I., Lou, X., Lu, J., Huryeva, I., Alam, A., Schneggenburger, R., Südhof, T.C., and Rizo, J. (2005). A Munc13/RIM/Rab3 tripartite complex: from priming to plasticity? EMBO J. *24*, 2839–2850.

Dulubova, I., Khvotchev, M., Liu, S., Huryeva, I., Südhof, T.C., and Rizo, J. (2007). Munc18-1 binds directly to the neuronal SNARE complex. Proc. Natl. Acad. Sci. U. S. A. *104*, 2697–2702.

Edwards, J.P., Hatton, P.A., and Wareham, A.C. (1998). Electrophysiology of the neuromuscular junction of the laminin-2 (merosin) deficient C57 BL/6J dy2J/dy2J dystrophic mouse. Brain Res. *788*, 262–268.

Eglen, R.M. (2006). Muscarinic receptor subtypes in neuronal and non-neuronal cholinergic function. Auton. Autacoid Pharmacol. *26*, 219–233.

Ellisman, M.H., Rash, J.E., Staehelin, L.A., and Porter, K.R. (1976). Studies of excitable membranes. II. A comparison of specializations at neuromuscular junctions and nonjunctional sarcolemmas of mammalian fast and slow twitch muscle fibers. J. Cell Biol. *68*, 752–774.

Endo, M. (2009). Calcium-induced calcium release in skeletal muscle. Physiol. Rev. *89*, 1153–1176.

Engel, J., Odermatt, E., Engel, A., Madri, J.A., Furthmayr, H., Rohde, H., and Timpl, R. (1981). Shapes, domain organizations and flexibility of laminin and fibronectin, two multifunctional proteins of the extracellular matrix. J. Mol. Biol. *150*, 97–120.

Ervasti, J.M. (2003). Costameres: the Achilles' heel of Herculean muscle. J. Biol. Chem. *278*, 13591–13594.

Ervasti, J.M., and Campbell, K.P. (1993). A role for the dystrophin-glycoprotein complex as a transmembrane linker between laminin and actin. J. Cell Biol. *122*, 809–823.

Exposito, J.-Y., Valcourt, U., Cluzel, C., and Lethias, C. (2010). The fibrillar collagen family. Int. J. Mol. Sci. *11*, 407–426.

Fariñas, I., Egea, G., Blasi, J., Cases, C., and Marsal, J. (1993). Calcium channel antagonist omega-conotoxin binds to intramembrane particles of isolated nerve terminals. Neuroscience *54*, 745–752.

Fässler, R., and Meyer, M. (1995). Consequences of lack of beta 1 integrin gene expression in mice. Genes Dev. *9*, 1896–1908.

Fatt, P., and Katz, B. (1952). Spontaneous subthreshold activity at motor nerve endings. J. Physiol. *117*, 109–128.

Favero, M., Busetto, G., and Cangiano, A. (2012). Spike timing plays a key role in synapse elimination at the neuromuscular junction. Proc. Natl. Acad. Sci. U. S. A. *109*, E1667–E1675.

Favier, F.B., Benoit, H., and Freyssenet, D. (2008). Cellular and molecular events controlling skeletal muscle mass in response to altered use. Pflugers Arch. *456*, 587–600.

Fdez, E., and Hilfiker, S. (2006). Vesicle pools and synapsins: new insights into old enigmas. Brain Cell Biol. *35*, 107–115.

Ferraro, E., Molinari, F., and Berghella, L. (2012). Molecular control of neuromuscular junction development. J. Cachexia. Sarcopenia Muscle *3*, 13–23.

Fertuck, H.C., and Salpeter, M.M. (1976). Quantitation of junctional and extrajunctional acetylcholine receptors by electron microscope autoradiography after 125I-alpha-bungarotoxin binding at mouse neuromuscular junctions. J. Cell Biol. *69*, 144–158.

Finlayson, S., Spillane, J., Kullmann, D.M., Howard, R., Webster, R., Palace, J., and Beeson, D. (2013). Slow channel congenital myasthenic syndrome responsive to a combination of fluoxetine and salbutamol. Muscle Nerve *47*, 279–282.

Van der Flier, A., Gaspar, A.C., Thorsteinsdottir, S., Baudoin, C., Groeneveld, E., Mummery, C.L., and Sonnenberg, A. (1997). Spatial and temporal expression of the beta1D integrin during mouse development. Dev. Dyn. *210*, 472–486.

Fox, M. a, Tapia, J.C., Kasthuri, N., and Lichtman, J.W. (2011). Delayed synapse elimination in mouse levator palpebrae superioris muscle. J. Comp. Neurol. *519*, 2907–2921.

Fox, M.A., Sanes, J.R., Borza, D.-B., Eswarakumar, V.P., Fässler, R., Hudson, B.G., John, S.W.M., Ninomiya, Y., Pedchenko, V., Pfaff, S.L., et al. (2007). Distinct target-derived signals organize formation, maturation, and maintenance of motor nerve terminals. Cell *129*, 179–193.

Fox, M.A., Ho, M.S.P., Smyth, N., and Sanes, J.R. (2008). A synaptic nidogen: developmental regulation and role of nidogen-2 at the neuromuscular junction. Neural Dev. *3*, 24.

Frank, T., Rutherford, M. a, Strenzke, N., Neef, A., Pangršič, T., Khimich, D., Fejtova, A., Fetjova, A., Gundelfinger, E.D., Liberman, M.C., et al. (2010). Bassoon and the synaptic ribbon organize Ca^{2+} channels and vesicles to add release sites and promote refilling. Neuron *68*, 724–738.

Froehner, S.C. (1993). Regulation of ion channel distribution at synapses. Annu. Rev. Neurosci. *16*, 347–368.

Fu, A.K.Y., Ip, F.C.F., Fu, W.-Y., Cheung, J., Wang, J.H., Yung, W.-H., and Ip, N.Y. (2005). Aberrant motor axon projection, acetylcholine receptor clustering, and neurotransmission in cyclin-dependent kinase 5 null mice. Proc. Natl. Acad. Sci. U. S. A. *102*, 15224–15229.

Fuchs, P., Zörer, M., Reipert, S., Rezniczek, G.A., Propst, F., Walko, G., Fischer, I., Bauer, J., Leschnik, M.W., Lüscher, B., et al. (2009). Targeted inactivation of a developmentally regulated neural plectin isoform (plectin 1c) in mice leads to reduced motor nerve conduction velocity. J. Biol. Chem. *284*, 26502–26509.

Fujita, M., Mitsuhashi, H., Isogai, S., Nakata, T., Kawakami, A., Nonaka, I., Noguchi, S., Hayashi, Y.K., Nishino, I., and Kudo, A. (2012). Filamin C plays an essential role in the maintenance of the structural integrity of cardiac and skeletal muscles, revealed by the medaka mutant zacro. Dev. Biol. *361*, 79–89.

Gallardo, E., Martínez-Hernández, E., Titulaer, M.J., Huijbers, M.G., Martínez, M.A., Ramos, A., Querol, L., Díaz-Manera, J., Rojas-García, R., Hayworth, C.R., et al. (2014). Cortactin autoantibodies in myasthenia gravis. Autoimmun. Rev.

Gans, C., and Northcutt, R.G. (1983). Neural crest and the origin of vertebrates: a new head. Science *220*, 268–273.

Gattenlohner, S. (2002). Expression of foetal type acetylcholine receptor is restricted to type 1 muscle fibres in human neuromuscular disorders. Brain *125*, 1309–1319.

Gautel, M. (2008). The sarcomere and the nucleus: functional links to hypertrophy, atrophy and sarcopenia. Adv. Exp. Med. Biol. *642*, 176–191.

Geis, T., Marquard, K., Rödl, T., Reihle, C., Schirmer, S., von Kalle, T., Bornemann, A., Hehr, U., and Blankenburg, M. (2013). Homozygous dystroglycan mutation associated with a novel muscle-eye-brain disease-like phenotype with multicystic leucodystrophy. Neurogenetics *14*, 205–213.

Gesemann, M., Denzer, A.J., and Ruegg, M.A. (1995). Acetylcholine receptor-aggregating activity of agrin isoforms and mapping of the active site. J. Cell Biol. *128*, 625–636.

Gillies, A.R., and Lieber, R.L. (2011). Structure and function of the skeletal muscle extracellular matrix. Muscle Nerve *44*, 318–331.

Giniatullin, R., Nistri, A., and Yakel, J.L. (2005). Desensitization of nicotinic ACh receptors: shaping cholinergic signaling. Trends Neurosci. *28*, 371–378.

Godfrey, C., Foley, a R., Clement, E., and Muntoni, F. (2011). Dystroglycanopathies: coming into focus. Curr. Opin. Genet. Dev. *21*, 278–285.

Gokhin, D.S., and Fowler, V.M. (2011). Tropomodulin capping of actin filaments in striated muscle development and physiology. J. Biomed. Biotechnol. *2011*, 103069.

Gonzalez-Freire, M., de Cabo, R., Studenski, S.A., and Ferrucci, L. (2014). The Neuromuscular Junction: Aging at the Crossroad between Nerves and Muscle. Front. Aging Neurosci. *6*, 208.

Goulet, B.B., Kothary, R., and Parks, R.J. (2013). At the "junction" of spinal muscular atrophy pathogenesis: the role of neuromuscular junction dysfunction in SMA disease progression. Curr. Mol. Med. *13*, 1160–1174.

Grady, R.M., Merlie, J.P., and Sanes, J.R. (1997). Subtle Neuromuscular Defects in Utrophin-deficient Mice. J Neurosci *136*, 871–882.

Grady, R.M., Zhou, H., Cunningham, J.M., Henry, M.D., Campbell, K.P., and Sanes, J.R. (2000). Maturation and maintenance of the neuromuscular synapse: genetic evidence for roles of the dystrophin--glycoprotein complex. Neuron *25*, 279–293.

Granger, B.L., and Lazarides, E. (1979). Desmin and vimentin coexist at the periphery of the myofibril Z disc. Cell *18*, 1053–1063.

Greensmith, L., Dick, J., Emanuel, A.O., and Vrbová, G. (1996). Induction of transmitter release at the neuromuscular junction prevents motoneuron death after axotomy in neonatal rats. Neuroscience *71*, 213–220.

Grinnell, A.D., Chen, B.-M., Kashani, A., Lin, J., Suzuki, K., and Kidokoro, Y. (2004). The role of integrins in the modulation of neurotransmitter release from motor nerve terminals by stretch and hypertonicity. J. Neurocytol. *32*, 489–503.

Guerra, M., Cartaud, A., Cartaud, J., and Legay, C. (2005). Acetylcholinesterase and molecular interactions at the neuromuscular junction. Chem. Biol. Interact. *157-158*, 57–61.

Gui, P., Wu, X., Ling, S., Stotz, S.C., Winkfein, R.J., Wilson, E., Davis, G.E., Braun, A.P., Zamponi, G.W., and Davis, M.J. (2006). Integrin receptor activation triggers converging regulation of Cav1.2 calcium channels by c-Src and protein kinase A pathways. J. Biol. Chem. *281*, 14015–14025.

Gulledge, A.T., Kampa, B.M., and Stuart, G.J. (2005). Synaptic integration in dendritic trees. J. Neurobiol. *64*, 75–90.

Guo, C., Willem, M., Werner, A., Raivich, G., Emerson, M., Neyses, L., and Mayer, U. (2006). Absence of alpha 7 integrin in dystrophin-deficient mice causes a myopathy similar to Duchenne muscular dystrophy. Hum. Mol. Genet. *15*, 989–998.

Haase, H., Alvarez, J., Petzhold, D., Doller, A., Behlke, J., Erdmann, J., Hetzer, R., Regitz-Zagrosek, V., Vassort, G., and Morano, I. (2005). Ahnak is critical for cardiac Ca(V)1.2 calcium channel function and its beta-adrenergic regulation. FASEB J. *19*, 1969–1977.

Haenggi, T., and Fritschy, J.-M. (2006). Role of dystrophin and utrophin for assembly and function of the dystrophin glycoprotein complex in non-muscle tissue. Cell. Mol. Life Sci. *63*, 1614–1631.

Hallermann, S., Fejtova, A., Schmidt, H., Weyhersmüller, A., Silver, R.A., Gundelfinger, E.D., and Eilers, J. (2010). Bassoon speeds vesicle reloading at a central excitatory synapse. Neuron *68*, 710–723.

Hantaï, D., Nicole, S., and Eymard, B. (2013). Congenital myasthenic syndromes: an update. Curr. Opin. Neurol. *26*, 561–568.

Harburger, D.S., and Calderwood, D. a. (2009). Integrin signalling at a glance. J. Cell Sci. *122*, 1472–1472.

Hartzell, H.C., Kuffler, S.W., and Yoshikami, D. (1975). Post-synaptic potentiation: interaction between quanta of acetylcholine at the skeletal neuromuscular synapse. J. Physiol. *251*, 427–463.

Has, C., Sparta, G., Kiritsi, D., Weibel, L., Moeller, A., Vega-Warner, V., Waters, A., He, Y., Anikster, Y., Esser, P., et al. (2012). Integrin α3 mutations with kidney, lung, and skin disease. N. Engl. J. Med. *366*, 1508–1514.

Heeroma, J.., Plomp, J.., Roubos, E.., and Verhage, M. (2003). Development of the mouse neuromuscular junction in the absence of regulated secretion. Neuroscience *120*, 733–744.

Van der Heijden, E.P., Kroese, A.B., Werker, P.M., de With, M.C., de Smet, M., Kon, M., and Bär, D.P. (2000). Improving the preservation of isolated rat skeletal muscles stored for 16 hours at 4 degrees C. Transplantation *69*, 1310–1322.

Hesser, B. a., Henschel, O., and Witzemann, V. (2006). Synapse disassembly and formation of new synapses in postnatal muscle upon conditional inactivation of MuSK. Mol. Cell. Neurosci. *31*, 470–480.

Hirokawa, N., and Heuser, J.E. (1982). Internal and external differentiations of the postsynaptic membrane at the neuromuscular junction. J. Neurocytol. *11*, 487–510.

Hirsch, E., Gullberg, D., Balzac, F., Altruda, F., Silengo, L., and Tarone, G. (1994). Alpha v integrin subunit is predominantly located in nervous tissue and skeletal muscle during mouse development. Dev. Dyn. *201*, 108–120.

Hodges, B.L., Hayashi, Y.K., Nonaka, I., Wang, W., Arahata, K., and Kaufman, S.J. (1997). Altered expression of the alpha7beta1 integrin in human and murine muscular dystrophies. J. Cell Sci. *110 (Pt 2*, 2873–2881.

Hoffman, E.P., Brown, R.H., and Kunkel, L.M. (1987). Dystrophin: the protein product of the Duchenne muscular dystrophy locus. Cell *51*, 919–928.

Hohenester, E., and Yurchenco, P.D. (2013). Laminins in basement membrane assembly. Cell Adh. Migr. *7*, 56–63.

Holmberg, J., and Durbeej, M. (2013). Laminin-211 in skeletal muscle function. 1–11.

Hoshijima, M. (2006). Mechanical stress-strain sensors embedded in cardiac cytoskeleton: Z disk, titin, and associated structures. Am. J. Physiol. Heart Circ. Physiol. *290*, H1313–H1325.

Hotulainen, P., and Lappalainen, P. (2006). Stress fibers are generated by two distinct actin assembly mechanisms in motile cells. J. Cell Biol. *173*, 383–394.

Houlden, H. (2013). Defective N-linked protein glycosylation pathway in congenital myasthenic syndromes. Brain *136*, 692–695.

Hu, P., and Luo, B.H. (2013). Integrin bi-directional signaling across the plasma membrane. J. Cell. Physiol. *228*, 306–312.

Huang, X., Li, J., Foster, D., Lemanski, S.L., Dube, D.K., Zhang, C., and Lemanski, L.F. (2002). Protein kinase C-mediated desmin phosphorylation is related to myofibril disarray in cardiomyopathic hamster heart. Exp. Biol. Med. (Maywood). *227*, 1039–1046.

Huard, J., Fortier, L.P., Labrecque, C., Dansereau, G., and Tremblay, J.P. (1991). Is dystrophin present in the nerve terminal at the neuromuscular junction? An immunohistochemical study of the heterozygote dystrophic (mdx) mouse. Synapse *7*, 135–140.

Huhtala, M., Heino, J., Casciari, D., de Luise, A., and Johnson, M.S. (2005). Integrin evolution: insights from ascidian and teleost fish genomes. Matrix Biol. *24*, 83–95.

Hutter, O.F., and Trautwein, W. (1956). Neuromuscular facilitation by stretch of motor nerve-endings. J. Physiol. *133*, 610–625.

Hynes, R.O. (2002a). Integrins: bidirectional, allosteric signaling machines. Cell *110*, 673–687.

Hynes, R.O. (2002b). Integrins : Bidirectional , Allosteric Signaling Machines In their roles as major adhesion receptors , integrins. *110*, 673–687.

Hynes, R.O. (2004). The emergence of integrins: a personal and historical perspective. Matrix Biol. *23*, 333–340.

Hynes, R.O. (2009). The extracellular matrix: not just pretty fibrils. Science *326*, 1216–1219.

Iannaccone, S.T., and Castro, D. (2013). Congenital muscular dystrophies and congenital myopathies. Continuum (Minneap. Minn). *19*, 1509–1534.

Inoue, A., Setoguchi, K., Matsubara, Y., Okada, K., Sato, N., Iwakura, Y., Higuchi, O., and Yamanashi, Y. (2009). Dok-7 activates the muscle receptor kinase MuSK and shapes synapse formation. Sci. Signal. *2*, ra7.

Janssen, I., Shepard, D.S., Katzmarzyk, P.T., and Roubenoff, R. (2004). The healthcare costs of sarcopenia in the United States. J. Am. Geriatr. Soc. *52*, 80–85.

Jaworski, A., and Burden, S.J. (2006). Neuromuscular synapse formation in mice lacking motor neuron- and skeletal muscle-derived Neuregulin-1. J. Neurosci. *26*, 655–661.

Jiao, W., Masich, S., Franzén, O., and Shupliakov, O. (2010). Two pools of vesicles associated with the presynaptic cytosolic projection in Drosophila neuromuscular junctions. J. Struct. Biol. *172*, 389–394.

Juranek, J., Mukherjee, K., Rickmann, M., Martens, H., Calka, J., Südhof, T.C., and Jahn, R. (2006). Differential expression of active zone proteins in neuromuscular junctions suggests functional diversification. Eur. J. Neurosci. *24*, 3043–3052.

Kaech, S.M., Whitfield, C.W., and Kim, S.K. (1998). The LIN-2/LIN-7/LIN-10 complex mediates basolateral membrane localization of the C. elegans EGF receptor LET-23 in vulval epithelial cells. Cell *94*, 761–771.

Kaeser, P.S., Deng, L., Wang, Y., Dulubova, I., Liu, X., Rizo, J., and Südhof, T.C. (2011). RIM proteins tether Ca2+ channels to presynaptic active zones via a direct PDZ-domain interaction. Cell *144*, 282–295.

Kanagawa, M., Michele, D.E., Satz, J.S., Barresi, R., Kusano, H., Sasaki, T., Timpl, R., Henry, M.D., and Campbell, K.P. (2005). Disruption of perlecan binding and matrix assembly by post-translational or genetic disruption of dystroglycan function. FEBS Lett. *579*, 4792–4796.

Kassar-Duchossoy, L., Gayraud-Morel, B., Gomès, D., Rocancourt, D., Buckingham, M., Shinin, V., and Tajbakhsh, S. (2004). Mrf4 determines skeletal muscle identity in Myf5:Myod double-mutant mice. Nature *431*, 466–471.

Katz, B., and Miledi, R. (1968). The role of calcium in neuromuscular facilitation. J. Physiol. *195*, 481–492.

Katz, B., and Miledi, R. (1973). The binding of acetylcholine to receptors and its removal from the synaptic cleft. J. Physiol. *231*, 549–574.

Katz, B., and Miledi, R. (1979). Estimates of quantal content during "chemical potentiation" of transmitter release. Proc. R. Soc. Lond. B. Biol. Sci. *205*, 369–378.

Kawaguchi, S., and Hirano, T. (2006). Integrin alpha3beta1 suppresses long-term potentiation at inhibitory synapses on the cerebellar Purkinje neuron. Mol. Cell. Neurosci. *31*, 416–426.

Kerrisk, M.E., Greer, C. a, and Koleske, A.J. (2013). Integrin α3 is required for late postnatal stability of dendrite arbors, dendritic spines and synapses, and mouse behavior. J. Neurosci. *33*, 6742–6752.

Knöll, R., Buyandelger, B., and Lab, M. (2011). The sarcomeric Z-disc and Z-discopathies. J. Biomed. Biotechnol. *2011*, 569628.

Kong, L., Wang, X., Choe, D.W., Polley, M., Burnett, B.G., Bosch-Marcé, M., Griffin, J.W., Rich, M.M., and Sumner, C.J. (2009). Impaired synaptic vesicle release and immaturity of neuromuscular junctions in spinal muscular atrophy mice. J. Neurosci. *29*, 842–851.

Koper, A., Schenck, A., and Prokop, A. (2012). Analysis of adhesion molecules and basement membrane contributions to synaptic adhesion at the Drosophila embryonic NMJ. PLoS One *7*, e36339.

Kreidberg, J.A., Donovan, M.J., Goldstein, S.L., Rennke, H., Shepherd, K., Jones, R.C., and Jaenisch, R. (1996). Alpha3beta1 integrin has a crucial role in kidney and lung organogenesis. Development *122*, 3537–3547.

Kuffler, S.W., and Yoshikami, D. (1975). The number of transmitter molecules in a quantum: an estimate from iontophoretic application of acetylcholine at the neuromuscular synapse. J. Physiol. *251*, 465–482.

Kummer, T.T., Misgeld, T., Lichtman, J.W., and Sanes, J.R. (2004). Nerve-independent formation of a topologically complex postsynaptic apparatus. J. Cell Biol. *164*, 1077–1087.

Kuo, H.-J., Maslen, C.L., Keene, D.R., and Glanville, R.W. (1997). Type VI Collagen Anchors Endothelial Basement Membranes by Interacting with Type IV Collagen. J. Biol. Chem. *272*, 26522–26529.

Lafuste, P., Sonnet, C., Chazaud, B., Dreyfus, P.A., Gherardi, R.K., Wewer, U.M., and Authier, F.-J.J. (2005). ADAM12 and alpha9beta1 integrin are instrumental in human myogenic cell differentiation. Mol. Biol. Cell *16*, 861–870.

Lampe, A.K., and Bushby, K.M.D. (2005). Collagen VI related muscle disorders. J. Med. Genet. *42*, 673–685.

Lapidos, K.A., Kakkar, R., and McNally, E.M. (2004). The dystrophin glycoprotein complex: signaling strength and integrity for the sarcolemma. Circ. Res. *94*, 1023–1031.

Latvanlehto, A., Fox, M.A., Sormunen, R., Tu, H., Oikarainen, T., Koski, A., Naumenko, N., Shakirzyanova, A., Kallio, M., Ilves, M., et al. (2010). Muscle-derived collagen XIII regulates maturation of the skeletal neuromuscular junction. J. Neurosci. *30*, 12230–12241.

Lepper, C., Partridge, T. a., and Fan, C.-M.M. (2011). An absolute requirement for Pax7-positive satellite cells in acute injury-induced skeletal muscle regeneration. Development *138*, 3639–3646.

Li, D., Bareja, A., Judge, L., Yue, Y., Lai, Y., Fairclough, R., Davies, K.E., Chamberlain, J.S., and Duan, D. (2010). Sarcolemmal nNOS anchoring reveals a qualitative difference between dystrophin and utrophin. J. Cell Sci. *123*, 2008–2013.

Li, Y., Lee, Y., and Thompson, W. (2011). Changes in aging mouse neuromuscular junctions are explained by degeneration and regeneration of muscle fiber segments at the synapse. J Neurosci *31*, 14910–14919.

Li, Y., Arora, Y., and Levin, K. (2013). Myasthenia gravis: newer therapies offer sustained improvement. Cleve. Clin. J. Med. *80*, 711–721.

Lin, W., Burgess, R.W., Dominguez, B., Pfaff, S.L., Sanes, J.R., and Lee, K.F. (2001). Distinct roles of nerve and muscle in postsynaptic differentiation of the neuromuscular synapse. Nature *410*, 1057–1064.

Ling, S.M., Conwit, R.A., Ferrucci, L., and Metter, E.J. (2009). Age-associated changes in motor unit physiology: observations from the Baltimore Longitudinal Study of Aging. Arch. Phys. Med. Rehabil. *90*, 1237–1240.

Linke, W.A., and Hamdani, N. (2014). Gigantic business: titin properties and function through thick and thin. Circ. Res. *114*, 1052–1068.

Liu, H., Niu, A., Chen, S.-E., and Li, Y.-P. (2011a). Beta3-integrin mediates satellite cell differentiation in regenerating mouse muscle. FASEB *25*, 1914–1921.

Liu, K., Cheng, L., Flesken-Nikitin, A., Huang, L., Nikitin, A.Y., and Pauli, B.U. (2010). Conditional knockout of fibronectin abrogates mouse mammary gland lobuloalveolar differentiation. Dev. Biol. *346*, 11–24.

Liu, K.S.Y., Siebert, M., Mertel, S., Knoche, E., Wegener, S., Wichmann, C., Matkovic, T., Muhammad, K., Depner, H., Mettke, C., et al. (2011b). RIM-binding protein, a central part of the active zone, is essential for neurotransmitter release. Science *334*, 1565–1569.

Llewellyn, M.E., Thompson, K.R., Deisseroth, K., and Delp, S.L. (2010). Orderly recruitment of motor units under optical control in vivo. Nat. Med. *16*, 1161–1165.

Lopes, L.R., and Elliott, P.M. (2014). A straightforward guide to the sarcomeric basis of cardiomyopathies. Heart.

Lu, Q.L., Rabinowitz, A., Chen, Y.C., Yokota, T., Yin, H., Alter, J., Jadoon, A., Bou-Gharios, G., and Partridge, T. (2005). Systemic delivery of antisense oligoribonucleotide restores dystrophin expression in body-wide skeletal muscles. Proc. Natl. Acad. Sci. U. S. A. *102*, 198–203.

Lucas, C.A., and Hoh, J.F. (1997). Extraocular fast myosin heavy chain expression in the levator palpebrae and retractor bulbi muscles. Invest. Ophthalmol. Vis. Sci. *38*, 2817–2825.

Luxenburg, C., Parsons, J.T., Addadi, L., and Geiger, B. (2006). Involvement of the Src-cortactin pathway in podosome formation and turnover during polarization of cultured osteoclasts. J. Cell Sci. *119*, 4878–4888.

Ma, C., Li, W., Xu, Y., and Rizo, J. (2011). Munc13 mediates the transition from the closed syntaxin-Munc18 complex to the SNARE complex. Nat. Struct. Mol. Biol. *18*, 542–549.

MacIntosh, B.R., Gardiner, P.F., and McComas, A.J. (2006). Skeletal Muscle: Form and Function (Human Kinetics).

Maglione, M., and Sigrist, S.J. (2013). Seeing the forest tree by tree: super-resolution light microscopy meets the neurosciences. Nat. Neurosci. *16*, 790–797.

Mainguy, V., Maltais, F., Saey, D., Gagnon, P., Martel, S., Simon, M., and Provencher, S. (2010). Peripheral muscle dysfunction in idiopathic pulmonary arterial hypertension. Thorax *65*, 113–117.

Marques, M.J., Conchello, J.A., and Lichtman, J.W. (2000). From plaque to pretzel: fold formation and acetylcholine receptor loss at the developing neuromuscular junction. J. Neurosci. *20*, 3663–3675.

Martin, A.R. (1994). Amplification of neuromuscular transmission by postjunctional folds. Proc. Biol. Sci. *258*, 321–326.

Martin, P.T. (2003). Dystroglycan glycosylation and its role in matrix binding in skeletal muscle. Glycobiology *13*, 55R – 66R.

Martin, P.T., Kaufman, S.J., Kramer, R.H., and Sanes, J.R. (1996a). Synaptic Integrins in Developing , Adult , and Mutant Muscle : Selective Association of a 1 , a 7A , and a 7B Integrins with the Neuromuscular Junction. *139*, 125–139.

Martin, P.T., Kaufman, S.J., Kramer, R.H., and Sanes, J.R. (1996b). Synaptic integrins in developing, adult, and mutant muscle: selective association of alpha1, alpha7A, and alpha7B integrins with the neuromuscular junction. Dev. Biol. *174*, 125–139.

Martínez-Hernández, R., Bernal, S., Also-Rallo, E., Alías, L., Barceló, M.J., Hereu, M., Esquerda, J.E., and Tizzano, E.F. (2013). Synaptic defects in type I spinal muscular atrophy in human development. J. Pathol. *229*, 49–61.

Martínez-Martínez, P., Phernambucq, M., Steinbusch, L., Schaeffer, L., Berrih-Aknin, S., Duimel, H., Frederik, P., Molenaar, P., De Baets, M.H., and Losen, M. (2009). Silencing rapsyn in vivo decreases acetylcholine receptors and augments sodium channels and secondary postsynaptic membrane folding. Neurobiol. Dis. *35*, 14–23.

Maselli, R. a, Arredondo, J., Ferns, M.J., and Wollmann, R.L. (2012). Synaptic basal lamina-associated congenital myasthenic syndromes. Ann. N. Y. Acad. Sci. *1275*, 36–48.

Maselli, R.A., Ng, J.J., Anderson, J.A., Cagney, O., Arredondo, J., Williams, C., Wessel, H.B., Abdel-Hamid, H., and Wollmann, R.L. (2009). Mutations in LAMB2 causing a severe form of synaptic congenital myasthenic syndrome. J. Med. Genet. *46*, 203–208.

Massaro, C.M., Pielage, J., and Davis, G.W. (2009). Molecular mechanisms that enhance synapse stability despite persistent disruption of the spectrin/ankyrin/microtubule cytoskeleton. J. Cell Biol. *187*, 101–117.

Matthews-Bellinger, J.A., and Salpeter, M.M. (1983). Fine structural distribution of acetylcholine receptors at developing mouse neuromuscular junctions. J. Neurosci. *3*, 644–657.

Mayer, U. (2003). Integrins: redundant or important players in skeletal muscle? J. Biol. Chem. *278*, 14587–14590.

Mayer, A., Wickner, W., and Haas, A. (1996). Sec18p (NSF)-driven release of Sec17p (alpha-SNAP) can precede docking and fusion of yeast vacuoles. Cell *85*, 83–94.

Mayer, U., Saher, G., Fassler, R., Bornemann, A., Echtermeyer, F., von der Mark, H., Miosge, N., Poschl, E., and von der Mark, K. (1997). Absence of integrin alpha 7 causes a novel form of muscular dystrophy. Nat. Genet. *17*, 318–323.

McDonald, K.A., Lakonishok, M., and Horwitz, A.F. (1995). αv and α3 integrin subunits are associated with myofibrils during myofibrillogenesis. J. Cell Sci. *2581*, 2573–2581.

McMahan, U.J. (1990). The agrin hypothesis. Cold Spring Harb. Symp. Quant. Biol. *55*, 407–418.

Melia, T.J. (2007). Putting the clamps on membrane fusion: how complexin sets the stage for calcium-mediated exocytosis. FEBS Lett. *581*, 2131–2139.

Mendell, L.M. (2005). The size principle: a rule describing the recruitment of motoneurons. J. Neurophysiol. *93*, 3024–3026.

Merker, H.J. (1994). Morphology of the basement membrane. Microsc. Res. Tech. *28*, 95–124.

Milner-Brown, H.S., Stein, R.B., and Yemm, R. (1973). The orderly recruitment of human motor units during voluntary isometric contractions. J. Physiol. *230*, 359–370.

Miner, J.H., Patton, B.L., Lentz, S.I., Gilbert, D.J., Snider, W.D., Jenkins, N.A., Copeland, N.G., and Sanes, J.R. (1997). The laminin alpha chains: expression, developmental transitions, and chromosomal locations of alpha1-5, identification of heterotrimeric laminins 8–11, and cloning of a novel alpha3 isoform. JCB *137*, 685–701.

Misgeld, T., Burgess, R.W., Lewis, R.M., Cunningham, J.M., Lichtman, J.W., and Sanes, J.R. (2002). Roles of neurotransmitter in synapse formation: development of neuromuscular junctions lacking choline acetyltransferase. Neuron *36*, 635–648.

Moloney, E.B., de Winter, F., and Verhaagen, J. (2014). ALS as a distal axonopathy: molecular mechanisms affecting neuromuscular junction stability in the presymptomatic stages of the disease. Front. Neurosci. *8*, 252.

Montarras, D., Morgan, J., Collins, C., Relaix, F., Zaffran, S., Cumano, A., Partridge, T., and Buckingham, M. (2005). Direct isolation of satellite cells for skeletal muscle regeneration. Science (80-.). *309*, 2064–2067.

Moore, C.J., and Winder, S.J. (2012). The inside and out of dystroglycan post-translational modification. Neuromuscul. Disord. *22*, 959–965.

Mootoosamy, R.C., and Dietrich, S. (2002). Distinct regulatory cascades for head and trunk myogenesis. Development *129*, 573–583.

Morgan, J.E., and Partridge, T.A. (2003). Muscle satellite cells. Int. J. Biochem. Cell Biol. *35*, 1151–1156.

Morley, J.E., von Haehling, S., Anker, S.D., and Vellas, B. (2014). From sarcopenia to frailty: a road less traveled. J. Cachexia. Sarcopenia Muscle *5*, 5–8.

Moscoso, L.M., Cremer, H., and Sanes, J.R. (1998). Organization and reorganization of neuromuscular junctions in mice lacking neural cell adhesion molecule, tenascin-C, or fibroblast growth factor-5. J. Neurosci. *18*, 1465–1477.

Mould, A.P., Travis, M.A., Barton, S.J., Hamilton, J.A., Askari, J.A., Craig, S.E., Macdonald, P.R., Kammerer, R.A., Buckley, P.A., and Humphries, M.J. (2005). Evidence that monoclonal antibodies directed against the integrin beta subunit plexin/semaphorin/integrin domain stimulate function by inducing receptor extension. J. Biol. Chem. *280*, 4238–4246.

Mozrzymas, J.W. (2008). Electrophysiological description of mechanisms determining synaptic transmission and its modulation. Acta Neurobiol. Exp. (Wars). *68*, 256–263.

Muiznieks, L.D., and Keeley, F.W. (2013). Molecular assembly and mechanical properties of the extracellular matrix: A fibrous protein perspective. Biochim. Biophys. Acta *1832*, 866–875.

Mukherjee, K., Yang, X., Gerber, S.H., Kwon, H.-B., Ho, A., Castillo, P.E., Liu, X., and Südhof, T.C. (2010). Piccolo and bassoon maintain synaptic vesicle clustering without directly participating in vesicle exocytosis. Proc. Natl. Acad. Sci. U. S. A. *107*, 6504–6509.

Muntoni, F., Torelli, S., Wells, D.J., and Brown, S.C. (2011). Muscular dystrophies due to glycosylation defects: diagnosis and therapeutic strategies. Curr. Opin. Neurol. *24*, 437–442.

Murphy, D. a., and Courtneidge, S. a. (2011). The “ins” and “outs” of podosomes and invadopodia: characteristics, formation and function. Nat. Rev. Mol. Cell Biol. *12*, 413–426.

Musil, L.S., Frail, D.E., and Merlie, J.P. (1989). The mammalian 43-kD acetylcholine receptor-associated protein (RAPsyn) is expressed in some nonmuscle cells. J. Cell Biol. *108*, 1833–1840.

Nagano, Y., Matsuda, Y., Desaki, J., Oki, S., Kitaoka, K., Okumura, H., and Shibata, T. (1998). Morphodifferentiation of skeletal muscle fiber ends at the myotendinous junction in the postnatal Chinese hamster: a scanning electron microscopic study. Arch. Histol. Cytol. *61*, 89–92.

Nagwaney, S., Harlow, M.L., Jung, J.H., Szule, J. a, Ress, D., Xu, J., Marshall, R.M., and McMahan, U.J. (2009). Macromolecular connections of active zone material to docked synaptic vesicles and presynaptic membrane at neuromuscular junctions of mouse. J. Comp. Neurol. *513*, 457–468.

Nakashima, H., Kibe, T., and Yokochi, K. (2009). “Congenital muscular dystrophy caused by integrin alpha7 deficiency”. Dev. Med. Child Neurol. *51*, 245.

Nakata, T., Kitamura, Y., Shimizu, K., Tanaka, S., Fujimori, M., Yokoyama, S., Ito, K., and Emi, M. (1999). Fusion of a novel gene, ELKS, to RET due to translocation t(10;12)(q11;p13) in a papillary thyroid carcinoma. Genes. Chromosomes Cancer *25*, 97–103.

Nawrotzki, R. (2003). Defective integrin switch and matrix composition at alpha 7-deficient myotendinous junctions precede the onset of muscular dystrophy in mice. Hum. Mol. Genet. *12*, 483–495.

Nelson, B.R., Wu, F., Liu, Y., Anderson, D.M., McAnally, J., Lin, W., Cannon, S.C., Bassel-Duby, R., and Olson, E.N. (2013a). Skeletal muscle-specific T-tubule protein STAC3 mediates voltage-induced Ca2+ release and contractility. Proc Natl Acad Sci U S A *110*, 11881–11886.

Nelson, J.C., Stavoe, A.K.H., and Colón-Ramos, D.A. (2013b). The actin cytoskeleton in presynaptic assembly. Cell Adh. Migr. *7*, 379–387.

Nishimune, H. (2012). Molecular mechanism of active zone organization at vertebrate neuromuscular junctions. Mol. Neurobiol. *45*, 1–16.

Nishimune, H., Sanes, J.R., and Carlson, S.S. (2004). A synaptic laminin-calcium channel interaction organizes active zones in motor nerve terminals. Nature *432*, 580–587.

Nishimune, H., Valdez, G., Jarad, G., Moulson, C.L., Müller, U., Miner, J.H., and Sanes, J.R. (2008). Laminins promote postsynaptic maturation by an autocrine mechanism at the neuromuscular junction. J. Cell Biol. *182*, 1201–1215.

Nishimune, H., Numata, T., Chen, J., Aoki, Y., Wang, Y., Starr, M.P., Mori, Y., and Stanford, J.A. (2012). Active zone protein Bassoon co-localizes with presynaptic calcium channel, modifies channel function, and recovers from aging related loss by exercise. PLoS One *7*, e38029.

Nishimune, H., Stanford, J.A., and Mori, Y. (2014). Role of exercise in maintaining the integrity of the neuromuscular junction. Muscle Nerve *49*, 315–324.

Noakes, P.G., Gautam, M., Mudd, J., Sanes, J.R., and Merlie, J.P. (1995). Aberrant differentiation of neuromuscular junctions in mice lacking s-laminin/laminin beta2. Nature *374*, 258–262.

Norden, M.A., Rao, V.K., and Southard, J.H. (1997). Improved preservation of rat hindlimbs with the University of Wisconsin solution and butanedione monoxime. Plast. Reconstr. Surg. *100*, 957–965.

Ottenheijm, C.A.C., and Granzier, H. (2010). Lifting the nebula: novel insights into skeletal muscle contractility. Physiology (Bethesda). *25*, 304–310.

Pacifici, P.G., Peter, C., Yampolsky, P., Koenen, M., McArdle, J.J., and Witzemann, V. (2011). Novel mouse model reveals distinct activity-dependent and -independent contributions to synapse development. PLoS One *6*, e16469.

Pankov, R., and Yamada, K.M. (2002). Fibronectin at a glance. J. Cell Sci. *115*, 3861–3863.

Parames, S.F., Coletta-Yudice, E.D., Nogueira, F.M., Nering de Sousa, M.B., Hayashi, M.A., Lima-Landman, M.T.R., Lapa, A.J., and Souccar, C. (2014). Altered acetylcholine release in the hippocampus of dystrophin-deficient mice. Neuroscience *269*, 173–183.

Parlati, F., McNew, J.A., Fukuda, R., Miller, R., Söllner, T.H., and Rothman, J.E. (2000). Topological restriction of SNARE-dependent membrane fusion. Nature *407*, 194–198.

Patton, B.L. (2000). Laminins of the neuromuscular system. Microsc. Res. Tech. *51*, 247–261.

Patton, B.L., Cunningham, J.M., Thyboll, J., Kortesmaa, J., Westerblad, H., Edström, L., Tryggvason, K., Sanes, J.R., and Edstrom, L. (2001). Properly formed but improperly localized synaptic specializations in the absence of laminin alpha4. Nat. Neurosci. *4*, 597–604.

Peter, A.K., Cheng, H., Ross, R.S., Knowlton, K.U., and Chen, J. (2011). The costamere bridges sarcomeres to the sarcolemma in striated muscle. Prog. Pediatr. Cardiol. *31*, 83–88.

Petty, R. (2007). Lambert Eaton myasthenic syndrome. Pract. Neurol. *7*, 265–267.

Pilgram, G.S.K., Potikanond, S., Baines, R. a, Fradkin, L.G., and Noordermeer, J.N. (2010). The roles of the dystrophin-associated glycoprotein complex at the synapse. Mol. Neurobiol. *41*, 1–21.

Playford, M.P., and Schaller, M.D. (2004). The interplay between Src and integrins in normal and tumor biology. Oncogene *23*, 7928–7946.

Plomp, J.J., Van Kempen, G.T., De Baets, M.B., Graus, Y.M., Kuks, J.B., and Molenaar, P.C. (1995). Acetylcholine release in myasthenia gravis: regulation at single end-plate level. Ann. Neurol. *37*, 627–636.

Poage, R.E., and Meriney, S.D. (2002). Presynaptic calcium influx, neurotransmitter release, and neuromuscular disease. Physiol. Behav. *77*, 507–512.

Pöschl, E., Schlötzer-Schrehardt, U., Brachvogel, B., Saito, K., Ninomiya, Y., and Mayer, U. (2004). Collagen IV is essential for basement membrane stability but dispensable for initiation of its assembly during early development. Development *131*, 1619–1628.

Postel, R., Vakeel, P., Topczewski, J., Knöll, R., and Bakkers, J. (2008). Zebrafish integrin-linked kinase is required in skeletal muscles for strengthening the integrin-ECM adhesion complex. Dev. Biol. *318*, 92–101.

Power, G.A., Dalton, B.H., Behm, D.G., Vandervoort, A.A., Doherty, T.J., and Rice, C.L. (2010). Motor unit number estimates in masters runners: use it or lose it? Med. Sci. Sports Exerc. *42*, 1644–1650.

Prokop, A., Martín-Bermudo, M.D., Bate, M., and Brown, N.H. (1998). Absence of PS integrins or laminin A affects extracellular adhesion, but not intracellular assembly, of hemiadherens and neuromuscular junctions in Drosophila embryos. Dev. Biol. *196*, 58–76.

Proszynski, T.J., and Sanes, J.R. (2013). Amotl2 interacts with LL5β, localizes to podosomes and regulates postsynaptic differentiation in muscle. J. Cell Sci. *126*, 2225–2235.

Proszynski, T.J., Gingras, J., Valdez, G., Krzewski, K., and Sanes, J.R. (2009). Podosomes are present in a postsynaptic apparatus and participate in its maturation. Proc. Natl. Acad. Sci. U. S. A. *106*, 18373–18378.

Przewoźniak, M., Czaplicka, I., Czerwińska, A.M., Markowska-Zagrajek, A., Moraczewski, J., Stremińska, W., Jańczyk-Ilach, K., Ciemerych, M. a, and Brzoska, E. (2013). Adhesion proteins--an impact on skeletal myoblast differentiation. PLoS One *8*, e61760.

Pumplin, D.W., Reese, T.S., and Llinás, R. (1981). Are the presynaptic membrane particles the calcium channels? Proc. Natl. Acad. Sci. U. S. A. *78*, 7210–7213.

Punga, A.R., Lin, S., Oliveri, F., Meinen, S., and Rüegg, M.A. (2011). Muscle-selective synaptic disassembly and reorganization in MuSK antibody positive MG mice. Exp. Neurol. *230*, 207–217.

Purves, D., Augustine, G.J., Fitzpatrick, D., Katz, L.C., LaMantia, A.-S., McNamara, J.O., and Williams, S.M. (2001). Local Recycling of Synaptic Vesicles.

Qadota, H., and Benian, G.M. (2010). Molecular structure of sarcomere-to-membrane attachment at M-Lines in C. elegans muscle. J. Biomed. Biotechnol. *2010*, 864749.

Qin, J., and Wu, C. (2012). ILK: a pseudokinase in the center stage of cell-matrix adhesion and signaling. Curr. Opin. Cell Biol. *24*, 607–613.

Raeker, M.O., Su, F., Geisler, S.B., Borisov, A.B., Kontrogianni-Konstantopoulos, A., Lyons, S.E., and Russell, M.W. (2006). Obscurin is required for the lateral alignment of striated myofibrils in zebrafish. Dev. Dyn. *235*, 2018–2029.

Rafuse, V.F., Polo-Parada, L., and Landmesser, L.T. (2000). Structural and functional alterations of neuromuscular junctions in NCAM-deficient mice. J. Neurosci. *20*, 6529–6539.

Reid, B., Slater, C.R., and Bewick, G.S. (1999). Synaptic vesicle dynamics in rat fast and slow motor nerve terminals. J. Neurosci. *19*, 2511–2521.

Relaix, F., Rocancourt, D., Mansouri, A., and Buckingham, M. (2005). A Pax3/Pax7-dependent population of skeletal muscle progenitor cells. Nature *435*, 948–953.

Relaix, F., Montarras, D., Zaffran, S., Gayraud-Morel, B., Rocancourt, D., Tajbakhsh, S., Mansouri, A., Cumano, A., and Buckingham, M. (2006). Pax3 and Pax7 have distinct and overlapping functions in adult muscle progenitor cells. J. Cell Biol. *172*, 91–102.

Ridge, J.C., Tidball, J.G., Ahl, K., Law, D.J., and Rickoll, W.L. (1994). Modifications in myotendinous junction surface morphology in dystrophin-deficient mouse muscle. Exp. Mol. Pathol. *61*, 58–68.

Rifes, P., and Thorsteinsdóttir, S. (2012). Extracellular matrix assembly and 3D organization during paraxial mesoderm development in the chick embryo. Dev. Biol. *368*, 370–381.

Rigoard, P., Buffenoir, K., Bauche, S., Fares, M., Koenig, J., Hantaï, D., Giot, J.-P., Seguin, F., Huze, C., Schaeffer, L., et al. (2009). [Tools and techniques dedicated to neuromuscular junction observation]. Neurochirurgie. *55 Suppl 1*, S43–S48.

Robinson, S.D., and Norton, R.S. (2014). Conotoxin Gene Superfamilies. Mar. Drugs *12*, 6058–6101.

Roche, S.L., Sherman, D.L., Dissanayake, K., Soucy, G., Desmazieres, A., Lamont, D.J., Peles, E., Julien, J.-P., Wishart, T.M., Ribchester, R.R., et al. (2014). Loss of Glial Neurofascin155 Delays Developmental Synapse Elimination at the Neuromuscular Junction. J. Neurosci. *34*, 12904–12918.

Rohrbough, J., Grotewiel, M.S., Davis, R.L., and Broadie, K. (2000). Integrin-mediated regulation of synaptic morphology, transmission, and plasticity. J. Neurosci. *20*, 6868–6878.

Ross, T.D., Coon, B.G., Yun, S., Baeyens, N., Tanaka, K., Ouyang, M., and Schwartz, M. a (2013). Integrins in mechanotransduction. Curr. Opin. Cell Biol. *25*, 613–618.

Rossetto, O., Pirazzini, M., and Montecucco, C. (2014). Botulinum neurotoxins: genetic, structural and mechanistic insights. Nat. Rev. Microbiol. *12*, 535–549.

Rudolf, R., Khan, M.M., Labeit, S., and Deschenes, M.R. (2014). Degeneration of neuromuscular junction in age and dystrophy. Front. Aging Neurosci. *6*, 99.

Ruiz, R., Casañas, J.J., Südhof, T.C., and Tabares, L. (2008). Cysteine string protein-α is essential for the high calcium sensitivity of exocytosis in a vertebrate synapse. Eur. J. Neurosci. *27*, 3118–3131.

Sambasivan, R., Kuratani, S., and Tajbakhsh, S. (2011a). An eye on the head: the development and evolution of craniofacial muscles. Development *138*, 2401–2415.

Sambasivan, R., Yao, R., Kissenpfennig, a., Van Wittenberghe, L., Paldi, a., Gayraud-Morel, B., Guenou, H., Malissen, B., Tajbakhsh, S., and Galy, a. (2011b). Pax7-expressing satellite cells are indispensable for adult skeletal muscle regeneration. Development *138*, 3647–3656.

Samuel, M.A., Valdez, G., Tapia, J.C., Lichtman, J.W., and Sanes, J.R. (2012). Agrin and synaptic laminin are required to maintain adult neuromuscular junctions. PLoS One *7*, e46663.

Sandonà, D., and Betto, R. (2009). Sarcoglycanopathies: molecular pathogenesis and therapeutic prospects. Expert Rev. Mol. Med. *11*, e28.

Sanes, J.R. (2003). The basement membrane/basal lamina of skeletal muscle. J. Biol. Chem. *278*, 12601–12604.

Sanes, J.R., and Lichtman, J.W. (1999). Development of the vertebrate neuromuscular junction. Annu. Rev. Neurosci. *22*, 389–442.

Sanford, J.L., Mays, T.A., and Rafael-Fortney, J.A. (2004). CASK and Dlg form a PDZ protein complex at the mammalian neuromuscular junction. Muscle Nerve *30*, 164–171.

Savige, J. (2014). Alport syndrome: its effects on the glomerular filtration barrier and implications for future treatment. J. Physiol. *592*, 4013–4023.

Schiavo, G., Benfenati, F., Poulain, B., Rossetto, O., Polverino de Laureto, P., DasGupta, B.R., and Montecucco, C. (1992). Tetanus and botulinum-B neurotoxins block neurotransmitter release by proteolytic cleavage of synaptobrevin. Nature *359*, 832–835.

Schmidt, N., Basu, S., Sladecek, S., Gatti, S., van Haren, J., Treves, S., Pielage, J., Galjart, N., and Brenner, H.R. (2012). Agrin regulates CLASP2-mediated capture of microtubules at the neuromuscular junction synaptic membrane. J. Cell Biol. *198*, 421–437.

Schoch, S., Mittelstaedt, T., Kaeser, P.S., Padgett, D., Feldmann, N., Chevaleyre, V., Castillo, P.E., Hammer, R.E., Han, W., Schmitz, F., et al. (2006). Redundant functions of RIM1alpha and RIM2alpha in Ca(2+)-triggered neurotransmitter release. EMBO J. *25*, 5852–5863.

Schulz, A.M., Jing, Z., Sánchez Caro, J.M., Wetzel, F., Dresbach, T., Strenzke, N., Wichmann, C., and Moser, T. (2014). Bassoon-disruption slows vesicle replenishment and induces homeostatic plasticity at a CNS synapse. EMBO J. *33*, 512–527.

Schwander, M., Leu, M., Stumm, M., Dorchies, O.M., Ruegg, U.T., Schittny, J., and Müller, U. (2003). Beta1 integrins regulate myoblast fusion and sarcomere assembly. Dev. Cell *4*, 673–685.

Schwander, M., Shirasaki, R., Pfaff, S.L., and Müller, U. (2004). Beta1 integrins in muscle, but not in motor neurons, are required for skeletal muscle innervation. J. Neurosci. *24*, 8181–8191.

Scott, W., Stevens, J., and Binder–Macleod, S. (2001). Human Skeletal Muscle Fiber Type Classifications. Phys. Ther. 1810–1816.

Seabrooke, S., Qiu, X., and Stewart, B.A. (2010). Nonmuscle Myosin II helps regulate synaptic vesicle mobility at the Drosophila neuromuscular junction. BMC Neurosci. *11*, 37.

Seale, P. (2000). Pax7 Is Required for the Specification of Myogenic Satellite Cells. Cell *102*, 777–786.

Seals, D.F., Azucena Jr., E.F., Pass, I., Tesfay, L., Gordon, R., Woodrow, M., Resau, J.H., and Courtneidge, S.A. (2005). The adaptor protein Tks5/Fish is required for podosome formation and function, and for the protease-driven invasion of cancer cells. Cancer Cell *7*, 155–165.

Selcen, D. (2011). Myofibrillar myopathies. Neuromuscul. Disord. *21*, 161–171.

Selverston, A.I., and Moulins, M. (1985). Oscillatory neural networks. Annu. Rev. Physiol. *47*, 29–48.

Sendtner, M., Pei, G., Beck, M., Schweizer, U., and Wiese, S. (2000). Developmental motoneuron cell death and neurotrophic factors. Cell Tissue Res. *301*, 71–84.

Sens, K.L., Zhang, S., Jin, P., Duan, R., Zhang, G., Luo, F., Parachini, L., and Chen, E.H. (2010). An invasive podosome-like structure promotes fusion pore formation during myoblast fusion. J. Cell Biol. *191*, 1013–1027.

Shafrir, E. (1994). Julius Axelrod, Bernard Katz and Ulf von Euler--Nobel Prize winners for the discovery of mechanisms of nerve signal transmission. Isr. J. Med. Sci. *30*, 869.

Shen, J., Tareste, D.C., Paumet, F., Rothman, J.E., and Melia, T.J. (2007). Selective activation of cognate SNAREpins by Sec1/Munc18 proteins. Cell *128*, 183–195.

Sheng, L., Leshchyns'ka, I., and Sytnyk, V. (2013). Cell adhesion and intracellular calcium signaling in neurons. Cell Commun. Signal. *11*, 94.

Shi, L., Butt, B., Ip, F.C.F., Dai, Y., Jiang, L., Yung, W.-H., Greenberg, M.E., Fu, A.K.Y., and Ip, N.Y. (2010). Ephexin1 is required for structural maturation and neurotransmission at the neuromuscular junction. Neuron *65*, 204–216.

Short, B. (2012). Stress fibers guide focal adhesions to maturity. J. Cell Biol. *196*, 301–301.

Sigoillot, S.M., Bourgeois, F., Lambergeon, M., Strochlic, L., and Legay, C. (2010). ColQ controls postsynaptic differentiation at the neuromuscular junction. J. Neurosci. *30*, 13–23.

Singhal, N., and Martin, P.T. (2011). Role of extracellular matrix proteins and their receptors in the development of the vertebrate neuromuscular junction. Dev. Neurobiol. *71*, 982–1005.

Slater, C.R. (2003). Structural determinants of the reliability of synaptic transmission at the vertebrate neuromuscular junction. J. Neurocytol. *32*, 505–522.

Slater, C.R. (2008). Structural factors influencing the efficacy of neuromuscular transmission. Ann. N. Y. Acad. Sci. *1132*, 1–12.

Slater, C.R., Lyons, P.R., Walls, T.J., Fawcett, P.R., and Young, C. (1992). Structure and function of neuromuscular junctions in the vastus lateralis of man. A motor point biopsy study of two groups of patients. Brain *115 (Pt 2*, 451–478.

Snow, C.J., Peterson, M.T., Khalil, A., and Henry, C.A. (2008). Muscle development is disrupted in zebrafish embryos deficient for fibronectin. Dev. Dyn. *237*, 2542–2553.

Son, Y.J., Scranton, T.W., Sunderland, W.J., Baek, S.J., Miner, J.H., Sanes, J.R., and Carlson, S.S. (2000). The synaptic vesicle protein SV2 is complexed with an alpha5-containing laminin on the nerve terminal surface. J. Biol. Chem. *275*, 451–460.

Song, W.K., Wang, W., Sato, H., Bielser, D.A., and Kaufman, S.J. (1993). Expression of alpha 7 integrin cytoplasmic domains during skeletal muscle development: alternate forms, conformational change, and homologies with serine/threonine kinases and tyrosine phosphatases. J. Cell Sci. *106 (Pt 4*, 1139–1152.

Sons, M.S., Busche, N., Strenzke, N., Moser, T., Ernsberger, U., Mooren, F.C., Zhang, W., Ahmad, M., Steffens, H., Schomburg, E.D., et al. (2006). Alpha-neurexins are required for efficient transmitter release and synaptic homeostasis at the mouse neuromuscular junction. Neuroscience *138*, 433–446.

Sons, S., Plomp, J.J., and Brose, N. (2005). Aberrant Morphology and Residual Transmitter Release at the Munc13-Deficient Mouse Neuromuscular Synapse †. *25*, 5973–5984.

Sparrow, J.C., and Schöck, F. (2009). The initial steps of myofibril assembly: integrins pave the way. Nat. Rev. Mol. Cell Biol. *10*, 293–298.

Spence, H.J., Dhillon, A.S., James, M., and Winder, S.J. (2004). Dystroglycan, a scaffold for the ERK-MAP kinase cascade. EMBO Rep. *5*, 484–489.

Spillane, J., Beeson, D.J., and Kullmann, D.M. (2010). Myasthenia and related disorders of the neuromuscular junction. J. Neurol. Neurosurg. Psychiatry *81*, 850–857.

Stephens, L.E., Sutherland, A.E., Klimanskaya, I. V, Andrieux, A., Meneses, J., Pedersen, R.A., and Damsky, C.H. (1995). Deletion of beta 1 integrins in mice results in inner cell mass failure and peri-implantation lethality. Genes Dev. *9*, 1883–1895.

Stevens, E., Carss, K.J., Cirak, S., Foley, a R., Torelli, S., Willer, T., Tambunan, D.E., Yau, S., Brodd, L., Sewry, C. a, et al. (2013). Mutations in B3GALNT2 cause congenital muscular dystrophy and hypoglycosylation of α-dystroglycan. Am. J. Hum. Genet. *92*, 354–365.

Südhof, T.C. (2012). The presynaptic active zone. Neuron *75*, 11–25.

Südhof, T.C. (2013). A molecular machine for neurotransmitter release: synaptotagmin and beyond. Nat. Med. *19*, 1227–1231.

Südhof, T.C., and Rothman, J.E. (2009). Membrane fusion: grappling with SNARE and SM proteins. Science *323*, 474–477.

Südhof, T.C., De Camilli, P., Niemann, H., and Jahn, R. (1993). Membrane fusion machinery: insights from synaptic proteins. Cell *75*, 1–4.

Sumikawa, K., and Miledi, R. (1989). Assembly and N-glycosylation of all ACh receptor subunits are required for their efficient insertion into plasma membranes. Brain Res. Mol. Brain Res. *5*, 183–192.

Sun, M., Xing, G., Yuan, L., Gan, G., Knight, D., With, S.I., He, C., Han, J., Zeng, X., Fang, M., et al. (2011). Neuroligin 2 is required for synapse development and function at the Drosophila neuromuscular junction. J. Neurosci. *31*, 687–699.

Suzuki, N., Yokoyama, F., and Nomizu, M. (2005). Functional sites in the laminin alpha chains. Connect. Tissue Res. *46*, 142–152.

Tajbakhsh, S., Rocancourt, D., Cossu, G., and Buckingham, M. (1997). Redefining the Genetic Hierarchies Controlling Skeletal Myogenesis: Pax-3 and Myf-5 Act Upstream of MyoD. Cell *89*, 127–138.

Taniguchi, M., Kurahashi, H., Noguchi, S., Fukudome, T., Okinaga, T., Tsukahara, T., Tajima, Y., Ozono, K., Nishino, I., Nonaka, I., et al. (2006). Aberrant neuromuscular junctions and delayed terminal muscle fiber maturation in alpha-dystroglycanopathies. Hum. Mol. Genet. *15*, 1279–1289.

Taverna, D., Disatnik, M.H., Rayburn, H., Bronson, R.T., Yang, J., Rando, T.A., and Hynes, R.O. (1998). Dystrophic muscle in mice chimeric for expression of alpha5 integrin. J. Cell Biol. *143*, 849–859.

Teriakidis, A., Willshaw, D.J., and Ribchester, R.R. (2012). Prevalence and elimination of sibling neurite convergence in motor units supplying neonatal and adult mouse skeletal muscle. J. Comp. Neurol. *520*, 3203–3216.

Thompson, O., Kleino, I., Crimaldi, L., Gimona, M., Saksela, K., and Winder, S.J. (2008). Dystroglycan, Tks5 and Src mediated assembly of podosomes in myoblasts. PLoS One *3*, e3638.

Thompson, O., Moore, C.J., Hussain, S.-A., Kleino, I., Peckham, M., Hohenester, E., Ayscough, K.R., Saksela, K., and Winder, S.J. (2010). Modulation of cell spreading and cell-substrate adhesion dynamics by dystroglycan. J. Cell Sci. *123*, 118–127.

Thorsteinsdóttir, S., Deries, M., Cachaço, A.S., and Bajanca, F. (2011). The extracellular matrix dimension of skeletal muscle development. Dev. Biol. *354*, 191–207.

Tokuyasu, K.T., and Maher, P.A. (1987). Immunocytochemical studies of cardiac myofibrillogenesis in early chick embryos. II. Generation of alpha-actinin dots within titin spots at the time of the first myofibril formation. J. Cell Biol. *105*, 2795–2801.

tom Dieck, S., Sanmartí-Vila, L., Langnaese, K., Richter, K., Kindler, S., Soyke, a, Wex, H., Smalla, K.H., Kämpf, U., Fränzer, J.T., et al. (1998). Bassoon, a novel zinc-finger CAG/glutamine-repeat protein selectively localized at the active zone of presynaptic nerve terminals. J. Cell Biol. *142*, 499–509.

Tonino, P., Pappas, C.T., Hudson, B.D., Labeit, S., Gregorio, C.C., and Granzier, H. (2010). Reduced myofibrillar connectivity and increased Z-disk width in nebulin-deficient skeletal muscle. J. Cell Sci. *123*, 384–391.

Tozawa, T., Itoh, K., Yaoi, T., Tando, S., Umekage, M., Dai, H., Hosoi, H., and Fushiki, S. (2012). The shortest isoform of dystrophin (Dp40) interacts with a group of presynaptic proteins to form a presumptive novel complex in the mouse brain. Mol. Neurobiol. *45*, 287–297.

Tremblay, J.P., Grégoire, L., Sasseville, R., Guay, G., and Belhumeur, C. (1988). Reduction of postjunctional fold density and depth in dystrophic mice. Synapse *2*, 148–156.

Trimbuch, T., Xu, J., Flaherty, D., Tomchick, D.R., Rizo, J., and Rosenmund, C. (2014). Re-examining how complexin inhibits neurotransmitter release. Elife *3*, e02391.

Truett, G.E., Heeger, P., Mynatt, R.L., Truett, A.A., Walker, J.A., and Warman, M.L. (2000). Preparation of PCR-quality mouse genomic DNA with hot sodium hydroxide and tris (HotSHOT). Biotechniques *29*, 52–54.

Turner, C.E., Glenney Jr., J.R., Burridge, K., and Glenney, J.R. (1990). Paxillin: a new vinculin-binding protein present in focal adhesions. J. Cell Biol. *111*, 1059–1068.

Unwin, N. (2013). Nicotinic acetylcholine receptor and the structural basis of neuromuscular transmission: insights from Torpedo postsynaptic membranes. Q. Rev. Biophys. *46*, 283–322.

Urbano, F.J., Piedras-Rentería, E.S., Jun, K., Shin, H.-S., Uchitel, O.D., and Tsien, R.W. (2003). Altered properties of quantal neurotransmitter release at endplates of mice lacking P/Q-type Ca2+ channels. Proc. Natl. Acad. Sci. U. S. A. *100*, 3491–3496.

Vainzof, M., Ayub-Guerrieri, D., Onofre, P.C.G., Martins, P.C.M., Lopes, V.F., Zilberztajn, D., Maia, L.S., Sell, K., and Yamamoto, L.U. (2008). Animal models for genetic neuromuscular diseases. J. Mol. Neurosci. *34*, 241–248.

Valdez, G., Tapia, J.C., Kang, H., Clemenson, G.D., Gage, F.H., Lichtman, J.W., and Sanes, J.R. (2010). Attenuation of age-related changes in mouse neuromuscular synapses by caloric restriction and exercise. Proc. Natl. Acad. Sci. U. S. A. *107*, 14863–14868.

Valenzuela, D.M., Stitt, T.N., DiStefano, P.S., Rojas, E., Mattsson, K., Compton, D.L., Nuñez, L., Park, J.S., Stark, J.L., and Gies, D.R. (1995). Receptor tyrosine kinase specific for the skeletal muscle lineage: expression in embryonic muscle, at the neuromuscular junction, and after injury. Neuron *15*, 573–584.

Vandervoort, A.A. (2002). Aging of the human neuromuscular system. Muscle Nerve *25*, 17–25.

Varoqueaux, F., Sigler, A., Rhee, J.-S., Brose, N., Enk, C., Reim, K., and Rosenmund, C. (2002). Total arrest of spontaneous and evoked synaptic transmission but normal synaptogenesis in the absence of Munc13-mediated vesicle priming. Proc. Natl. Acad. Sci. U. S. A. *99*, 9037–9042.

Varoqueaux, F., Sons, M.S., Plomp, J.J., and Brose, N. (2005). Aberrant Morphology and Residual Transmitter Release at the Munc13-Deficient Mouse Neuromuscular Synapse Aberrant Morphology and Residual Transmitter Release at the Munc13-Deficient Mouse Neuromuscular Synapse †.

Velling, T., Collo, G., Sorokin, L., Durbeej, M., Zhang, H., and Gullberg, D. (1996). Distinct alpha 7A beta 1 and alpha 7B beta 1 integrin expression patterns during mouse development: alpha 7A is restricted to skeletal muscle but alpha 7B is expressed in striated muscle, vasculature, and nervous system. Dev. Dyn. *207*, 355–371.

Voermans, N.C., Bönnemann, C.G., Huijing, P. a, Hamel, B.C., van Kuppevelt, T.H., de Haan, a, Schalkwijk, J., van Engelen, B.G., and Jenniskens, G.J. (2008). Clinical and molecular overlap between myopathies and inherited connective tissue diseases. Neuromuscul. Disord. *18*, 843–856.

Volk, T., Fessler, L.I., and Fessler, J.H. (1990). A role for integrin in the formation of sarcomeric cytoarchitecture. Cell *63*, 525–536.

Volknandt, W., and Karas, M. (2012). Proteomic analysis of the presynaptic active zone. Exp. Brain Res. *217*, 449–461.

Waite, A., Brown, S.C., and Blake, D.J. (2012). The dystrophin-glycoprotein complex in brain development and disease. Trends Neurosci. *35*, 487–496.

Waites, C.L., Leal-Ortiz, S.A., Andlauer, T.F.M., Sigrist, S.J., and Garner, C.C. (2011). Piccolo regulates the dynamic assembly of presynaptic F-actin. J. Neurosci. *31*, 14250–14263.

Waites, C.L., Leal-Ortiz, S. a, Okerlund, N., Dalke, H., Fejtova, A., Altrock, W.D., Gundelfinger, E.D., and Garner, C.C. (2013). Bassoon and Piccolo maintain synapse integrity by regulating protein ubiquitination and degradation. EMBO J. 1–16.

Wang, H.-V., Chang, L.-W., Brixius, K., Wickström, S.A., Montanez, E., Thievessen, I., Schwander, M., Müller, U., Bloch, W., Mayer, U., et al. (2008). Integrin-linked kinase stabilizes myotendinous junctions and protects muscle from stress-induced damage. J. Cell Biol. *180*, 1037–1049.

Wang, P., Yang, G., Mosier, D.R., Chang, P., Zaidi, T., Gong, Y.-D., Zhao, N.-M., Dominguez, B., Lee, K.-F., Gan, W.-B., et al. (2005). Defective neuromuscular synapses in mice lacking amyloid precursor protein (APP) and APP-Like protein 2. J. Neurosci. *25*, 1219–1225.

Wang, X., Kibschull, M., Laue, M.M., Lichte, B., Petrasch-Parwez, E., and Kilimann, M.W. (1999). Aczonin, a 550-kD putative scaffolding protein of presynaptic active zones, shares homology regions with Rim and Bassoon and binds profilin. J. Cell Biol. *147*, 151–162.

Wang, Y., Okamoto, M., Schmitz, F., Hofmann, K., and Südhof, T.C. (1997). Rim is a putative Rab3 effector in regulating synaptic-vesicle fusion. Nature *388*, 593–598.

Wasicky, R., Ziya-Ghazvini, F., Blumer, R., Lukas, J.-R., and Mayr, R. (2000). Muscle Fiber Types of Human Extraocular Muscles: A Histochemical and Immunohistochemical Study. Invest. Ophthalmol. Vis. Sci. *41*, 980–990.

Webster, R.G., Cossins, J., Lashley, D., Maxwell, S., Liu, W.W., Wickens, J.R., Martinez-Martinez, P., de Baets, M., and Beeson, D. (2013). A mouse model of the slow channel myasthenic syndrome: Neuromuscular physiology and effects of ephedrine treatment. Exp. Neurol. *248*, 286–298.

Wegener, K.L., Partridge, A.W., Han, J., Pickford, A.R., Liddington, R.C., Ginsberg, M.H., and Campbell, I.D. (2007). Structural basis of integrin activation by talin. Cell *128*, 171–182.

Welser, J. V, Rooney, J.E., Cohen, N.C., Gurpur, P.B., Singer, C.A., Evans, R.A., Haines, B.A., and Burkin, D.J. (2009). Myotendinous junction defects and reduced force transmission in mice that lack alpha7 integrin and utrophin. Am. J. Pathol. *175*, 1545–1554.

Whitmore, C., and Morgan, J. (2014). What do mouse models of muscular dystrophy tell us about the DAPC and its components? Int. J. Exp. Pathol.

Wicklund, M.P. (2013). The muscular dystrophies. Continuum (Minneap. Minn). *19*, 1535–1570.

Witzemann, V. (2006). Development of the neuromuscular junction. Cell Tissue Res. *326*, 263–271.

Wong, K.C., Meyer, T., Harding, D.I., Dick, J.R., Vrbova, G., and Greensmith, L. (1999). Integrins at the neuromuscular junction are important for motoneuron survival. Eur. J. Neurosci. *11*, 3287–3292.

Wood, S.J., and Slater, C.R. (2001). Safety factor at the neuromuscular junction.

Wozniak, M.A., Modzelewska, K., Kwong, L., and Keely, P.J. (2004). Focal adhesion regulation of cell behavior. Biochim. Biophys. Acta *1692*, 103–119.

Wu, H., Xiong, W.C., and Mei, L. (2010). To build a synapse: signaling pathways in neuromuscular junction assembly. Development *137*, 1017–1033.

Xiong, J.P., Stehle, T., Diefenbach, B., Zhang, R., Dunker, R., Scott, D.L., Joachimiak, A., Goodman, S.L., and Arnaout, M.A. (2001). Crystal structure of the extracellular segment of integrin alpha Vbeta3. Science *294*, 339–345.

Yang, J.T., Rando, T.A., Mohler, W.A., Rayburn, H., Blau, H.M., and Hynes, R.O. (1996). Genetic analysis of alpha 4 integrin functions in the development of mouse skeletal muscle. J. Cell Biol. *135*, 829–835.

Yang, W., Shimaoka, M., Chen, J., and Springer, T.A. (2004). Activation of integrin subunit I-like domains by one-turn C-terminal helix deletions. Proc. Natl. Acad. Sci. *101*, 2333–2338.

Yang, X., Arber, S., William, C., Li, L., Tanabe, Y., Jessell, T.M., Birchmeier, C., and Burden, S.J. (2001). Patterning of muscle acetylcholine receptor gene expression in the absence of motor innervation. Neuron *30*, 399–410.

Zhang, W., and Benson, D.L. (2001). Stages of Synapse Development Defined by Dependence on F-Actin. J Neurosci *21*, 5169–5181.

Ziober, B.L., Vu, M.P., Waleh, N., Crawford, J., Lin, C.S., and Kramer, R.H. (1993). Alternative extracellular and cytoplasmic domains of the integrin alpha 7 subunit are differentially expressed during development. J. Biol. Chem. *268*, 26773–26783.

Zong, Y., and Jin, R. (2013). Structural mechanisms of the agrin-LRP4-MuSK signaling pathway in neuromuscular junction differentiation. Cell. Mol. Life Sci. *70*, 3077–3088.